ESSENTIAL PATHWAYS AND GENE REGULATION FOR CELL WALL HOMEOSTASIS IN *BACILLUS SUBTILIS*

A dissertation

Presented to the Faculty of the Graduate School

of Cornell University

in Partial Fulfillment of the Requirements for the Degree of

Doctor of Philosophy

By

Heng Zhao

August 2018

ESSENTIAL PATHWAYS AND GENE REGULATION FOR CELL WALL HOMEOSTASIS IN *BACILLUS SUBTILIS*

Heng Zhao, Ph.D.

Cornell University 2018

The cell wall is an essential component of most bacterial cells, and cell wall targeting antibiotics have greatly improved human health and life span. Despite intense research over the last 50 years, we still lack a complete understanding of how bacteria maintain cell wall homeostasis. Here we attempt to integrate new data from the last few years with some established ideas in the field, and we propose a new model of cell wall biogenesis in rod-shaped bacteria (Chapter 1).

The lipid II cycle is central to peptidoglycan (PG) synthesis. A common C_{55} lipid carrier, undecaprenyl-pyrophosphate (UPP) is used for the synthesis of both peptidoglycan and wall teichoic acids to ferry precursors across the cytoplasmic membrane. Here we demonstrate that *B. subtilis* requires either one of two UPP phosphatases, UppP or BcrC, for the recycling of this essential molecule for continuous synthesis of cell wall (Chapter 2).

Peptidoglycan synthesis relies on intermediates derived from central metabolism. We found that an *aspB* mutant is auxotrophic for aspartate and lyses when grown on Difco sporulation medium due to limitation of the peptidoglycan precursor meso-2,6-diaminopimelate (mDAP), a downstream metabolic intermediate of aspartate. Interestingly, we found that when bacteria experience a shortage of aspartate, the first breakpoint is not protein but peptidoglycan synthesis, which predisposes them to cell wall weakness and sensitizes them to antibiotics targeting late steps of PG synthesis. This work highlights the ability of perturbations of central metabolism to sensitize cells to peptidoglycan synthesis inhibitors (Chapter 3).

Bacillus subtilis uses alternative sigma factors to regulate gene transcription upon stresses. Being a powerful double-edged sword, it is essential to keep this regulatory network under check. Here we show that the absence of its anti-sigma factor(s) leads to dysregulation of SigM, which drives a positive feedback loop for its own synthesis and SigM accumulates to a toxic level. High SigM activity overproduces membrane proteins and causes protein secretion stress, which lead to cell morphology and severe growth defects (Chapter 4). Collectively, the work in this dissertation provides additional insights of essential pathways and gene regulation for cell wall homeostasis in *Bacillus subtilis*.

BIOGRAPHICAL SKETCH

Heng Zhao was born on November 21st, 1986 in Nanjing, Jiangsu, China. Raised by his parents and grandparents, he has always faced high expectations for his academic development. When asked what he wanted to be when grows up, he gave the standard answer of becoming a scientist, without any understanding of what it really meant at the age of five.

Being convinced that Biology is the discipline of the future, Heng went to Nanjing Agricultural University for college and chose biological science as his major. During his thesis work in senior year, he was amazed of how complex a bacterium is, and how much impact bacteria can have on the environment and human life despite their tiny size. He went on and did three years of master work in the field of Microbiology in Dr. Xiafang Sheng's laboratory at Nanjing Agricultural University. By the end of his masters study, he had become passionate about science, and somehow the childhood wish of becoming a scientist turned out to be a real career possibility. He applied to a few graduate schools in the US and was thrilled when offered into Cornell University.

After a year of rotations in three different laboratories, Heng joined the John Helmann group in May 2013 to study cell wall homeostasis in the Gram-Positive model organism *Bacillus subtilis*. There he met the best mentor in the world and learnt how to study fundamental biological questions using various methods including microbial genetics. This dissertation summarizes his findings during his Ph.D. work.

ACKNOWLEDGMENTS

I am sincerely grateful to my advisor and mentor, Dr. John D. Helmann, who welcomed me into his laboratory and supported me through my Ph.D. study. During my years in his laboratory, I was deeply impressed by his incredible knowledge and passion in science, and enjoyed tremendously his kind and humorous personality. I have greatly benefited from his mentorship, as he always has the passion and patience to teach me any aspect of science, from big scientific questions to small experiment setup, and from manuscript structure to wording choices. He also adjusts his mentorship as I went through different stages in my learning process, providing me with close attention and detailed help in the first few years, and much trust and freedom for me to explore myself as I gradually mature. In addition, he has always been very supportive to my personal life, and very kind to my family. He is a great role model for me to know what kind of PI I should strive to become.

I want to thank my two other committee members, Dr. Esther Angert and Dr. Gerald Feigenson, who are very supportive for my academic growth and are always there for me when I need help. I would also like to thank Dr. Tobias Doerr who has generously provided both scientific and technical help for my projects.

I want to thank Dr. James P. Shapleigh for welcoming me into Cornell University and the U.S. He made my transition so easy and enjoyable.

It has been a great experience working in the Helmann group. I want to especially thank Dr. Ahmed Gaballa, who has trained me very well, taught me so many techniques and tips, and is always there to help me planning, carrying out, and troubleshooting experiments. I also want to thank Dr. Anthony Kingston, who mentored me in my rotation period, let me enjoy both the

scientific and personal life in the lab, and made it a very easy decision for me to join the lab. I would like to thank all the Helmann lab members who have overlapped with me, as they have always been kind, supportive and helpful.

All of this would not be possible without the unconditional love and support from my family. I am extremely fortunate to have a loving wife who gave me a lovely family and support my work wholeheartedly despite of the heavy burden of taking care of young kids at home. My family are all the motivation for me to work hard. I want to thank my father, who has showed me what a good father is and what a huge impact a good father can have on his child. I also want to thank all the support from other family members, especially my mother and mother-in-law, who came here and stayed through Ithaca winters to help me with family, enabling me to focus on my work. I am deeply grateful for all their help and devotion.

TABLE OF CONTENTS

LIST OF TABLES

LIST OF FIGURES

Chapter 1. Don’t let sleeping dogmas lie: New views of peptidoglycan synthesis and its regulation

1.1 Abstract

Bacterial cell wall synthesis is the target for some of our most powerful antibiotics and has thus been the subject of intense research focus for more than 50 years. Surprisingly, we still lack a fundamental understanding of how bacteria build, maintain and expand their cell wall. Due to technical limitations, directly testing hypotheses about the coordination and biochemistry of cell wall synthesis enzymes or architecture has been challenging, and interpretation of data has therefore often relied on circumstantial evidence and implicit assumptions. A number of recent papers have exploited new technologies, like single molecule tracking and real-time, high resolution temporal mapping of cell wall synthesis processes, to address fundamental questions of bacterial cell wall biogenesis. The results have challenged established dogmas and it is therefore timely to integrate new data and old observations into a new model of cell wall biogenesis in rod-shaped bacteria.

1.2 Introduction

Most bacteria surround themselves with a cell wall, a complex biopolymer with a crucial role in maintaining cellular integrity and cell shape. Due to its essentiality for bacterial growth and survival, the bacterial cell wall constitutes an ideal target for antibiotics, and there has been a longstanding scientific interest in the mechanisms of its synthesis and turnover. Pioneering work beginning over 50 years ago established the general composition of the cell wall (or sacculus) as a single large molecule made primarily of peptidoglycan (PG). The Gram-positive cell wall also contains a large amount of teichoic acid, including wall teichoic acids covalently linked to PG

(Brown *et al.*, 2013, Reichmann & Grundling, 2011)). PG is a mesh-like macromolecule comprising roughly parallel glycan strands of polymerized disaccharide (*N*-acetylglucosamine-*N*-acetylmuramic acid; or NAG-NAM), which are intermittently crosslinked with neighboring strands by peptide bonds between short oligopeptides (pentapeptides) attached to the NAM residues (Strominger *et al.*, 1971, Strominger *et al.*, 1959, Anderson *et al.*, 1967, Anderson *et al.*, 1966).

This basic PG structure is conserved amongst essentially all Bacteria, although there are variations in the details. These include differences in glycan strand chain length and a diversity of peptide crosslinks. The peptide crosslinks vary in amino acid composition and modifications (e.g. amidation), the addition in some species of interstrand bridging peptides, the precise site of interstrand linkage, and their overall density (Espaillat *et al.*, 2016, Quintela *et al.*, 1995). The PG sacculus can be further modified after synthesis by occasional additions to the glycan strands, for example of acetyl residues (O-acetylation, (Moynihan *et al.*, 2014)). Despite these subtle variations, the overall PG structure is highly conserved when compared to other bacterial surface layers (including capsules, S-layers, and enterobacterial O-antigen) and therefore PG and its derivatives serve as effective pathogen-associated molecular patterns (PAMPs) for host recognition of bacterial infection (Mogensen, 2009).

Despite being the focus of intense research, conspicuous gaps in our knowledge of PG biogenesis have persisted over decades, and some long-entrenched ideas have been found to be either incorrect or incomplete. Recent studies of the enzymology, genetics and cell biology of PG synthesis have challenged many long-standing assumptions. Here, we review recent insights into PG synthesis, largely from studies of the rod-shaped model organisms *Escherichia coli* and *Bacillus subtilis*. The focus will be the enzymology and cell biology of proteins involved in cell

elongation and division. We conclude by proposing a new model of cell wall biogenesis that incorporates these recent findings.

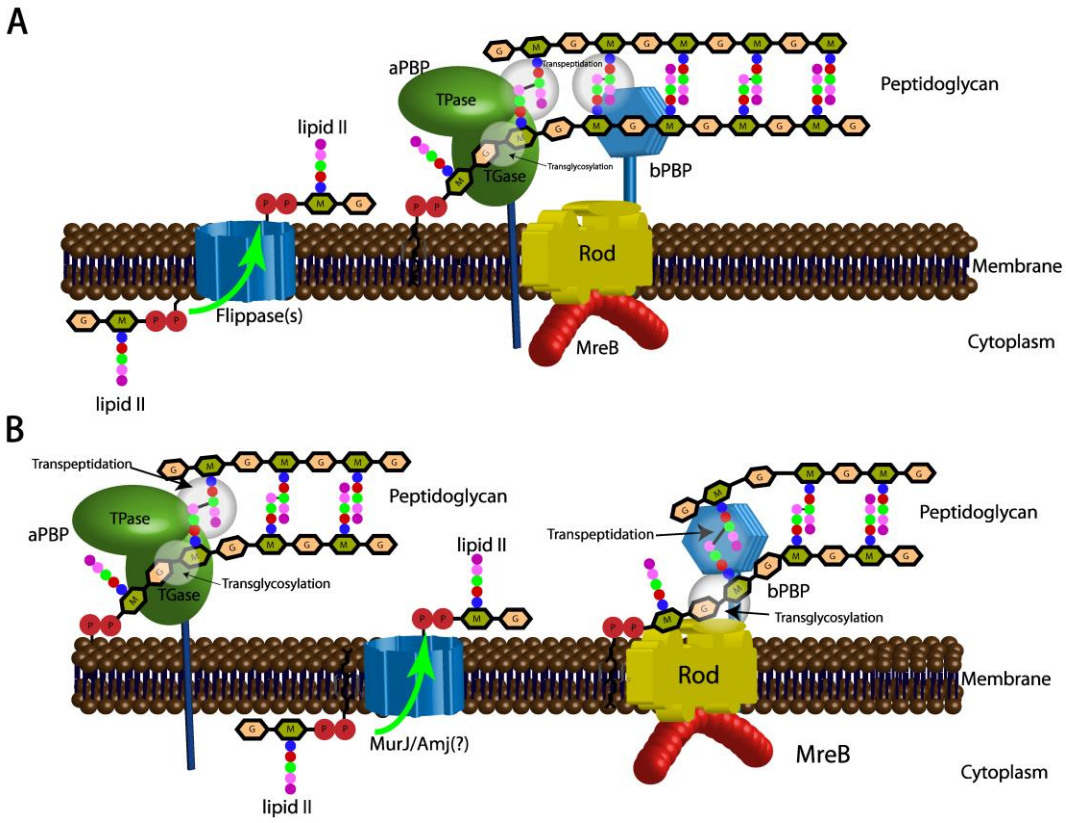

Figure 1.1. Unified (A) and Interdependent (B) models of peptidoglycan (PG) synthesis complexes.

(A) In the unified model, RodAZ, MreB, aPBPs and bPBPs form one protein complex: guided by MreB, the aPBPs produce peptidoglycan strands via their TG domains while both aPBPs and bPBPs crosslink these strands into a tight PG mesh.

(B) In the interdependent model, RodAZ, bPBP and MreB form one complex, while aPBP works in a different spatial and temporal frame. Glycan strands are produced by the transglycosylase RodA and are crosslinked by bPBP to existing PG. PG synthesis provides the force for pushing circumferential MreB movement. aPBPs exhibit a different movement pattern distinct from MreB, including two modes of movement: fast diffusion and slow movement (pause). These two systems are spatially distinct, but functionally interdependent for PG synthesis.

1.3 Enzymology of PG synthesis: variations, nuances, and the key points of controversy

Assembly of the PG layer requires three major stages: precursor synthesis in the cytoplasm to generate the key intermediate lipid II, the lipid II cycle (translocation, transglycosylation, and recycling of the carrier lipid), and glycan strand crosslinking and maturation. As would be expected for such a central process in bacterial cell biology, the key enzymes for PG synthesis are generally well-established. However, the overall process displays more plasticity than originally envisioned, some key enzymes have remained elusive or controversial, and several puzzling genetic observations have only recently been resolved.

PG synthesis starts in the cytoplasm, where the precursor molecule UDP-NAM-pentapeptide is produced by enzymes encoded by the *mur* genes as well as the D-Ala-D-Ala ligase Ddl as the last soluble precursor (Lovering *et al.*, 2012). Ligation of this precursor to an undecaprenyl (C_{55}) carrier lipid by the membrane-associated enzyme MraY generates lipid I, the first membrane-associated intermediate. MurG ligates a NAG residue to lipid I to generate the final, lipidated disaccharide-pentapeptide precursor referred to as lipid II (Scheffers & Tol, 2015). Once synthesis is complete on the cytoplasmic face of the inner membrane, the lipid II precursor must be translocated (flipped) to the outer face of the membrane by a flippase, where the final steps of PG assembly occur. Following assembly, PG may be further modified and serves as a scaffold for the anchoring of wall teichoic acids (in Gram-positive bacteria), proteins, and other surface structures and appendages (Siegel *et al.*, 2016, Brown *et al.*, 2013, Guest & Raivio, 2016).

Lipid II provides the subunits that are polymerized into glycan strands via a transglycosylation (TG) reaction. The lipid carrier is released as undecaprenyl-pyrophosphate and

recycled into the cytoplasm by a putative, as yet unidentified C_{55}-pyrophosphate flippase, which may or may not be the same as the lipid II flippase. The TG reaction has historically been thought to be mediated solely by bifunctional (class A) penicillin binding proteins, here designated as aPBPs (Goffin & Ghuysen, 1998, Sauvage *et al.*, 2008). The polysaccharide strands resulting from the TG reaction are subsequently covalently linked via D, D transpeptidation (TP) reactions to form peptide bond crosslinks between the glycan strands (Sauvage *et al.*, 2008). The acceptor amino group derives from the side chain of the third amino acid (typically diaminopimelic acid, DAP_3 or lysine, Lys_3, depending on the species) with D-Ala_4 as the donor (generating a 4-3 crosslink); this results in the release of the terminal D-Ala_5 from the donor strand (McDonough *et al.*, 2002, Mainardi *et al.*, 2008). The TP reaction can be mediated by either aPBPs (which possess both TG and TP activity) or by monofunctional D, D-transpeptidases (class B PBPs, designated here as bPBPs).

This basic, textbook version of PG synthesis provides a framework for a more detailed consideration of how this process may differ between organisms or be modified in response to stress. Moreover, some of the central steps in PG synthesis have retained an aura of mystery, with a lack of consensus about the identity of key enzymes and some confounding genetic observations. Recent excitement centers on three major advances. First, the proteins that translocate the lipid II precursor from the cytosolic to the external face of the membrane are now becoming clear. Second, a long predicted but elusive PBP-independent TG activity has been defined. Third, variations in the nature of the PG intra-strand crosslinking reactions, and in particular the presence and impact of 3-3 in place of 4-3 crosslinks, is an emerging area of focus.

1.3.1 MurJ and functionally redundant lipid II flippases

After its generation in the cytoplasm, the PG precursor lipid II must be translocated ("flipped") across the cytoplasmic membrane to provide the substrate for cell wall synthesis enzymes. The identity of the lipid II flippase(s) has been the subject of a longstanding controversy. Using a reductionist bioinformatics approach, Ruiz first proposed the membrane-anchored protein MurJ as the lipid II flippase in *E. coli* and supported this notion by demonstrating that MurJ is essential and required for PG synthesis (both of which would be expected of a flippase) (Ruiz, 2008). This was later challenged by Mohammadi *et al*., who used an *in vitro* assay to demonstrate flippase activity of purified FtsW protein, and thus speculated that SEDS (shape, elongation, division, and sporulation) family proteins (including RodA, FtsW and SpoVE in *B. subtilis*), rather than MurJ, were flippases (Mohammadi *et al.*, 2011). Another key point of their argument was that while a flippase is expected to be universally essential, all MurJ homologues could be deleted in *B. subtili*s (Fay & Dworkin, 2009).

Two recent studies have shed some more light on this controversy. Using an *in vivo* biochemical assay, Sham *et al*. demonstrated that MurJ does have lipid II flippase activity (Sham *et al.*, 2014). Importantly, in the same study, depleting FtsW in a Δ*rodA* background (essentiality of *rodA* was suppressed by overexpression of the *ftsQAZ* operon (Kruse *et al.*, 2005)) did not affect precursor translocation, suggesting that RodA and FtsW are entirely dispensable for this process. Another recent study addressed the important question of why MurJ proteins were (collectively) non-essential in *B. subtilis.* Using a synthetic lethal screen (via transposon insertion sequencing), Meeske *et al*. searched for genes that become essential in the absence of all MurJ homologs, arguing that an alternative flippase must exist and should be synthetic lethal with MurJ (Meeske *et al.*, 2015). The screen was answered by a locus that was renamed *amj* ("alternate to MurJ");

intriguingly, the predicted Amj protein bears no sequence or structural homology to MurJ. Using the *in vivo* biochemical assay mentioned above (Sham *et al.*, 2014) it was demonstrated that both MurJ and Amj can mediate lipid II translocation across the inner membrane; in addition, Amj could functionally replace MurJ in *E. coli*. Interestingly, *amj* is induced in the absence of MurJ, and its expression depends on the cell wall stress responsive alternative sigma factor SigM (Helmann, 2016, Eiamphungporn & Helmann, 2008, Meeske *et al.*, 2015). Thus, *B. subtilis* can respond to inhibition of one of its flippases, perhaps by currently unknown antibiotics, with the expression of an alternative, structurally unrelated enzyme. In summary, there are now strong data supporting the role of MurJ and Amj as lipid II flippases. The role of FtsW remains controversial; however, recent revelations about the similar SEDS family protein RodA provide us with some room to speculate on FtsW function (see next section).

Important open questions remain concerning the reverse side of the flippase reaction; after transglycosylation, the undecaprenyl pyrophosphate (UPP) portion of lipid II remains on the outer leaflet of the cytoplasmic membrane. UPP molecules in the cell membrane are limited and UPP must therefore be efficiently recycled. This is accomplished by known, membrane-associated enzymes (UPP phosphatases) that convert UPP to undecaprenyl phosphate (UP), which can be reintroduced into the lipid II cycle (El Ghachi *et al.*, 2005, Zhao *et al.*, 2016). Due to the size and charge of the lipid carrier, it is generally expected to be translocated back into the cytoplasm by an enzyme facilitator rather than via spontaneous flipping, but the identity of this putative facilitator remains unknown.

1.3.2 The SEDS protein RodA has TG activity

The transglycosylation (TG) reaction is a crucial step in periplasmic cell wall assembly. Until recently, two classes of enzymes were known or predicted to perform the TG reaction: monofunctional transglycosylases (MTGs) and the TG domains of aPBPs. While MTGs have a demonstrated role in cell wall synthesis in some coccoid Gram-positive bacteria like *Staphylococcus aureus* (Reed *et al.*, 2011), they are not widely conserved (absent for example in *B. subtilis*) and their physiological role in rod-shaped bacteria is unclear as there are no strong phenotypes associated with deletion or overexpression mutants (Denome *et al.*, 1999, Di Berardino *et al.*, 1996). Hence, the aPBPs were generally considered as the principal TGases during cell wall biosynthesis.

This dogma was challenged over a decade ago, when David Popham's group found that *B. subtilis* was able to grow (albeit poorly) in the absence of all aPBPs (McPherson & Popham, 2003). This striking finding strongly suggested that an unidentified TGase could compensate for the loss of aPBPs by collaborating with the TP function of a bPBP. Other groups have reported similar observations in *Enterococcus* spp. (Arbeloa *et al.*, 2004, Rice *et al.*, 2009). Intriguingly, a study from more than 30 years ago had already provided a candidate for Popham's "missing" transglycosylase. Ishino *et al*., while conducting studies on PG synthesis processes mediated by the bPBP2 (for clarity, we will add the a/b class prefix to specific PBPs throughout the text), found that crude membrane extracts of *E. coli* produced cell wall material when they were isolated from a strain in which bPBP2 as well as RodA were overproduced (the aPBPs were at the same time inactivated using antibiotics) (Ishino *et al.*, 1986). Using bPBP2-specific antibiotics and thermosensitive variants of both bPBP2 and RodA, these authors dissected the contribution of each protein to the PG synthesis process and found that while bPBP2 was, as expected, required for the

crosslinking part of assembly, RodA was required for chain elongation. They then discussed the possibility that RodA itself possessed transglycosylase activity, but dismissed this as "unlikely" and rather concluded (in light of what was known about PBPs in 1986) that bPBP2 itself had TG activity that was somehow stimulated by RodA. These observations were thus not integrated into later models of cell wall synthesis. Later, the idea that RodA possessed TG activity was further obscured by the proposal (as noted above) that another SEDS protein, FtsW, functioned as a lipid II flippase based on an *in vitro* biochemical assay (Mohammadi *et al.*, 2011), fueling the assumption that this was true for RodA as well. FtsW and RodA were thus tentatively assigned as flippases, as noted above.

Several recent papers from the Bernhardt, Ruiz, Rudner and Errington labs have provided new insights into the roles of SEDS proteins. First, the identification of MurJ (and Amj in *B. subtilis*, see previous section) as a lipid II flippase (Meeske *et al.*, 2015), re-established the possibility that RodA and FtsW have activities other than (or in addition to) precursor translocation. Then, using independent approaches (homology search (Meeske *et al.*, 2016) or candidate genes elimination (Emami *et al.*, 2017)), it was discovered that RodA has TGase activity *in vitro* (Meeske et al., 2016), and that overexpression of RodA rescued the strong growth defect of the *B. subtilis* strain lacking all aPBPs (Meeske *et al.*, 2016, Emami *et al.*, 2017). Possible natural molecule inhibitors of RodA were also identified (Emami *et al.*, 2017).

Interestingly, these data provided an explanation for another curious feature of *B. subtilis*: its resistance to moenomycin. Moenomycin is a potent aPBP transglycosylase inhibitor (Welzel, 2007, Gampe *et al.*, 2013, Rebets *et al.*, 2014) whereas RodA TG activity was found to be unaffected by moenomycin *in vitro* (Meeske *et al.*, 2016, McPherson & Popham, 2003). In *B. subtilis*, resistance to moenomycin depends on the SigM dependent cell envelope damage response,

and SigM induces expression of *rodA* (Eiamphungporn & Helmann, 2008, Meeske *et al.*, 2016, Mascher *et al.*, 2007). Thus, similar to Amj (see above), or PBP2a in Methicillin Resistant *Staphylococcus aureus* (Hao *et al.*, 2012), *B. subtilis* enhances the expression of one cell wall synthesis enzyme (RodA) upon inhibition of another (aPBPs) (Meeske *et al.*, 2015, Helmann, 2016).

RodA was also shown to contribute significant TG activity to cell wall synthesis mediated by the "elongasome" in *E. coli* (Cho *et al.*, 2016). However, unlike its Gram-positive counterpart, this activity does not suffice to sustain growth in the absence of aPBPs. This might be a common feature in Gram-negative bacteria, as in these organisms depletion or inhibition of aPBPs typically leads to cessation of growth and/or lysis and death (Dorr *et al.*, 2014, Yousif *et al.*, 1985, Satta *et al.*, 1995).

Whether FtsW possesses TG activity has not been completely resolved. Recent biochemical evidence suggests that in *E. coli*, FtsW forms a complex with bPBP3 and aPBP1B at the division site (Leclercq *et al.*, 2017). FtsW was also shown to bind lipid II and to negatively regulate aPBP1b activity using *in vitro* assays, and this inhibition was alleviated by the presence of bPBP3 (Leclercq *et al.*, 2017). Importantly, FtsW did not exhibit TGase activity under these experimental conditions.

1.3.3 L,D-transpeptidases and diversification of PG architecture

D-Ala$_4$-D-DAP$_3$ or D-Ala$_4$-D-Lys$_3$ (D,D) crosslinks (generally referred to as 4,3 crosslinks), whose formation is mediated by D,D transpeptidases (the PBPs), have been established as the major type of PG crosslink. However, many bacteria also harbor L,D transpeptidases (LDT) (Magnet *et al.*, 2008, Lavollay *et al.*, 2008, Hernandez *et al.*, 2015, Mainardi *et al.*, 2000, Lam *et al.*, 2009, Cava *et al.*, 2011, Bramkamp, 2010, Magnet *et al.*, 2007). These enzymes also catalyze TP reactions between two amino acids, e.g. between two DAP molecules in neighboring PG strands (using the energy stored in the DAP$_3$-D-Ala$_4$ bond), which at least in principle could lead to fully crosslinked PG. Intriguingly, even mutants deleted in multiple or all L,D transpeptidases exhibit only minor phenotypes (Sanders & Pavelka, 2013) and the types of crosslinks these enzymes create (DAP-DAP or 3,3 crosslinks) are typically too rare to provide full structural integrity (Glauner *et al.*, 1988, Desmarais *et al.*, 2013). A notable exception is *Agrobacterium tumefaciens*, whose PG naturally consists of ~45% L,D crosslinks (Quintela *et al.*, 1995). An increase in 3,3 crosslinks has been observed in multiple other species when cells enter stationary phase (where in *Mycobacterium tuberculosis*, up to 80% of PG can be crosslinked via DAP-DAP (Lavollay *et al.*, 2008)), and under envelope stress conditions: activation of the Cpx response in *E. coli* for example led to a ~1.5-fold increase in DAP-DAP crosslinks (Lavollay *et al.*, 2008, Bernal-Cabas *et al.*, 2015). It is therefore possible that L,D transpeptidation serves a supporting role for D,D crosslinks to further strengthen the PG meshwork under certain conditions.

Early evidence that L,D transpeptidases could assume a more fundamental role in cell wall biogenesis came from the work of the Gutmann and Arthur labs. In a series of papers (Mainardi *et al.*, 2000, Mainardi *et al.*, 2002, Mainardi *et al.*, 2005), these authors described the selection for a β-lactam resistant mutant of *Enterococcus faecalis*, whose cell wall was found to be essentially

devoid of the classical D,D crosslinks mediated by PBPs. This mutant could grow in the presence of β-lactam antibiotics by substituting the D,D crosslinks formed by the β-lactam sensitive PBPs with those formed by a β-lactam-insensitive L,D transpeptidase named Ldt_{fm}, which catalyzed transpeptidation between D-asparagine and L-lysine residues situated in neighboring PG strands, resulting in L,D (3,3) bonds (Mainardi *et al.*, 2005). Interestingly, the activity or abundance of the Ldt_{fm} or PBPs was unaltered in the resistant mutant. Instead, this strain showed an increase in the activity of a carboxypeptidase that removes the terminal D-Ala_5; the resulting tetrapeptide sidestem is recognized by L,D transpeptidases, but not PBPs as a substrate. Thus, *E. faecalis* provides intrinsic substrate cues to reprogram the activity of PG crosslinking enzymes and thus the nature of its PG crosslinks.

Another study recently reported that a similar mechanism of β-lactam resistance can evolve in *E. coli* (Hugonnet *et al.*, 2016). Upon multistep selection on β-lactam antibiotics, a mutant emerged that had upregulated one of its L,D transpeptidases (YcbB) as well as the stringent response, a starvation response that leads to the accumulation of the alarmone ppGpp and subsequent reprogramming of transcription. While the connection between the stringent response and L,D-TP activity is unclear, this strain utilizes the TG activity of the aPBP1B in conjunction with TP activity of YcbB for cell wall synthesis and crosslinking. Like in *E. faecium*, the ability to form L,D crosslinks depended on the presence of a carboxypeptidase, in this case PBP5. Although these experiments involved mutants that were generated under severe and artificial selection conditions, these results clearly demonstrate that L,D-TPase activity can, at least in principle, be contribute significantly to the structural integrity of the cell wall. It remains to be seen whether the primary reliance on L,D transpeptidation for bacterial growth is an oddity

resulting from stringent conditions of mutant selection or can be an adaptive response (for example as a stress response mechanism in the presence of β-lactam antibiotics) in nature as well.

1.4 Cell biology of PG synthesis: New insights into the roles of the cytoskeletal proteins MreB and FtsZ

The basic enzymology of PG synthesis was established in early studies following conventional approaches that integrated *in vitro* enzyme assays with chemical and structural characterization of reaction mechanisms and products. However, efforts to decipher the larger scale coordination of PG synthesis with cell growth and division did not make great strides until the advent of bacterial cell biology. The introduction of fluorescently labeled proteins, high resolution light microscopy methods, and, more recently, single-molecule tracking approaches has invigorated the field and enabled the development of new models of PG synthesis and its coordination. It is not enough to just be able to stitch together new PG; the newly synthesized glycan strands must be integrated into the existing sacculus in a manner that does not compromise the overall integrity and load-bearing properties of the wall, and old wall material must be simultaneously shed and recycled. How new areas of synthesis are defined in a manner appropriate for the maintenance of cell shape, as seen for example in rods, cocci, and helically shaped bacteria, has been a challenging problem. Here, we focus on the emerging view of the two primary biosynthetic, macromolecular complexes involved in synthesis of rod-shaped bacteria: the "elongasome" and the "divisome".

1.4.1 MreB and the "elongasome"

The transmembrane and periplasmic proteins associated with cell wall synthesis processes have been shown, or at least implicitly assumed, to be part of a single multiprotein complex called the "elongasome" (Laddomada *et al.*, 2016, Egan *et al.*, 2017, Errington, 2015) that contains structural components, as well as aPBPs, bPBPs, cell wall lytic enzymes ("autolysins"), and presumably a flippase. The "elongasome" was assumed to be spatio-temporally directed by the cytoskeletal protein MreB, a homologue of eukaryotic actin (van den Ent *et al.*, 2001) that localizes to the lateral wall of the bacterial cell (Jones *et al.*, 2001). One model suggests that MreB mediates the formation of regions with increased fluidity (RIFs), which affect distribution and diffusion of membrane proteins and may contribute to the organization of the "elongasome" (Strahl *et al.*, 2014). Until recently, a generally accepted model of cell wall synthesis proposed that MreB served to guide the aPBPs, which in turn produce peptidoglycan strands via their TG domains while the aPBPs and the bPBPs crosslink these strands into a tight PG mesh, fitting new material into cell wall gaps provided by the cleavage activity of autolysins (Figure 1.1A). However, the existence of an "elongasome" protein complex could never be demonstrated *in vivo* and recent single molecule tracking experiments revealed that MreB and aPBPs operate in distinct complexes (Cho *et al.*, 2016). This, in addition to the recent revelation that RodA itself possesses TG activity, calls for a re-evaluation of MreB's contribution to cell wall synthesis (Meeske *et al.*, 2016, Emami *et al.*, 2017).

MreB is found in most rod-shaped bacteria and loss of MreB generally leads to the cessation of lateral cell wall synthesis and concomitant loss of rod-shape, establishing the cytoskeleton's crucial role in directional PG insertion during cell elongation. MreB strongly interacts with RodA and RodZ in *E. coli* (Morgenstein *et al.*, 2015) and the latter mediates the

indirect interaction between MreB and a bPBP. This established complex (MreB-RodAZ-bPBP) will be referred to hereafter as the "Rod complex".

Early localization studies using immunofluorescence and epifluorescence microscopy to visualize fluorescently tagged proteins in *B. subtilis, E. coli* and *Caulobacter crescentus* suggested that MreB localizes in helical filaments along the inner face of the cytoplasmic membrane spanning the lateral cell (Shih *et al.*, 2003, Figge *et al.*, 2004, Jones *et al.*, 2001). However, using microscopy techniques that allowed for higher spatio-temporal resolution, it was later shown that instead of forming continuous filaments, MreB rotates around the cell in patches (arcs) whose motion depends on bPBP transpeptidation activity and the presence of RodA, but, at least in *E. coli*, not on the activity of aPBPs (Dominguez-Escobar *et al.*, 2011, Garner *et al.*, 2011, van Teeffelen *et al.*, 2011). More recent data show that MreB locates to regions of negative curvature, and "corrects" this negative curvature by filling this region with newly synthesized PG, suggesting a self-correcting feedback mechanism for cells to maintain rod shape (Ursell *et al.*, 2014). Overall these data strongly support a model in which cell wall synthesis during cell elongation is mediated primarily by the Rod complex.

Importantly, these single molecule studies have provided evidence for a spatial independence of the Rod complex and aPBPs (Figure 1.1B). In contrast, the Rod complex and bPBPs appear to move along the same trajectories, suggesting that they may be coupled (Cho *et al.*, 2016) (though it has to be noted that another study had previously found that MreB and bPBP2 move at different velocities (Lee *et al.*, 2014); this can be attributed to differences in imaging parameters and/or intrinsic differences between different fusion constructs, and may suggest that bPBP2's circumferential motion is not essential for its function). In contrast, aPBPs showed a bimodal pattern of movement, with two distinct subpopulations: one exhibiting fast, diffusive

motion, and another moving at a speed an order of magnitude slower (Cho *et al.*, 2016, Lee *et al.*, 2016). When considering the behavior of a single PBP molecule, these data can be interpreted as short periods of fast diffusion interspersed with temporary pauses. Although spatially independent, the partially redundant TG activities of the Rod complex and aPBPs are functionally coupled, as inactivation of one or the other leads to the same dramatic (~80%) decrease in incorporation of new cell wall material (Cho *et al.*, 2016). This, together with the observation that in *E. coli* a bPBP interacts directly with aPBP1A (Banzhaf *et al.*, 2012), suggests that the two seemingly independent activities of aPBPs and the Rod complex are somehow synergistic, and that they may at least transiently interface. A recent paper has exposed an additional layer of complexity about the relationship between the Rod complex and aPBPs. Using TIRF, Billaudeau *et al*. showed that in *B. subtilis,* MreB not only shows rotational movement, but has subpopulations that, similar to aPBPs, diffuse slowly or stop altogether (Billaudeau *et al.*, 2017). This, coupled with indirect evidence of an interaction between MreB and aPBPs (Kawai *et al.*, 2009) opens up the possibility that MreB and aPBPs associate. It is important to note that neither MreB patch rotational movement, nor aPBP activity, depend on each other (Cho *et al.*, 2016, van Teeffelen *et al.*, 2011); but whether diffusive MreB molecules functionally interact with aPBPs is not known. Further work is thus required to investigate the spatial and functional relationship between MreB (or at least a sub-population of it) and aPBPs.

How does Rod-mediated cell wall synthesis apparently drive its own motion, while aPBPs, in principle mediating the exact same reactions, are more diffusive? One possibility is that RodA's TG activity drives directional movement, and that its interaction with short, dynamic MreB arcs essentially reinforces this movement, while the aPBPs move along a similar trajectory for a short time, but produce shorter PG chains and diffuse away when the TG reaction is terminated (e.g.

through interaction with a putative chain termination factor, or due to an intrinsic capability to produce shorter PG chains). It is noteworthy that MreB was shown to interact with cytoplasmic cell wall precursor synthesis proteins and their localization changed during MreB depletion (Favini-Stabile *et al.*, 2013, White *et al.*, 2010, Rueff *et al.*, 2014, Divakaruni *et al.*, 2007), suggesting that MreB might coordinate the availability of precursors to generate a local pool of lipid II to support the activity of the Rod complex. This might be beneficial if RodA's TG activity intrinsically generates longer PG strands than the aPBPs (generating shorter chains may enable the aPBPs to operate on a more limited local supply of lipid II).

In the light of the existence of two independent cell wall synthesis complexes, an important open question is whether flippase activity is associated with one of the complexes, both, or is completely independent. Current data favor the latter hypothesis: heterologous expression of the *Helicobacter pylori* O-antigen flippase Wzk (Elhenawy *et al.*, 2016) or *B. subtilis* Amj (Meeske *et al.*, 2015) can functionally replace MurJ in *E. coli*. Amj has no homologs in *E. coli* and is thus unlikely to specifically interact with this organism's cell wall synthesis machinery, suggesting that unguided lipid II flipping may be sufficient to sustain bacterial growth. Furthermore, cell wall incorporation after inhibition of either the Rod complex or aPBPs is not zero, implying residual flippase activity. Thus, it is likely that lipid II flippase activity is not strictly dependent on either complex.

1.4.2 FtsZ and the divisome: FtsZ treadmilling drives PG synthesis at the septum

FtsZ, a homolog of tubulin, is essential for cell division in many bacteria. Cytoplasmic FtsZ molecules polymerize at the inner face of the cytoplasmic membrane as a dynamic ring of FtsZ filaments of varying lengths (Michie & Lowe, 2006). This so-called "Z-ring" and various accessory factors anchor the assembly of a dynamic, spatio-temporally ordered multiprotein

complex called the divisome. The divisome contains what are generally assumed to be structural proteins, but also proteins involved in cell wall synthesis (PBPs) and turnover, like amidases and lytic transglycosylases (Egan & Vollmer, 2013). Ultimately, the FtsZ-guided divisome serves the function of facilitating cytokinesis, membrane constriction, synthesis of new cell wall material and finally daughter cell separation. Purified FtsZ is sufficient to initiate constriction of elongated liposomes (Osawa *et al.*, 2009, Osawa *et al.*, 2008), suggesting that FtsZ itself generates the forces for cell division, powered by GTP hydrolysis (RayChaudhuri & Park, 1992, de Boer *et al.*, 1992). This was later challenged by results from experiments showing that constriction does not initiate in the absence of cell wall synthesis (Daley *et al.*, 2016). Beyond these observations, the role of FtsZ outside of its anchor function remained largely mysterious.

Several recent studies have addressed this issue with newly available super-resolution techniques. In two parallel studies, Bisson-Filho *et al.* and Yang *et al.* used single molecule tracking and super-resolution microscopy combined with targeted perturbations of division processes to assess the role of FtsZ filaments in the division process in *B. subtilis* and *E. coli (Bisson-Filho et al., 2017, Yang et al., 2017b).* Both groups found that short FtsZ filaments display a rotational, inward movement that coincides with the deposition of new cell wall material. Strikingly, and in contrast to MreB, FtsZ movement was independent of cell wall synthesis and driven by treadmilling, which depended on its GTPase activity. It thus appears that FtsZ generates its own motion, and induces cell wall synthesis during the constriction process. This observation could provide an explanation for previously inconsistent data: while FtsZ treadmilling by itself probably generates enough force to initiate membrane constriction, it is the reinforcement of these constrictions via guided traces of PG material that enables the completion of outer membrane constriction and cytokinesis. This more active, cytoskeleton-driven process of movement (as

opposed to MreB's passive motion) might thus be necessary to apply the forces needed for cell division.

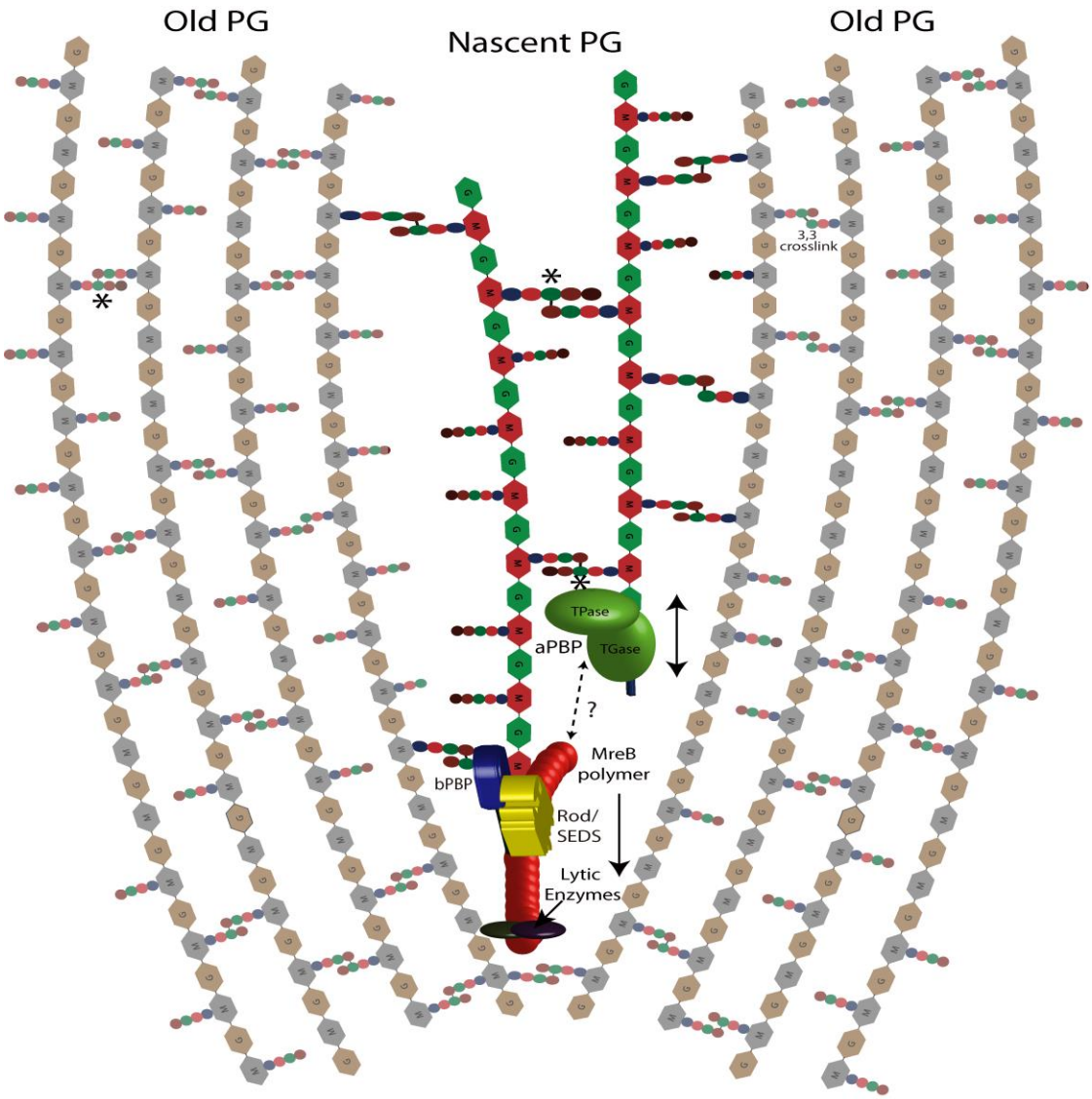

Figure 1.2. "Break before Make" model of peptidoglycan (PG) synthesis complexes.

Rod/SEDS/MreB-associated endopeptidases locally cleave crosslinks in mature PG. RodA generates a PG template, which is attached to the sacculus via bPBPs (only one strand is shown here, note that in principle this could also be a raft structure of multiple parallel strands). The aPBPs then generate additional strands, which are crosslinked with nascent PG on one side and mature PG on the other, ensuring maintenance of structural integrity. Whether the Rod/SEDS/MreB complex interacts with aPBPs remains an open question. Crosslinked pentapeptide (asterisk) is formed when a nascent PG strand containing pentapeptide is crosslinked with another one. PBP-independent 3,3 crosslinks also exist albeit at low abundance under normal growth conditions.

1.5 An emerging model of PG synthesis for rod-shaped bacteria

One of the most influential unified models of cell wall growth coordination was put forth in a seminal review paper by Höltje (Holtje, 1998). Asking how PG lytic and synthetic processes might be coordinated without compromising cell wall structural integrity, the author proposed that bacteria synthesize a precursor of three parallel, crosslinked PG strands, which would substitute for a single strand concomitantly removed by the coordinated activity of PG hydrolases; he termed this the "3-for-1" model. Höltje assumed that the parallel strands were generated before breaking any bonds in the PG meshwork (to ensure structural integrity), or a "make before break" mode of sacculus expansion. This model has remained an important conceptual framework, but has not been re-evaluated in the light of subsequent new observations.

We will attempt here to integrate new data on the mechanisms of PG biogenesis with previous observations into an updated model of cell wall biogenesis (Figure 1.2). Perhaps one of the most striking recent realizations is that the Rod complex and aPBPs are spatially distinct, yet their activities are interdependent. A possible model is that one cell wall synthesis complex creates a template structure for the other, consistent with what has been suggested by Wientjes et al. (Wientjes & Nanninga, 1991) and Cho et al. (Cho *et al.*, 2016). We speculate that template generation is accomplished by the circumferentially moving population of the Rod complex, as steady, circumferential motion would be conducive to providing a regular template structure. In contrast, the aPBPs exhibit a diffusive motion interspersed with prolonged local persistence (Cho *et al.*, 2016, Lee *et al.*, 2016), which could suggest that their role is to diffuse freely until they recognize a PG trace or gap (e.g. one generated by the Rod complex) and then add new material to the template. Inhibition of a bPBP (PBP2) in *E. coli* results in the generation of PG fragments that are not incorporated into the PG meshwork but rather are rapidly degraded and recycled (Cho

et al., 2014, Uehara & Park, 2008), suggesting that in Rod-mediated PG synthesis, PBP2 provides the first point of attachment for nascent PG after (or while) it emerges from RodA-mediated transglycosylation. This first point of attachment would also be an important anchor providing a fulcrum for RodA-driven MreB movement; perhaps this is why inhibition of bPBPs stops MreB motion (van Teeffelen *et al.*, 2011, Garner *et al.*, 2011, Dominguez-Escobar *et al.*, 2011) but allows futile synthesis of PG by RodA (Cho *et al.*, 2016, Cho *et al.*, 2014).

Interestingly, at least in *E. coli*, a bPBP (PBP2) was shown to activate an aPBP (PBP1A) (Banzhaf *et al.*, 2012). The fact that the Rod-associated bPBP stimulates the aPBP's TG activity may suggest that rod-driven PG synthesis starts prior to aPBP-driven PG synthesis. We propose that the aPBPs likely use the Rod-mediated PG template to attach parallel (or possibly antiparallel) PG strands (Figure 1.2). In addition to providing lateral directionality of sacculus expansion, this is consistent with the observed existence of crosslinked PG strands containing pentapeptide: enzymatically, the only way to generate PG containing pentapeptides is when nascent PG is crosslinked with another strand of nascent PG (since the terminal D-Ala of the donor strand is lost in the crosslinking reaction). Moreover, pentapeptides are likely rapidly processed by carboxypeptidases associated with cell wall synthesis (Potluri *et al.*, 2010, Santos *et al.*, 2002, Atrih *et al.*, 1999, Moll *et al.*, 2015)), but nascent-nascent crosslinks are indeed observed during pulse-chase PG labeling experiments (Burman & Park, 1984). Alternatively, these crosslinked PG strands containing pentapeptide may come from region with presumably less carboxypeptidase activity, for example the septum (Morales Angeles *et al.*, 2017), or from PG generated by several Rod complexes working in parallel, as recently suggested for *B. subtilis* (Billaudeau *et al.*, 2017). It is therefore possible that the Rod template actually consists of a PG "raft" structure of several strands that are then woven tightly into the cell wall by aPBPs. Why are the aPBPs partially

dispensable in *B. subtilis* (dependent on stress-response mediated upregulation of RodA) and not in *E. coli*? Perhaps the Rod complex template itself is enough to mediate sacculus expansion, as long as it is made in sufficient quantity (*B. subtilis* upregulates RodA upon aPBP deletion via the Sigma M cell wall stress sensing pathway) and as long as there is a sufficient stress-bearing "buffer", i.e. a thick cell wall that can partially compensate for localized, inefficient crosslinking.

Our model suggests that the Rod complex might coordinate its cell wall synthesis activity with PG cleavage by endopeptidases, which are required for the insertion of new PG material during cell elongation (Vollmer, 2012, Singh *et al.*, 2012, Dorr *et al.*, 2013) and should therefore immediately precede template attachment. Consistent with this hypothesis, MreB homologs in *B. subtilis* have been shown to direct the activities of elongation-specific endopeptidases LytE and (indirectly) CwlO (Dominguez-Cuevas *et al.*, 2013, Meisner *et al.*, 2013). Further, at least in Gram-negative bacteria, inhibition or depletion of aPBPs (leaving the putative RodA-autolysin complex active) typically leads to a catastrophic loss of the cell wall (Dorr *et al.*, 2014, Yousif *et al.*, 1985, Satta *et al.*, 1995), while defects associated with the Rod complex (which might cause concurrent lack of major autolysin activation) are generally milder and simply result in an abrogation of cell elongation with loss of cellular integrity only after prolonged exposure (Tybring & Melchior, 1975, Iwai *et al.*, 2002). Measurements of the incorporation of new cell wall material in the presence of antibiotics previously showed that inhibition of aPBPs resulted in a delayed inhibition of cell wall incorporation, and cessation of cell wall synthesis coincided with the onset of lysis (Wientjes & Nanninga, 1991). These observations are also consistent with Rod-associated cell wall cleavage and template generation, which would proceed even in the absence of aPBPs until a "tipping point" is reached where accumulated damage caused by the lack of subsequent aPBP-mediated crosslinking results in catastrophic failure of structural integrity. Recent results

demonstrate that *E. coli* endopeptidase activity increases aPBP-mediated cell wall attachment during inhibition of bPBP2 (Lai *et al.*, 2017), suggesting that endopeptidases might, in addition to priming the Rod system, provide Rod-independent starting points (gaps) for PG synthesis by aPBPs.

It remains to be seen what the roles of lytic transglycosylases (LTGs) are in the cell wall biosynthesis process. The typical PG breakdown products of these enzymes are detected during growth and at increased levels upon exposure to cell wall synthesis inhibitors; however, it is currently unclear whether removal of a strand (or strands) of mature PG is actually necessary for the insertion of new material. Alternatively, LTG breakdown products could be the result of the removal of the outer cell layer in Gram-positive bacteria, a proofreading capacity (removing erroneously crosslinked and thus potentially unstable cell wall material), as has been suggested previously (Cho *et al.*, 2014), or simply the fact that nascent PG is produced in longer chains at first and then trimmed down to the length most appropriate for the current growth condition (Yunck *et al.*, 2016, Vollmer & Holtje, 2004).

In summary, we propose a "break before make" model. Endopeptidases locally cleave crosslinks in mature PG. RodA generates a PG template, which is attached to the sacculus via bPBPs. Since the Rod complex is not expected to perform an entire rotation around the cell (based on short PG chain lengths measured in various bacteria), these PG degradation events are initially localized and overall structural integrity is thus not immediately compromised. The aPBPs then generate additional strands, which are crosslinked with nascent PG on one side and mature PG on the other, ensuring that the local degradation events initiated by the Rod complex do not accumulate with harmful consequences. Previous simulations and observations regarding bPBP2 inactivation have indeed shown that the cell wall synthesis machinery, even in Gram-negative

bacteria, is surprisingly well-buffered and can sustain a fairly high amount of degradation before experiencing catastrophic failure (Lee *et al.*, 2014, Huang *et al.*, 2008).

Important questions remain unanswered in the context of this model; most importantly, how the Rod complex defines start sites for PG synthesis, how aPBPs recognize the putative Rod template and what role the modulators of PBP activity play (such as the outer membrane localized activators in Gram-negative bacteria, (Typas *et al.*, 2010, Paradis-Bleau *et al.*, 2010)). After all, more than 50 years after its emergence, bacterial cell wall research still holds surprises, and is expected to continue doing so.

1.5 Acknowledgment

This chapter is adapted from "Don't let sleeping dogmas lie: new views of peptidoglycan synthesis and its regulation", *Mol Microbiol*. 2017 Dec;106(6):847-860. doi: 10.1111/mmi.13853. The list of the authors is Zhao H, Patel V, Helmann JD, and Dörr T. Patel V is a graduate student in the field of microbiology. Helmann JD and Dörr T are faculty members of the department of microbiology at Cornell University.

1.6 References

Anderson, J.S., M. Matsuhashi, M.A. Haskin & J.L. Strominger, (1967) Biosythesis of the peptidoglycan of bacterial cell walls. II. Phospholipid carriers in the reaction sequence. *J Biol Chem* **242**: 3180-3190.

Anderson, J.S., P.M. Meadow, M.A. Haskin & J.L. Strominger, (1966) Biosynthesis of the peptidoglycan of bacterial cell walls. I. Utilization of uridine diphosphate acetylmuramyl pentapeptide and uridine diphosphate acetylglucosamine for peptidoglycan synthesis by

particulate enzymes from *Staphylococcus aureus* and *Micrococcus lysodeikticus*. *Arch Biochem Biophys* **116**: 487-515.

Arbeloa, A., H. Segal, J.E. Hugonnet, N. Josseaume, L. Dubost, J.P. Brouard, L. Gutmann, D. Mengin-Lecreulx & M. Arthur, (2004) Role of class A penicillin-binding proteins in PBP5-mediated beta-lactam resistance in *Enterococcus faecalis*. *J Bacteriol* **186**: 1221-1228.

Atrih, A., G. Bacher, G. Allmaier, M.P. Williamson & S.J. Foster, (1999) Analysis of peptidoglycan structure from vegetative cells of *Bacillus subtilis* 168 and role of PBP 5 in peptidoglycan maturation. *J Bacteriol* **181**: 3956-3966.

Banzhaf, M., B. van den Berg van Saparoea, M. Terrak, C. Fraipont, A. Egan, J. Philippe, A. Zapun, E. Breukink, M. Nguyen-Disteche, T. den Blaauwen & W. Vollmer, (2012) Cooperativity of peptidoglycan synthases active in bacterial cell elongation. *Mol Microbiol* **85**: 179-194.

Bernal-Cabas, M., J.A. Ayala & T.L. Raivio, (2015) The Cpx envelope stress response modifies peptidoglycan cross-linking via the L,D-transpeptidase LdtD and the novel protein YgaU. *J Bacteriol* **197**: 603-614.

Billaudeau, C., A. Chastanet, Z. Yao, C. Cornilleau, N. Mirouze, V. Fromion & R. Carballido-Lopez, (2017) Contrasting mechanisms of growth in two model rod-shaped bacteria. *Nat Commun* **8**: 15370.

Bisson-Filho, A.W., Y.P. Hsu, G.R. Squyres, E. Kuru, F. Wu, C. Jukes, Y. Sun, C. Dekker, S. Holden, M.S. VanNieuwenhze, Y.V. Brun & E.C. Garner, (2017) Treadmilling by FtsZ filaments drives peptidoglycan synthesis and bacterial cell division. *Science* **355**: 739-743.

Bramkamp, M., (2010) The putative *Bacillus subtilis* L,D-transpeptidase YciB is a lipoprotein that localizes to the cell poles in a divisome-dependent manner. *Arch Microbiol* **192**: 57-68.

Brown, S., J.P. Santa Maria, Jr. & S. Walker, (2013) Wall teichoic acids of gram-positive bacteria. *Annu Rev Microbiol* **67**: 313-336.

Burman, L.G. & J.T. Park, (1984) Molecular model for elongation of the murein sacculus of *Escherichia coli*. *Proc Natl Acad Sci U S A* **81**: 1844-1848.

Cava, F., M.A. de Pedro, H. Lam, B.M. Davis & M.K. Waldor, (2011) Distinct pathways for modification of the bacterial cell wall by non-canonical D-amino acids. *EMBO J* **30**: 3442-3453.

Cho, H., T. Uehara & T.G. Bernhardt, (2014) Beta-lactam antibiotics induce a lethal malfunctioning of the bacterial cell wall synthesis machinery. *Cell* **159**: 1300-1311.

Cho, H., C.N. Wivagg, M. Kapoor, Z. Barry, P.D. Rohs, H. Suh, J.A. Marto, E.C. Garner & T.G. Bernhardt, (2016) Bacterial cell wall biogenesis is mediated by SEDS and PBP polymerase families functioning semi-autonomously. *Nat Microbiol*: 16172.

Daley, D.O., U. Skoglund & B. Soderstrom, (2016) FtsZ does not initiate membrane constriction at the onset of division. *Sci Rep* **6**: 33138.

de Boer, P., R. Crossley & L. Rothfield, (1992) The essential bacterial cell-division protein FtsZ is a GTPase. *Nature* **359**: 254-256.

Denome, S.A., P.K. Elf, T.A. Henderson, D.E. Nelson & K.D. Young, (1999) *Escherichia coli* mutants lacking all possible combinations of eight penicillin binding proteins: viability, characteristics, and implications for peptidoglycan synthesis. *J Bacteriol* **181**: 3981-3993.

Desmarais, S.M., M.A. De Pedro, F. Cava & K.C. Huang, (2013) Peptidoglycan at its peaks: how chromatographic analyses can reveal bacterial cell wall structure and assembly. *Mol Microbiol* **89**: 1-13.

Di Berardino, M., A. Dijkstra, D. Stuber, W. Keck & M. Gubler, (1996) The monofunctional glycosyltransferase of *Escherichia coli* is a member of a new class of peptidoglycan-synthesising enzymes. *FEBS Lett* **392**: 184-188.

Divakaruni, A.V., C. Baida, C.L. White & J.W. Gober, (2007) The cell shape proteins MreB and MreC control cell morphogenesis by positioning cell wall synthetic complexes. *Mol Microbiol* **66**: 174-188.

Dominguez-Cuevas, P., I. Porcelli, R.A. Daniel & J. Errington, (2013) Differentiated roles for MreB-actin isologues and autolytic enzymes in *Bacillus subtilis* morphogenesis. *Mol Microbiol* **89**: 1084-1098.

Dominguez-Escobar, J., A. Chastanet, A.H. Crevenna, V. Fromion, R. Wedlich-Soldner & R. Carballido-Lopez, (2011) Processive movement of MreB-associated cell wall biosynthetic complexes in bacteria. *Science* **333**: 225-228.

Dorr, T., F. Cava, H. Lam, B.M. Davis & M.K. Waldor, (2013) Substrate specificity of an elongation-specific peptidoglycan endopeptidase and its implications for cell wall architecture and growth of *Vibrio cholerae*. *Mol Microbiol* **89**: 949-962.

Dorr, T., H. Lam, L. Alvarez, F. Cava, B.M. Davis & M.K. Waldor, (2014) A novel peptidoglycan binding protein crucial for PBP1A-mediated cell wall biogenesis in *Vibrio cholerae*. *PLoS Genet* **10**: e1004433.

Egan, A.J., R.M. Cleverley, K. Peters, R.J. Lewis & W. Vollmer, (2017) Regulation of bacterial cell wall growth. *FEBS J* **284**: 851-867.

Egan, A.J. & W. Vollmer, (2013) The physiology of bacterial cell division. *Ann N Y Acad Sci* **1277**: 8-28.

Eiamphungporn, W. & J.D. Helmann, (2008) The *Bacillus subtilis* sigma(M) regulon and its contribution to cell envelope stress responses. *Mol Microbiol* **67**: 830-848.

El Ghachi, M., A. Derbise, A. Bouhss & D. Mengin-Lecreulx, (2005) Identification of multiple genes encoding membrane proteins with undecaprenyl pyrophosphate phosphatase (UppP) activity in *Escherichia coli*. *J Biol Chem* **280**: 18689-18695.

Elhenawy, W., R.M. Davis, J. Fero, N.R. Salama, M.F. Felman & N. Ruiz, (2016) The O-Antigen Flippase Wzk Can Substitute for MurJ in Peptidoglycan Synthesis in *Helicobacter pylori* and *Escherichia coli*. *PLoS One* **11**: e0161587.

Emami, K., A. Guyet, Y. Kawai, J. Devi, L.J. Wu, N. Allenby, R.A. Daniel & J. Errington, (2017) RodA as the missing glycosyltransferase in *Bacillus subtilis* and antibiotic discovery for the peptidoglycan polymerase pathway. *Nat Microbiol* **2**: 16253.

Errington, J., (2015) Bacterial morphogenesis and the enigmatic MreB helix. *Nat Rev Microbiol* **13**: 241-248.

Espaillat, A., O. Forsmo, K. El Biari, R. Bjork, B. Lemaitre, J. Trygg, F.J. Canada, M.A. de Pedro & F. Cava, (2016) Chemometric Analysis of Bacterial Peptidoglycan Reveals Atypical Modifications That Empower the Cell Wall against Predatory Enzymes and Fly Innate Immunity. *J Am Chem Soc* **138**: 9193-9204.

Favini-Stabile, S., C. Contreras-Martel, N. Thielens & A. Dessen, (2013) MreB and MurG as scaffolds for the cytoplasmic steps of peptidoglycan biosynthesis. *Environ Microbiol* **15**: 3218-3228.

Fay, A. & J. Dworkin, (2009) *Bacillus subtilis* homologs of MviN (MurJ), the putative *Escherichia coli* lipid II flippase, are not essential for growth. *J Bacteriol* **191**: 6020-6028.

Figge, R.M., A.V. Divakaruni & J.W. Gober, (2004) MreB, the cell shape-determining bacterial actin homologue, co-ordinates cell wall morphogenesis in *Caulobacter crescentus*. *Mol Microbiol* **51**: 1321-1332.

Gampe, C.M., H. Tsukamoto, E.H. Doud, S. Walker & D. Kahne, (2013) Tuning the moenomycin pharmacophore to enable discovery of bacterial cell wall synthesis inhibitors. *J Am Chem Soc* **135**: 3776-3779.

Garner, E.C., R. Bernard, W. Wang, X. Zhuang, D.Z. Rudner & T. Mitchison, (2011) Coupled, circumferential motions of the cell wall synthesis machinery and MreB filaments in B. *subtilis*. *Science* **333**: 222-225.

Glauner, B., J.V. Holtje & U. Schwarz, (1988) The composition of the murein of *Escherichia coli*. *J Biol Chem* **263**: 10088-10095.

Goffin, C. & J.M. Ghuysen, (1998) Multimodular penicillin-binding proteins: an enigmatic family of orthologs and paralogs. *Microbiol Mol Biol Rev* **62**: 1079-1093.

Guest, R.L. & T.L. Raivio, (2016) Role of the Gram-Negative Envelope Stress Response in the Presence of Antimicrobial Agents. *Trends Microbiol* **24**: 377-390.

Hao, H., M. Dai, Y. Wang, L. Huang & Z. Yuan, (2012) Key genetic elements and regulation systems in methicillin-resistant *Staphylococcus aureus*. *Future Microbiol* **7**: 1315-1329.

Helmann, J.D., (2016) *Bacillus subtilis* extracytoplasmic function (ECF) sigma factors and defense of the cell envelope. *Curr Opin Microbiol* **30**: 122-132.

Hernandez, S.B., F. Cava, M.G. Pucciarelli, F. Garcia-Del Portillo, M.A. de Pedro & J. Casadesus, (2015) Bile-induced peptidoglycan remodelling in *Salmonella enterica*. *Environ Microbiol* **17**: 1081-1089.

Holtje, J.V., (1998) Growth of the stress-bearing and shape-maintaining murein sacculus of *Escherichia coli*. *Microbiol Mol Biol Rev* **62**: 181-203.

Huang, K.C., R. Mukhopadhyay, B. Wen, Z. Gitai & N.S. Wingreen, (2008) Cell shape and cell-wall organization in Gram-negative bacteria. *Proc Natl Acad Sci U S A* **105**: 19282-19287.

Hugonnet, J.E., D. Mengin-Lecreulx, A. Monton, T. den Blaauwen, E. Carbonnelle, C. Veckerle, Y.V. Brun, M. van Nieuwenhze, C. Bouchier, K. Tu, L.B. Rice & M. Arthur, (2016) Factors essential for L,D-transpeptidase-mediated peptidoglycan cross-linking and beta-lactam resistance in *Escherichia coli*. *Elife* **5**.

Ishino, F., W. Park, S. Tomioka, S. Tamaki, I. Takase, K. Kunugita, H. Matsuzawa, S. Asoh, T. Ohta, B.G. Spratt & et al., (1986) Peptidoglycan synthetic activities in membranes of *Escherichia coli* caused by overproduction of penicillin-binding protein 2 and *rodA* protein. *J Biol Chem* **261**: 7024-7031.

Iwai, N., K. Nagai & M. Wachi, (2002) Novel S-benzylisothiourea compound that induces spherical cells in *Escherichia coli* probably by acting on a rod-shape-determining protein(s) other than penicillin-binding protein 2. *Biosci Biotechnol Biochem* **66**: 2658-2662.

Jones, L.J., R. Carballido-Lopez & J. Errington, (2001) Control of cell shape in bacteria: helical, actin-like filaments in *Bacillus subtilis*. *Cell* **104**: 913-922.

Kawai, Y., R.A. Daniel & J. Errington, (2009) Regulation of cell wall morphogenesis in *Bacillus subtilis* by recruitment of PBP1 to the MreB helix. *Mol Microbiol* **71**: 1131-1144.

Kruse, T., J. Bork-Jensen & K. Gerdes, (2005) The morphogenetic MreBCD proteins of *Escherichia coli* form an essential membrane-bound complex. *Mol Microbiol* **55**: 78-89.

Laddomada, F., M.M. Miyachiro & A. Dessen, (2016) Structural Insights into Protein-Protein Interactions Involved in Bacterial Cell Wall Biogenesis. *Antibiotics (Basel)* **5**.

Lai, G.C., H. Cho & T.G. Bernhardt, (2017) The mecillinam resistome reveals a role for peptidoglycan endopeptidases in stimulating cell wall synthesis in *Escherichia coli*. *PLoS Genet* **13**: e1006934.

Lam, H., D.C. Oh, F. Cava, C.N. Takacs, J. Clardy, M.A. de Pedro & M.K. Waldor, (2009) D-amino acids govern stationary phase cell wall remodeling in bacteria. *Science* **325**: 1552-1555.

Lavollay, M., M. Arthur, M. Fourgeaud, L. Dubost, A. Marie, N. Veziris, D. Blanot, L. Gutmann & J.L. Mainardi, (2008) The peptidoglycan of stationary-phase *Mycobacterium tuberculosis* predominantly contains cross-links generated by L,D-transpeptidation. *J Bacteriol* **190**: 4360-4366.

Leclercq, S., A. Derouaux, S. Olatunji, C. Fraipont, A.J. Egan, W. Vollmer, E. Breukink & M. Terrak, (2017) Interplay between Penicillin-binding proteins and SEDS proteins promotes bacterial cell wall synthesis. *Sci Rep* **7**: 43306.

Lee, T.K., K. Meng, H. Shi & K.C. Huang, (2016) Single-molecule imaging reveals modulation of cell wall synthesis dynamics in live bacterial cells. *Nat Commun* **7**: 13170.

Lee, T.K., C. Tropini, J. Hsin, S.M. Desmarais, T.S. Ursell, E. Gong, Z. Gitai, R.D. Monds & K.C. Huang, (2014) A dynamically assembled cell wall synthesis machinery buffers cell growth. *Proc Natl Acad Sci U S A* **111**: 4554-4559.

Lovering, A.L., S.S. Safadi & N.C. Strynadka, (2012) Structural perspective of peptidoglycan biosynthesis and assembly. *Annu Rev Biochem* **81**: 451-478.

Magnet, S., A. Arbeloa, J.L. Mainardi, J.E. Hugonnet, M. Fourgeaud, L. Dubost, A. Marie, V. Delfosse, C. Mayer, L.B. Rice & M. Arthur, (2007) Specificity of L,D-transpeptidases from gram-positive bacteria producing different peptidoglycan chemotypes. *J Biol Chem* **282**: 13151-13159.

Magnet, S., L. Dubost, A. Marie, M. Arthur & L. Gutmann, (2008) Identification of the L,D-transpeptidases for peptidoglycan cross-linking in *Escherichia coli*. *J Bacteriol* **190**: 4782-4785.

Mainardi, J.L., M. Fourgeaud, J.E. Hugonnet, L. Dubost, J.P. Brouard, J. Ouazzani, L.B. Rice, L. Gutmann & M. Arthur, (2005) A novel peptidoglycan cross-linking enzyme for a beta-lactam-resistant transpeptidation pathway. *J Biol Chem* **280**: 38146-38152.

Mainardi, J.L., R. Legrand, M. Arthur, B. Schoot, J. van Heijenoort & L. Gutmann, (2000) Novel mechanism of beta-lactam resistance due to bypass of DD-transpeptidation in *Enterococcus faecium*. *J Biol Chem* **275**: 16490-16496.

Mainardi, J.L., V. Morel, M. Fourgeaud, J. Cremniter, D. Blanot, R. Legrand, C. Frehel, M. Arthur, J. Van Heijenoort & L. Gutmann, (2002) Balance between two transpeptidation mechanisms determines the expression of beta-lactam resistance in *Enterococcus faecium*. *J Biol Chem* **277**: 35801-35807.

Mainardi, J.L., R. Villet, T.D. Bugg, C. Mayer & M. Arthur, (2008) Evolution of peptidoglycan biosynthesis under the selective pressure of antibiotics in Gram-positive bacteria. *FEMS Microbiol Rev* **32**: 386-408.

Mascher, T., A.B. Hachmann & J.D. Helmann, (2007) Regulatory overlap and functional redundancy among *Bacillus subtilis* extracytoplasmic function sigma factors. *J Bacteriol* **189**: 6919-6927.

McDonough, M.A., J.W. Anderson, N.R. Silvaggi, R.F. Pratt, J.R. Knox & J.A. Kelly, (2002) Structures of two kinetic intermediates reveal species specificity of penicillin-binding proteins. *J Mol Biol* **322**: 111-122.

McPherson, D.C. & D.L. Popham, (2003) Peptidoglycan synthesis in the absence of class A penicillin-binding proteins in *Bacillus subtilis*. *J Bacteriol* **185**: 1423-1431.

Meeske, A.J., E.P. Riley, W.P. Robins, T. Uehara, J.J. Mekalanos, D. Kahne, S. Walker, A.C. Kruse, T.G. Bernhardt & D.Z. Rudner, (2016) SEDS proteins are a widespread family of bacterial cell wall polymerases. *Nature* **537**: 634-638.

Meeske, A.J., L.T. Sham, H. Kimsey, B.M. Koo, C.A. Gross, T.G. Bernhardt & D.Z. Rudner, (2015) MurJ and a novel lipid II flippase are required for cell wall biogenesis in *Bacillus subtilis*. *Proc Natl Acad Sci U S A* **112**: 6437-6442.

Meisner, J., P. Montero Llopis, L.T. Sham, E. Garner, T.G. Bernhardt & D.Z. Rudner, (2013) FtsEX is required for CwlO peptidoglycan hydrolase activity during cell wall elongation in *Bacillus subtilis*. *Mol Microbiol* **89**: 1069-1083.

Michie, K.A. & J. Lowe, (2006) Dynamic filaments of the bacterial cytoskeleton. *Annu Rev Biochem* **75**: 467-492.

Mogensen, T.H., (2009) Pathogen recognition and inflammatory signaling in innate immune defenses. *Clin Microbiol Rev* **22**: 240-273, Table of Contents.

Mohammadi, T., V. van Dam, R. Sijbrandi, T. Vernet, A. Zapun, A. Bouhss, M. Diepeveen-de Bruin, M. Nguyen-Disteche, B. de Kruijff & E. Breukink, (2011) Identification of FtsW as a transporter of lipid-linked cell wall precursors across the membrane. *EMBO J* **30**: 1425-1432.

Moll, A., T. Dorr, L. Alvarez, B.M. Davis, F. Cava & M.K. Waldor, (2015) A D, D-carboxypeptidase is required for *Vibrio cholerae* halotolerance. *Environ Microbiol* **17**: 527-540.

Morales Angeles, D., Y. Liu, A.M. Hartman, M. Borisova, A. de Sousa Borges, N. de Kok, K. Beilharz, J.W. Veening, C. Mayer, A.K. Hirsch & D.J. Scheffers, (2017) Pentapeptide-rich peptidoglycan at the *Bacillus subtilis* cell-division site. *Mol Microbiol* **104**: 319-333.

Morgenstein, R.M., B.P. Bratton, J.P. Nguyen, N. Ouzounov, J.W. Shaevitz & Z. Gitai, (2015) RodZ links MreB to cell wall synthesis to mediate MreB rotation and robust morphogenesis. *Proc Natl Acad Sci U S A* **112**: 12510-12515.

Moynihan, P.J., D. Sychantha & A.J. Clarke, (2014) Chemical biology of peptidoglycan acetylation and deacetylation. *Bioorg Chem* **54**: 44-50.

Osawa, M., D.E. Anderson & H.P. Erickson, (2008) Reconstitution of contractile FtsZ rings in liposomes. *Science* **320**: 792-794.

Osawa, M., D.E. Anderson & H.P. Erickson, (2009) Curved FtsZ protofilaments generate bending forces on liposome membranes. *EMBO J* **28**: 3476-3484.

Paradis-Bleau, C., M. Markovski, T. Uehara, T.J. Lupoli, S. Walker, D.E. Kahne & T.G. Bernhardt, (2010) Lipoprotein cofactors located in the outer membrane activate bacterial cell wall polymerases. *Cell* **143**: 1110-1120.

Potluri, L., A. Karczmarek, J. Verheul, A. Piette, J.M. Wilkin, N. Werth, M. Banzhaf, W. Vollmer, K.D. Young, M. Nguyen-Disteche & T. den Blaauwen, (2010) Septal and lateral wall localization of PBP5, the major D,D-carboxypeptidase of *Escherichia coli*, requires substrate recognition and membrane attachment. *Mol Microbiol* **77**: 300-323.

Quintela, J.C., M. Caparros & M.A. de Pedro, (1995) Variability of peptidoglycan structural parameters in gram-negative bacteria. *FEMS Microbiol Lett* **125**: 95-100.

RayChaudhuri, D. & J.T. Park, (1992) *Escherichia coli* cell-division gene ftsZ encodes a novel GTP-binding protein. *Nature* **359**: 251-254.

Rebets, Y., T. Lupoli, Y. Qiao, K. Schirner, R. Villet, D. Hooper, D. Kahne & S. Walker, (2014) Moenomycin resistance mutations in *Staphylococcus aureus* reduce peptidoglycan chain length and cause aberrant cell division. *ACS Chem Biol* **9**: 459-467.

Reed, P., H. Veiga, A.M. Jorge, M. Terrak & M.G. Pinho, (2011) Monofunctional transglycosylases are not essential for *Staphylococcus aureus* cell wall synthesis. *J Bacteriol* **193**: 2549-2556.

Reichmann, N.T. & A. Grundling, (2011) Location, synthesis and function of gly*coli*pids and polyglycerolphosphate lipoteichoic acid in Gram-positive bacteria of the phylum Firmicutes. *FEMS Microbiol Lett* **319**: 97-105.

Rice, L.B., L.L. Carias, S. Rudin, R. Hutton, S. Marshall, M. Hassan, N. Josseaume, L. Dubost, A. Marie & M. Arthur, (2009) Role of class A penicillin-binding proteins in the expression of beta-lactam resistance in *Enterococcus faecium*. *J Bacteriol* **191**: 3649-3656.

Rueff, A.S., A. Chastanet, J. Dominguez-Escobar, Z. Yao, J. Yates, M.V. Prejean, O. Delumeau, P. Noirot, R. Wedlich-Soldner, S.R. Filipe & R. Carballido-Lopez, (2014) An early cytoplasmic step of peptidoglycan synthesis is associated to MreB in *Bacillus subtilis*. *Mol Microbiol* **91**: 348-362.

Ruiz, N., (2008) Bioinformatics identification of MurJ (MviN) as the peptidoglycan lipid II flippase in *Escherichia coli*. *Proc Natl Acad Sci U S A* **105**: 15553-15557.

Sanders, A.N. & M.S. Pavelka, (2013) Phenotypic analysis of Eschericia *coli* mutants lacking L,D-transpeptidases. *Microbiology* **159**: 1842-1852.

Santos, J.M., M. Lobo, A.P. Matos, M.A. De Pedro & C.M. Arraiano, (2002) The gene *bolA* regulates *dacA* (PBP5), dacC (PBP6) and *ampC* (AmpC), promoting normal morphology in *Escherichia coli*. *Mol Microbiol* **45**: 1729-1740.

Satta, G., G. Cornaglia, A. Mazzariol, G. Golini, S. Valisena & R. Fontana, (1995) Target for bacteriostatic and bactericidal activities of beta-lactam antibiotics against *Escherichia coli* resides in different penicillin-binding proteins. *Antimicrob Agents Chemother* **39**: 812-818.

Sauvage, E., F. Kerff, M. Terrak, J.A. Ayala & P. Charlier, (2008) The penicillin-binding proteins: structure and role in peptidoglycan biosynthesis. *FEMS Microbiol Rev* **32**: 234-258.

Scheffers, D.J. & M.B. Tol, (2015) LipidII: Just Another Brick in the Wall? *PLoS Pathog* **11**: e1005213.

Sham, L.T., E.K. Butler, M.D. Lebar, D. Kahne, T.G. Bernhardt & N. Ruiz, (2014) Bacterial cell wall. MurJ is the flippase of lipid-linked precursors for peptidoglycan biogenesis. *Science* **345**: 220-222.

Shih, Y.L., T. Le & L. Rothfield, (2003) Division site selection in *Escherichia coli* involves dynamic redistribution of Min proteins within coiled structures that extend between the two cell poles. *Proc Natl Acad Sci U S A* **100**: 7865-7870.

Siegel, S.D., J. Liu & H. Ton-That, (2016) Biogenesis of the Gram-positive bacterial cell envelope. *Curr Opin Microbiol* **34**: 31-37.

Singh, S.K., L. SaiSree, R.N. Amrutha & M. Reddy, (2012) Three redundant murein endopeptidases catalyse an essential cleavage step in peptidoglycan synthesis of *Escherichia coli* K12. *Mol Microbiol* **86**: 1036-1051.

Strahl, H., F. Burmann & L.W. Hamoen, (2014) The actin homologue MreB organizes the bacterial cell membrane. *Nat Commun* **5**: 3442.

Strominger, J.L., P.M. Blumberg, H. Suginaka, J. Umbreit & G.G. Wickus, (1971) How penicillin kills bacteria: progress and problems. *Proc R Soc Lond B Biol Sci* **179**: 369-383.

Strominger, J.L., J.T. Park & R.E. Thompson, (1959) Composition of the cell wall of *Staphylococcus aureus*: its relation to the mechanism of action of penicillin. *J Biol Chem* **234**: 3263-3268.

Tybring, L. & N.H. Melchior, (1975) Mecillinam (FL 1060), a 6beta-amidinopenicillanic acid derivative: bactericidal action and synergy in vitro. *Antimicrob Agents Chemother* **8**: 271-276.

Typas, A., M. Banzhaf, B. van den Berg van Saparoea, J. Verheul, J. Biboy, R.J. Nichols, M. Zietek, K. Beilharz, K. Kannenberg, M. von Rechenberg, E. Breukink, T. den Blaauwen, C.A. Gross & W. Vollmer, (2010) Regulation of peptidoglycan synthesis by outer-membrane proteins. *Cell* **143**: 1097-1109.

Uehara, T. & J.T. Park, (2008) Growth of *Escherichia coli*: significance of peptidoglycan degradation during elongation and septation. *J Bacteriol* **190**: 3914-3922.

Ursell, T.S., J. Nguyen, R.D. Monds, A. Colavin, G. Billings, N. Ouzounov, Z. Gitai, J.W. Shaevitz & K.C. Huang, (2014) Rod-like bacterial shape is maintained by feedback between cell curvature and cytoskeletal localization. *Proc Natl Acad Sci U S A* **111**: E1025-1034.

van den Ent, F., L.A. Amos & J. Lowe, (2001) Prokaryotic origin of the actin cytoskeleton. *Nature* **413**: 39-44.

van Teeffelen, S., S. Wang, L. Furchtgott, K.C. Huang, N.S. Wingreen, J.W. Shaevitz & Z. Gitai, (2011) The bacterial actin MreB rotates, and rotation depends on cell-wall assembly. *Proc Natl Acad Sci U S A* **108**: 15822-15827.

Vollmer, W., (2012) Bacterial growth does require peptidoglycan hydrolases. *Mol Microbiol* **86**: 1031-1035.

Vollmer, W. & J.V. Holtje, (2004) The architecture of the murein (peptidoglycan) in gram-negative bacteria: vertical scaffold or horizontal layer(s)? *J Bacteriol* **186**: 5978-5987.

Welzel, P., (2007) A long research story culminates in the first total synthesis of moenomycin A. *Angew Chem Int Ed Engl* **46**: 4825-4829.

White, C.L., A. Kitich & J.W. Gober, (2010) Positioning cell wall synthetic complexes by the bacterial morphogenetic proteins MreB and MreD. *Mol Microbiol* **76**: 616-633.

Wientjes, F.B. & N. Nanninga, (1991) On the role of the high molecular weight penicillin-binding proteins in the cell cycle of *Escherichia coli*. *Res Microbiol* **142**: 333-344.

Yang, X., Z. Lyu, A. Miguel, R. McQuillen, K.C. Huang & J. Xiao, (2017) GTPase activity-coupled treadmilling of the bacterial tubulin FtsZ organizes septal cell wall synthesis. *Science* **355**: 744-747.

Yousif, S.Y., J.K. Broome-Smith & B.G. Spratt, (1985) Lysis of *Escherichia coli* by beta-lactam antibiotics: deletion analysis of the role of penicillin-binding proteins 1A and 1B. *J Gen Microbiol* **131**: 2839-2845.

Yunck, R., H. Cho & T.G. Bernhardt, (2016) Identification of MltG as a potential terminase for peptidoglycan polymerization in bacteria. *Mol Microbiol* **99**: 700-718.

Zhao, H., Y. Sun, J.M. Peters, C.A. Gross, E.C. Garner & J.D. Helmann, (2016) Depletion of Undecaprenyl Pyrophosphate Phosphatases Disrupts Cell Envelope Biogenesis in *Bacillus subtilis*. *J Bacteriol* **198**: 2925-2935.

Chapter 2. Depletion of undecaprenyl pyrophosphate phosphatases (UPP-Pases) disrupts cell envelope biogenesis in *Bacillus subtilis*

2.1 Abstract

The integrity of the bacterial cell envelope is essential to sustain life by countering the high turgor pressure of the cell and providing a barrier against chemical insults. In *Bacillus subtilis*, synthesis of both peptidoglycan and wall teichoic acids requires a common C_{55} lipid carrier, undecaprenyl-pyrophosphate (UPP), to ferry precursors across the cytoplasmic membrane. The synthesis and recycling of UPP requires a phosphatase to generate the monophosphate form Und-P, which is the substrate for peptidoglycan and wall teichoic acid synthases. Using an optimized CRISPR-dCas9 based transcriptional repression system (CRISPRi), we demonstrate that *B. subtilis* requires either of two UPP phosphatases, UppP or BcrC, for viability. We show that a third predicted lipid phosphatase (YodM), with homology to diacylglycerol pyrophosphatases, can also support growth when overexpressed. Depletion of UPP phosphatase activity leads to morphological defects consistent with a failure of cell envelope synthesis and strongly activates the σ^M-dependent cell envelope stress response, including *bcrC* which encodes one of the two UPP phosphatases. These results highlight the utility of an optimized CRISPRi system for investigation of synthetic lethal gene pairs, clarify the nature of the *B. subtilis* UPP-Pase enzymes, and provide further evidence linking the σ^M regulon to cell envelope homeostasis pathways.

2.2 Introduction

In bacterial peptidoglycan synthesis, a 55 carbon polyisoprenoid lipid carrier called undecaprenyl-pyrophosphate (UPP) is required to transport peptidoglycan precursor across the cell membrane (Jorgenson *et al.*, 2015). UPP is synthesized by UppS and then dephosphorylated by a UPP phosphatase (UPP-Pase) to Und-P (Payne *et al.*, 2007). The MraY enzyme uses Und-P as a

substrate together with UDP-MurNAc-pentapeptide to synthesize lipid I, the first membrane-bound precursor of peptidoglycan synthesis (Lovering *et al.*, 2012). Addition of N-acetylglucosamine (GlcNAc) by MurG completes the synthesis of the critical intermediate, lipid II. Lipid II is a single GlcNAc-MurNAc-pentapeptide unit linked to UPP as the lipid carrier and serves as a substrate for penicillin-binding proteins (PBPs) which incorporate the disaccharide unit into the growing glycan strands.

Our understanding of this critical lipid II cycle is compromised by a lack of mechanistic understanding for key steps. The identity of the lipid II flippase required for the export of this essential precursor from the cytoplasmic to the external face of the membrane has been controversial. Recent results provide strong support for a role of MurJ as the lipid II flippase (Sham *et al.*, 2014) and have further shown that this enzyme is redundant in function with a stress-regulated alternate to MurJ (Amj) protein (Meeske *et al.*, 2015). The recycling of the UPP carrier to Und-P also involves redundant enzymes, perhaps to allow the conversion to occur on either the inner or outer face of the membrane. UppS synthesizes UPP on the cytosolic face of the membrane. Subsequent dephosphorylation of UPP, also presumed to occur on the cytosolic face of the inner membrane, generates Und-P as substrate for MraY and TagO (Guillaume Manat, 2014). After transporting cell wall precursors to the outside of membrane, the lipid carrier is released as UPP, which must again be recycled back to Und-P by the action of a UPP-Pase (El Ghachi *et al.*, 2005). This may occur by dephosphorylation on the outer face of the membrane, or by flipping of the UPP across the membrane to serve as a substrate for a UPP-Pase active on the inner face of the membrane. It is assumed that flipping of UPP (or Und-P) from the outer to the inner face of the membrane is facilitated by proteins, but the flippase has not been identified (Guillaume Manat, 2014). It may be advantageous, in general, for cells to have UPP-Pase activity localized to both

faces of the membrane to facilitate *de novo* Und-P synthesis (on the inner face) and UPP recycling (on the outer face), and this may account in part for the redundancy commonly observed in UPP-Pases (Bickford & Nick, 2013, Guillaume Manat, 2014, El Ghachi *et al.*, 2005).

In Gram-positive bacteria, the same UPP carrier is shared between the peptidoglycan and the wall teichoic acid (WTA) biosynthesis pathways. For WTA synthesis, Und-P serves as a substrate for TagO (Brown *et al.*, 2013). As a result, mutations in later steps in WTA synthesis are lethal due to the sequestration of the limiting UPP carrier in dead-end products (D'Elia *et al.*, 2006), and this observation has motivated the search for antibiotics active on late stages of WTA synthesis (Pasquina *et al.*, 2013). A similar sequestration effect has been reported in *Escherichia coli*, when synthesis of the enterobacterial common antigen was impaired (Jorgenson *et al.*, 2015), and in *Streptococcus pneumoniae* mutants defective in synthesis of serotype 2 capsule (Xayarath & Yother, 2007).

As expected for a critical lipid carrier, the synthesis and recycling of UPP is essential and is therefore an excellent target for antibacterials. Recent *in silico*, *in vitro*, and *in vivo* approaches have identified inhibitors of UppS (Durrant *et al.*, 2011, Zhu *et al.*, 2013, Farha *et al.*, 2015), including a method that used CRISPR (clustered regularly interspersed short palindromic repeats) interference (CRISPRi) to identify drug targets (Peters *et al.*, 2016a). We demonstrated previously that a ribosome-binding site mutation that decreased expression of UppS led to vancomycin resistance and activation of the σ^M-dependent cell envelope stress response (Lee & Helmann, 2013). Compounds that inhibit the recycling of UPP may also serve as effective antibiotics. The most widely used antibiotic of this class is bacitracin, which binds tightly to the pyrophosphate group on surface-exposed UPP to inhibit its dephosphorylation (Economou *et al.*, 2013). Bacitracin also activates the σ^M stress response and contributes to bacitracin resistance by

increasing synthesis of BcrC (Cao & Helmann, 2002, Ohki *et al.*, 2003, Kingston *et al.*, 2014), a predicted UPP-Pase presumed to act on the outer face of the membrane to convert UPP (the target of bacitracin) into Und-P (Bernard *et al.*, 2005). Finally, a variety of structurally diverse antibiotics, including glycopeptides and lantibiotics, bind to lipid II which serves to both inhibit cell wall synthesis and sequester the UPP carrier lipid (Schneider & Sahl, 2010).

The identity of the UPP-Pases has been clearly established in *E. coli* where there are three UPP-pase enzymes (BacA, YbjG, and PgpB) and a fourth enzyme (YeiU, later renamed LpxT) exhibiting UPP-Pase activity *in vitro* (El Ghachi *et al.*, 2005). The BacA family includes the eponymous BacA protein, while YbjG, PgpB and LpxT all belong to type 2 phosphatidic acid phosphatase (PAP2) superfamily. BacA provides 75% of the cell's UPP-Pase activity, and overexpression of BacA makes cells bacitracin resistant (El Ghachi *et al.*, 2005). PgpB was originally identified in mutant cells lacking phosphatidylglycerol phosphate phosphatase activity (Icho & Raetz, 1983), and is shown to have broad substrate specificity (Fan *et al.*, 2014, Touze *et al.*, 2008a). The BacA, YbjG, and PgpB enzymes are functionally redundant, and single mutants lacking any one of the three genes do not show significant growth defects. However, a triple mutant missing all three genes is not viable. Although LpxT displayed *in vitro* UPP-Pase activity, it could not support growth in the absence of at least one of the other three UPP-Pases (El Ghachi *et al.*, 2005). It was later found out that LpxT transfers phosphate from UPP to lipid A to produce lipid A 1-diphosphate, and in the process generates Und-P (Touze *et al.*, 2008b). In contrast, the number and identity of the UPP-Pases in *B. subtilis* has not been resolved.

Genetic approaches to analyze the function of essential genes often rely on conditional mutants in which either gene expression or protein activity can be regulated. Optimization of conditional gene expression systems can be challenging (as reported also here), since leaky

expression may suffice to support viability even in the absence of induction, or the induced level may be insufficient to support viability. Recently, the CRISPR system, used by many bacterial and archaeal species to defend against foreign DNA, has been adapted as a powerful tool for conditionally regulating bacterial gene expression (Qi *et al.*, 2013, Gilbert *et al.*, 2014, Peters *et al.*, 2015, Peters *et al.*, 2016a).

Here we report the use of an optimized CRISPR interference (CRISPRi) system to investigate the essentiality of candidate UPP-Pases in *B. subtilis*. Using CRISPRi, we have identified UppP and BcrC as two functionally redundant UPP-Pases. We have also identified a third lipid phosphatase (YodM) capable of supporting growth in the absence of these two enzymes, but only when artificially overexpressed. Depletion of essential UPP-Pases, predicted to interrupt synthesis of both peptidoglycan and WTA, results in cells that cannot maintain their rod shape and leads to induction of the σ^M-dependent cell envelope stress response.

2.3 Materials and Methods

2.3.1 Strains, plasmids and growth condition

All strains and plasmids used in this work are listed in Tables S2.4. Bacteria were grown in liquid lysogeny broth (LB) medium with shaking, or on LB plates (1.5% agar; Difco) at 37 ˚C unless otherwise stated. Plasmids were constructed using standard methods (Luo *et al.*, 2010), and amplified in *E. coli* DH5α before transforming into *B. subtilis*. For selection of transformants, 100 μg/ml ampicillin was used for *E. coli*. Antibiotics used for selection of *B. subtilis* transformants include: kanamycin 15 μg/ml, spectinomycin 100 μg/ml, macrolide-lincosamide-streptogramin B (MLS, contains 1 μg/ml erythromycin and 25 μg/ml lincomycin), neomycin 10 μg/ml, chloramphenicol 10 μg/ml.

2.3.2 Genetic techniques

Chromosomal and plasmid DNA transformation was performed as previously stated (Luo & Helmann, 2012). Markerless in-frame deletion mutants were constructed from BKE strains as described (Meeske *et al.*, 2015). Briefly, BKE strains were acquired from the Bacillus Genetics Stock Center, chromosomal DNA was extracted, and the mutation containing an *erm* cassette was transformed into our WT 168 strain. The *erm* cassette was subsequently removed by introduction of plasmid pDR244, which was later cured by growing at the non-permissive temperature of 42 ˚C. Gene deletions were confirmed by PCR screening using flanking primers. Transduction was performed to move SPβ derivatives into the 168 strain as previously described (Harwood & Cutting, 1990). Unless otherwise described, all PCR products were generated using *B. subtilis* 168 strain chromosomal DNA as template. DNA fragments used for gene over-expression were sequence verified. Null mutant construction was PCR screen verified to have the right size band.

2.3.3 Construction of the CRISPRi-based transcriptional repression system

The CRISPRi system was based on plasmid vectors that replicate in *E. coli* and integrate into the *B. subtilis* chromosome. Briefly, the gene encoding dCas9 is inserted into plasmid pAX01 to form pJPM1. pJMP1 is then integrated into the *B. subtilis ganA* gene by double cross-over recombination. sgRNAs targeting *bcrC* or *uppP* were incorporated into integrative vectors by inverse PCR followed by cyclization by self-ligation. Expression of sgRNA is constitutive, and expression of dCas9 is induced by xylose. sgRNAs were selected based on their specificity for, and location within, target genes. We identified all PAM (Protospacer Adjacent Motif) sites (NGG for *S. pyogenes* dCas9) within target genes and designed all possible sgRNAs for those targets. We then assigned each sgRNA a specificity score by aligning progressive truncations of the

sgRNA sequences to the *B. subtilis* 168 genome using Bowtie (Langmead *et al.*, 2009); sgRNAs that retained specificity after several truncations received better scores. We then selected the most specific sgRNAs that targeted the non-template strand and were near the 5´ end of the gene where CRISPR interference is thought to be most effective in bacteria (Qi *et al.*, 2013, Peters *et al.*, 2015). After choosing sgRNAs sequences, the constructs were made by inverse PCR using forward primer containing sequence specific to gene of interest (base paring region), and universal reverse primer which binds to the complementary strand of DNA adjacent to the base paring region. For example, *bcrC*-1 was made using pJMP3 as template, primer 6411 CRISPRi bcrC-1 F and 6415 CRISPRi universal R. Inverse PCR product was self-ligated, and transformed into *E. coli* DH5α. Plasmids extracted from successful transformations were confirmed by sequencing before being used to transform *B. subtilis*.

Construction of pSPβ-dCas9 was done by ligating a fragment containing P_{xyl}-*dCas9* from pJMP1 into backbone of pJPM122, a plasmid that can integrate into SPβ prophage in strain ZB307A as described (Slack *et al.*, 1993). To get the fragment containing P_{xyl}-*dCas9*, pJMP1 was first digested by SacII, treated with T4 DNA polymerase (NEB) to make a blunt-end, and then digested by SalI. DNA fragment containing P_{xyl}-*dCas9* was gel purified. pJPM122 was digested with SalI and EcoRV, and backbone was recovered from agarose gel. The fragment containing P_{xyl}-*dCas9* from pJMP1 was then ligated with pJPM122, forming plasmid pSPβ-dCas9. pSPβ-dCas9 was then used to transform *B. subtilis* ZB307A. Transformants were PCR screened to confirm that a double cross-over recombination event occurred into the chromosome of ZB307A and named ZB307A-pSPβ-dCas9. Phage lysate from ZB307A-pSPβ-dCas9 was prepared using heat shock and was used to transduce *B. subtilis* 168 and its derivatives.

2.3.4 Disk diffusion assays

Disk diffusion assays were performed as previously described (Kingston *et al.*, 2014). Overnight cultures of test strains were re-inoculated into fresh LB liquid medium and grown to early log phase (OD_{600} ~0.4), and a 100 µl aliquot of the culture was mixed briefly with 4 ml LB soft agar (containing 0.75% agar, kept at 50 ˚C) before poured onto LB plates (containing 15 ml LB with 1.5% agar). Plates were then cooled and dried in a laminar airflow hood for 5 minutes. Filter paper disks were placed on the surface of the plate, and chemicals were added to the paper disks. Plates were then incubated at 37˚C for 16 h before the diameter of the zone of inhibition was measured. Numbers reported are diameter minus the 6.5 mm diameter of the filter paper disk. The chemicals added to the disks include: xylose 20 µl of 50% solution, bacitracin 400 µg, ampicillin 1 mg, penicillin 1 mg, cefuroxime 10 mg, vancomycin 100 µg, fosfomycin 1mg, D-cycloserine 100 µg, lysozyme 100 µg, daptomycin 100 µg, nisin 1 mg, SDS 10 µl of 10% solution, Triton X-100 10 µl of 25% solution, EDTA 10 µl of 0.5 M (pH 8.0) solution, novobiocin 100 µg.

2.3.5 Measurement of the fraction of suppressors

Strains were grown in liquid LB medium supplemented with 1% glucose overnight, and then the overnight culture was re-inoculated into fresh LB liquid medium supplemented with 1% glucose and grown to early log phase (OD_{600} ~0.4). Serial dilutions were performed up to 10^{-6}. Cultures with 10^{-4}, 10^{-5}, and 10^{-6} dilutions were plated on LB plate supplemented with 1% glucose, and cultures with no dilution, 10^{-1}, and 10^{-2} dilutions were plated on LB plate supplemented with 2% xylose. Colonies were counted from plates having between 20-200 colonies, and colony forming units (CFU) were calculated. Fraction of suppressors is calculated by dividing CFU of

strains growing on xylose LB by CFU of the same strain growing on glucose LB. This experiment was done at least three times using biological replicates.

2.3.6 Phase contrast time-lapse and fluorescence microscopy

Strains were grown in CH medium (Sterlini & Mandelstam, 1969) in presence of 1% (w/v) glucose at 37 °C. Then the cells were harvested when the OD of the culture reaches ~0.4. Then cells were grown in CH in presence of 2%(w/v) xylose in a micro-fluidic chamber. The phase contrast time lapse images were acquired on a Nikon N-STORM microscope equipped with Plan Apo lambda 100x objective and a Hamamatsu ORCA CMOS camera. Images were taken every 30 s. Images of FM5-95 (ThermoFisher) membrane staining were acquired on a GE DeltaVision Elite with DeltaVision connected to a PCO Edge sSCOS camera. A 561-nm laser and a 60X 1.45 NA Plan Apo-objective were used. The excitation filter was YFP (with center wave length at 513nm and 17nm bandwidth) and the emission filter was mCherry (with center wave length at 632nm and 60nm bandwidth). The cells were stained with 1X FM5-69 (2 μM) mounted on 1% agarose in CH medium pads and immediately imaged with an exposure time of 2 s. All images were analyzed using Morphometrics (Ursell *et al.*, 2014) and home built MATLAB program.

2.3.7 Whole genome sequencing and sequence analysis

Chromosomal DNA of suppressor strains was extracted using Qiagen DNeasy Blood & Tissue Kit. DNA was then sent for sequencing using Illumina HiSeq2500 High Output Mode with Single-end 100 bp reads. Sequencing results were analyzed using CLC workbench version 8.5.1. Single nucleotide variants (SNVs) were detected using default settings.

2.3.8 Microarray analysis

The wild type and depletion strains were grown separately in liquid LB medium to OD_{600} ~0.4, and then each diluted 100-fold into two 250 ml flasks each containing fresh 50 ml LB medium. After 1.5 hours of initial growth, one of the two flasks of each strain was supplemented with 50% xylose to a final concentration of 2%, while the other flask was left untreated as control. After another 2.5 hours of growth, cells were collected and total RNA was extracted using phenol-chloroform based method. Total RNA was quantified and quality of RNA was tested using Bio-analyzer. RNA quality numbers for all four RNA samples are 10 out of 10. Total RNA were then treated with Turbo-DNAse (Thermo Fisher Scientific) to remove any possible DNA contamination, and then reverse transcribed using SuperScript™ Indirect cDNA Labeling System (Thermo Fisher Scientific) into cDNA. cDNA was aliquoted and labelled with either fluorescent dye 555 or dye 647, and hybridized to microarray slides containing 60 nt oligonucleotides for each coding region according to laboratory protocol (Luo *et al.*, 2010). Dye swap was performed to reduce systematic error caused by difference in labelling and hybridization efficiency for different dyes. For instance, in one hybridization cDNA of WT strain is labelled with dye 555 and cDNA of depletion strain is labelled with dye 647. In the dye swap experiment, cDNA from the WT will then be labelled with dye 647 and depletion strain dye 555. Transcriptome results have been deposited in the NCBI GEO database under accession number (*to be added*).

Comparison of transcriptome among different strains and conditions were performed by comparing fluorescent signal from different pairs. Among the treated group, transcriptomes of the WT and depletion strains were compared to reveal change in gene transcription, and untreated WT and depletion strains were used as controls. Fold change for each gene is the average of two experiments containing a dye swap. Up- and down-regulated genes after UPP-Pase depletion were

defined as those with an average fold change of at least 3-fold, and at least 2-fold in each hybridization. It is also crucial that only signals well above background are considered trustworthy. Gene function and regulon information was acquired from SubtiWiki (http://subtiwiki.uni-goettingen.de/;(Michna *et al.*, 2014)) and prior publications.

Cluster 3.0 (http://bonsai.hgc.jp/~mdehoon/software/cluster/software.htm) and Java Treeview (https://sourceforge.net/projects/jtreeview/) were used to generate heat maps. Briefly, we chose genes regulated by ECF sigma factors and two component systems involved in cell envelope homeostasis (e.g. WalR, BceR, LiaR, PsdR and YvrHb). Gene *bcrC* was not included in the list of genes (even though it is controlled by multiple ECF sigma factors), as it was artificially repressed using CRISPRi. Microarray fold change data were $\log_{10}$ transformed and used for hierarchical clustering (using uncentered correlation and complete linkage functions) showing genes that were up-regulated (red) or down-regulated (green).

2.4 Results

2.4.1 UppP and BcrC are functionally redundant UPP-Pases

We identified *B. subtilis* UppP, BcrC and YodM as homologs of known UPP-Pases in *E. coli* using BLASTp with default parameters. UppP is a homolog of BacA whereas BcrC and YodM are homologs of YbjG, PgpB and LpxT, members of the PAP2 superfamily (Table S2.1). BcrC was previously shown to have UPP-Pase activity and to be regulated by σ^M (Bernard *et al.*, 2005, Cao & Helmann, 2002). UppP (YubB) was also speculated to function as a UPP-Pase based on homology, but played a less important role than BcrC in bacitracin resistance (Bernard *et al.*, 2005). Mutations that affect UPP levels were later found to affect the sensitivity of *B. subtilis* to rare earth metals and, based on this phenotype, it was also suggested that BcrC was the major enzyme with

UppP having a minor role (Inaoka & Ochi, 2012). However, this assay may report specifically on the levels of extracellular UPP which is accessible for binding by rare earth metals.

To investigate functional redundancy amongst these candidate UPP-Pases, we constructed single mutants with each UPP-Pase gene replaced by an antibiotic cassette, followed by transformation to make mutants missing two or all three UPP-Pases. While we could construct *yodM bcrC* and *yodM uppP* double mutants, we were unable to obtain the *bcrC uppP* double mutant in multiple attempts, despite previous suggestions that a double mutant had been obtained (Bernard *et al.*, 2005, Inaoka & Ochi, 2012). For example, when chromosomal DNA from a *bcrC*::*mls* (macrolide-lincosamide-streptogramin B) strain was used to transform a *uppP*::*spc* (spectinomycin) strain, we recovered MLS^R transformants, but only if the cells simultaneously acquired a functional copy of *uppP* (and therefore lost Spc^R). This phenomenon, in which a cell acquires two unlinked markers by transformation, is referred to as congression. Overall, our findings indicate that *bcrC* and *uppP* are a synthetic lethal gene pair and likely encode the only functional UPP-Pases in *B. subtilis,* at least in our laboratory conditions.

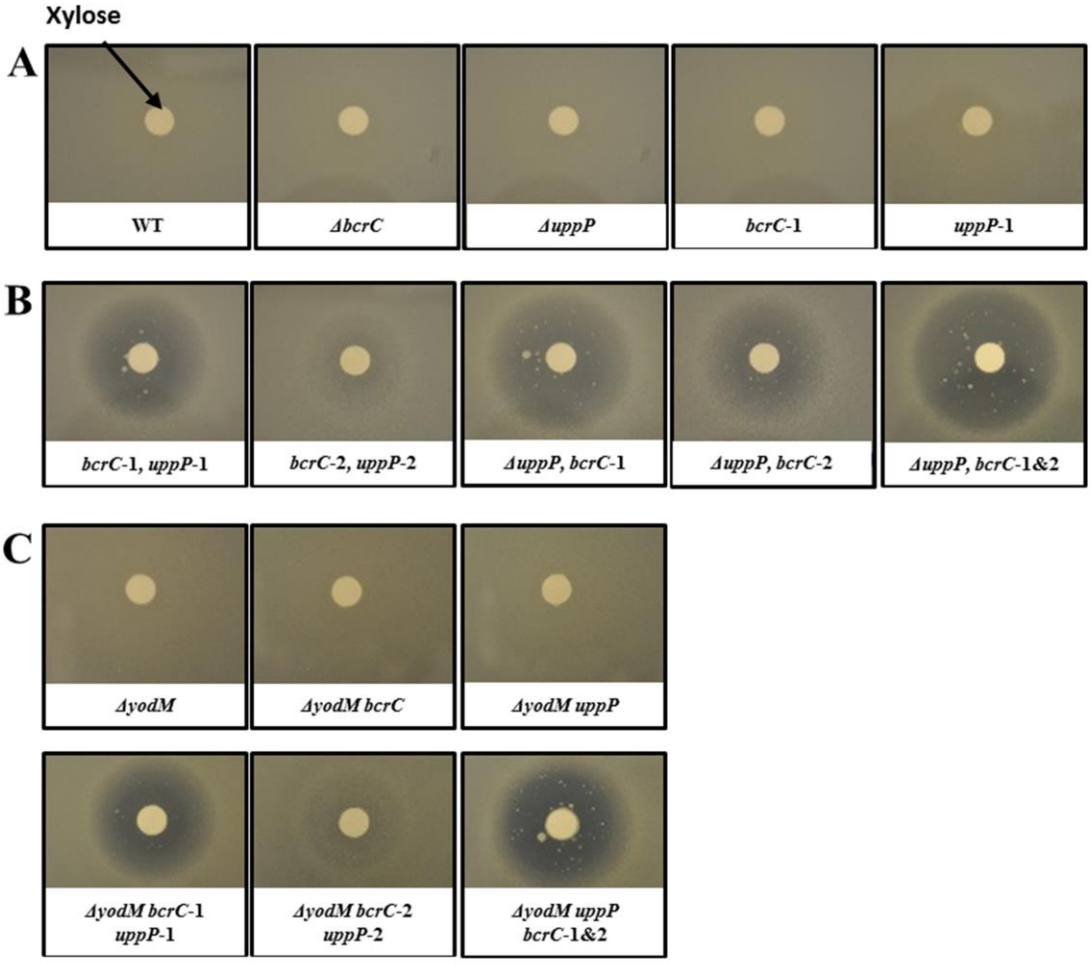

Figure 2.1. Growth inhibition by depletion of BcrC and UppP.

Photos of disk diffusion assay of WT and mutant strains. Cells were grown on LB plates with xylose on the filter paper disk to induce dCas9 and inhibit transcription of *bcrC* and/or *uppP*. **(A)** WT and mutants with either *bcrC* or *uppP* null mutations, or containing sgRNA targeting only one UPP-Pase are not sensitive to induction of dCas9 by xylose. **(B)** Mutants containing sgRNA for both *bcrC* and *uppP* (*bcrC*-1*, uppP*-1*; bcrC*-2*, uppP*-2), and mutants with a *uppP* null mutant and sgRNA for *bcrC* (*ΔuppP, bcrC*-1*; ΔuppP, bcrC*-2*; ΔuppP, bcrC*-1&2) are sensitive to xylose. **(C)** Mutant strain shows similar phenotypes in a Δ*yodM* background.

2.4.2 The YodM protein can provide UPP-Pase activity when overexpressed

To characterize the physiological consequences of limiting UPP-Pase activity, we sought to generate conditional depletion strains. We introduced ectopic copies of *bcrC*, *uppP*, or *yodM* under the control of the IPTG inducible promoter $P_{spac(hy)}$. Next, we attempted to sequentially delete *bcrC* and *uppP* under conditions where the ectopic gene was expressed. However, due to either leakiness or insufficient expression, we were unable to construct a depletion strain conditionally expressing *bcrC* or *uppP*, even after attempts to modify the ribosome binding site to change translational efficiency (Table S2.2)(Vellanoweth & Rabinowitz, 1992).

One interesting result that emerged from this exercise is that YodM, if overexpressed, can support growth even in the absence of BcrC and UppP. In this strain, the native *yodM* RBS was replaced with a strong RBS (Vellanoweth & Rabinowitz, 1992) and the start codon was changed from TTG to ATG. The resulting $P_{spac(hy)}$-*yodM* construct allowed generation of a *bcrC uppP* double mutant strain that could grow in the presence, but not in the absence of IPTG (Figure S2.1). Note that this strain has two copies of *yodM* with one native copy and an ectopic copy controlled by $P_{spac(hy)}$ and optimized for expression. Because of the homology between YodM and *E. coli* UPP-Pases and the fact that overexpression of YodM can rescue growth defect of *bcrC uppP* double mutant, we infer that YodM has some UPP-Pase activity, and this activity is sufficient to support growth in absence of the other two UPP-Pases when it is expressed at an artificially high level. However, YodM is not able to support growth of a *bcrC uppP* double mutant at its normal expression levels. Overall we conclude that BcrC and UppP are the two primary UPP-Pases, at least in our laboratory conditions.

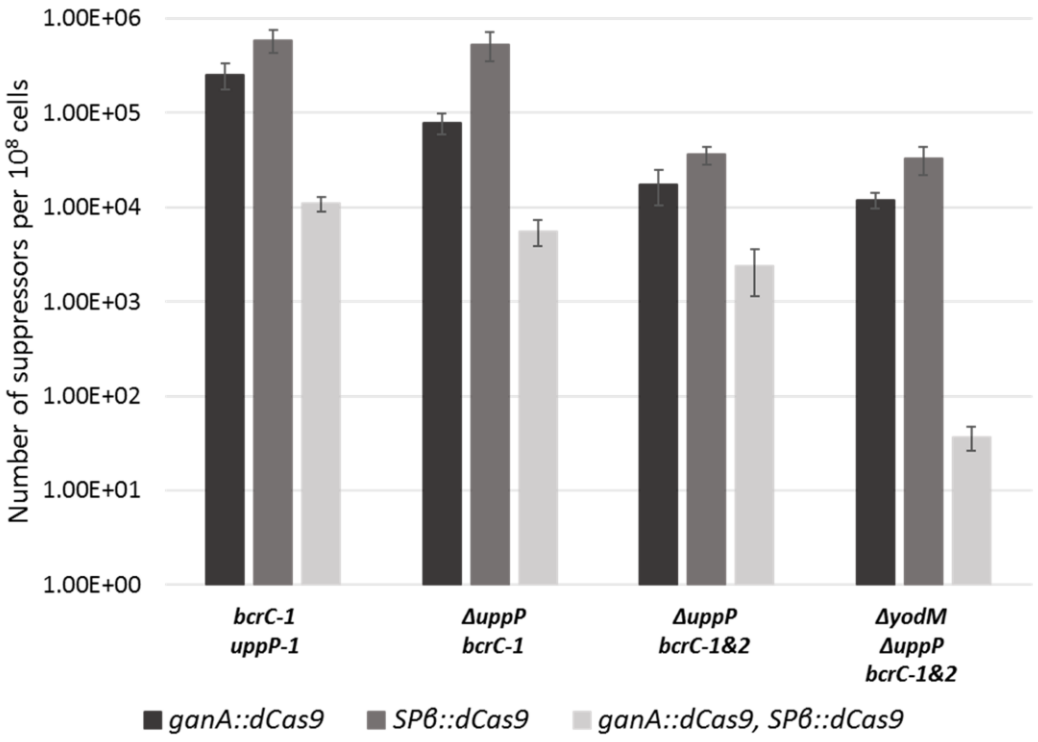

Figure 2.2. Reduction of suppressor mutations in depletion strains.

Fraction of suppressors in populations of various depletion strains. UPP-Pases depletion strains cannot grow on LB plates containing 2% xylose unless they have a suppressor mutation. Cells were plated on LB plates with or without 2% xylose, and the number of cells on each type of plate were counted and back calculated to CFU/ml. Fraction of suppressor in each population was calculated by dividing CFU of suppressors over CFU of total cells.

2.4.3 Demonstration of essentiality of UPP-Pases using CRISPRi

We next explored the use of CRISPRi as a tool to monitor the effects of UPP-Pase depletion on cell physiology. The CRISPRi system uses a catalytically inactive form of the Cas9 endonuclease (dCas9) and a single guide RNA (sgRNA) (Qi *et al.*, 2013, Hawkins *et al.*, 2015). The sgRNA contains a customizable 20-nt base pairing region to direct dCas9 to specific DNA sequences, and the dCas9:sgRNA complex binds DNA and serves as a road block to transcription. In the system used in this work, dCas9 gene is expressed from a xylose-inducible promoter and the sgRNAs were constitutively expressed (Peters *et al.*, 2016a). Based on previous studies in *E. coli* (Qi *et al.*, 2013) and mycobacteria (Choudhary *et al.*, 2015), we anticipated that the strength of transcriptional repression would be increased by promoter proximal targeted complexes and by the use of two sgRNAs. We therefore designed *bcrC*-1 and *uppP*-1 sgRNAs to bind close to the transcription start site (predicted to have a strong repressive effect) and *bcrC*-2 and *uppP*-2 sgRNAs to bind further downstream (predicted to have weaker repressive effects).

The conditional depletion strains did not show any growth defect in the absence of the dCas9 inducer xylose, but were growth impaired in medium with xylose. In order to illustrate the functional redundancy of BcrC and UppP, we used disk diffusion assays as a measure of xylose sensitivity. *B. subtilis* is not sensitive to xylose *per se,* and can use it as a carbon source (Schmiedel & Hillen, 1996). As expected based on the phenotype of the null mutant strains, depletion of either *uppP* or *bcrC* using CRISPRi did not lead to xylose sensitivity (Figure 2.1A). However, strains in which both genes were targeted for transcriptional repression showed a notable sensitivity to xylose as shown by a clear zone of inhibition around the paper disk containing xylose (Figure 2.1B). A similar effect was noted in strains where *uppP* was deleted and *bcrC* was targeted for transcriptional repression. Strains containing the weak sgRNAs *bcrC*-2 and *uppP*-2 showed a small

zone of inhibition, demonstrating that these cells are less xylose sensitive, and suggesting that *bcrC*-2 and *uppP*-2 provide less efficient in transcriptional repression (Figure 2.1B). This is consistent with the previous observation that sgRNAs farther from 5' end of transcription start site caused weaker repression (Choudhary *et al.*, 2015). In the *uppP* null mutant, depleting *bcrC* led to xylose-sensitivity. The use of the promoter proximal sgRNA *bcrC*-1 led to a high level of xylose sensitivity, and this was modestly increased with the inclusion of the second sgRNA, *bcrC*-2. We were not able to construct a strain with *bcrC* deleted and containing *uppP*-1, possibly due to leaky expression of dCas9 which has been shown to have moderate repressive activity even in the absence of xylose induction (Peters *et al.*, 2016a).

2.4.4 Optimization of CRISPRi to reduce suppressor formation in conditional depletion strains

It is apparent that suppressors arise frequently in the zone of xylose-dependent growth inhibition (Figure 2.1B). Whole genome sequencing of ten independent suppressors revealed frameshift mutations in the dCas9 gene (nine strains), and a single base pair mutation in the *bcrC* gene which altered the PAM (Protospacer Adjacent Motif) sequence for sgRNA *bcrC*-1 and thus prevent binding of dCas9:sgRNA complex (one strain). To facilitate further physiological studies, we sought to first reduce the frequency of suppressors. Since our sequencing results indicate that inactivation of the gene encoding dCas9 is the single most frequent class of suppressor mutation, we constructed a merodiploid strain containing a second copy of dCas9 integrated into the SPβ prophage. We then monitored the frequency with which suppressors arise by plating the depletion strain on LB medium supplemented with 1% glucose or 2% xylose and comparing the colony forming units (CFU). As expected, strains with two copies of the gene encoding dCas9 displayed

a reduction (approximately 10-fold) in the frequency of suppressors (Figure 2.2). We also note that suppressor formation is somewhat higher in strains with dCas9 expressed only from the SPβ prophage locus rather than the *ganA* locus (Figure 2.2, Figure S2.2A). Since it is also possible to isolate suppressors that mutate either the sgRNA or its target, we reasoned that having two sgRNAs targeted to the same gene would further decrease the frequency of suppressors. In general, the frequency of suppressors was reduced in the *uppP* null strain carrying both *bcrC*-1 and *bcrC*-2 sgRNAs relative to the strain with only *bcrC*-1, however these effects were rather modest. We hypothesized that another possible class of suppressors might result from up-regulation of *yodM*. Indeed, introduction of a *yodM* null mutation into the *uppP bcrC*-1 *bcrC*-2 strain greatly reduced the frequency of suppressors, but only if dCas9 was present in two copies (Figure 2.2**,** Figure S2.2B, C). These results indicate that inactivation of dCas9 is the most frequent cause of suppression (as inferred from the whole genome sequencing studies), and that the use of two sgRNAs and elimination of known or predicted pathways of suppression (such as upregulation of *yodM*) may be required for a significant further reduction in suppressor occurrence.

We then isolated two independent suppressors from the optimized strain (HB17235) and performed whole genome sequencing. While we might have expected to discover mutations revealing novel UPP-Pase(s), each suppressor contained a frameshift mutation (base deletion) in a homopolymeric stretch within both dCas9 genes (one suppressor in TTCCTTTGAAAAAAA and the other in CAGTATCAAAAAAAA). The fact that both dCas9 genes in each suppressor strain have the same point mutation in each copy of the gene leads us to speculate that the first mutation may have resulted from a relatively frequent strand slippage event in the homopolymeric sequence followed by a gene conversion event to generate the double mutant.

One of our goals in generating depletion strains for UPP-Pases was to monitor the terminal phenotype, and this is complicated if suppressors arise at a high frequency. To determine if our optimized CRISPRi system had sufficiently reduced the appearance of suppressors to allow growth studies, we inoculated ~$4x10^4$ cells into 200 µl of xylose-containing medium using an automated BioScreen growth analyzer. For each strain, we monitored 30 replicate cultures (3 biological replicates containing 10 technical replicates each). In this assay, the majority of the cultures for each strain grew after a long lag phase (Table S2.3), suggesting that suppressors were arising that might therefore complicate analysis of the terminal phenotype. The single exception was our optimized strain (HB17235) which is a dCas9 merodiploid lacking both UppP and YodM and with two sgRNAs targeting *bcrC*. With this strain, there was outgrowth in less than 10% of the wells.

2.4.5 Dynamics of UPP-Pase depletion

To determine how long it takes for the existing BcrC protein to be depleted in the optimized (HB17235) strain and thereby limit growth, we monitored growth curves as a function of the initial inoculum in LB with either 1% glucose or 2% xylose. With a starting culture at initial OD_{600} 0.14, the culture reached a final OD_{600} of 0.7 in the presence of 2% xylose, while it could reach OD_{600} ~1.2 with glucose (Figure 2.3). With each two-fold dilution of the initial inoculum, the final OD_{600} reached under depletion conditions was also decreased by nearly 2-fold, consistent with a growth-limiting depletion of pre-existing BcrC after 3 to 4 doublings.

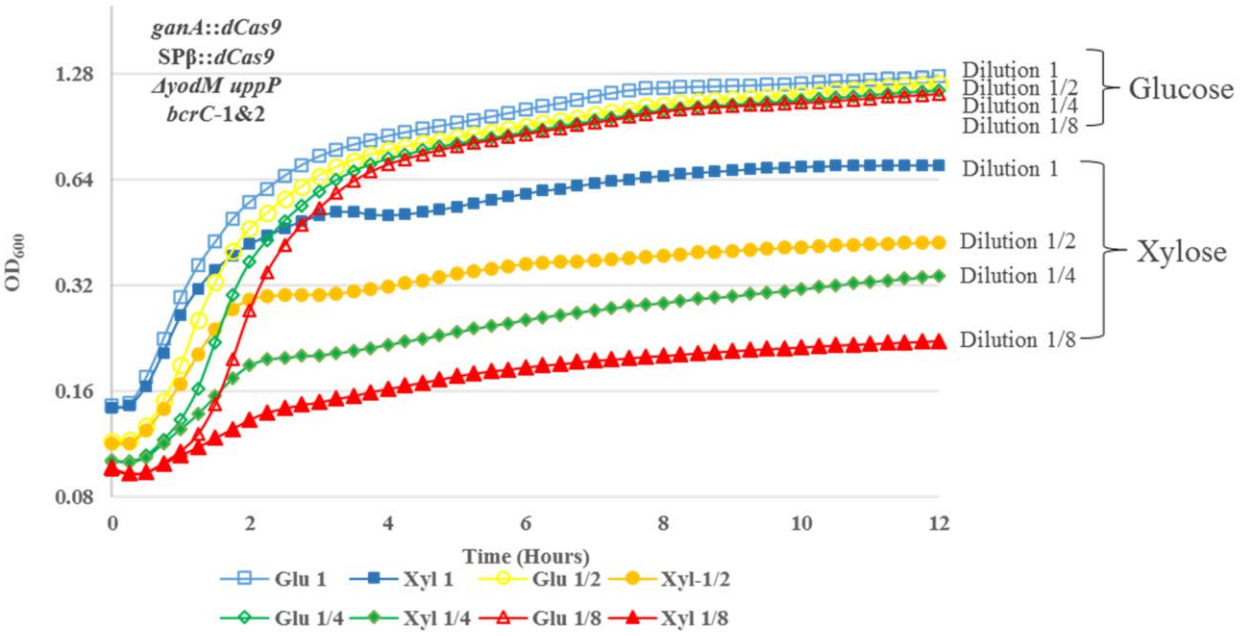

Figure 2.3. Growth of depletion strain in depletion/non-depletion condition with different initial culture population size.

Depletion strain (*ganA*::*dCas9* SPβ::*dCas9 ΔyodM uppP bcrC*-1&2) growing at logarithm phase was diluted and re-inoculate into liquid LB medium supplemented with either 1% (w/v) glucose or 2% (w/v) xylose. Growth was carried at 37℃ with shaking. OD_{600} was measured every 15 minutes. Starting OD_{600} of ~0.1 was designated at "Dilution 1", and further two-fold dilution was performed until the smallest inoculum contained 1/8 amount of the cells in "Dilution 1". Different amount of initial inoculums affects final OD of cells growing in LB xylose medium, while had no significant on cells growing in LB glucose medium.

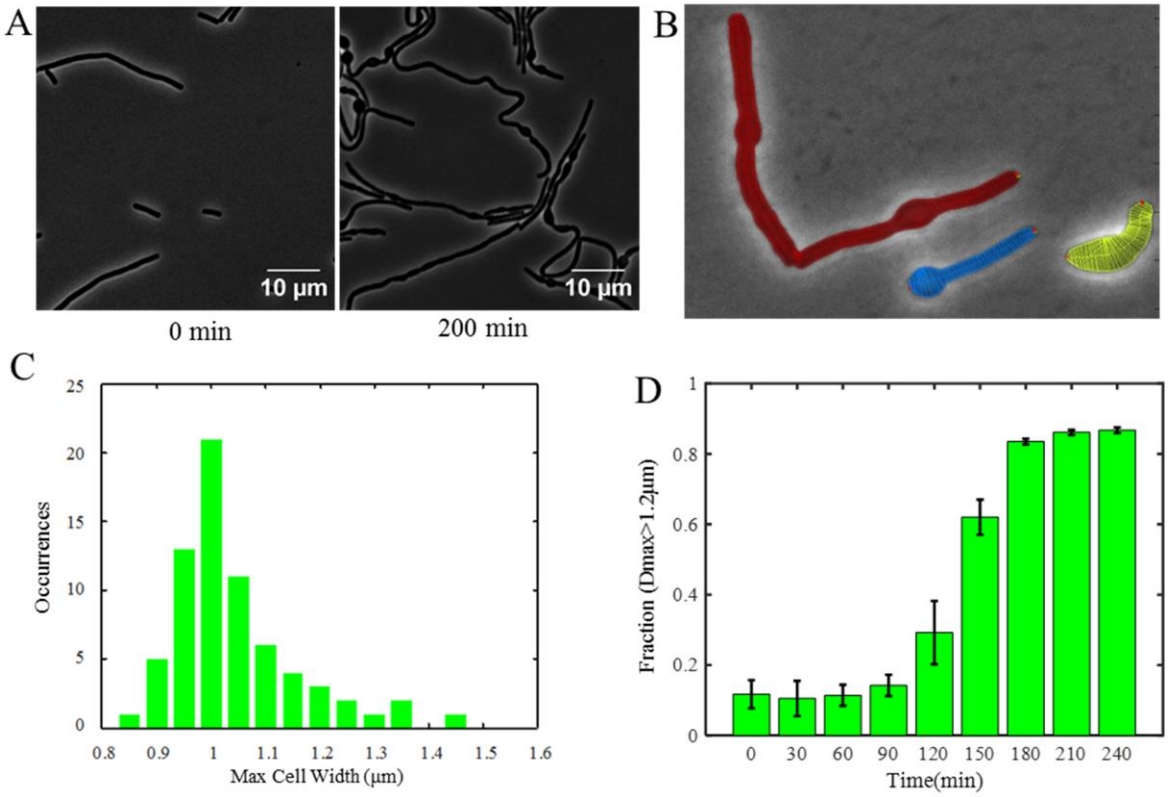

Figure 2.4. UPP-Pase depletion leads to curved and bulged cells.

Microscopy images of depletion strains under depletion conditions. Cells were observed using phase contract and under 100X magnification (each pixel size is 65 nm). **(A)** Depletion strain (HB17325) growing in CH medium supplemented with 2% xylose at 37˚C. Cells showed normal morphology at the beginning of the experiment (0 min) and showed curved and bulged cells as UPP-Pases were depleted (200 min). **(B)** Example showing how cell width was measured. Lines were draw across cell width, and cell width at each line was measured. The max width of each cell was used for quantification. **(C)** Distribution of max cell width of depletion strain at the beginning of treatment (0 min). The majority of cells had max width of 0.95-1.05 μm, while approximately 10% of cells have max width bigger than 1.2 μm. **(D)** Change of fraction of cells having max cell width (Dmax, max diameter of cells) larger than 1.2 μm through time. The fraction increased significantly after 120 minutes and reached its peak after 180 minutes, indicating more and more cells began to form bulge as UPP-Pases were depleted.

2.4.6 Changes in cell morphology upon depletion of UPP-Pases

Defects in cell wall synthesis often cause morphological changes as the integrity of the cell wall is compromised. For example, depletion of MreB and its homologs leads to a loss of rod shape and formation of bulged cells (Formstone & Errington, 2005), and cells missing all class A PBPs form longer and bent cells with abnormal protrusions into the cell plasma (McPherson & Popham, 2003). Cells with UppS expression repressed by CRISPRi also show bulged cells without significant lysis (Peters *et al.*, 2016a). We therefore anticipated a similar phenotype from the UPP-Pase depletion strain. Cells were grown in a micro-fluidic chamber in CH medium supplemented with 2% xylose, and images were taken every 30 seconds. At the beginning of the experiment, cells did not show any obvious morphological defect relative to WT. After about 2 hours, cells grown with xylose began to form bulges (Figure 2.4, Movie S1). In comparison, WT cells did not exhibit any growth defect in presence of 2% xylose (Movie S2). Surprisingly, few cell lysis events were observed during the time lapse experiment. This is similar to what was observed in the UppS depletion strain (Schirner *et al.*, 2015, Peters *et al.*, 2016a), and in a strain depleted for lipid II flippases (Meeske *et al.*, 2015). The lantibiotic NAI-107 (which targets UPP linked cell wall precursors such as lipid I, II and precursors of WTA) leads to a similar terminal phenotype (Munch *et al.*, 2014).

To quantify the fraction of cells forming bulges when UPP-Pases are depleted, we observed more than 200 cells at each time point and used Morphometrics and an in-house MATLAB script to measure cell width across the whole length of the cell, and determined the maximum cell width for each cell (Figure 2.4B). Before depletion of UPP-Pases, the majority of cells exhibited a maximum width of between 0.95 and 1.05 μm (Figure 2.4C) and only ~10% of cells had a width >1.2 μm (Figure 2.4C, D). As the cells grew under depletion conditions, the percentage of

cells with a maximal width above 1.2 μm increased significantly (Figure 2.4D). Septum formation was still present in the depletion strain as visualized with the membrane stain FM5-95, even when cells exhibited bulging (Figure S2.3).

2.4.7 The UPP-Pase depletion strain is sensitive to cell envelope stress

It has been reported that leaky expression of dCas9 in absence of xylose may lead to ~3-fold repression of target genes (Peters *et al.*, 2016a). We therefore hypothesized that our depletion strain may have reduced expression of UPP-Pases even in the absence of inducer. Indeed, the depletion strain exhibited more lysis than WT when stored on plates. To test this hypothesis, we used disk diffusion assays under non-inducing condition to monitor sensitivity to cell envelope stress conditions (Figure 2.5). In fact, the depletion strain is significantly ($P<0.01$) more sensitive to both bacitracin, which binds UPP and thereby inhibits UPP-Pase activity, and daptomycin. A more modest level of sensitivity ($P<0.05$) was noted for the peptidoglycan synthesis inhibitors vancomycin and fosfomycin. The depletion strain was not more sensitive to several other tested stress conditions including compounds that elicit membrane stress (Nisin, SDS, and Triton X-100). The reason for the increased sensitivity to some, but not other, peptidoglycan synthesis inhibitors is presently unclear, but interpreting such effects can be complex, as previously discussed (Lee & Helmann, 2013).

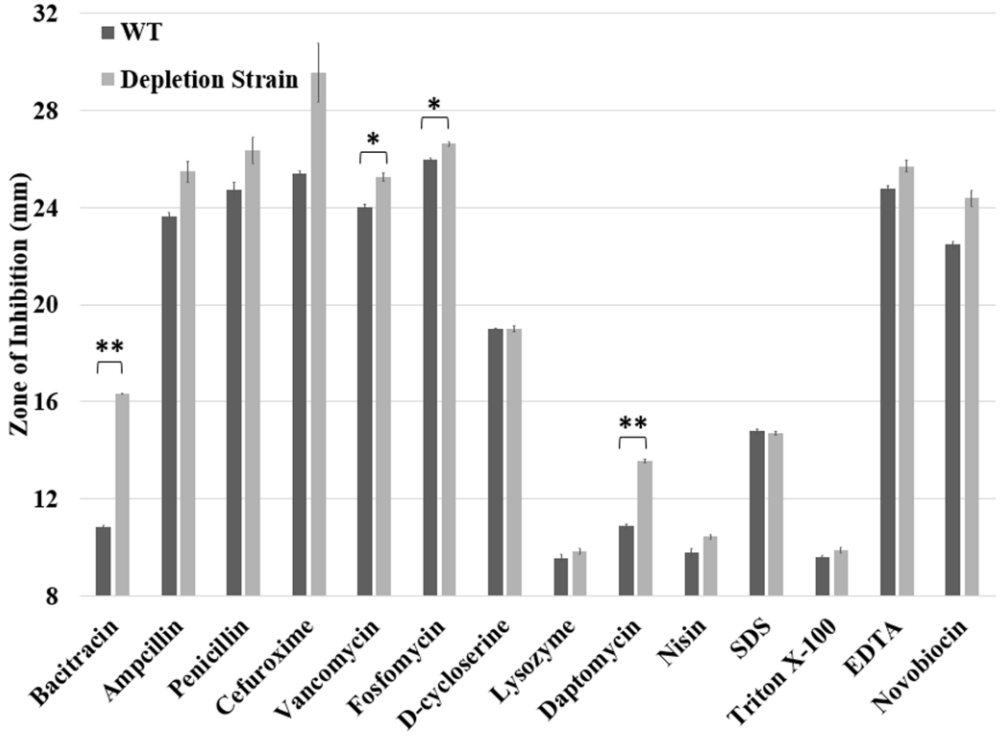

Figure 2.5. Sensitivity of depletion strain against stresses under partial depletion condition. Cells were grown on LB plates with chemicals added onto the filter paper disk. Sensitivity of depletion strain was measured as the clear zone of inhibition around the paper disk. Chemicals used in this assay include bacitracin 400 µg, ampicillin 1 mg, penicillin 1 mg, cefuroxime 10 mg, vancomycin 100 µg, fosfomycin 1 mg, D-cycloserine 100 µg, lysozyme 100 µg, daptomycin 100 µg, nisin 1 mg, SDS 10 µl of 10% solution, Triton X-100 10 µl of 25% solution, EDTA 10 µl of 0.5 M (pH 8.0) solution, novobiocin 100 µg. The data are expressed as mean ± standard error (n=3). Statistical assay was performed using T test with two samples assuming unequal variances. * means two tail P value <0.05, ** means two tail P value <0.01.

2.4.8 Depletion of UPP-Pases triggers a cell envelope stress response

To further characterize the effects of UPP-Pase depletion, we monitored changes in the transcriptome 2.5 h after addition of xylose to deplete BcrC, a time known to coincide with the onset of visible morphological changes and decreased growth (Figure 2.3, 2.4). In the depletion strain, >150 genes were >3-fold up-regulated and nearly 300 genes were >3-fold down-regulated (SI Excel Sheets). The set of up-regulated genes includes known cell envelope stress responses including, most notably, the σ^M regulon. In contrast, down-regulated genes include many genes and regulons consistent with catabolite repression in the xylose-treated cultures, and with entry of the untreated cells into transition phase during the 2.5 h of incubation. The up-regulation of the flagellar and motility systems controlled by σ^D in the control cells as they enter into transition phase likely explains the apparent down-regulation of these genes in the depletion strain.

To gain further insights into the effects of UPP-Pase depletion on cell envelope stress responses we used hierarchical clustering to compare the expression of genes regulated by ECF sigma factors and the WalR, BceR, PsdR, LiaR and YvrHb two component system regulons (Figure 2.6). Microarray data generated in this study (UPP-Pase depletion), as well as for cells treated with targocil (Schirner *et al.*, 2015), bacitracin (Mascher *et al.*, 2003), D-cycloserine (Hutter *et al.*, 2004), Triton X-100 (Hutter *et al.*, 2004), and vancomycin (Eiamphungporn & Helmann, 2008) (SI Excel Sheets) were used for clustering and heat map generation as previously described (Eiamphungporn & Helmann, 2008). Based on the observations above, we anticipated that the effects of UPP-Pase depletion (occurring over 2.5 h) might not be directly comparable to those elicited by relatively short treatments with cell envelope antibiotics. Nevertheless, we noted several striking similarities. Specifically, the σ^M regulon is selectively induced by UPP-Pase depletion, with comparatively weak effects noted for other ECF σ factor stress responses.

Induction of the σ^M regulon is consistent with the inclusion of the BcrC UPP-Pase as part of this regulon (Cao & Helmann, 2002), as well as the previously noted induction in cells treated with bacitracin (Mascher *et al.*, 2003) or containing mutations that decrease UPP synthesis (Lee & Helmann, 2013). In contrast with σ^M, the σ^W regulon, most strongly activated by membrane stress conditions (Eiamphungporn & Helmann, 2008), was down-regulated in the depleted cells compared to the control.

In addition to clustering based on genes, we also determined the clustering based on treatments. Among the antibiotics used for comparison, the treatment condition most similar to UPP-Pase depletion is targocil, which inhibits WTA export and therefore also causes a gradual depletion of the Und-P pool. D-cycloserine, an inhibitor of early steps in PG synthesis that converge with Und-P to allow lipid II synthesis, also leads to a similar set of stress responses. We might have expected bacitracin (which binds directly to UPP) to trigger a response similar to UPP-Pase depletion. However, despite several similarities, bacitracin additionally elicits strong (albeit transient) induction of the BceR and LiaR regulons after 5 min of treatment (Radeck *et al.*, 2016). This activation can happen at bacitracin concentrations well below the MIC and does not depend on cell wall damage (Fritz *et al.*, 2015). The least similar stress conditions, compared to UPP-Pase depletion, were those elicited by Triton-X-100 and vancomycin, which both lead to induction of the large σ^W regulon under the tested conditions.

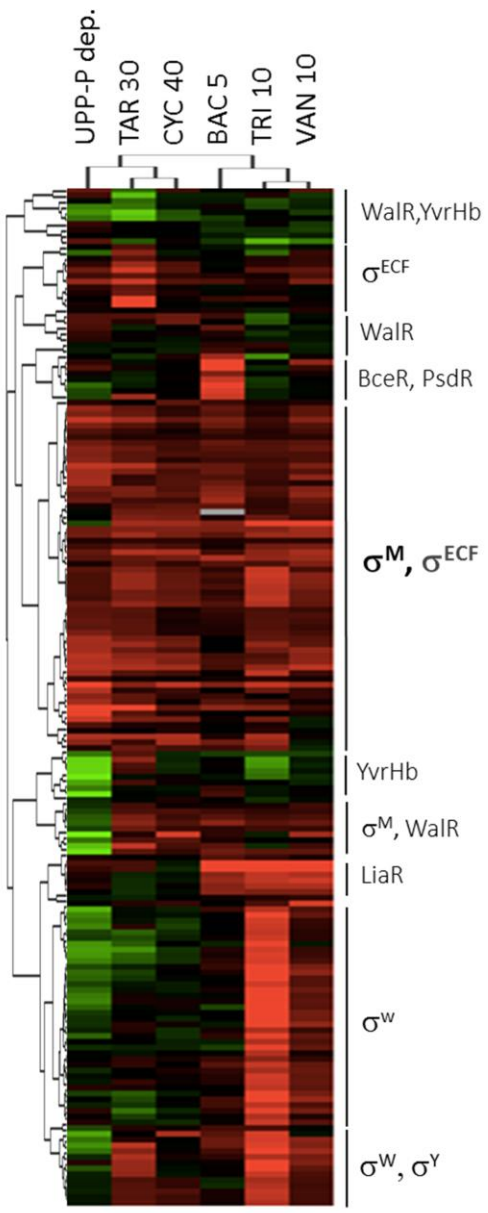

Figure 2.6. UPP-Pase depletion induces the σ^M cell envelope stress response.

Hierarchical clustering was used to generate a heat map of up-regulation (red) or down-regulation (green) of known cell envelope stress responsive genes (regulons indicated to the right). Cells were either depleted of UPP-Pase (compared to non-depletion control cells), or treated with targocil (TAR), D-cycloserine (CYC), bacitracin (BAC), Triton X-100 (TRI), or vancomycin (VAN). Numbers indicate the minutes of treatment with each antibiotic.

2.5 Discussion

UPP is a crucial lipid carrier for synthesis of the cell envelope, including both peptidoglycan and WTA. In peptidoglycan synthesis, UPP serves as lipid carrier for the disaccharide-pentapeptide precursor in the central intermediate lipid II. Although initially synthesized as the pyrophosphate form (UPP), dephosphorylation is required to generate the substrate (Und-P) for MraY. Similarly, in *B. subtilis* strain 168, Und-P is required for WTA synthesis which is initiated by transfer of GlcNac-1-P from UDP-GlcNac to Und-P by TagO to generate the initial membrane-bound precursor. The peptidoglycan precursor, lipid II, is flipped across the membrane by either of two flippases, MurJ or Amj, where it serves as substrate for synthesis of the glycan polymer by PBPs. In contrast, synthesis of the WTA polymer occurs in the cytosol and the completed polymer (a glycerol-phosphate alternating copolymer in *B. subtilis*) is exported and then attached to PG. In both peptidoglycan and WTA synthesis, the UPP carrier is released on the extracytoplasmic face of the membrane (by PBPs or the TagTUV family of WTA-attachases) and recycled (Brown *et al.*, 2013).

Disruption of cell envelope synthesis is one of the most effective strategies for inhibiting bacterial growth and numerous antibiotics target these processes. The lipid II cycle can be disrupted by compounds that inhibit UPP synthesis or that bind directly to lipid II (nisin, vancomycin, ramoplanin), and to UPP itself (bacitracin). Other PG synthesis inhibitors target the PBPs and thereby inhibit the transpeptidation (β-lactams) or transglycosylation (moenomycin) reactions. It is also possible to disrupt the lipid II cycle by blocking the synthesis of WTA at late steps, thereby leading to sequestration of this limiting lipid carrier (Pasquina *et al.*, 2013).

A common feature of many different compounds that inhibit the lipid II cycle is that they invoke cell envelope stress responses including activation of the σ^M regulon (Helmann, 2016). A

major function of the σ^M regulon is to increase the expression of key enzymes involved in cell envelope synthesis and to up-regulate alternative enzymes to replace those that might be inhibited. Notable examples of σ^M-dependent compensation reactions include up-regulation of the lipid II flippase Amj (which substitutes for MurJ; (Meeske *et al.*, 2015)), the lipoteichoic acid synthase LtaSa (YfnI, which substitutes for LtaS), and BcrC (which substitutes for UppP; (Cao & Helmann, 2002, Eiamphungporn & Helmann, 2008)). Similarly, antibiotics that inhibit the lipid II cycle, including bacitracin (Mascher *et al.*, 2003), vancomycin (Eiamphungporn & Helmann, 2008), moenomycin (Salzberg *et al.*, 2011), and the WTA-targeting targocil (Schirner *et al.*, 2015), all activate the σ^M regulon (Helmann, 2016).

Here, we set out to explore the role of three genes encoding candidate UPP-Pases in the lipid II cycle in *B. subtilis*. The CRISPRi system has been recently adapted as a tool to repress bacterial gene expression and facilitate the analysis of essential gene functions (Peters *et al.*, 2016a). Our inability to construct a *uppP bcrC* double mutant suggested that these two genes might be a synthetic lethal pair (in contrast with a previous report; (Bernard *et al.*, 2005, Inaoka & Ochi, 2012)), although they could both be deleted when a third candidate phosphatase, YodM, was overexpressed. The ability of YodM to rescue cell growth in a *uppP bcrC* double mutant and its homology to other UPP-Pases support a possible role for YodM as a UPP-Pase that is active under growth conditions not yet identified. Alternatively, this may be an adventitious reaction that only occurs when this enzyme is artifically overexpressed. This may be similar to the case in *E.coli*, where LpxT transfers phosphate from UPP to lipid A and as a product also generates Und-P (Touze *et al.*, 2008b). The efficiency of recycling UPP by this reaction is not enough to support cell growth, but this enzyme indeed has UPP-Pase activity. To test the hypothesis that *uppP* and *bcrC* are a synthetic lethal pair, and to explore the physiological consequences of UPP-Pase depletion, we

optimized a previously described CRISPRi repression system (Peters *et al.*, 2016a) to minimize the appearance of suppressor mutations. We have here used two copies of dCas9 to reduce the occurrence of suppressor mutations. The frequency of suppressor mutations varies significantly between loci (unpublished results), and may be affected by the length of time required to deplete the cell of essential proteins. Whereas one sgRNA generally suffices for gene knockdown (Peters *et al.*, 2016a), here we included two sgRNAs targeting the *bcrC* gene. The presence of two sgRNAs leads to a modest increase in repression efficiency as judged by xylose sensitivity (Figure 2.1B), and also slightly reduced the frequency of suppressors (Figure 2.2). In this system, the greatest reduction in suppressor frequency required deletion of *yodM* which eliminates the only other known protein with UPP-Pase activity (Figure 2.2). In general, optimization of CRISPRi for knockdown of essential genes (or sets of genes) may benefit from use of a dCas9 merodiploid since inactivation of dCas9 is one frequent cause of suppression. Further modifications worth exploring include the use of two sgRNAs per gene (although this effect may be minor) and elimination of known or predicted pathways of suppression.

The two independent suppressor analyzed from our optimized strain each contained mutations in both copies of the dCas9 gene. The occurrence of frameshift mutations in runs of adenines suggests that these may be hot spots for mutagenesis, and the fact that each strain contains the same point mutation in both dCas9 genes suggests a gene conversion event after the first mutation. One way to further reduce the fraction of suppressors might be to use a dCas9 with a different coding sequence as the second copy. For example, swapping alternate but still preferred codons for *B. subtilis* (Moszer *et al.*, 1999) could be used to reduce the number of homopolymeric sequences and also to reduce sequence-sequence similarity between two dCas9 genes.

Nevertheless, the fraction of suppressors in the optimized strain used in this study is sufficiently low to carry out the physiological assays performed here.

Depletion of UPP-Pases leads to a cessation of growth after ~3-4 doublings. Even mild depletion (due to the leaky expression of dCas9 in the depletion strain) leads to an increase in sensitivity to bacitracin. As UPP is further depleted, the cells begin to display morphological abnormalities including a prominent bulging of the cells. This is consistent with the morphological changes induced by other genetic and chemical perturbations known to affect PG synthesis. Concomitant with the onset of morphological defects resulting from depletion of UPP, the cells strongly activate the σ^M cell envelope stress response, consistent with the effects of other antibiotics targeting the lipid II cycle (Helmann, 2016).

In conclusion, our results establish that *B. subtilis* requires either of two UPP-Pases for viability, UppP and BcrC. Because of the nature of Und-P synthesis and recycling, it is reasonable to speculate that one UPP-Pase has a cytosolic-facing active site and functions to convert UPP produced by UppS into Und-P for use in cell wall synthesis, while the other one recycles UPP produced as a product of the transglycosylase reaction catalyzed by class A PBPs. We speculate that the former activity is UppP, which might account for the minor role of this enzyme with respect to sensitivity to rare earth metals (Inaoka & Ochi, 2012). After each addition to the growing peptidoglycan (or WTA) polymer, UPP is released and must be dephosphorylated and flipped back to the cytoplasmic face of the membrane for reuse. This is the likely role for BcrC, which by reducing surface exposed UPP can prevent binding of bacitracin to its target. In contrast, all four of the *E. coli* UPP-Pases may have active sites on the outer face of the membrane. These include the PAP2 family UPP-Pases PgpB (Touze *et al.*, 2008a), YbjG and YeiU (Tatar *et al.*, 2007) and,

based on protein modeling, BacA (Chang *et al.*, 2014). Manat and co-workers provided supporting evidence for this model using truncated BacA-β-lactamase reporters (Manat *et al.*, 2015).

Regardless of whether the two UPP-Pases in *B. subtilis* have their active sites on the same or opposite faces of the membrane, the fact that *B. subtilis* can survive with only one UPP-Pase suggests that UPP-Pase function needs only be localized to one face to support viability. This suggests that either *de novo* synthesized UPP is dephosphorylated inside the cell and the UPP product released by the transglycosylase reaction can be flipped from outside to inside, or that UPP synthesized in the cytoplasm is first flipped to the outside to be dephosphorylated, and then flipped back to the cytoplasmic face to support peptidoglycan (MraY) and WTA (TagO) synthesis. Flipping of Und-P or UPP is unlikely to be spontaneous, although the identity of any proteins that help catalyze this reaction is not yet clear. Ongoing efforts to define this and other poorly understood steps in the lipid II cycle will help to identify new candidates for the targeting of antibacterials and will refine our understanding of the complex mechanisms of acclimation to antibiotics in bacteria.

2.6 Acknowledgment

This chapter is adapted from "Depletion of Undecaprenyl Pyrophosphate Phosphatases Disrupts Cell Envelope Biogenesis in *Bacillus subtilis*", *J Bacteriol.* 2016 Oct 7;198(21):2925-2935. The list of the authors is Zhao H, Sun Y, Peters JM, Gross CA, Garner EC, Helmann JD. Sun Y and Garner EC contributed the microscopy data in Figure 2.4 and Figure S2.3. Peters JM and Gross CA contributed the CRISPRi plasmids and designed the sgRNA. All other data were acquired by Zhao H. Zhao H and Helmann JD drafted the manuscript, and all authors contributed in editing the paper.

2.7 Reference

Bernard, R., M. El Ghachi, D. Mengin-Lecreulx, M. Chippaux & F. Denizot, (2005) BcrC from Bacillus subtilis acts as an undecaprenyl pyrophosphate phosphatase in bacitracin resistance. *J Biol Chem* **280**: 28852-28857.

Bickford, J.S. & H.S. Nick, (2013) Conservation of the PTEN catalytic motif in the bacterial undecaprenyl pyrophosphate phosphatase, BacA/UppP. *Microbiology* **159**: 2444-2455.

Brown, S., J.P. Santa Maria, Jr. & S. Walker, (2013) Wall teichoic acids of gram-positive bacteria. *Annu Rev Microbiol* **67**: 313-336.

Cao, M. & J.D. Helmann, (2002) Regulation of the Bacillus subtilis bcrC bacitracin resistance gene by two extracytoplasmic function sigma factors. *J Bacteriol* **184**: 6123-6129.

Chang, H.Y., C.C. Chou, M.F. Hsu & A.H. Wang, (2014) Proposed carrier lipid-binding site of undecaprenyl pyrophosphate phosphatase from Escherichia coli. *J Biol Chem* **289**: 18719-18735.

Choudhary, E., P. Thakur, M. Pareek & N. Agarwal, (2015) Gene silencing by CRISPR interference in mycobacteria. *Nat Commun* **6**: 6267.

D'Elia, M.A., K.E. Millar, T.J. Beveridge & E.D. Brown, (2006) Wall teichoic acid polymers are dispensable for cell viability in Bacillus subtilis. *J Bacteriol* **188**: 8313-8316.

Durrant, J.D., R. Cao, A.A. Gorfe, W. Zhu, J. Li, A. Sankovsky, E. Oldfield & J.A. McCammon, (2011) Non-bisphosphonate inhibitors of isoprenoid biosynthesis identified via computer-aided drug design. *Chem Biol Drug Des* **78**: 323-332.

Economou, N.J., S. Cocklin & P.J. Loll, (2013) High-resolution crystal structure reveals molecular details of target recognition by bacitracin. *Proc Natl Acad Sci U S A* **110**: 14207-14212.

Eiamphungporn, W. & J.D. Helmann, (2008) The Bacillus subtilis sigma(M) regulon and its contribution to cell envelope stress responses. *Mol Microbiol* **67**: 830-848.

El Ghachi, M., A. Derbise, A. Bouhss & D. Mengin-Lecreulx, (2005) Identification of multiple genes encoding membrane proteins with undecaprenyl pyrophosphate phosphatase (UppP) activity in Escherichia coli. *J Biol Chem* **280**: 18689-18695.

Fan, J., D. Jiang, Y. Zhao, J. Liu & X.C. Zhang, (2014) Crystal structure of lipid phosphatase Escherichia coli phosphatidylglycerophosphate phosphatase B. *Proc Natl Acad Sci U S A* **111**: 7636-7640.

Farha, M.A., T.L. Czarny, C.L. Myers, L.J. Worrall, S. French, D.G. Conrady, Y. Wang, E. Oldfield, N.C. Strynadka & E.D. Brown, (2015) Antagonism screen for inhibitors of bacterial cell wall biogenesis uncovers an inhibitor of undecaprenyl diphosphate synthase. *Proc Natl Acad Sci U S A* **112**: 11048-11053.

Formstone, A. & J. Errington, (2005) A magnesium-dependent mreB null mutant: implications for the role of mreB in Bacillus subtilis. *Mol Microbiol* **55**: 1646-1657.

Fritz, G., S. Dintner, N.S. Treichel, J. Radeck, U. Gerland, T. Mascher & S. Gebhard, (2015) A New Way of Sensing: Need-Based Activation of Antibiotic Resistance by a Flux-Sensing Mechanism. *MBio* **6**: e00975.

Gilbert, L.A., M.A. Horlbeck, B. Adamson, J.E. Villalta, Y. Chen, E.H. Whitehead, C. Guimaraes, B. Panning, H.L. Ploegh, M.C. Bassik, L.S. Qi, M. Kampmann & J.S. Weissman, (2014) Genome-Scale CRISPR-Mediated Control of Gene Repression and Activation. *Cell* **159**: 647-661.

Guillaume Manat, S.R., Rodolphe Auger, Ahmed Bouhss, He´ le`ne Barreteau,Dominique Mengin-Lecreulx, and Thierry Touze, (2014) Deciphering the Metabolism of Undecaprenyl-Phosphate: The Bacterial Cell-Wall Unit Carrier at the Membrane Frontier. *MICROBIAL DRUG RESISTANCE* **20**: 199-214.

Harwood, C.R. & S.M. Cutting, (1990) Molecular biological methods for Bacillus. *New York: Wiley*.

Hawkins, J.S., S. Wong, J.M. Peters, R. Almeida & L.S. Qi, (2015) Targeted Transcriptional Repression in Bacteria Using CRISPR Interference (CRISPRi). *Methods Mol Biol* **1311**: 349-362.

Helmann, J.D., (2016) Bacillus subtilis extracytoplasmic function (ECF) sigma factors and defense of the cell envelope. *Curr Opin Microbiol* **30**: 122-132.

Hutter, B., C. Schaab, S. Albrecht, M. Borgmann, N.A. Brunner, C. Freiberg, K. Ziegelbauer, C.O. Rock, I. Ivanov & H. Loferer, (2004) Prediction of mechanisms of action of antibacterial compounds by gene expression profiling. *Antimicrob Agents Chemother* **48**: 2838-2844.

Icho, T. & C.R. Raetz, (1983) Multiple genes for membrane-bound phosphatases in Escherichia coli and their action on phospholipid precursors. *J Bacteriol* **153**: 722-730.

Inaoka, T. & K. Ochi, (2012) Undecaprenyl pyrophosphate involvement in susceptibility of Bacillus subtilis to rare earth elements. *J Bacteriol* **194**: 5632-5637.

Jorgenson, M.A., S. Kannan, M.E. Laubacher & K.D. Young, (2015) Dead-end intermediates in the enterobacterial common antigen pathway induce morphological defects in Escherichia coli by competing for undecaprenyl phosphate. *Mol Microbiol*.

Kingston, A.W., H. Zhao, G.M. Cook & J.D. Helmann, (2014) Accumulation of heptaprenyl diphosphate sensitizes Bacillus subtilis to bacitracin: implications for the mechanism of resistance mediated by the BceAB transporter. *Mol Microbiol* **93**: 37-49.

Langmead, B., C. Trapnell, M. Pop & S.L. Salzberg, (2009) Ultrafast and memory-efficient alignment of short DNA sequences to the human genome. *Genome Biol* **10**: R25.

Lee, Y.H. & J.D. Helmann, (2013) Reducing the Level of Undecaprenyl Pyrophosphate Synthase Has Complex Effects on Susceptibility to Cell Wall Antibiotics. *Antimicrob Agents Chemother*.

Lovering, A.L., S.S. Safadi & N.C. Strynadka, (2012) Structural perspective of peptidoglycan biosynthesis and assembly. *Annu Rev Biochem* **81**: 451-478.

Luo, Y., K. Asai, Y. Sadaie & J.D. Helmann, (2010) Transcriptomic and phenotypic characterization of a Bacillus subtilis strain without extracytoplasmic function sigma factors. *J Bacteriol* **192**: 5736-5745.

Luo, Y. & J.D. Helmann, (2012) Analysis of the role of Bacillus subtilis sigma(M) in beta-lactam resistance reveals an essential role for c-di-AMP in peptidoglycan homeostasis. *Mol Microbiol* **83**: 623-639.

Manat, G., M. El Ghachi, R. Auger, K. Baouche, S. Olatunji, F. Kerff, T. Touze, D. Mengin-Lecreulx & A. Bouhss, (2015) Membrane Topology and Biochemical Characterization of the Escherichia coli BacA Undecaprenyl-Pyrophosphate Phosphatase. *PLoS One* **10**: e0142870.

Mascher, T., N.G. Margulis, T. Wang, R.W. Ye & J.D. Helmann, (2003) Cell wall stress responses in Bacillus subtilis: the regulatory network of the bacitracin stimulon. *Mol Microbiol* **50**: 1591-1604.

McPherson, D.C. & D.L. Popham, (2003) Peptidoglycan synthesis in the absence of class A penicillin-binding proteins in Bacillus subtilis. *J Bacteriol* **185**: 1423-1431.

Meeske, A.J., L.T. Sham, H. Kimsey, B.M. Koo, C.A. Gross, T.G. Bernhardt & D.Z. Rudner, (2015) MurJ and a novel lipid II flippase are required for cell wall biogenesis in Bacillus subtilis. *Proc Natl Acad Sci U S A* **112**: 6437-6442.

Michna, R.H., F.M. Commichau, D. Todter, C.P. Zschiedrich & J. Stulke, (2014) SubtiWiki-a database for the model organism Bacillus subtilis that links pathway, interaction and expression information. *Nucleic Acids Res* **42**: D692-698.

Moszer, I., E.P. Rocha & A. Danchin, (1999) Codon usage and lateral gene transfer in Bacillus subtilis. *Curr Opin Microbiol* **2**: 524-528.

Munch, D., A. Muller, T. Schneider, B. Kohl, M. Wenzel, J.E. Bandow, S. Maffioli, M. Sosio, S. Donadio, R. Wimmer & H.G. Sahl, (2014) The lantibiotic NAI-107 binds to bactoprenol-bound cell wall precursors and impairs membrane functions. *J Biol Chem* **289**: 12063-12076.

Ohki, R., K. Tateno, Y. Okada, H. Okajima, K. Asai, Y. Sadaie, M. Murata & T. Aiso, (2003) A bacitracin-resistant Bacillus subtilis gene encodes a homologue of the membrane-spanning subunit of the Bacillus licheniformis ABC transporter. *J Bacteriol* **185**: 51-59.

Pasquina, L.W., J.P. Santa Maria & S. Walker, (2013) Teichoic acid biosynthesis as an antibiotic target. *Curr Opin Microbiol* **16**: 531-537.

Payne, D.J., M.N. Gwynn, D.J. Holmes & D.L. Pompliano, (2007) Drugs for bad bugs: confronting the challenges of antibacterial discovery. *Nat Rev Drug Discov* **6**: 29-40.

Peters, J.M., A. Colavin, H. Shi, T.L. Czarny, M.H. Larson, S. Wong, J.S. Hawkins, C.H.S. Lu, B.M. Koo, E. Marta, A.L. Shiver, E.H. Whitehead, J.S. Weissman, E.D. Brown, L.S. Qi, K.C. Huang & C.A. Gross, (2016) A Comprehensive, CRISPR-based Approach to Functional Analysis of Essential Genes in Bacteria. *Cell* **In Press**.

Peters, J.M., M.R. Silvis, D. Zhao, J.S. Hawkins, C.A. Gross & L.S. Qi, (2015) Bacterial CRISPR: accomplishments and prospects. *Curr Opin Microbiol* **27**: 121-126.

Qi, L.S., M.H. Larson, L.A. Gilbert, J.A. Doudna, J.S. Weissman, A.P. Arkin & W.A. Lim, (2013) Repurposing CRISPR as an RNA-guided platform for sequence-specific control of gene expression. *Cell* **152**: 1173-1183.

Radeck, J., S. Gebhard, P.S. Orchard, M. Kirchner, S. Bauer, T. Mascher & G. Fritz, (2016) Anatomy of the bacitracin resistance network in Bacillus subtilis. *Mol Microbiol*.

Salzberg, L.I., Y. Luo, A.B. Hachmann, T. Mascher & J.D. Helmann, (2011) The Bacillus subtilis GntR family repressor YtrA responds to cell wall antibiotics. *J Bacteriol* **193**: 5793-5801.

Schirner, K., Y.J. Eun, M. Dion, Y. Luo, J.D. Helmann, E.C. Garner & S. Walker, (2015) Lipid-linked cell wall precursors regulate membrane association of bacterial actin MreB. *Nat Chem Biol* **11**: 38-45.

Schmiedel, D. & W. Hillen, (1996) A Bacillus subtilis 168 mutant with increased xylose uptake can utilize xylose as sole carbon source. *Fems Microbiology Letters* **135**: 175-178.

Schneider, T. & H.G. Sahl, (2010) Lipid II and other bactoprenol-bound cell wall precursors as drug targets. *Curr Opin Investig Drugs* **11**: 157-164.

Sham, L.T., E.K. Butler, M.D. Lebar, D. Kahne, T.G. Bernhardt & N. Ruiz, (2014) Bacterial cell wall. MurJ is the flippase of lipid-linked precursors for peptidoglycan biogenesis. *Science* **345**: 220-222.

Slack, F.J., J.P. Mueller & A.L. Sonenshein, (1993) Mutations That Relieve Nutritional Repression of the *Bacillus subtilis* Dipeptide Permease Operon. *Journal of Bacteriology* **175**: 4605-4614.

Sterlini, J.M. & J. Mandelstam, (1969) Commitment to sporulation in Bacillus subtilis and its relationship to development of actinomycin resistance. *Biochem J* **113**: 29-37.

Tatar, L.D., C.L. Marolda, A.N. Polischuk, D. van Leeuwen & M.A. Valvano, (2007) An Escherichia coli undecaprenyl-pyrophosphate phosphatase implicated in undecaprenyl phosphate recycling. *Microbiology* **153**: 2518-2529.

Touze, T., D. Blanot & D. Mengin-Lecreulx, (2008a) Substrate specificity and membrane topology of Escherichia coli PgpB, an undecaprenyl pyrophosphate phosphatase. *J Biol Chem* **283**: 16573-16583.

Touze, T., A.X. Tran, J.V. Hankins, D. Mengin-Lecreulx & M.S. Trent, (2008b) Periplasmic phosphorylation of lipid A is linked to the synthesis of undecaprenyl phosphate. *Mol Microbiol* **67**: 264-277.

Ursell, T.S., J. Nguyen, R.D. Monds, A. Colavin, G. Billings, N. Ouzounov, Z. Gitai, J.W. Shaevitz & K.C. Huang, (2014) Rod-like bacterial shape is maintained by feedback between cell curvature and cytoskeletal localization. *Proc Natl Acad Sci U S A* **111**: E1025-1034.

Vellanoweth, R.L. & J.C. Rabinowitz, (1992) The influence of ribosome-binding-site elements on translational efficiency in Bacillus subtilis and Escherichia coli in vivo. *Mol Microbiol* **6**: 1105-1114.

Xayarath, B. & J. Yother, (2007) Mutations blocking side chain assembly, polymerization, or transport of a Wzy-dependent Streptococcus pneumoniae capsule are lethal in the absence of suppressor mutations and can affect polymer transfer to the cell wall. *J Bacteriol* **189**: 3369-3381.

Zhu, W., Y. Zhang, W. Sinko, M.E. Hensler, J. Olson, K.J. Molohon, S. Lindert, R. Cao, K. Li, K. Wang, Y. Wang, Y.L. Liu, A. Sankovsky, C.A. de Oliveira, D.A. Mitchell, V. Nizet, J.A. McCammon & E. Oldfield, (2013) Antibacterial drug leads targeting isoprenoid biosynthesis. *Proc Natl Acad Sci U S A* **110**: 123-128.

2.8 Supplemental Material

2.8.1 Supplemental Figures

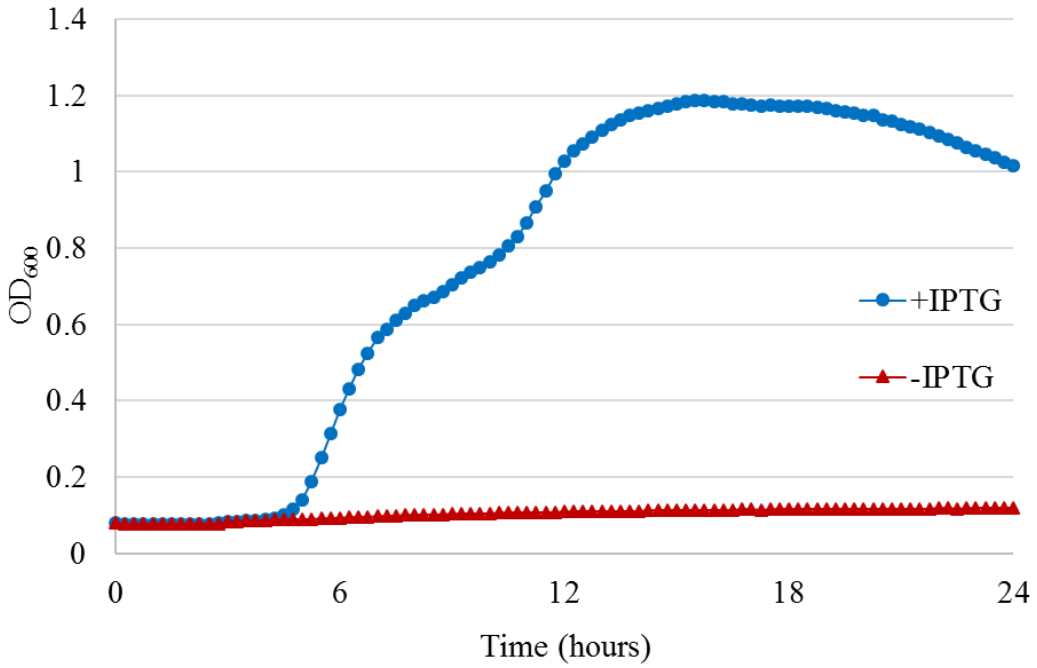

Figure S2.1. Overexpression of YodM rescues growth defect of a *uppP bcrC* double mutant. Growth of *yodM* overexpression strain in absence and presence of 1 mM IPTG. An ectopic copy of *yodM* was overexpressed from the *Pspac(hy)* promoter with a strong RBS and ATG as start codon.

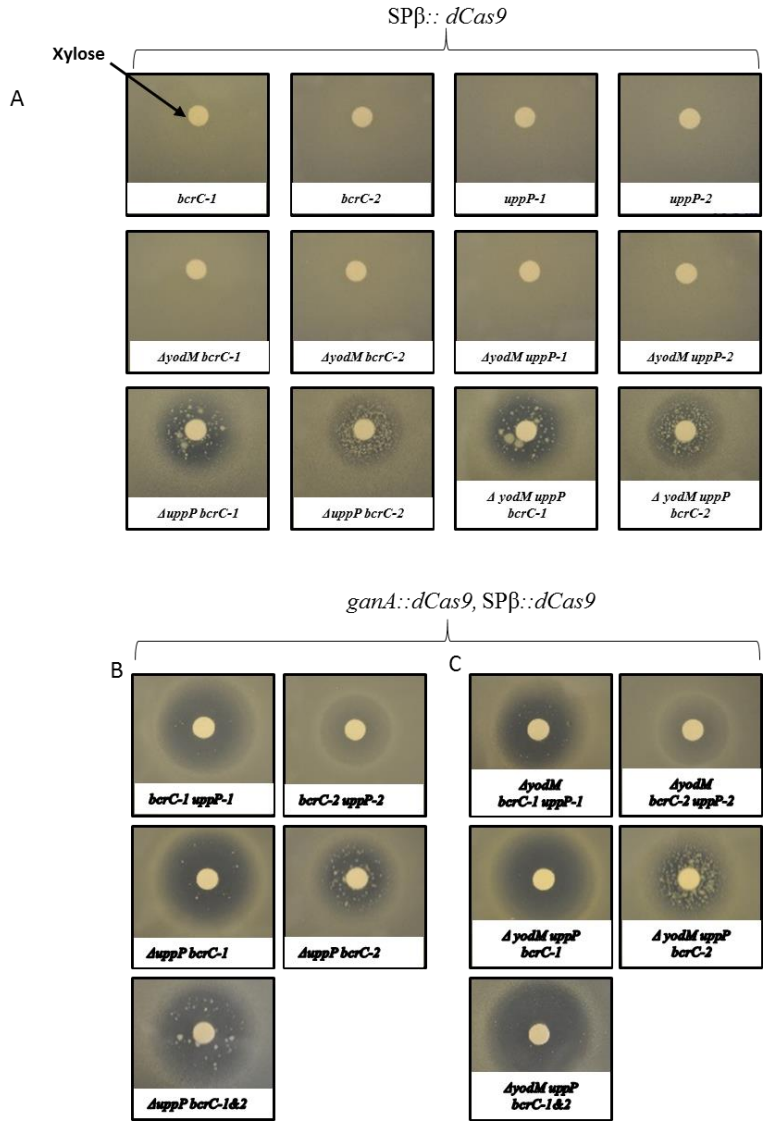

Figure S2.2 A dCas9 merodiploid reduces the frequency of spontaneous suppressor mutations.

Photos of disk diffusion assay of WT and mutant strains. Cells were grown on LB plates with xylose added onto the filter paper disk. **(A).** Strains having single *dCas9* in SPβ showed similar phenotype as having single *dCas9* in *ganA* site, but had more of suppressors inside the clear zone. **(B).** Mutants containing two *dCas9* is more sensitive to induction of *dCas9* by addition of xylose. With chromosomal copy of *yodM* intact, there were still many suppressors inside the clear zone. **(C).**Mutants having two copies of *dCas9* show similar phenotype in Δ*yodM* background. The number of suppressors is much smaller in *ΔuppP bcrC*-1&2 background lacking *yodM*.

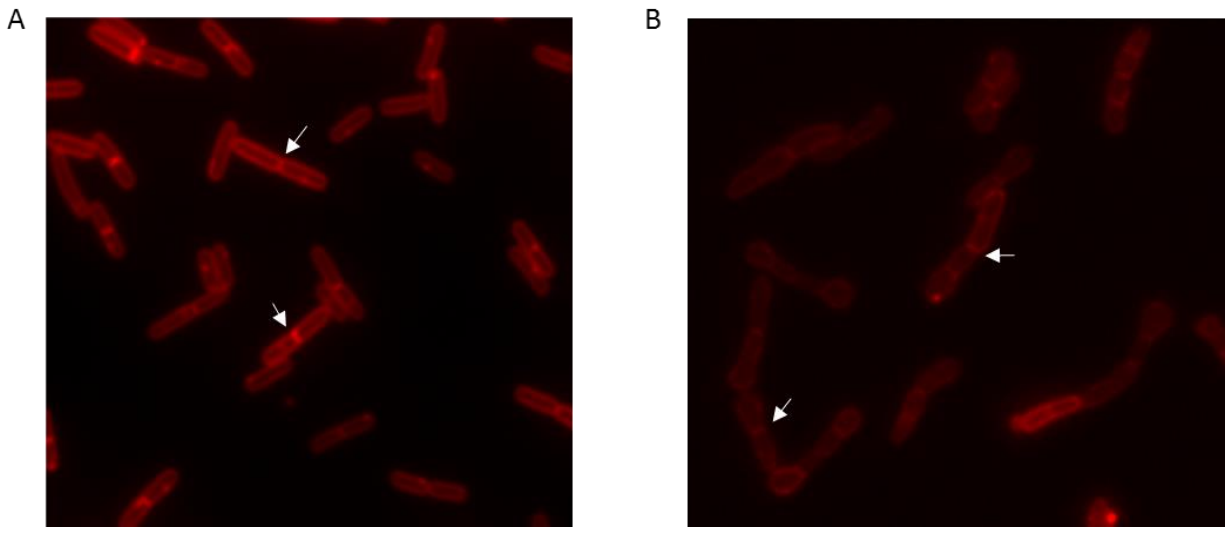

Figure S2.3. Membrane stain of **WT (A)** and **optimized depletion strain (B)** after growing in presence of xylose. Cells were growing in CH medium containing 2% xylose and membrane was strained by FM5-95. Images were taken 4 hours after addition of xylose. Depletion strain (B) still formed septum (arrows) as WT strain (A) but exhibited bulging phenotype after depletion of UPP-Pases.

2.8.2 Supplemental Tables

Table S2.1. Homologs of *E.coli* UPP-Pases in *B.subtilis*

E.coli **UPP-Pase**	***B.subtilis*** **Homologue**	**Query coverage**	**E Value**	**Identity**
BacA	UppP	93%	5.00E-79	48%
YbjG	BcrC	78%	3.00E-18	30%
	YodM	33%	0.003	36%
PgpB	YodM	23%	0.01	34%
YeiU (LpxT)	BcrC	63%	0.005	23%

Table S2.2. IPTG-regulated expression of candidate UPP-Pases with altered RBS sequences in a *bcrC uppP* double mutant

Ectopic copy of gene[a]	RBS*	Growth[b]	
$P_{spac(hy)}$-*bcrC*		*+IPTG*	*-IPTG*
Native RBS	aaat**gtaaaagg** *tgattat* ttg	+	+
Native 6[c]	aaat**gtaaaagg** *gattat* ttg	(-)	
Native 5	aaat**gtaaaagg** *attat* ttg	(-)	
Native 4	aaat**gtaaaagg** *ttat* ttg	(-)	
$P_{spac(hy)}$-*uppP*			
Native RBS	aat**ggggagaa** *tcaaaatc* atg	(-)	
Strong[c] 7	**taaggagg** *caaaatc* atg	+	+
Strong 6	**taaggagg** *aaaatc* atg	+	+
Strong 5	**taaggagg** *aaatc* atg	+	+
Strong 4	**taaggagg** *aatc* atg	+	+
$P_{spac(hy)}$-*yodM*			
Native RBS and Start Codon	t**tgaggtgg** *ttaaaa* ttg	(-)	
Strong 7	**taaggagg** *tgattat* atg	+	-

*Predicted Ribosome Binding Site (RBS) is in **bold**, spacer region between RBS and start codon is in *italic*, and start codon is underlined. For purposes of clarity, one or more space was used between RBS, spacer region and start codon.

[a] Transformation deleting *bcrC* and *uppP* in two consecutive steps was performed in strains with ectopic copy of indicated gene. In a successful transformation, resulting strain should miss both chromosomal copy of *bcrC* and *uppP*.

[b] "+" indicates growth and "-" indicates no growth. (-) indicates that the strain could not be constructed due to failure to get transformants even under IPTG-inducing conditions.

[c] Number after "strong" or "native" is the number of base pairs for the spacer region.

Table S2.3. Percentage of suppressor outgrowth in selected strain backgrounds

Strain Number	Genotype	Number of cultures with outgrowth [a]	Percentage of cultures with outgrowth [b]
HB17177	*ganA*::*dCas9*, *bcrC*-1, *uppP*-1	30	100%
HB17190	*ganA*::*dCas9*, *yodM* null markerless, *uppP* null markerless, *bcrC*-1, *bcrC*-2	30	100%
HB17221	*ganA*::*dCas9*, *SPβ*::*dCas9*, *bcrC*-1, *uppP*-1	22	73.3%
HB17235	*ganA*::*dCas9*, *SPβ*::*dCas9*, *yodM*, *uppP* null markerless, *bcrC*-1, *bcrC*-2	2	6.7%

a. Suppressor outgrowth was monitored using an automated BioScreen growth analyzer. Approximately $4x10^4$ logarithmic phase cells were inoculated into 200 µl of LB medium supplemented with final concentration of 2% (w/v) xylose. 30 replicate cultures (3 biological replicates containing 10 technical replicates each) were used for each strain. Outgrowth is defined as OD_{600}>0.3 after 12 hours of incubation.

b. Percentage of outgrowth cultures was calculated by dividing number of cultures with outgrowth by the total number (30) of cultures.

Table S2.4. Strains, plasmids and primers used in this study

Strain Number	Genotype
168	Wild Type
ZB307	*trp*$^{+}$ *phe*$^{+}$ SPβc2Δ2::Tn917::pSK10Δ6
HB17042	*bcrC*::MLS
HB17043	*uppp*::spec
HB17044	*yodM*::tet
HB17046	P$_{spac(hy)}$-*uppP*
HB17045	P$_{spac(hy)}$-*bcrC*
HB17047	P$_{spac(hy)}$-*yodM*
HB17071	P$_{spac(hy)}$-*uppP, bcrC*::*MLS*
HB17072	P$_{spac(hy)}$-*uppP, uppP*::*spec*
HB17073	P$_{spac(hy)}$-*yodM, bcrC*::*MLS*
HB17074	P$_{spac(hy)}$-*yodM, uppP*::*spec*
HB17075	P$_{spac(hy)}$-*bcrC*, bcrC*::*MLS, uppP*::*spec*
HB17076	P$_{spac(hy)}$-*bcrC** RBS *wk6*
HB17077	P$_{spac(hy)}$-*bcrC** RBS *wk5*
HB17078	P$_{spac(hy)}$-*bcrC** RBS *wk4*
HB17079	P$_{spac(hy)}$-*uppP** RBS *st7*
HB17080	P$_{spac(hy)}$-*uppP** RBS *st6*
HB17081	P$_{spac(hy)}$-*uppP** RBS *st5*
HB17082	P$_{spac(hy)}$-*uppP** RBS *st4*
HB17083	P$_{spac(hy)}$-*bcrC** RBS *wk6, bcrC*::*MLS*
HB17084	P$_{spac(hy)}$-*bcrC** RBS *wk5, bcrC*::*MLS*
HB17085	P$_{spac(hy)}$-*bcrC** RBS *wk4, bcrC*::*MLS*
HB17086	P$_{spac(hy)}$-*uppP** RBS *st7, bcrC*::*MLS*
HB17087	P$_{spac(hy)}$-*uppP** RBS *st6, bcrC*::*MLS*
HB17088	P$_{spac(hy)}$-*uppP** RBS *st5, bcrC*::*MLS*
HB17089	P$_{spac(hy)}$-*uppP** RBS *st4, bcrC*::*MLS*
HB17090	P$_{spac(hy)}$-*bcrC** RBS *wk6, uppP*::*spec*
HB17091	P$_{spac(hy)}$-*bcrC** RBS *wk5, uppP*::*spec*
HB17092	P$_{spac(hy)}$-*bcrC** RBS *wk4, uppP*::*spec*
HB17093	P$_{spac(hy)}$-*uppP** RBS *st7, uppP*::*spec*
HB17094	P$_{spac(hy)}$-*uppP** RBS *st6, uppP*::*spec*
HB17095	P$_{spac(hy)}$-*uppP** RBS *st5, uppP*::*spec*
HB17096	P$_{spac(hy)}$-*uppP** RBS *st4, uppP*::*spec*
HB17132	*bcrC* null makerless
HB17160	*uppP* null markerless
HB17162	*yodM* null markerless
HB17164	*bcrC, yodM* null markerless
HB17166	*uppP, yodM* null markerless

HB17167	*ganA*::*dCas9*
HB17168	*ganA*::*dCas9*, *bcrC* null markerless
HB17169	*ganA*::*dCas9*, *uppP* null markerless
HB17170	*ganA*::*dCas9*, *yodM* null markerless
HB17171	*ganA*::*dCas9*, *bcrC*, *yodM* null markerless
HB17172	*ganA*::*dCas9*, *uppP*, *yodM* null markerless
HB17173	*ganA*::*dCas9*, *bcrC*-1
HB17174	*ganA*::*dCas9*, *bcrC*-2
HB17175	*ganA*::*dCas9*, *uppP*-1
HB17176	*ganA*::*dCas9*, *uppP*-2
HB17177	*ganA*::*dCas9*, *bcrC*-1, *uppP*-1
HB17178	*ganA*::*dCas9*, *bcrC*-2, *uppP*-2
HB17179	*ganA*::*dCas9*, *uppP* null markerless, *bcrC*-1
HB17180	*ganA*::*dCas9*, *uppP* null markerless, *bcrC*-2
HB17181	*ganA*::*dCas9*, *uppP* null markerless, *bcrC*-1, *bcrC*-2
HB17182	*ganA*::*dCas9*, *yodM* null markerless, *bcrC*-1
HB17183	*ganA*::*dCas9*, *yodM* null markerless, *bcrC*-2
HB17184	*ganA*::*dCas9*, *yodM* null markerless, *uppP*-1
HB17185	*ganA*::*dCas9*, *yodM* null markerless, *uppP*-2
HB17186	*ganA*::*dCas9*, *yodM* null markerless, *bcrC*-1, *uppP*-1
HB17187	*ganA*::*dCas9*, *yodM* null markerless, *bcrC*-2, *uppP*-2
HB17188	*ganA*::*dCas9*, *yodM* null markerless, *uppP* null markerless, *bcrC*-1
HB17189	*ganA*::*dCas9*, *yodM* null markerless, *uppP* null markerless, *bcrC*-2
HB17190	*ganA*::*dCas9*, *yodM* null markerless, *uppP* null markerless, *bcrC*-1, *bcrC*-2
HB17191	SPβ::*dCas9*
HB17192	SPβ::*dCas9*, *bcrC* null markerless
HB17193	SPβ::*dCas9*, *uppP* null markerless
HB17194	SPβ::*dCas9*, *yodM* null markerless
HB17195	SPβ::*dCas9*, *bcrC*, *yodM* null markerless
HB17196	SPβ::*dCas9*, *uppP*, *yodM* null markerless
HB17197	SPβ::*dCas9*, *bcrC*-1
HB17198	SPβ::*dCas9*, *bcrC*-2
HB17199	SPβ::*dCas9*, *uppP*-1
HB17200	SPβ::*dCas9*, *uppP*-2
HB17201	SPβ::*dCas9*, *bcrC*-1, *uppP*-1
HB17202	SPβ::*dCas9*, *bcrC*-2, *uppP*-2
HB17203	SPβ::*dCas9*, *uppP* null markerless, *bcrC*-1
HB17204	SPβ::*dCas9*, *uppP* null markerless, *bcrC*-2
HB17205	SPβ::*dCas9*, *uppP* null markerless, *bcrC*-1, *bcrC*-2
HB17206	SPβ::*dCas9*, *yodM* null markerless, *bcrC*-1
HB17207	SPβ::*dCas9*, *yodM* null markerless, *bcrC*-2
HB17208	SPβ::*dCas9*, *yodM* null markerless, *uppP*-1
HB17209	SPβ::*dCas9*, *yodM* null markerless, *uppP*-2

HB17210	SPβ::*dCas9*, *yodM* null markerless, *bcrC*-1, *uppP*-1
HB17211	SPβ::*dCas9*, *yodM* null markerless, *bcrC*-2, *uppP*-2
HB17212	SPβ::*dCas9*, *yodM* null markerless, *uppP* null markerless, *bcrC*-1
HB17213	SPβ::*dCas9*, *yodM* null markerless, *uppP* null markerless, *bcrC*-2
HB17214	SPβ::*dCas9*, *yodM* null markerless, *uppP* null markerless, *bcrC*-1, *bcrC*-2
HB17216	*ganA*::*dCas9*, SPβ::*dCas9*, *bcrC*-1
HB17217	*ganA*::*dCas9*, SPβ::*dCas9*, *bcrC*-2
HB17218	*ganA*::*dCas9*, SPβ::*dCas9*, *uppP*-1
HB17219	*ganA*::*dCas9*, SPβ::*dCas9*, *uppP*-2
HB17220	*ganA*::*dCas9*, SPβ::*dCas9*, *uppP* null markerless
HB17221	*ganA*::*dCas9*, SPβ::*dCas9*, *bcrC*-1, *uppP*-1
HB17222	*ganA*::*dCas9*, SPβ::*dCas9*, *bcrC*-2, *uppP*-2
HB17223	*ganA*::*dCas9*, SPβ::*dCas9*, *uppP* null markerless, *bcrC*-1
HB17224	*ganA*::*dCas9*, SPβ::*dCas9*, *uppP* null markerless, *bcrC*-2
HB17225	*ganA*::*dCas9*, SPβ::*dCas9*, *uppP* null markerless, *bcrC*-1, *bcrC*-2
HB17226	*ganA*::*dCas9*, SPβ::*dCas9*, *yodM* null markerless, *bcrC*-1
HB17227	*ganA*::*dCas9*, SPβ::*dCas9*, *yodM* null markerless, *bcrC*-2
HB17228	*ganA*::*dCas9*, SPβ::*dCas9*, *yodM* null markerless, *uppP*-1
HB17229	*ganA*::*dCas9*, SPβ::*dCas9*, *yodM* null markerless, *uppP*-2
HB17230	*ganA*::*dCas9*, SPβ::*dCas9*, *yodM*, *uppP* null markerless
HB17231	*ganA*::*dCas9*, SPβ::*dCas9*, *yodM* null markerless, *bcrC*-1, *uppP*-1
HB17232	*ganA*::*dCas9*, SPβ::*dCas9*, *yodM* null markerless, *bcrC*-2, *uppP*-2
HB17233	*ganA*::*dCas9*, SPβ::*dCas9*, *yodM*, *uppP* null markerless, *bcrC*-1
HB17234	*ganA*::*dCas9*, SPβ::*dCas9*, *yodM*, *uppP* null markerless, *bcrC*-2
HB17235	*ganA*::*dCas9*, SPβ::*dCas9*, *yodM*, *uppP* null markerless, *bcrC*-1, *bcrC*-2
HB17236	$P_{spac(hy)}$-*yodM** RBS st7
HB17237	$P_{spac(hy)}$-*yodM** RBS st7, *bcrC* null markerless
HB17239	$P_{spac(hy)}$-*yodM** RBS st7, *bcrC* null markerless, *uppP*::*spec*

Plasmid	**Description**
pPL82	Integration plasmid into *amyE* site
pJMP1	Integration plasmid containing *dCas9* into *ganA* site
pJMP2	Integration plasmid for sgRNA into *amyE* site
pJMP3	Integration plasmid for sgRNA into *thrC* site
pJPM122	Integration plasmid into modified SPβ phage strain ZB307
pSPβ::*dCas9*	Integration plasmid containing *dCas9* into modified SPβ phage strain ZB307
pJMP2-*bcrC*-2	pJMP2 with sgRNA *bcrC*-2
pJMP3-*bcrC*-1	pJMP3 with sgRNA *bcrC*-1
pJMP3-*uppP*-2	pJMP3 with sgRNA *uppP*-2
pJMP2-*uppP*-1	pJMP2 with sgRNA *uppP*-1

Primer Number	Name	Sequence
6048	*bcrC*-up-for	ACTTAACGATGCACGGGGAA
6049	*bcrC*-up-rev(mls)	GAGGGTTGCCAGAGTTAAAGGATCCCATGGATTGCTTTAAAAATTTCGT
6050	*bcrC*-down-for(mls)	CGATTATGTCTTTTGCGCAGTCGGCCGTGAGGATCTACGAAGCCA
6051	*bcrC*-down-rev	AGTGAAGACAGCGGAAACCA
6186	*uppP* up F	ACGATCGTGAACAGCACCTT
6189	*uppP* down R	TCCAAGACATTTTTGGCGGC
6221	*bcrC* depletion F XmaI	GATCCCCGGGTGTAAAAGGTGATTATTTGAACTAC
6222	*bcrC* depletion R XbaI	GATCTCTAGACTGTCTTGATTTCAGACGCC
6223	*uppP* depletion F XmaI	GATCCCCGGGTAATGGGGAGAATCAAAATC
6224	*uppP* depletion R XbaI	GATCTCTAGAAGGCTCGGAAAAGAGCCTTA
6233	*uppP* up R sepc	CGTTACGTTATTAGCGAGCCAGTCGGCGGCTACAAACAATTCCC
6234	*uppP* down F spec	CAATAAACCCTTGCCCTCGCTACGACTTGTCCCATTTGCAATCTATCG
6235	*yodM* Up F	GAGTGGCTTGAAACGGAGGA
6236	*yodM* up R tet	GAGAACAACCTGCACCATTGCAAGAAGAAACAAACTAACGGGCTTGT
6237	*yodM* Down F tet	GGGATCAACTTTGGGAGAGAGTTCCGAAAAGATTAAGCGGTTTCGAC
6238	*yodM* Down R	AAGGCGCAAAATCAACGCTT
6239	*yodM* F XmaI	GATCCCCGGGGCGGTCAGCTCCGGTTTTATT
6240	*yodM* R XbaI	GATCTCTAGAGCGTTTTTGCTGTGTTTTCCT
6254	*uppP* depletion F HindIII (st7)	GATCAAGCTTTAAGGAGGCAAAATCATGACTCTATGGGAATTG
6255	*uppP* depletion F HindIII (st6)	GATCAAGCTTTAAGGAGGAAAATCATGACTCTATGGGAATTGTTT
6256	*uppP* depletion F HindIII (st5)	GATCAAGCTTTAAGGAGGAAATCATGACTCTATGGGAATTGTTTG
6257	*uppP* depletion F HindIII (st4)	GATCAAGCTTTAAGGAGGAATCATGACTCTATGGGAATTGTTTG
6258	*bcrC* depletion F HindIII (wk6)	GATCAAGCTTTGTAAAAGGGATTATTTGAACTACGAAATTTTTAAAGC
6259	*bcrC* depletion F HindIII (wk5)	GATCAAGCTTTGTAAAAGGATTATTTGAACTACGAAATTTTTAAAGC
6260	*bcrC* depletion F HindIII (wk4)	GATCAAGCTTTGTAAAAGGTTATTTGAACTACGAAATTTTTAAAGC
6411	CRISPRi *bcrC*-1 F	AATTGTGATGAGATAGTCCAGTTTTAGAGCTAGAAATAGCAAGTTAAAATAAGGC
6412	CRISPRi *bcrC*-2 F	TTCCGTGATGAAGACCATAAGTTTTAGAGCTAGAAATAGCAAGTTAAAATAAGGC
6413	CRISPRi *uppP*-1 F	CACGATAGCTACTGCTAAAAGTTTTAGAGCTAGAAATAGCAAGTTAAAATAAGGC
6414	CRISPRi *uppP*-2 F	AGCCCAGTAAATTTAAAATTGTTTTAGAGCTAGAAATAGCAAGTTAAAATAAGGC
6415	CRISPRi universal R	ACATTTATTGTACAACACGAGCC
6424	CRISPRi check F	TGACAAAAATGGGCTCGTGT
6425	CRISPRi check R	ACTTCTGAGTTCGGCATGGG
6426	*yodM* F HindIII (RBS st7)	GATCAAGCTTTAAGGAGGTGATTATATGTACAAGCCCGTTAGTTTGTTTC
6429	*dCas9* check F	CCGTCGTTGGAACTGCTTTG
6430	*dCas9* check R	AGCATCCGTTTACGACCGTT
6326	BKE MLS check R	TTTTCTCGTTCATAGTAGTTCCTCC

Chapter 3. Aspartate deficiency limits peptidoglycan synthesis and sensitizes cells to antibiotics targeting cell wall synthesis in *Bacillus subtilis*

3.1 Summary

Peptidoglycan synthesis is an important target for antibiotics and relies on intermediates derived from central metabolism. As a result, alterations of metabolism may affect antibiotic sensitivity. An *aspB* mutant is auxotrophic for aspartate (Asp) and asparagine (Asn) and lyses when grown on Difco sporulation medium (DSM), but not on LB medium. Genetic and physiological studies, supported by amino acid analysis, reveal that cell lysis in DSM results from Asp limitation due to a relatively low Asp and high glutamate (Glu) concentrations, with Glu functioning as a competitive inhibitor of Asp uptake by the major Glu/Asp transporter GltT. Lysis can be specifically suppressed by supplementation with 2,6-diaminopimelate (DAP), which is imported by two different cystine uptake systems. These studies suggest that aspartate limitation depletes the peptidoglycan precursor meso-2,6-diaminopimelate (mDAP), inhibits peptidoglycan synthesis, upregulates the cell envelope stress response mediated by σ^M and eventually leads to cell lysis. Aspartate limitation sensitizes cells to antibiotics targeting late steps of PG synthesis, but not steps prior to the addition of mDAP into the pentapeptide sidechain. This work highlights the ability of perturbations of central metabolism to sensitize cells to peptidoglycan synthesis inhibitors.

3.2 Introduction

Bacillus subtilis is a metabolically versatile soil bacterium and can synthesize all 20 amino acids. Amino acids are essential for synthesis of proteins and other macromolecules, and many can also be catabolized to yield intermediates of the tricarboxylic acid (TCA) cycle. Amino acid metabolism is governed by master regulators, such as CcpA, TnrA, and CodY, working in concert

with pathway-specific regulation by transcriptional, translational and post-translational mechanisms in a complex, interlinked network (Geiger & Wolz, 2014, Brantl & Licht, 2010, Sonenshein, 2007).

Glutamate (Glu) serves as a central link between nitrogen and carbon metabolism and, together with aspartate, functions as a key branch point amino acid linking amino acid biosynthesis with central carbon metabolism (Figure 3.1). Glutamate is synthesized by glutamate synthase (also known as glutamine oxoglutarate aminotransferase, GOGAT), encoded by *gltAB* in *B. subtilis*, which converts one molecule each of Gln and α-ketoglutarate into two molecules of Glu. Glutamate can be imported into the cell by GltT (Zaprasis *et al.*, 2015), GltP (Tolner *et al.*, 1995) and YveA (Lorca *et al.*, 2003).

Glutamate homeostasis is tightly regulated in *B. subtilis* (Gunka & Commichau, 2012). Expression of *gltAB* is under control of GltC, which senses the ratio between Glu (the product) and α-ketoglutarate (the substrate) (Picossi *et al.*, 2007). When growing on medium containing glucose and ammonium, cells are rich in TCA cycle intermediates and GltC is bound to α-ketoglutarate and activates expression of *gltAB* (Commichau *et al.*, 2007, Picossi *et al.*, 2007). When intracellular Glu is high, Glu binds to GltC and represses *gltAB* (Picossi *et al.*, 2007). In the presence of Arg or other amino acids that can be metabolized into Glu, the glutamate dehydrogenase RocG is induced and degrades Glu into α-ketoglutarate and ammonium (Belitsky & Sonenshein, 1998). GltC can also physically interact with RocG and it was suggested that this interaction affects GltC activity (Commichau *et al.*, 2007, Picossi *et al.*, 2007). *B. subtilis* 168 contains two genes encoding glutamate dehydrogenases, a functional *rocG* gene and cryptic *gudB* gene (Belitsky & Sonenshein, 1998). When a *rocG* null mutant grows on complex sporulation medium, there is strong selection for mutations that regenerate functional *gudB* (Gunka *et al.*,

2012), highlighting the importance of maintaining Glu homeostasis in the cell. In addition to serving as a major nitrogen donor and anion in the cell and a precursor for protein synthesis, Glu is also important for cell wall synthesis. D-glutamate, synthesized by glutamate racemase from L-glutamate, is incorporated into the pentapeptide side-chain of the peptidoglycan (PG) precursor lipid II. Mutations that affect Glu homeostasis have been found to affect resistance to antibiotics targeting early (fosfomycin) and late (beta-lactams) stages of PG synthesis (Lee *et al.*, 2012).

In contrast with Glu, synthesis of Asp is not known to be tightly regulated. The main pathway of Asp synthesis in *B. subtilis* is through aspartate transaminase AspB, which transfers an amino group from Glu to oxaloacetate to form Asp (Figure 3.1) (Ochi *et al.*, 1981). AspB is constitutively and highly expressed, and is one of the most abundant proteins in vegetative cells (Eymann *et al.*, 2004). Asp is imported by GltT, GltP and YveA (Zaprasis *et al.*, 2015), which are also involved in Glu uptake. In *B. subtilis*, Asp can also be generated from Asn by L-asparaginases AnsA and AnsZ (Sun & Setlow, 1991). However, their regulation indicates that these asparaginases function in degradation of Asn (and then Asp) ultimately yielding fumarate (Daniel & Errington, 1993; Fisher & Wray, 2002).

Aspartate is the starting point for synthesis of the Asp family amino acids, which include Asn, Lys, Thr, Met and Ile. The pathway that generates Lys includes both meso-diaminopimelate (mDAP), which is used in PG synthesis in many bacteria, and a branch point to dipicolinate, important for heat resistance of endospores (Daniel & Errington, 1993, Chen *et al.*, 1993) (Figure 1). The regulation of Asp usage mostly results from feedback inhibition (Dumas *et al.*, 2012). For example, three aspartokinases convert L-aspartate into L-aspartyl-4-phosphate, the first committed step for generating Asp family amino acids (except Asn). Aspartokinase I (DapG) is feedback inhibited by mDAP but not L,L-diaminopimelate (DAP) (Rosner & Paulus, 1971, Chen *et al.*,

1993), aspartokinase II (LysC) by Lys (Zhang *et al.*, 1990), and aspartokinase III (ThrD) by the simultaneous presence of Thr and Lys (Kobashi *et al.*, 2001, Graves & Switzer, 1990). The branch point enzyme Hom initiates the synthesis of Met, Thr, and Ile, and can be feedback inhibited by these products (Gutierrez-Preciado *et al.*, 2009).

In bacteria, the amino acid composition of the stem pentapeptide of PG is typically L-Ala_1-D-Glu_2-$mDAP_3$-D-Ala_4-D-Ala_5, with the third amino acid being L-lysine in some bacteria (Zhao *et al.*, 2017). Whether $mDAP_3$ or L-Lys_3 is used is mainly dependent on the substrate specificity of the corresponding ligase (MurE), as well as the cytoplasmic concentration of L-lysine versus mDAP (Ruane *et al.*, 2013). Because of its essential role in PG synthesis, the stem pentapeptide serves as an important target for antibiotics including D-cycloserine, vancomycin and teicoplanin. D-cycloserine is a mimic of D-Ala, and inhibits D-Ala-D-Ala synthesis by inhibiting both alanine racemase (Alr) and D-Ala-D-Ala ligase (Ddl) (Strominger *et al.*, 1960). Vancomycin inhibits PG synthesis by binding to the D-Ala_4-D-Ala_5 termini of stem peptides thereby preventing transpeptidation (Arthur *et al.*, 1996).

In this work, we characterized the growth properties of a *B. subtilis aspB* mutant in a variety of nutrient conditions, which revealed that Asp limitation under otherwise nutrient rich conditions leads to depletion of mDAP and cell lysis. Aspartate limitation is exacerbated by high concentrations of Glu, which competitively inhibits Asp import. Depletion of mDAP can be rescued by addition of its precursor DAP, which is imported through two cystine uptake systems, TcyABC and TcyP. Under these conditions, Asp deficiency sensitizes cells to antibiotics targeting late steps of PG synthesis, thereby highlighting the intimate connection between central metabolism, PG synthesis and antibiotic susceptibility.

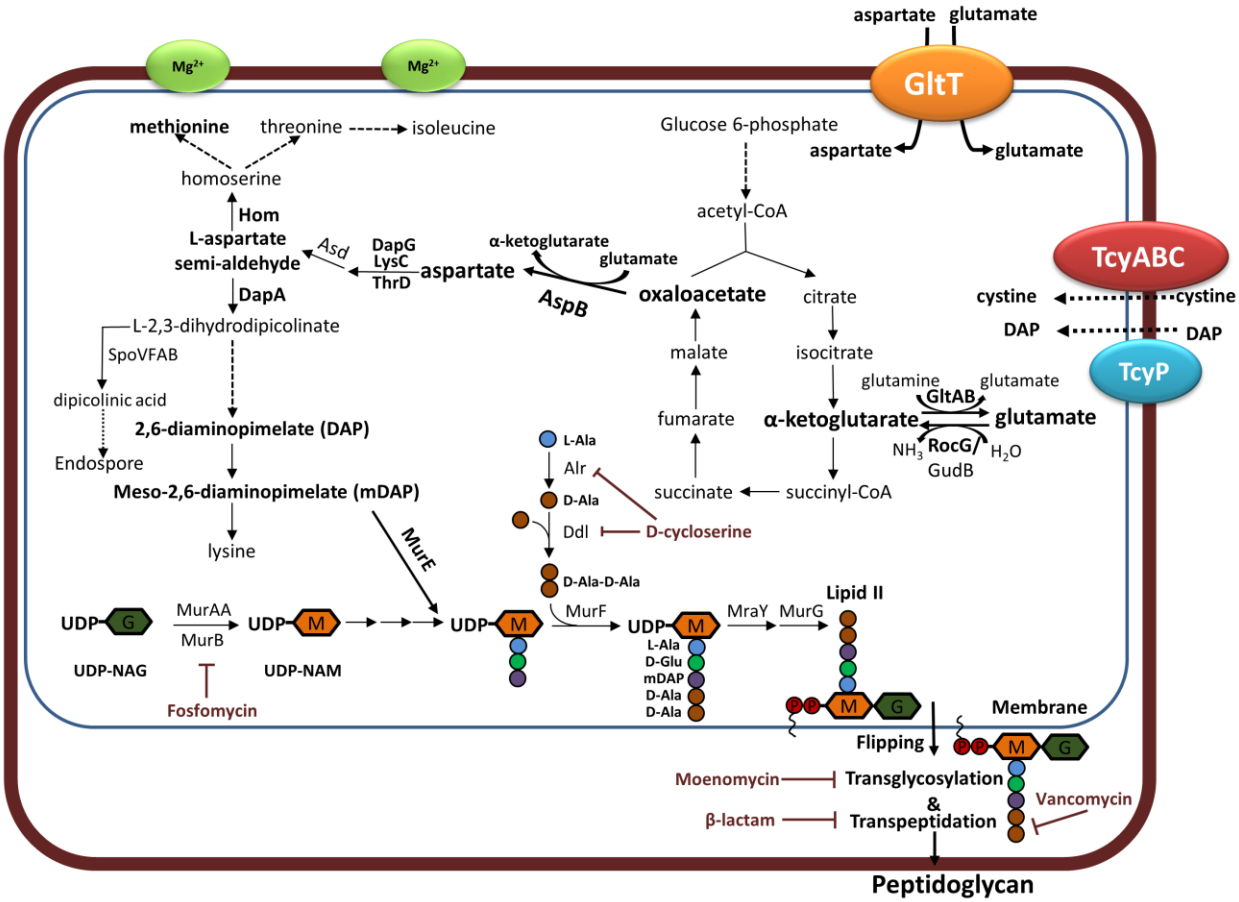

Figure 3.1. Metabolic pathways relevant to this study. Cofactors such as NAD^+/NADH are not shown in the reactions for simplicity. Solid lines indicate steps requiring a single enzyme, and dashed lines indicate multiple enzymatic reactions between two compounds. Other processes, such as uptake of cystine or DAP or incorporation of dipicolinic acid into endospore, are indicated with dotted lines. Fosfomycin inhibits the synthesis of UDP-N-acetylmuramic acid (UDP-NAM) from UDP-N-acetylglucosamine (UDP-NAG) by inactivating MurAA. D-cycloserine mimics D-Ala and inhibits both the alanine racemase (Alr) and D-Ala-D-Ala ligase (Ddl), which form D-Ala-D-Ala to be added to complete the pentapeptide side chain. After synthesis at the cytoplasmic membrane, lipid II needs to be flipped to the outside of the membrane by lipid II flippase (the flipping step) and oligomerized into glycan strands (transglycosylation). The glycan strands are then crosslinked by the transpeptidase activity of penicillin binding proteins (PBP) into the mesh-like structure of peptidoglycan (transpeptidation). Vancomycin binds to the D-Ala-D-Ala motif of lipid II and prevent transpeptidation. β-lactam antibiotics such as cefuroxime (CEF) bind to PBPs and prevent transpeptidation. Mg^{2+} can bind to and stabilize the cell envelope even under conditions of reduced peptidoglycan synthesis.

3.3 Results

3.3.1 An aspartate transaminase mutant lyses on Difco sporulation medium (DSM)

Moenomycin (MOE) is an antibiotic that inhibits the transglycosylase activity of class A PBPs for peptidoglycan synthesis (Figure 3.1). During a transposon library selection for MOE resistant (MOE^R) mutants, we identified multiple independent insertions in *ypmB (*Hachmann, 2010*),* encoding a membrane protein of unknown function. A *ypmB* mutant has recently been shown to suppress the tetracycline sensitivity of an *ezrA* mutation (and the name *tseB* was therefore proposed) and has a reduced cell length (Gamba *et al.*, 2015). However, the physiological function of YpmB remains unknown.

Interestingly, when grown on Difco sporulation medium (DSM) plates (a medium that induces sporulation), a *ypmB*::*mls* mutant exhibited pronounced cell lysis (Guariglia, 2013). Since *ypmB* is the second gene in a three-gene operon (*ypmA-ypmB(tseB)-aspB*) (Figure 3.2A), we tested if the MOE^R and DSM lysis phenotypes were due to a polar effect on the downstream *aspB* gene. The MOE^R phenotype of the *ypmB*::*mls* mutant can be suppressed by ectopic expression of *ypmB* (cells become MOE sensitive), but not *aspB* (Figure 3.2B). Indeed, ectopic expression of *aspB* increased MOE^R rather than restoring sensitivity (Figure 3.2B). In contrast, the DSM lysis phenotype was suppressed by *aspB,* but not *ypmB* (Figure 3.2C, D). We conclude that MOE^R results from lack of *ypmB,* but the DSM lysis phenotype results from reduced expression of *aspB.* The mechanism underlying the increased MOE^R of the *ypmB* mutant strain is not yet clear, but we note that YpmB is predicted to have PEPSY domains that are implicated in regulation of peptidase and perhaps other enzymatic activities of cell-membrane localized proteins (Yeats *et al.*, 2004, Gamba *et al.*, 2015). Here, we focus on the role of AspB in preventing cell lysis on DSM.

Since the DSM lysis phenotype of the *ypmB*::*mls* mutant strain appeared to result from polarity, we next tested the growth properties of an *aspB* null mutant. When grown on a DSM plate at 37˚C overnight, an *aspB* null mutant lysed and this phenotype was complemented by ectopic expression of *aspB* (Figure 3.2C). When grown in liquid DSM, an *aspB* null mutant grew to OD_{600} ~0.25 and lysed back to OD_{600} ~0.1 (Figure 3.2D), suggestive of nutrient limitation. In comparison, an *aspB* mutant grew almost as well as the *B. subtilis* 168 parent strain (WT) in LB medium (Figure 3.2B), which is richer in amino acids (Table 3.1).

The *aspB* gene encodes aspartate transaminase (interconverting L-glutamate and oxaloacetate to with L-aspartate and α-ketoglutarate; Figure 3.1), and an *aspB* null mutant is an Asp/Asn auxotroph (Figure S3.1A, B), as previously reported (Ochi *et al.*, 1981). Supplementation of DSM with 10 mM Asp (final concentration) greatly increased cell yield and completely suppressed lysis (Figure 3.3A), suggesting that limitation for Asp may trigger lysis. Asn can be converted to Asp by two asparaginases, AnsA and AnsZ (Fisher & Wray, 2002). Consistently, addition of 10 mM Asn (final concentration) also suppressed the lysis phenotype in DSM (Figure 3.3A).

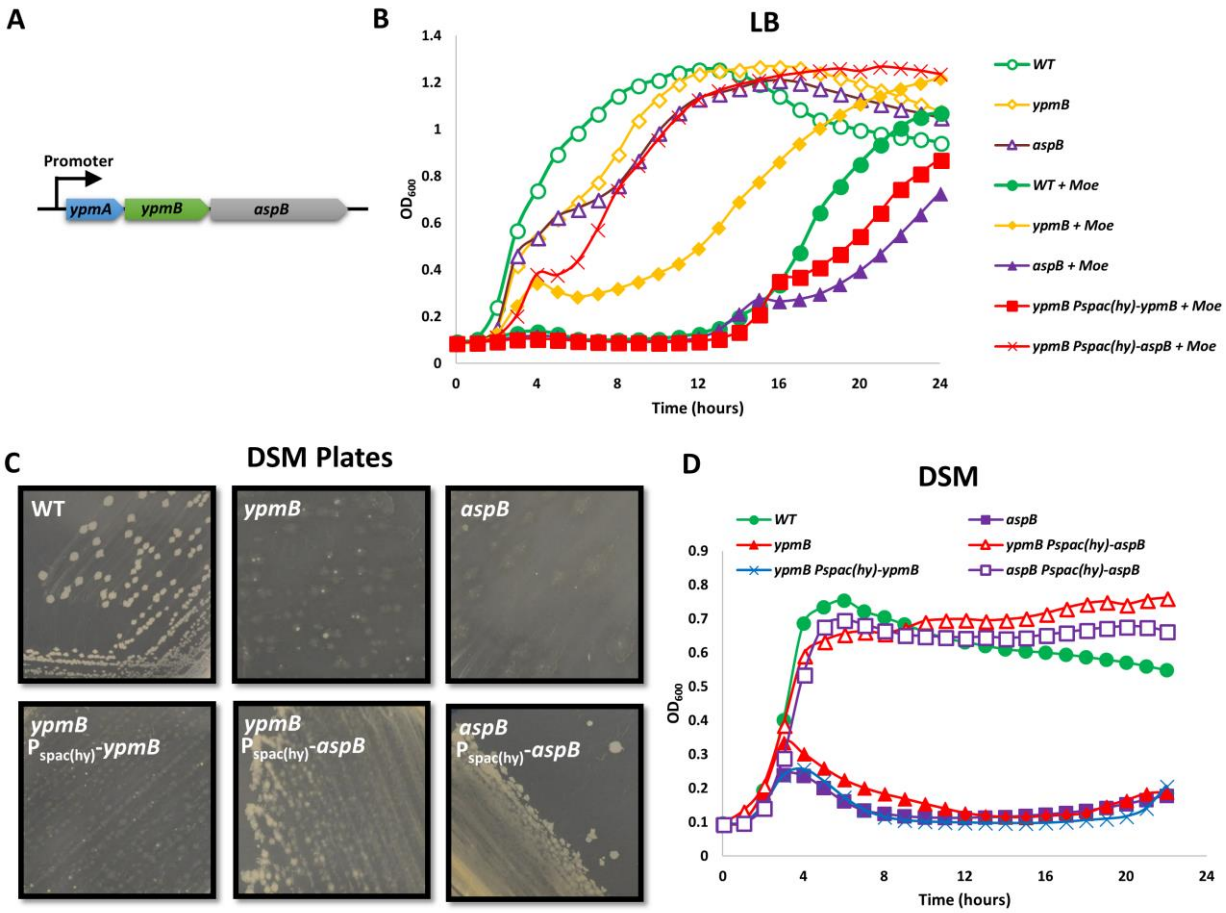

Figure 3.2. Dissection of phenotypes caused by *ypmB* and *aspB* mutations.

A. Genetic arrangement of the *ypmAypmBaspB* operon. **B.** Representative growth curves of strains in liquid LB with or without 1 μg ml^{-1} moenomycin. **C**. Colony morphology of strains on DSM plates after 20 hours of incubation at 37˚C. **D**. Representative growth curves of strains in liquid DSM. 1 mM final concentration of IPTG are used to induce $P_{spac(hy)}$ promoter. All growth curves were measured at least 3 times with similar results. A representative measurement is shown. Strains used were *ypmB*::*mls* **(**HB12259), Δ*aspB* (HB17401), *ypmB*::*mls* $P_{spac(hy)}$-*ypmB* **(**HB22913), *ypmB*::*mls* $P_{spac(hy)}$-*aspB* (HB17062), and *aspB*::*kan* $P_{spac(hy)}$-*aspB* (HB17060). Note that indistinguishable phenotypes were observed for the Δ*aspB* and *aspB*::*kan* strains.

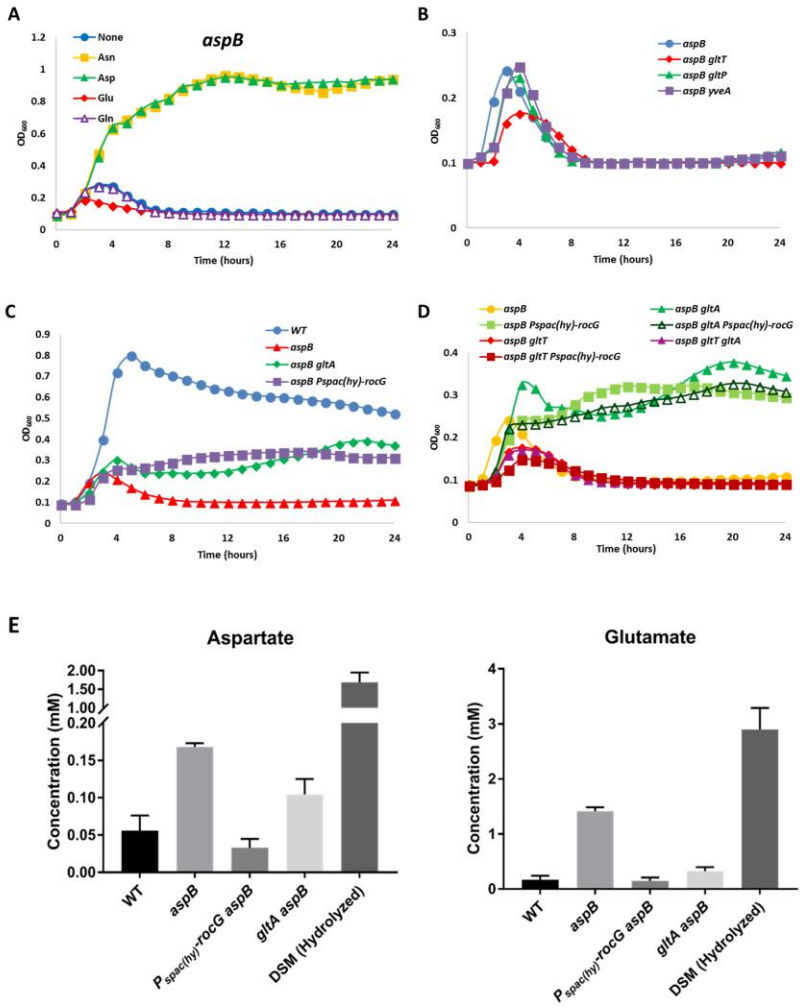

Figure 3.3. Lysis of the *aspB* mutant results from depletion of Asp and competition with Glu for GltT. Representative growth curves of *aspB* mutants in DSM:

A. Effect of supplementation with 10 mM (final concentration) of the following amino acids: Asn, asparagine; Asp, aspartate; Glu, glutamate; Gln, glutamine. **B.** Effects of mutation of each of the known glutamate/aspartate importers. **C**. Effects of mutations affecting intracellular Glu synthesis and degradation. **D.** Effects of mutations in panel C combined with or without *gltT*. **E.** Residual concentration of Asp and Glu in DSM medium after growth of 24 hours of indicated bacterial strains, as well as acid hydrolyzed medium. The data is represented as the mean plus and minus one standard error of the mean.

Table 3.1. Amino Acid Composition of LB and DSM

Amino Acids[e] (mM)	LB[a]	Hydrolyzed LB[b]	DSM[a]	Hydrolyzed DSM[b]
Alanine	1.47	1.78	0.38	2.72
Arginine	1.34	0.81	0.52	1.45
Asparagine	0.49	0.11[c]	0.08	0.14[c]
Aspartate	0.55	3.39	0.14	1.68
Glutamine	4.50	5.51[c]	0.47	1.34[c]
Glutamate	2.32	7.17	0.93	2.90
Glycine	0.71	1.18	0.26	5.77
Histidine	0.33	0.88	0.07	0.65
Isoleucine	0.83	3.91	0.27	0.89
Leucine	1.75	2.60	0.32	1.23
Lysine	3.53	4.74	0.42	1.16
Methionine[d]	0.40	0.82	0.01	0.01
Phenylalanine	0.99	2.96	0.37	0.75
Proline	0.33	4.54	0.13	3.12
Serine[d]	0.88	3.36	0.30	1.50
Threonine[d]	2.38	5.55	0.27	1.14
Tryptophan[d]	0.45	0.07	0.06	0.07
Tyrosine[d]	0.31	0.94	0.21	0.08
Valine	1.13	2.14	0.17	1.05

a. The amino acid composition is measured in unhydrolyzed media. This method measures free amino acids in the medium, which includes amino acids sensitive to acid hydrolysis, but does not measure amino acids that are inside oligo- and polypeptides. One measurement was performed for each medium. The measurement was performed by Metabolomics Center, Roy J. Carver Biotechnology Center, University of Illinois at Urbana-Champaign using a GC/MS based method.
b. The acid hydrolysis was performed by addition of concentrated HCl into media to a final concentration of 6 M in sealed glass tubes. The mixture was placed in a sand bath at 110 ˚C for 24 hours for hydrolysis. The mixture was then neutralized to pH 7 by addition of NaOH. Two samples were measured for each medium and the average is shown. The measurement was performed by Metabolomics Center, Roy J. Carver Biotechnology Center, University of Illinois at Urbana-Champaign using GC/MS based method.
c. Asparagine and glutamine can be hydrolyzed to aspartate and glutamate, respectively. The presence of the amine form is likely due to incomplete hydrolysis.
d. Methionine, serine, threonine, tryptophan and tyrosine are known to be unstable under acid hydrolysis condition and the data acquired can be lower than the true value to different degrees according to the stability of each amino acid.
e. Cystine is not reported due to incomplete data acquired from the measurement.

3.3.2 Lysis of *aspB* results from depletion of Asp and competition with Glu for GltT

Deletion of *aspB* blocks both the synthesis of Asp and the consumption of Glu, and under conditions of limiting Asp supply from the medium could lead to either depletion of Asp or accumulation of Glu in the cells. Because of the importance of Glu homeostasis in *Bacillus subtilis*, we first investigated whether the lysis of *aspB* on DSM is due to intracellular accumulation of Glu. Indeed, addition of 10 mM Glu (final concentration) to DSM medium reduced the peak OD_{600} of the *aspB* null mutant from ~0.25 to ~0.15 (Figure 3.3A). Furthermore, in minimal medium (MM) high Glu antagonized the ability of Asp to support *aspB* growth (Figure S3.1C). In *B. subtilis*, Gln is a preferred nitrogen source and can be readily converted into Glu (Detsch & Stulke, 2003). However, a high concentration of Gln (5 or 10 mM) did not have a similar inhibitory effect (Figure 3.3A, S3.1C), although under this condition intracellular Glu levels should also be elevated. This led us to hypothesize that rather than being toxic itself, due to intracellular accumulation, Glu was acting as an antagonist of Asp import.

Glu and Asp can be imported by three Glu/Asp transporters, GltP, YveA and GltT (Tolner *et al.*, 1995, Lorca *et al.*, 2003), with GltT being the major importer for both amino acids (Zaprasis *et al.*, 2015). To test whether growth inhibition of the *aspB* mutant by Glu might be caused by competitive inhibition of Asp import, we mutated each of the three Asp/Glu importers in an *aspB* null mutant to see if the deletion of an importer would mimic the addition of Glu. Although deletion of *gltP* or *yveA* in the *aspB* mutant did not cause a noticeable growth defect, inactivation of *gltT* greatly reduced the growth yield (peak OD_{600}) of the *aspB* mutant (Figure 3.3B), similar to that seen for the *aspB* single mutant growing in DSM supplemented with Glu (Figure 3.3A). Thus, direct inactivation of Asp uptake by deleting *gltT* mimics the presence of high Glu, which may competitively inhibit uptake of Asp by GltT.

To further demonstrate that lysis is affected by relative concentrations of Asp and Glu in the medium, we altered cells to increase consumption of Glu. Glutamate is degraded by glutamate dehydrogenases RocG and GudB (Commichau *et al.*, 2008). We reasoned that degradation of intracellular Glu may allow cells to deplete Glu from the medium and facilitate Asp uptake. Indeed, when RocG was overexpressed from an IPTG inducible $P_{spac(hy)}$ promoter it completely suppressed the lysis phenotype of the *aspB* null mutant, and the final OD_{600} increased from ~0.25 to about 0.35 (Figure 3.3C), possibly due to the ability of cells to more efficiently access Asp from the medium. Similarly, deletion of glutamate synthase GltA, which prevents Glu synthesis, also rescued the *aspB* lysis phenotype (Figure 3.3C). If these effects of altering Glu metabolism are due to effects on Asp import, then these mutations should be epistatic with *gltT*. Indeed, in a *gltT* null background, overexpression of *rocG* or deletion of *gltA* could no longer rescue *aspB* lysis (Figure 3.3D). This is consistent with the hypothesis that consumption of Glu facilitates Asp uptake.

This model makes several predictions about the levels of Glu and Asp in DSM medium (in which *aspB* cells lyse) and LB medium (in which they do not), and how these levels might be affected by mutations in central metabolism. Using amino acid analysis (Table 3.1), we found that DSM is relatively poor in Asp (0.14 mM free Asp without hydrolysis and 1.68 mM with hydrolysis, as hydrolysis releases free amino acids from oligopeptides) compared to LB (0.55 mM and 3.39 mM, respectively), consistent with published work (Sezonov *et al.*, 2007). These differences in amino acid levels are reflected in the growth yield (final OD_{600}) of the *aspB* mutant in the two media (Figure 3.2B, D), and are generally consistent with the dependence of growth yield on Asp supplementation as observed in MM (Figure S3.1A). In addition, DSM contains much more Glu (0.93 mM without and 2.90 mM with hydrolysis) than Asp. Since GltT has a similar

affinity for these two amino acids (Zaprasis *et al.*, 2015), it is likely that Glu competitively inhibits Asp uptake under conditions of our experiments.

This model is further supported by analysis of residual free amino acids after 24 hours of growth of the WT, *aspB, aspB gltA* and *aspB* $P_{spac(hy)}$-*rocG* mutants in DSM. WT cells, which grew to high density (Figure 3.3C), deplete both free Asp (0.05 mM remaining) and Glu (0.1 mM remaining) (Figure 3.3E). In contrast, the *aspB* mutant failed to grow to high density (Figure 3.3C) and there was considerable Asp (0.16 mM) and high Glu (1.4 mM) in the spent medium (Figure 3.3E). In *aspB* mutant cells overexpressing RocG, Glu in the medium was reduced to 0.21 mM and Asp to 0.04 mM, similar to WT (Figure 3.3E). Deletion of *gltA* also reduced residual Glu in a similar but less dramatic manner, and correspondingly increased the ability of cells to utilize Asp (Figure 3.3E). The additional Asp rendered accessible by lowering Glu is not large (estimated at ~0.1 mM). This is consistent with the small increase of final OD_{600} when *rocG* is overexpressed (from OD_{600} 0.25 to 0.4, Figure 3.3C), possibly because of limited Asp in DSM. Collectively, these results suggest that high exogeneous Glu competitively inhibits Asp uptake by GltT, thereby exacerbating Asp limitation of the *aspB* mutant in the relatively Asp-poor DSM medium.

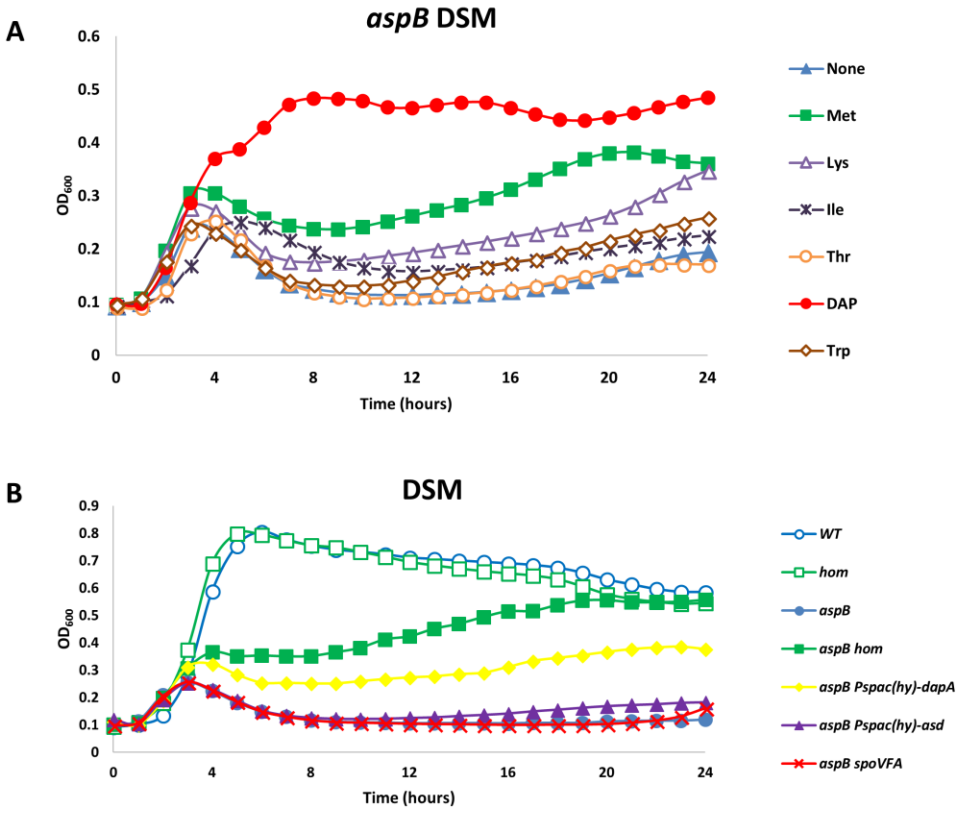

Figure 3.4. Lysis of the *aspB* mutant can be suppressed by biochemical or genetic manipulations that favor production of mDAP.

A. Representative growth curves of the *aspB* mutant in DSM supplemented with or without the following amino acids (final concentration of 10 mM each, except Trp is at 5 mM): DAP, L, L-diaminopimelate; Met, methionine; Lys, lysine; Ile, isoleucine; Thr, threonine; Trp, tryptophan. **B.** Representative growth curves of mutants in liquid DSM. 1 mM final concentration of IPTG is added to induce $P_{spac(hy)}$ promoter when present.

3.3.3 *aspB* lysis is caused by depletion of mDAP

In addition to being used for protein synthesis, Asp is used for the synthesis of Lys, Thr, Met, and Ile, as well as mDAP for peptidoglycan synthesis and dipicolinic acid for endospores (Figure 3.1). We next tested whether supplementation with any of these metabolites could suppress lysis in DSM. Supplementation with DAP (also known as L, L-diaminopimelic acid or 2,6-DAP, a precursor of mDAP) completely suppressed lysis and allowed cells to achieve a final OD_{600} of ~0.5 (Figure 3.4A), close to WT in this medium (maximal OD_{600} of 0.7-0.8; Figure 3.4C).

We hypothesized that DAP supplementation was providing mDAP for PG synthesis (Figure 3.1), and thereby suppressing cell lysis. However, DAP is also a precursor for Lys. In contrast with DAP, cells grown in DSM supplemented with Lys still showed an initial lysis before a gradual recovery (Figure 3.4A). The slow recovery was not specific to Lys as we also observed some recovery when supplemented with Ile or Trp (Figure 3.4A). Although the WT *B. subtilis* strain 168 used in this work is a tryptophan auxotroph, Trp is unlikely to be limited for cell growth, as DSM contains ~0.06 mM Trp (Table 3.1), which is over ten times higher than the required amount (~0.005 mM) for WT to grow to an OD_{600} of ~0.6 in minimal medium (Figure S3.2A). In addition, supplementing DSM with up to 10 mM Trp did not significantly increase cell yield (Figure S3.2B). Thus, both Lys and Trp facilitate recovery of the *aspB* mutant in a dose dependent manner after lysis, but have no effect on lysis itself (Figure S3.3). We speculate that this effect may result from increased nutrition supply to the not yet lysed cells, which facilitates the cannibalization of Asp from lysed cells. Indeed, supplementation with TCA cycle intermediates also facilitates post-lysis recovery, but has no effect in preventing lysis (Figure S3.4). Overall, the much more dramatic restoration of growth and complete prevention of lysis with DAP compared with Lys suggest that growth limitation and lysis results from a lack of mDAP for PG synthesis.

We also noticed a modest effect in suppressing lysis by supplementation with Met (Figure 3.4A). Met can be synthesized from Asp through a pathway starting with the branch point enzyme homoserine dehydrogenase (Hom) (Figure 3.1). Hom converts L-aspartate semi-aldehyde into homoserine, the precursor for synthesis of Met, Thr, and Ile, and can be feedback inhibited by Met (Gutierrez-Preciado *et al.*, 2009). We hypothesized that the partial rescue effect from Met may result from inhibition of Hom, which would spare L-aspartate semi-aldehyde for the DapA pathway and synthesis of mDAP (Figure 3.1). Because DSM contains all the amino acids produced by the Hom pathway (Table 3.1), we can delete *hom* under these growth conditions (Figure 3.4B) and test whether this allows a redirection of L-aspartate semi-aldehyde into the DAP pathway. Indeed, deletion of *hom* completely abolished lysis in the *aspB hom* double mutant (Figure 3.4B). Overexpression of DapA using an IPTG-inducible promoter led to a similar phenotype (Figure 3.4B), likely because it diverts more L-aspartate semi-aldehyde into the DAP pathway. In contrast, overexpression of Asd, the aspartate semi-aldehyde dehydrogenase that produces the common substrate for Hom and DapA, did not have much effect (Figure 3.4B). SpoVFAB synthesizes dipicolinic acid, an abundant component of endospores, and is a major pathway that consumes precursors for mDAP in sporulating cells (Daniel & Errington, 1993). Since this pathway is not active in vegetative cells, deletion of *spoVFA* had no effect on the *aspB* lysis phenotype (Figure 3.4B).

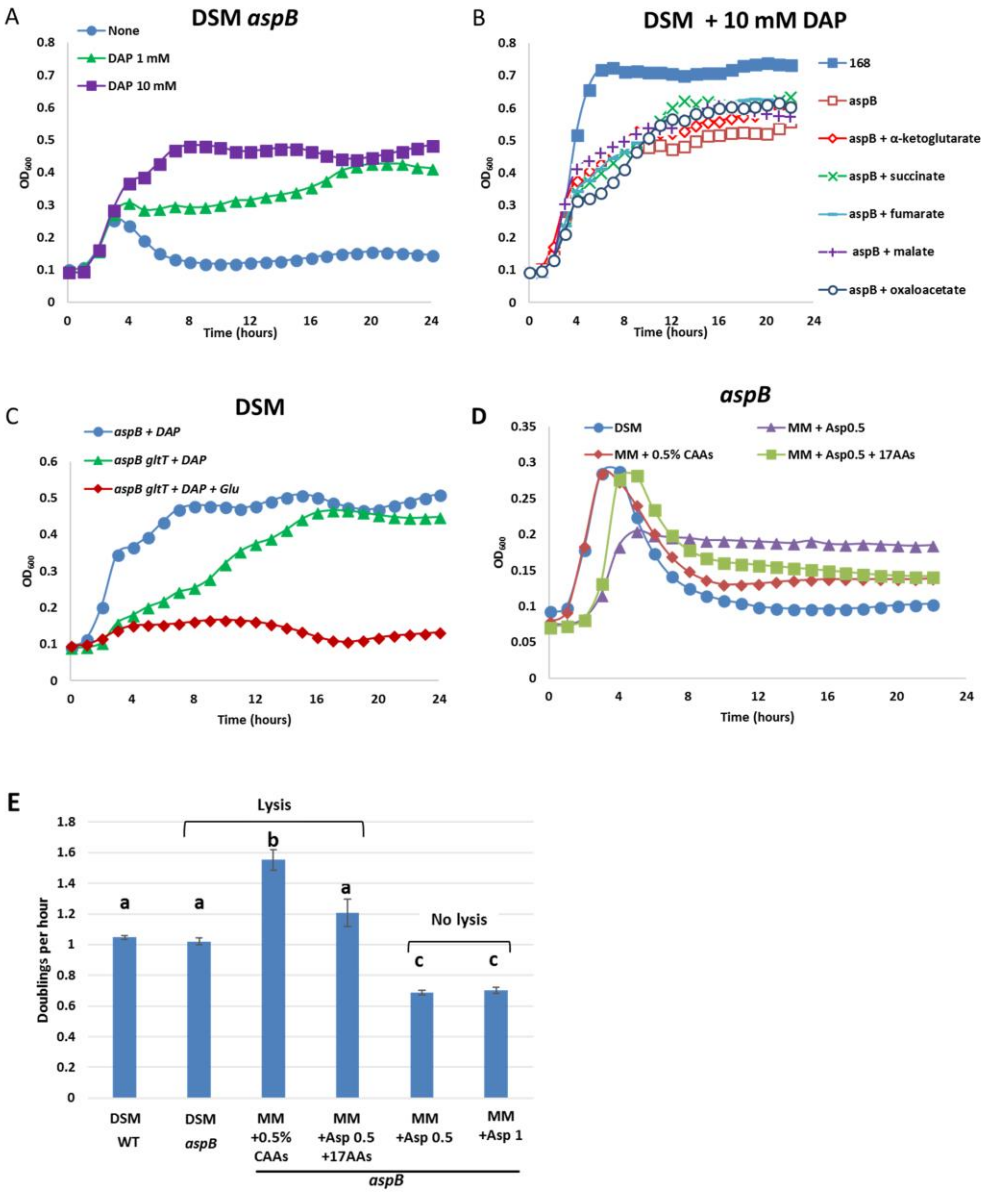

Figure 3.5. Amino acid and mDAP limitation are physiologically distinct.

A. Growth curve of the *aspB* mutant growing in DSM supplemented with 1 or 10 mM final concentration of DAP. **B.** Growth curve of WT and the *aspB* mutant in DSM supplemented with 10 mM final concentration of DAP, and with or without TCA cycle intermediates (10 mM final concentration). **C**. Growth curve of mutants in DSM supplemented with 10 mM final concentration

of DAP, or 10 mM each of DAP and Glu. **D**. Growth curve of the *aspB* mutant in DSM, or MM supplemented with 0.5 mM Asp, 0.5% (w/v) casamino acids, or 0.5 mM Asp and a mixture of 17 amino acids each at concentration of 0.1 mg ml^{-1}. **E**. Growth rate of *aspB* mutant in different media. The growth rate is calculated as $\log_2(OD_{600\text{-}T2}/OD_{600\text{-}T1})/(T_2\text{-}T_1)$, in which T_1 and T_2 are two time points in the exponential phase of cell growth. When $OD_{600}<0.3$, one doubling in cell cycle is approximated as a two-fold increase in OD_{600} value. The data is represented as the mean plus or minus one standard error of the mean, and statistically significant different samples (Student's t test, two-tailed $P<0.05$) are labelled with different letters. All growth curves were measured at least 3 times and yielded similar results. A representative measurement is shown.

3.3.4 Amino acid and mDAP limitation are physiologically distinct

An *aspB* mutant grown in DSM supplemented with 1 mM DAP temporarily ceases growth at roughly the same cell density as in the absence of DAP (OD_{600} ~0.3), but lysis (as defined by the loss of optical density) was inhibited and slow growth resumed to a final OD_{600} of ~0.45 after 20 hours (Figure 3.5A). With 10 mM DAP, cells grew to this same final OD_{600} after only 8 hours (Figure 3.5A). The similar final cell yield suggests that growth yield is ultimately determined by availability of Asp in the medium. Since the *aspB* mutant cannot grow to the same cell density as WT, even when supplemented with DAP (Figure 3.5B), we infer that the lowered growth rate and cell yield is due to insufficient Asp (or Asp family amino acids) for protein synthesis. We hypothesize that the growth rate stimulation with 10 mM compared to 1 mM DAP (Figure 3.5A) may be due to the known ability of mDAP to inhibit aspartokinase I (DapG) (Graves & Switzer, 1990, Rosner & Paulus, 1971), which will reduce the amount of Asp used to synthesize other Asp family amino acids.

In addition to its role in Asp synthesis, AspB could in principle function as an anaplerotic enzyme by providing α-ketoglutarate to sustain TCA cycle function. To test whether this might be a cause for the reduced cell yield, we tested the effect of supplementation with both DAP and 10 mM of various TCA cycle intermediates. None of the tested intermediates increased yield beyond that seen with DAP alone (Figure 3.5B), consistent with the idea that reduced growth of the *aspB* mutant under these conditions is due to an insufficiency of amino acids to support protein synthesis. Consistent results were observed in MM: an *aspB* mutant grown in MM supplemented with a limiting amount of Asp (1 mM) did not display an increase in cell yield when DAP was added (Figure S3.1D).

When an *aspB* mutant is grown in the presence of 10 mM DAP, cells no longer lyse, and are likely growth limited by the requirement of Asp and Asp family amino acids for protein synthesis (Figure 3.1). This limitation can be exacerbated by removal of the major Asp uptake system, GltT. In the presence of DAP the *aspB gltT* double mutant grew slowly to OD_{600} ~0.5 (Figure 3.5C). The similar final OD_{600} for the *gltT*$^{+}$ and *gltT* strains suggests that the remaining Asp uptake system(s), presumably GltP and YveA (Tolner *et al.*, 1995, Lorca *et al.*, 2003), can still import Asp from the medium, albeit at a lower rate. However, these Asp uptake systems are still sensitive to Glu competition, as addition of 10 mM Glu completely abolished *aspB gltT* growth, even in the presence of DAP (Figure 3.5C). Overall, these data strongly suggest that when DAP is provided, growth and cell yield of the *aspB* mutant is determined by the availability of Asp for protein synthesis, whereas when mDAP is limited cell lysis results from a deficiency in PG synthesis.

In contrast to the lysis observed in DSM, the *aspB* mutant did not lyse in MM when a low concentration of Asp was supplemented (0.5 mM or 1 mM, Figure S3.1D). One notable difference between these media is that in MM cells are synthesizing most amino acids and are only provided with Trp (0.24 mM) and a limiting amount of Asp, whereas DSM contains all 20 proteinaceous amino acids (Table 3.1). Indeed, when additional amino acids were supplemented into MM, either in the form of casamino acids (CAAs) or a mixture of 17 amino acids (17AAs; the 20 essential amino acids omitting Asp, Asn and Glu), the *aspB* mutant exhibited rapid lysis after reaching its peak OD_{600} (Figure 3.5D). We hypothesized that lysis might be correlated with growth rate, with fast-growing cells having more active autolysins and therefore being more vulnerable to a disruption in PG synthesis (Mah & O'Toole, 2001, Tuomanen *et al.*, 1986). Indeed, under growth conditions that caused lysis of the *aspB* mutant (DSM, or in MM supplemented with 0.5% CAA

or 17AAs) the *aspB* mutant grew at a rate similar to, or even faster than, that of WT in DSM until Asp was depleted (Figure 3.5E). In comparison, when the *aspB* mutant was grown in MM with limiting Asp and ammonium as nitrogen source, cells grew slower and did not lyse after Asp depletion. Overall, our results suggest a correlation between growth rate and lysis, with rapid growth contributing to lysis upon mDAP depletion in the cell.

3.3.5 DAP can be imported into *B. subtilis* by cystine uptake systems TcyABC and TcyP

Previous studies suggest that in *E. coli* and *Salmonella* Typhimurium, DAP can be imported by cystine uptake systems, likely due to their structural similarity (Leive & Davis, 1965, Stephen & Nicholas, 1986) (Figure 3.6A). There are two cystine uptake systems in *E. coli* (Berger & Heppel, 1972), with TcyJLN able to uptake DAP and TcyP more specific for cystine (Chonoles Imlay *et al.*, 2015). Uptake of DAP in *Bacillus megaterium* was resistant to the presence of cystine, suggesting the uptake is not through cystine import pathways (Gally *et al.*, 1991). However, in the same study *Bacillus subtilis* 168 exhibited no detectable DAP uptake with or without cystine (Gally *et al.*, 1991), in contrast to our observation that DAP can suppress the lysis of the *aspB* mutant.

To investigate if DAP is imported into the cells using cystine uptake systems in *B. subtilis*, we used the lysis phenotype of the *aspB* mutant as a readout and tested whether cystine can abolish the rescue of lysis by DAP. With supplementation with 600 μM cystine, 1 mM DAP could no longer prevent the *aspB* lysis (Figure 3.6B), suggesting that *B. subtilis* can indeed import DAP and this uptake is likely through cystine uptake pathways. However, the import is likely to be slow and unable to replace endogenous DAP synthesis, as supplementation with 10 mM DAP cannot bypass the essentiality of genes (such as *dapB* and *dapL*) upstream of DAP synthesis in the mDAP/lysine

pathway, as tested using CRISPRi based gene knockdown strains (Peters *et al.*, 2016b), either in LB and DSM (data not shown), or in minimal medium (no cystine to compete with DAP import) supplemented with 3.4 mM Lys(Figure S3.5).

In *B. subtilis*, there are three cystine uptake systems: TcyABC, TcyJKLMN and TcyP (Burguiere *et al.*, 2004). TcyABC and TcyJKLMN are ATP binding cassette (ABC) transporters and TcyP is a proton-cystine symporter. To determine which of these three cystine uptake systems are involved in DAP import, we tested mutant strains lacking one, two, or all three systems for the ability of DAP to prevent lysis of the *aspB* mutant (Figure 3.6C). The results suggest that TcyABC and TcyP are the two major DAP uptake systems, with TcyJKLMN playing little if any role. The limited role for TcyJKLMN was surprising since import of L-[^{14}C]-cystine by this system is known to be partially inhibited by mDAP (Burguiere *et al.*, 2004). Regardless, our results suggest that TcyJKLMN does not import sufficient DAP to suppress lysis and support growth under these conditions.

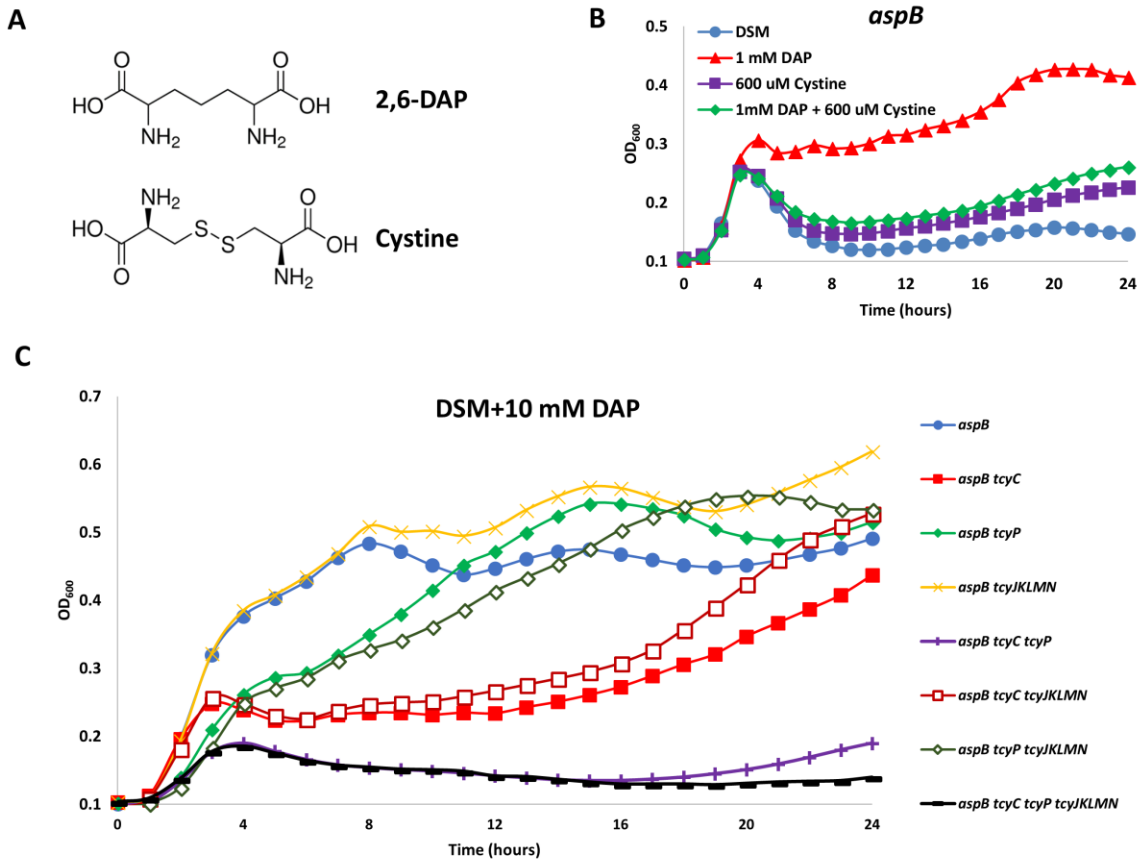

Figure 3.6. DAP can be imported through cystine uptake systems TcyABC and TcyP.

A. Chemical structure of 2,6-DAP and cystine. **B.** Growth curve of the *aspB* mutant growing in DSM with or without supplementation with DAP (1 mM final concentration), Cys (600 µM cystine), and DAP + Cys (1 mM DAP and 600 µM cystine). **C**. Growth curves of different strains in DSM supplemented with 10 mM DAP. All growth curves were measured at least 3 times and yielded similar results. A representative measurement is shown.

3.3.6 Depletion of mDAP causes cell wall stress and cell morphology defects

Since mDAP is an essential substrate for PG synthesis, mDAP limitation is predicted to impair PG synthesis ultimately leading to cell lysis. Indeed, microscopic images revealed many bulged cells and cell debris when the *aspB* mutant was grown in liquid DSM, while such deformed cells were rare in the 168 WT (Figure 3.7A, red arrows). When supplemented with DAP, the lysis phenotype was suppressed (Figure 3.7B), and bulged cells were much less frequent (Figure 3.7E). Divalent cations such as Mg^{2+} are known to suppress PG defects, in part through altering the acetylation level of mDAP in peptidoglycan (Dajkovic *et al.*, 2017) and possibly by other mechanisms including stabilization of negatively charged cell wall through cation-anion interactions. Consistent with the idea that lysis of an *aspB* null mutant is due to lack of mDAP and weakened PG, addition of 10 mM $MgSO_4$ suppressed the lysis phenotype of *aspB* (Figure 3.7B, E).

The alternative sigma factor σ^M is known to be upregulated when PG synthesis is inhibited (Helmann, 2016). Using a P_M-*lux* luciferase reporter containing the σ^M dependent autoregulatory promoter of the *sigM* gene, we found that σ^M activity was strongly induced after 3 hours of growth in DSM medium, around the same time that growth of the *aspB* mutant ceased (Figure 3.7C, dotted line). However, within the first hour after growth ceased and cells began to lyse, the σ^M activity increased another 2- to 3-fold, as measured by luciferase activity (Figure 3.7C, dashed line). It is worth noting that because the luciferase enzyme we used in this work has an estimated half-life of only 4.2 minutes (Radeck *et al.*, 2013) it seems that there is still ongoing protein synthesis even when the Asp pool is very limited and cells fail to generate enough mDAP for PG synthesis.

Although addition of either DAP or Mg^{2+} can suppress the lysis of the *aspB* mutant, their mechanisms are quite different: addition of DAP rescues PG synthesis by providing the limiting

mDAP precursor, whereas Mg^{2+} stabilizes the cell wall without solving the underlying problem. Consistently, addition of DAP almost completely suppressed induction of σ^M while supplementation with Mg^{2+} did not (Figure 3.7D). We also compared these two mechanisms of suppressing lysis by monitoring cell morphology after 24 hours of growth in supplemented DSM. In WT cultures, phase-bright endospores were readily visible after 24 hours of growth in DSM, while almost no endospores were present in the *aspB* mutant. Addition of DAP enabled a smaller population to form phase-bright endospores while addition of Mg^{2+} apparently did not. Using Oufti software (Paintdakhi *et al.,* 2016), we scored more than 600 cells (exclusive of spores) for each strain and growth condition, and measured cell length and width and calculated the width to length ratio (Figure 3.7E, F). Insufficient peptidoglycan synthesis in the *aspB* mutant significantly changed cell shape: the *aspB* mutant was about 11% shorter and 13% wider than WT cells, causing a 27% increase in the width to length ratio (Figure 3.7F). Addition of DAP or Mg^{2+} did not strongly affect the width/length ratio of WT cells. However, supplementation with DAP partially reversed the shape effects in the *aspB* mutant and reduced the change in aspect ratio from a 27% to a 9% increase relative to WT. In contrast, addition of Mg^{2+} did not restore cells to a more WT shape (Figure 3.7F). In fact, the *aspB* mutant supplemented with Mg^{2+} displayed a further increase of the width to length ratio relative to WT (Figure 3.7F). These data suggest that although addition of either DAP and Mg^{2+} suppress cell lysis, the intrinsic differences between the two mechanisms result in different cell morphologies.

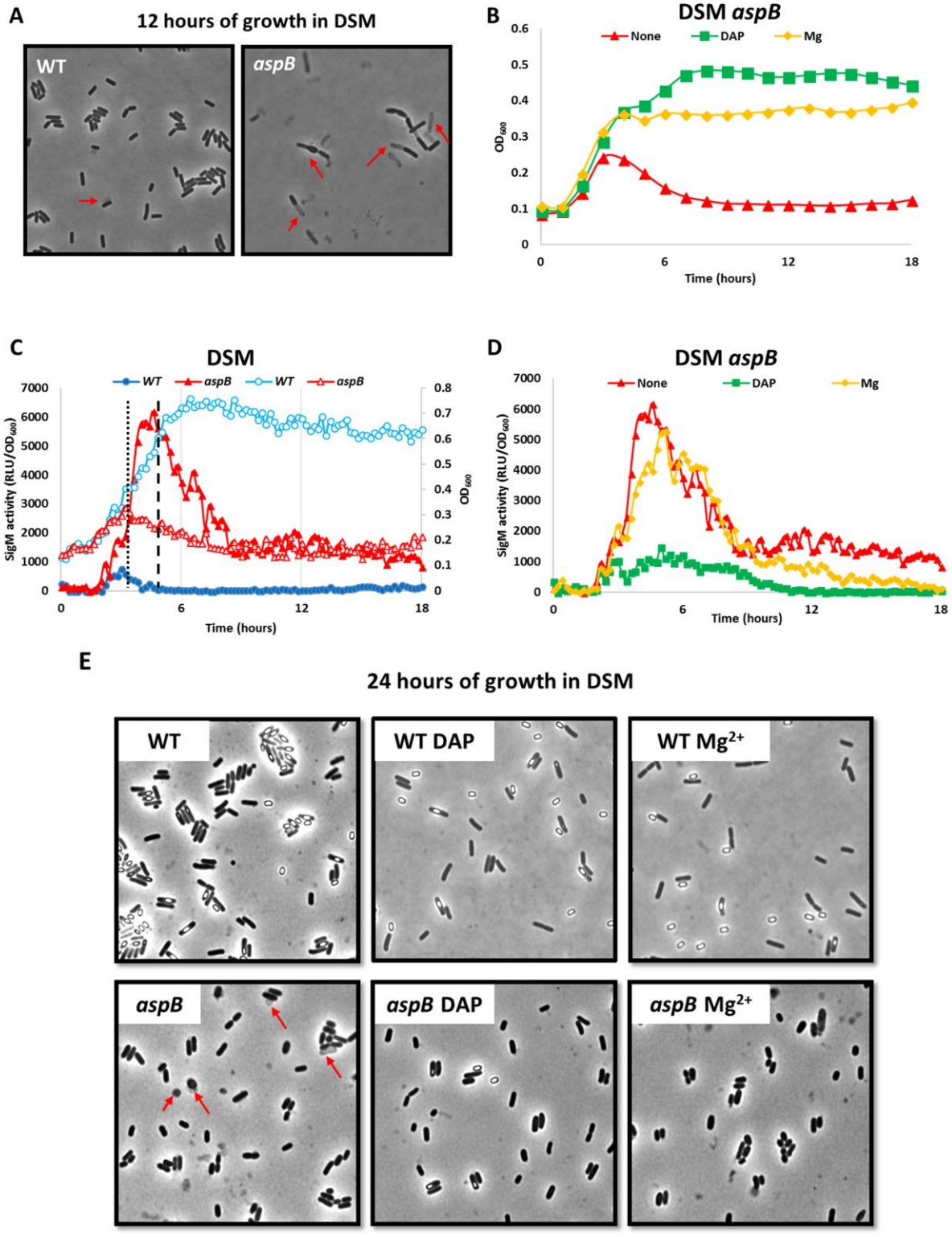
A
12 hours of growth in DSM
WT
aspB
B
DSM aspB
None
DAP
Mg
OD600
Time (hours)
C
DSM
WT
aspB
WT
aspB
SigM activity (RLU/OD600)
OD600
Time (hours)
D
DSM aspB
None
DAP
Mg
SigM activity (RLU/OD600)
Time (hours)
E
24 hours of growth in DSM
WT
WT DAP
WT Mg2+
aspB
aspB DAP
aspB Mg2+

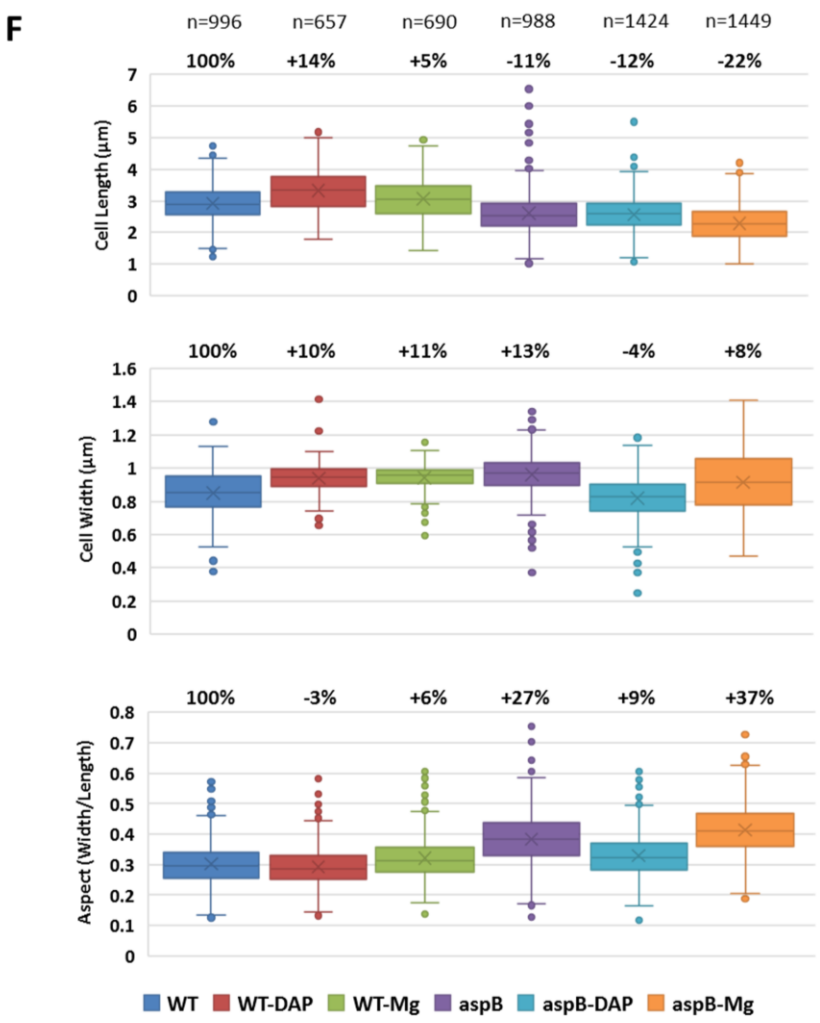

Figure 3.7. Limitation of mDAP causes cell wall stress and cell morphology defects.

A. Representative phase contrast microscopic images of WT and the *aspB* mutant after 12 hours of growth in DSM. Red arrows point to deformed or lysed cells. **B**. Growth curve of the *aspB* mutant in DSM with or without supplementation with 10 mM $MgSO_4$ or 10 mM DAP. **C**. σ^M activity (relative light unit (RLU)/OD_{600}, left axis, closed symbols) and OD_{600} (right axis, open symbols) of WT and the *aspB* mutant in DSM. The dotted line indicates the time when the *aspB*

mutant starts to lyse, and the dashed line indicates when the luciferase synthesis begins to decrease. Because the luciferase has a short half-life (~4 minutes), OD_{600} and luminescence were measured every 12 minutes to generate near real time gene expression data. **D**. σ^M activity (relative light unit (RLU)/OD_{600}) of the *aspB* mutant in DSM with or without supplement of 10 mM DAP or 10 mM $MgSO_4$. All growth curves were measured at least 3 times and yielded similar results. A representative measurement is shown. **E.** Representative phase contrast microscopic images of WT and the *aspB* mutant after 24 hours of growth in DSM, with or without supplementing 10 mM DAP or $MgSO_4$. Red arrows point to deformed or lysed cells. **F**. Comparison of cell length, width and aspect between WT and the *aspB* mutant under different growth conditions. n is the number of cells measured per strain per condition. Percentage change of the mean compared to WT is shown above each data plot. The bottom and top of the box are the first and third quartiles, the band inside the box is the second quartile (the median), and the X inside the box is the mean. Whiskers are one standard deviation above or below the mean. Outliers are shown as single dots.

3.3.7 Limitation of mDAP sensitizes cells to cell wall antibiotics

Since the *aspB* mutant is limited for mDAP availability, we tested the effect on sensitivity against several antibiotics targeting PG synthesis. For this analysis, we used Mueller-Hinton (MH) medium in which *aspB* mutant has less of a growth defect than in DSM: single colonies grow with normal morphology on MH plates, with comparatively mild lysis apparent in the colony centers and the inoculation loading zone (Figure S3.6). Using MH medium, we found that an *aspB* mutant was no more sensitive than WT to fosfomycin or D-cycloserine (Figure 3.8A), two antibiotics targeting early steps of PG synthesis (Figure 3.1). However, the *aspB* mutant was significantly more sensitive to antibiotics targeting PG synthesis steps downstream of lipid II, including vancomycin and the beta-lactam antibiotic cefuroxime (Figure 3.8A). Addition of 10 mM Asp completely rescued the sensitivity to vancomycin and partially to cefuroxime (Figure 3.8B, C), consistent with the sensitivity being caused by a restricted availability of mDAP. Addition of DAP did not rescue sensitivity to vancomycin or cefuroxime (data not shown), possibly due to slow import through the cystine uptake systems. Interestingly, while addition of α-ketoglutarate together with Asp did not have any effect on cefuroxime resistance, it reduced sensitivity to vancomycin in both WT and the *aspB* mutant background. The mechanism of this altered sensitivity is not yet clear.

Even when grown in the Asp-rich LB medium, the *aspB* mutant exhibited increased MOE^S (Figure 3.2B) and, consistently, our original *ypmB*::*mls* mutant (polar on the downstream *aspB*) can become further resistant to MOE when *aspB* is overexpressed ectopically from an IPTG inducible promoter. As a mimic for the substrate of class A PBPs (aPBPs), MOE is most potent when its aPBP targets are not bound to their true substrate lipid II. The reduced expression of *aspB* in the *ypmB*::*mls* mutant likely leads to partial mDAP depletion and reduced lipid II production.

Experiments using a non-polar *ypmB* mutant revealed strong MOE resistance, similar to a *ypmB*::*mls* complemented with an ectopic copy of *aspB* (data not shown). Overall, the sensitivity of *aspB* towards vancomycin, cefuroxime and MOE demonstrates that limitation of Asp (and consequently mDAP) sensitizes cells to antibiotics targeting PG synthesis, likely due to a reduced pool of lipid II.

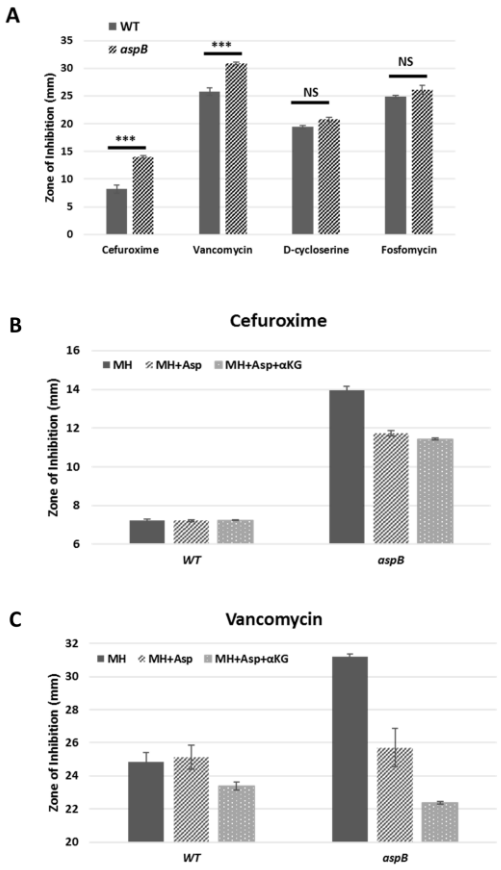

Figure 3.8. **Limitation of mDAP sensitizes cells to antibiotics targeting late steps in PG synthesis.**

A. Sensitivity of WT and the *aspB* mutant against cefuroxime, vancomycin, D-cycloserine and fosfomycin. Pairwise comparison was made to test if difference between samples are statistically significant (Student's t test, two-tailed. ***, P<0.01; NS, not significant.) **B**. Sensitivity of WT and the *aspB* mutant against cefuroxime when grown in MH, MH+Asp, or MH+Asp+αKG (α-ketoglutarate). **C**. Sensitivity of WT and the *aspB* mutant against vancomycin when grown in MH, MH+Asp, or MH+Asp+αKG. Pairwise comparison was made (Student's t test, two-tailed P<0.05), and samples with statistically significant differences are labelled with different letters. The data is represented as the mean plus or minus one standard error of the mean, with sample number n greater-than or equal to 3.

3.4 Discussion

It is increasingly appreciated that sensitivity to antibiotics is dependent on the metabolic state of the cell. Changes in carbon source, or from aerobic to anaerobic metabolism, can have dramatic effects on antibiotic susceptibility (Yang *et al.*, 2017a, Su *et al.*, 2018). It may be possible to exploit such effects by combining antibiotics that inhibit essential cellular processes with compounds that alter metabolism to increase susceptibility. Development of new antibiotics also relies on understanding cell metabolism: for example, inhibitors of pathways presumed to be essential, such as fatty acid synthesis, may in fact be ineffective if the targeted organism does not require this pathway in the host (Brinster *et al.*, 2009, Balemans *et al.*, 2010). To complicate matters further, cell populations are heterogeneous and variations in levels of metabolites or specific proteins may determine survival after antibiotic challenge, and can partially explain the phenomenon of highly resistant persister cells (Fisher *et al.*, 2017, Shan *et al.*, 2017, Lee & Collins, 2011).

In this work, we show that an *aspB* null mutation growing in rich medium with limited Asp ceases growth and lyses due to depletion of mDAP, an essential intermediate for PG synthesis. Lysis can be prevented by chemical complementation (DAP supplementation), and this property enabled us to assign two cystine uptake systems (TcyABC and TcyP) as the major DAP importers (Figure 3.6, Figure S3.5). Lysis could also be suppressed by addition of Asp or optimized utilization of available Asp or a variety of genetic manipulations that increased the flux of limited Asp into the DAP pathway. For example, increased consumption of Glu can alleviate competitive inhibition of Asp import (largely through GltT) (Figure 3.3), and provision of Met can spare the branch point intermediate L-aspartate semialdehyde for entry into the DAP pathway (Figure 3.4A, B). Interestingly, a recent study in *Salmonella* Typhimurium shows that a Met auxotroph (Δ*metB*)

also affects PG synthesis, and leads to a disproportionate increase relative to WT of UDP-NAM-L-Ala-D-Glu (1000-fold) compared to UDP-NAM-L-Ala-D-Glu-mDAP (5-fold) (Husna *et al.*, 2018). One possibility is that the *metB* mutation increases the amount of L-aspartate semi-aldehyde shunted into the Hom pathway for Met synthesis, thereby contributing to a depletion of mDAP and accumulation of the co-substrate for UDP-NAM-L-Ala-D-Glu-mDAP synthesis.

Because an *aspB* null mutant is unable to *de novo* synthesize Asp, cells rely on import from the medium to support protein and peptidoglycan synthesis. By measuring amino acid content in DSM and LB medium, we propose that the growth defect of the *aspB* null mutant is due to Asp limitation exacerbated by competition with Glu for Asp uptake. Our results suggest that GltT is the major Glu/Asp importer, and are in agreement with prior work (Zaprasis et al., 2015), even though our conditions are drastically different (our experiments are done in DSM, a complex medium containing all essential amino acids, whereas Zaprasis *et al.* used a glucose ammonium based minimal medium supplemented with 20 μM of Glu or Asp). Growth of the *aspB* mutant can be strongly inhibited by Glu, even in the presence of DAP, suggesting that all major Asp importers are sensitive to Glu-inhibition. Interestingly, Asp uptake is crucial for host colonization of *Mycobacterium tuberculosis* (Gouzy *et al.*, 2013a, Gouzy *et al.*, 2013b), highlighting the importance of understanding Asp uptake systems and their role in bacterial physiology.

A major finding of this work is that the growth defect of the *aspB* mutant on DSM can be separated into two parts. In the presence of added DAP, growth limitation results primarily from amino acid limitation for protein synthesis. In contrast, when no DAP is added the initial response to Asp limitation is cell wall stress, resulting from the lack of mDAP, inducing the σ^M regulon and predisposing cells to lysis. A reduced capacity for mDAP synthesis in the *aspB* null mutant contributes to an aberrant cell morphology (Figure 3.7) and sensitivity to antibiotics targeting late

steps in PG synthesis (Figure 3.8), likely caused by a limited pool of lipid II. These results are analogous to the cross-talk recently noted in *Caulobacter crescentus* in which mutations that lead to α-ketoglutarate accumulation can inhibit mDAP synthesis, leading to antibiotic sensitivity (Irnov *et al.*, 2017).

In conclusion, in the absence of exogenous DAP, PG synthesis is the first critical process that fails as Asp is depleted (Figure 3.7C). The resultant cell lysis may be dependent on growth rate: when growing slowly in MM, the *aspB* mutant does not lyse after depletion of Asp and mDAP, while addition of free amino acids increases growth rate and lysis. Interestingly, a similar observation was made over 35 years ago when it was noted that the depletion of mDAP in an auxotrophic strain of *E. coli* leads to more rapid lysis in fast-growing than slow-growing cells (Leduc *et al.*, 1982). One possible explanation is that both PG synthesizing and degrading enzymes are more active in fast growing cells than slow-growing cells, and thus the imbalance is more severe in fast-growing cells when PG synthesis is limited by mDAP depletion. Overall, this work highlights the important connection between central metabolism and cell wall synthesis and reveals how alterations in central metabolism that limit peptidoglycan sidechain biosynthesis may increase sensitivity to peptidoglycan synthesis inhibitors.

Table 3.2. Strains used in this study

Number	Genotype	Reference/Construction [a]
168	Wild type *B. subtilis* strain (*trpC2*)	Lab stock
HB12259	*ypmB*::*mls*	LFH PCR → 168 (Guariglia, 2013) [b]
HB17053	*aspB*::*kan*	LFH PCR → 168 [b]
HB17058	$P_{spac(hy)}$-*aspB*	pPL82-*aspB* → 168
HB17060	*aspB*::*kan*, $P_{spac(hy)}$-*aspB*	HB17053 → HB17058
HB17062	*ypmB*::*mls*, $P_{spac(hy)}$-*aspB*	HB12259 → HB17058
HB17325	P_M-*lux*	pBS3C*lux*-P_M → 168
HB17401	Δ*aspB*	BKE22370 → 168, then the erm cassette removed using pDR244
HB20720	$P_{spac(hy)}$-*rocG*	pPL82-*rocG* → 168
HB20749	$P_{spac(hy)}$-*rocG aspB-erm*	BKE22370 → HB20720
HB20873	Δ*gltA*	BKE18450 → 168, then the *erm* cassette removed using pDR244
HB22836	*yveA::erm*	BKE34470 → 168
HB20874	Δ*gltA aspB::erm*	BKE22370 → HB20873
HB22838	*gltP::erm*	BKE02340 → 168
HB22841	*gltT::erm aspB*::*kan*	HB17053 → HB22851
HB22842	*gltP::erm aspB*::*kan*	HB17053 → HB22838
HB22843	*yveA::erm aspB*::*kan*	HB17053 → HB22836
HB22851	*gltT::erm*	BKE10220 → 168
HB22869	Δ*tcyC*	BKE03590 → 168, then the *erm* cassette removed using pDR244
HB22870	Δ*tcyP*	BKE09130 → 168, then the *erm* cassette removed using pDR244
HB22871	Δ*tcyJKLMN*	See Experiment Procedure
HB22878	Δ*tcyC tcyP*	BKE03590 → HB22870, then the *erm* cassette removed using pDR244
HB22879	Δ*tcyC tcyJKLMN*	BKE03590 → HB22871, then the *erm* cassette removed using pDR244
HB22880	Δ*tcyP tcyJKLMN*	BKE09130 → HB22871, then the *erm* cassette removed using pDR244
HB22881	Δ*tcyC tcyP tcyJKLMN*	BKE03590 → HB22880, then the *erm* cassette removed using pDR244
HB22885	Δ*spoVFA*	BKE16730 → 168, then the *erm* cassette removed using pDR244
HB22887	Δ*hom*	BKE32260 → 168, then the *erm* cassette removed using pDR244
HB22890	Δ*spoVFA aspB*::*kan*	HB17053 → HB22885
HB22892	Δ*tcyC aspB*::*kan*	HB17053 → HB22869
HB22893	Δ*tcyP aspB*::*kan*	HB17053 → HB22870
HB22894	Δ*tcyJKLMN aspB*::*kan*	HB17053 → HB22871
HB22895	Δ*tcyC tcyP aspB*::*kan*	HB17053 → HB22878
HB22896	Δ*tcyC tcyJKLMN aspB*::*kan*	HB17053 → HB22879
HB22897	Δ*tcyP tcyJKLMN aspB*::*kan*	HB17053 → HB22880
HB22898	Δ*tcyC tcyP tcyJKLMN aspB*::*kan*	HB17053 → HB22881
HB22900	Δ*hom aspB*::*kan*	HB17053 → HB22887
HB22910	$P_{spac(hy)}$-*ypmB*	pPL82-*ypmB* → 168
HB22913	*ypmB*::*mls* $P_{spac(hy)}$-*ypmB*	HB12259 → HB22910
HB22917	$P_{spac(hy)}$-*asd*	pPL82-*asd* → 168
HB22919	$P_{spac(hy)}$-*dapA*	pPL82-*dapA* → 168
HB22921	$P_{spac(hy)}$-*asd aspB*::*kan*	HB17053 → HB22917
HB22923	$P_{spac(hy)}$-*dapA aspB*::*kan*	HB17053 → HB22919

HB22932	Δ*gltA* $P_{spac(hy)}$-*rocG*	HB20720 → HB20873
HB22933	Δ*gltA gltT-erm*	BKE10220 → HB20873
HB22934	$P_{spac(hy)}$-*rocG gltT-erm*	HB20720 → HB22851
HB22935	Δ*gltA* $P_{spac(hy)}$-*rocG aspB*::*kan*	HB17053 → HB22932
HB22937	Δ*gltA gltT-erm aspB*::*kan*	HB17053 → HB22933
HB22939	$P_{spac(hy)}$-*rocG gltT-erm aspB*::*kan*	HB17053 → HB22934
HB22951	P_M-*lux aspB*::*kan*	HB17053 → HB17325

a. "→" indicates transformation using DNA from the former (donor) into the latter (recipient).
b. Most of the open reading frame is replaced by an antibiotic cassette.

3.5 Experimental Procedures

3.5.1 Strains, primers, media and growth condition

All strains used in this work are listed in Table 2, and all DNA primers are listed in Table S1. Bacteria were routinely grown in liquid lysogeny broth (LB), Difco Sporulation Medium (DSM) or minimal medium (MM) with vigorous shaking, or on plates (1.5% agar; Difco) at 37 ˚C unless otherwise stated. LB medium contains 10 g tryptone, 5 g yeast extract, and 5 g NaCl per liter. DSM (per 500 ml) includes 5 ml 10% KCl, 5 ml 1.2% $MgSO_4$*$7H_2O$, 4 g Bacto nutrient broth powder, 0.25 ml 1 M NaOH, and water to bring the volume to 500 ml. The medium is autoclaved at 121 ˚C for 20 minutes. After autoclaving, the following filter sterilized ingredients were added: 0.5 ml 1 M $Ca(NO_3)_2$, 0.05 ml 0.1 M $MnCl_2$, and 10 mM $FeSO_4$. The minimal medium contains 2% glucose, 2 g l^{-1} $(NH_4)_2SO_4$, 40 mM MOPS (pH 7.4), 1.2 mM K_2HPO_4, 0.8 mM KH_2PO_4, 1 g l^{-1} sodium citrate·$2H_2O$, 245 μM L-tryptophan, 80 nM $MnCl_2$, 1 μM $FeSO_4$ and 0.5 mM $MgSO_4$. The mixture of 17 amino acids includes alanine, arginine, cysteine, glutamine, glycine, histidine, isoleucine, leucine, lysine, methionine, phenylalanine, proline, serine, threonine, tryptophan, tyrosine and valine. Final concentrations for each amino acid used in the growth measurement is 0.1 mg ml^{-1}. For growth curve measurements, 1 μl log phase culture (OD_{600} ~0.4) was inoculated into 200 μl of liquid medium per well in a Bioscreen 100-well plate, the plate was shaken vigorously and OD_{600} was measured every 15 minutes using an automated BioScreen growth analyzer. Plasmids were constructed using standard methods (Luo *et al.*, 2010), and amplified in *E. coli* DH5α before transforming into *B. subtilis*. For selection of transformants, 100 μg ml^{-1} ampicillin was used for *E. coli*. Antibiotics used for selection of *B. subtilis* transformants include: kanamycin 15 μg ml^{-1}, spectinomycin 100 μg ml^{-1}, macrolide-lincosamide-streptogramin

B (MLS, contains 1 μg ml^{-1} erythromycin and 25 μg ml^{-1} lincomycin), and chloramphenicol 10 μg ml^{-1}.

3.5.2 Genetic techniques

LFH PCR, chromosomal and plasmid DNA transformation was performed as previously stated (Zhao *et al.*, 2016). The kanamycin resistance and MLS resistance cassettes were PCR amplified from plasmids pDG780 and pDG646, respectively (Guerout-Fleury *et al.*, 1995). The pPL82 plasmid-based $P_{spac(hy)}$ overexpression constructs were linearized and integrated into the *amyE* locus (Quisel *et al.*, 2001). Markerless in-frame deletion mutants (indicated by Δ in Table 2) were constructed from BKE strains as described (Koo *et al.*, 2017). Briefly, BKE strains were acquired from the Bacillus Genetics Stock Center, chromosomal DNA was extracted, and the mutation containing an erm^R cassette was transformed into our WT 168 strain. The erm^R cassette was subsequently removed by introduction of the Cre recombinase carried on plasmid pDR244, which was later cured by growing at the non-permissive temperature of 42 ˚C. Gene deletions were confirmed by PCR screening using flanking primers. Unless otherwise described, all PCR products were generated using *B. subtilis* 168 strain chromosomal DNA as template. DNA fragments used for gene over-expression were sequence verified. Null mutant constructions were verified by PCR. The mutant missing the entire *tcyJKLMN* operon was constructed in three steps. Briefly, a fragment containing the region upstream of *tcyJ* and adjacent *erm* cassette was amplified from BKE29380 (*tcyJ*::*erm*), and another fragment containing the *erm* cassette and downstream region of *tcyN* was amplified from BKE29340 (*tcyN*::*erm*). These two fragments were joined by overlap PCR using the shared *erm* cassette and yielded a fragment containing the upstream of *tcyJ* and the downstream of *tcyN*, with the entire *tcyJKLMN* operon replaced by an *erm* cassette. The fragment was used to transform WT strain and the *erm* cassette was later removed by the Cre recombinase

encoded on plasmid pDR244. Unless otherwise stated, the Δ*aspB* strain was used as a representative null mutant, and the *aspB*::*kan* or *aspB*::*erm* allele was used for construction of strains with multiple mutations (Table 2). The Δ*aspB*, *aspB*::*kan* and *aspB*::*erm* strains were compared in most growth experiments and were phenotypically indistinguishable.

3.5.3 Disk Diffusion Assay

Disk diffusion assays was performed as previously described (Kingston *et al.*, 2014). Briefly, overnight cultures in LB medium were inoculated into fresh LB medium and grown to exponential phase with OD_{600} of 0.4. A 100 µl aliquot of each culture was mixed with 4 ml of 0.75% MH soft agar (kept at 50°C) and directly poured onto a prewarmed 37°C MH plate (containing 15 ml of 1.5% MH agar). After the soft agar solidified, a filter paper disk with diameter of 6.5 mm was placed on top of the soft agar, and an antibiotic to be tested was added to the paper disk. The plate was kept at room temperature for 5 minutes to let the antibiotic to be absorbed into the medium, and then moved to 37°C incubator for 20 hours. The overall diameter of the inhibition zone was measured along two pairs of orthogonal lines, and zones of inhibition are reported as the average diameter of the four measurements for each biological replicate. At least four biological replicates were used for each antibiotic and strain combination. The quantity of antibiotics used per disk is cefuroxime 10 µg, vancomycin 50 µg, D-cycloserine 500 µg, or fosfomycin 500 µg.

3.5.4 Amino Acid Analysis

Amino acid analysis (AAA) was performed by Metabolomics Center, Roy J. Carver Biotechnology Center, University of Illinois at Urbana-Champaign using GC/MS based method. For AAA of used medium, cells were grown in the medium for 24 hours, and then removed from the medium by centrifugation at 5000 g for 10 minutes, followed by filtration of the supernatant through 0.22 µm filter. Concentrations of free amino acids were then measured using quantitative

GC/MS based method. To measure total amino acids in media which contain oligo- and polypeptides, the medium was hydrolyzed (Davidson, 2003). Briefly, HCl was added to 6 M and samples kept at 110 ˚C in a sand bath for 24 hours. Hydrolyzed medium was then centrifuged at 5000 g for 10 minutes, followed by filtration through 0.22 μm filter to remove particles formed during the hydrolysis. Hydrolyzed medium containing 6 M HCl was neutralized by NaOH to pH 7.0 before AAA.

3.5.5 Luciferase reporter construction and measurement

The P_M-*lux* luciferase reporter was constructed by inserting the σ^M-controlled promoter of *sigM* (P_M) amplified using primers 6808 and 6809 into the multicloning sites of pBS3C*lux* (Radeck *et al.*, 2013). The insert was confirmed by sequencing, the plasmid was linearized and integrated into the *B. subtilis sacA* locus. For luciferase measurements, 1 μl of exponentially growing cells were inoculated into 99 μl of fresh medium in a 96 well plate, incubated at 37 ˚C with shaking using a SpectraMax i3x plate reader. Because the luciferase has a short half-life (~4 minutes), OD_{600} and luminescence were measured every 12 min. The data was analyzed using SoftMax Pro 7.0 software. P_M promoter activity was normalized by dividing the relative light units (RLU) by OD_{600}.

3.5.6 Phase contrast microscopy

Cells were grown in liquid medium for the time indicated and loaded on saline (0.90% NaCl, w/v) agarose pads (0.8% final concentration) on a glass slide. Phase contrast images were taken using a Leica DMi8 microscope equipped with a 100x immersion objective and Leica Application Suite X software. Cell length and width were measured using Oufti per the software's instruction (Paintdakhi *et al.*, 2016).

3.6 Acknowledgment

This chapter is adapted from "Aspartate deficiency limits peptidoglycan synthesis and sensitizes cells to antibiotics targeting cell wall synthesis in *Bacillus subtilis*", which was just accepted into *Mol Microbiol* in July 2018. The author list includes Zhao H, Roistacher DM, Helmann JD. Roistacher DM is an undergraduate student working with Zhao H, and helped with experiments, data acquisition, and manuscript editing. Zhao H and Helmann JD drafted and edited the manuscript.

3.7 References

Arthur, M., P.E. Reynolds, F. Depardieu, S. Evers, S. Dutka-Malen, R. Quintiliani, Jr. & P. Courvalin, (1996) Mechanisms of glycopeptide resistance in enterococci. *J Infect* **32**: 11-16.

Balemans, W., N. Lounis, R. Gilissen, J. Guillemont, K. Simmen, K. Andries & A. Koul, (2010) Essentiality of FASII pathway for Staphylococcus aureus. *Nature* **463**: E3; discussion E4.

Belitsky, B.R. & A.L. Sonenshein, (1998) Role and regulation of Bacillus subtilis glutamate dehydrogenase genes. *J Bacteriol* **180**: 6298-6305.

Berger, E.A. & L.A. Heppel, (1972) A binding protein involved in the transport of cystine and diaminopimelic acid in Escherichia coli. *J Biol Chem* **247**: 7684-7694.

Brantl, S. & A. Licht, (2010) Characterisation of Bacillus subtilis transcriptional regulators involved in metabolic processes. *Curr Protein Pept Sci* **11**: 274-291.

Brinster, S., G. Lamberet, B. Staels, P. Trieu-Cuot, A. Gruss & C. Poyart, (2009) Type II fatty acid synthesis is not a suitable antibiotic target for Gram-positive pathogens. *Nature* **458**: 83-86.

Burguiere, P., S. Auger, M.F. Hullo, A. Danchin & I. Martin-Verstraete, (2004) Three different systems participate in L-cystine uptake in Bacillus subtilis. *J Bacteriol* **186**: 4875-4884.

Chen, N.Y., S.Q. Jiang, D.A. Klein & H. Paulus, (1993) Organization and nucleotide sequence of the Bacillus subtilis diaminopimelate operon, a cluster of genes encoding the first three enzymes of diaminopimelate synthesis and dipicolinate synthase. *J Biol Chem* **268**: 9448-9465.

Chonoles Imlay, K.R., S. Korshunov & J.A. Imlay, (2015) Physiological Roles and Adverse Effects of the Two Cystine Importers of Escherichia coli. *J Bacteriol* **197**: 3629-3644.

Commichau, F.M., K. Gunka, J.J. Landmann & J. Stulke, (2008) Glutamate metabolism in Bacillus subtilis: gene expression and enzyme activities evolved to avoid futile cycles and to allow rapid responses to perturbations of the system. *J Bacteriol* **190**: 3557-3564.

Commichau, F.M., C. Herzberg, P. Tripal, O. Valerius & J. Stulke, (2007) A regulatory protein-protein interaction governs glutamate biosynthesis in Bacillus subtilis: the glutamate dehydrogenase RocG moonlights in controlling the transcription factor GltC. *Mol Microbiol* **65**: 642-654.

Dajkovic, A., B. Tesson, S. Chauhan, P. Courtin, R. Keary, P. Flores, C. Marliere, S.R. Filipe, M.P. Chapot-Chartier & R. Carballido-Lopez, (2017) Hydrolysis of peptidoglycan is modulated by amidation of meso-diaminopimelic acid and Mg2+ in Bacillus subtilis. *Mol Microbiol* **104**: 972-988.

Daniel, R.A. & J. Errington, (1993) Cloning, DNA sequence, functional analysis and transcriptional regulation of the genes encoding dipicolinic acid synthetase required for sporulation in Bacillus subtilis. *J Mol Biol* **232**: 468-483.

Davidson, I., (2003) Hydrolysis of samples for amino acid analysis. *Methods Mol Biol* **211**: 111-122.

Detsch, C. & J. Stulke, (2003) Ammonium utilization in Bacillus subtilis: transport and regulatory functions of NrgA and NrgB. *Microbiology* **149**: 3289-3297.

Dumas, R., D. Cobessi, A.Y. Robin, J.L. Ferrer & G. Curien, (2012) The many faces of aspartate kinases. *Arch Biochem Biophys* **519**: 186-193.

Eymann, C., A. Dreisbach, D. Albrecht, J. Bernhardt, D. Becher, S. Gentner, T. Tam le, K. Buttner, G. Buurman, C. Scharf, S. Venz, U. Volker & M. Hecker, (2004) A comprehensive proteome map of growing Bacillus subtilis cells. *Proteomics* **4**: 2849-2876.

Fisher, R.A., B. Gollan & S. Helaine, (2017) Persistent bacterial infections and persister cells. *Nat Rev Microbiol* **15**: 453-464.

Fisher, S.H. & L.V. Wray, Jr., (2002) Bacillus subtilis 168 contains two differentially regulated genes encoding L-asparaginase. *J Bacteriol* **184**: 2148-2154.

Gamba, P., E. Rietkotter, R.A. Daniel & L.W. Hamoen, (2015) Tetracycline hypersensitivity of an ezrA mutant links GalE and TseB (YpmB) to cell division. *Front Microbiol* **6**: 346.

Geiger, T. & C. Wolz, (2014) Intersection of the stringent response and the CodY regulon in low GC Gram-positive bacteria. *Int J Med Microbiol* **304**: 150-155.

Gouzy, A., G. Larrouy-Maumus, T.D. Wu, A. Peixoto, F. Levillain, G. Lugo-Villarino, J.L. Guerquin-Kern, L.P. de Carvalho, Y. Poquet & O. Neyrolles, (2013a) Mycobacterium tuberculosis nitrogen assimilation and host colonization require aspartate. *Nat Chem Biol* **9**: 674-676.

Gouzy, A., Y. Poquet & O. Neyrolles, (2013b) A central role for aspartate in Mycobacterium tuberculosis physiology and virulence. *Front Cell Infect Microbiol* **3**: 68.

Graves, L.M. & R.L. Switzer, (1990) Aspartokinase III, a new isozyme in Bacillus subtilis 168. *J Bacteriol* **172**: 218-223.

Grundy, F.J., S.C. Lehman & T.M. Henkin, (2003) The L box regulon: lysine sensing by leader RNAs of bacterial lysine biosynthesis genes. *Proc Natl Acad Sci U S A* **100**: 12057-12062.

Guariglia, V., (2013) CELL ENVELOPE STRESS RESPONSE AND ANTIMICROBIAL RESISTANCE IN BACILLUS SUBTILIS. In: Doctoral Dissertation in Department of Microbiology. Cornell University, pp. 149.

Gunka, K. & F.M. Commichau, (2012) Control of glutamate homeostasis in Bacillus subtilis: a complex interplay between ammonium assimilation, glutamate biosynthesis and degradation. *Mol Microbiol* **85**: 213-224.

Gunka, K., S. Tholen, J. Gerwig, C. Herzberg, J. Stulke & F.M. Commichau, (2012) A high-frequency mutation in Bacillus subtilis: requirements for the decryptification of the gudB glutamate dehydrogenase gene. *J Bacteriol* **194**: 1036-1044.

Gutierrez-Preciado, A., T.M. Henkin, F.J. Grundy, C. Yanofsky & E. Merino, (2009) Biochemical features and functional implications of the RNA-based T-box regulatory mechanism. *Microbiol Mol Biol Rev* **73**: 36-61.

Hachmann, A.-B.G., (2010) CELL ENVELOPE STRESS RESPONSE AND MECHANISMS OF ANTIBIOTIC RESISTANCE IN BACILLUS SUBTILIS. In: Doctoral Dissertation in Department of Microbiology. Cornell University, pp. 187.

Helmann, J.D., (2016) Bacillus subtilis extracytoplasmic function (ECF) sigma factors and defense of the cell envelope. *Curr Opin Microbiol* **30**: 122-132.

Kingston, A.W., H. Zhao, G.M. Cook & J.D. Helmann, (2014) Accumulation of heptaprenyl diphosphate sensitizes Bacillus subtilis to bacitracin: implications for the mechanism of resistance mediated by the BceAB transporter. *Mol Microbiol* **93**: 37-49.

Kobashi, N., M. Nishiyama & H. Yamane, (2001) Characterization of aspartate kinase III of Bacillus subtilis. *Biosci Biotechnol Biochem* **65**: 1391-1394.

Koo, B.M., G. Kritikos, J.D. Farelli, H. Todor, K. Tong, H. Kimsey, I. Wapinski, M. Galardini, A. Cabal, J.M. Peters, A.B. Hachmann, D.Z. Rudner, K.N. Allen, A. Typas & C.A. Gross, (2017) Construction and Analysis of Two Genome-Scale Deletion Libraries for Bacillus subtilis. *Cell Syst* **4**: 291-305 e297.

Lee, Y.H., A.W. Kingston & J.D. Helmann, (2012) Glutamate dehydrogenase affects resistance to cell wall antibiotics in Bacillus subtilis. *J Bacteriol* **194**: 993-1001.

Lorca, G., B. Winnen & M.H. Saier, Jr., (2003) Identification of the L-aspartate transporter in Bacillus subtilis. *J Bacteriol* **185**: 3218-3222.

Luo, Y., K. Asai, Y. Sadaie & J.D. Helmann, (2010) Transcriptomic and phenotypic characterization of a Bacillus subtilis strain without extracytoplasmic function sigma factors. *J Bacteriol* **192**: 5736-5745.

Mah, T.F. & G.A. O'Toole, (2001) Mechanisms of biofilm resistance to antimicrobial agents. *Trends Microbiol* **9**: 34-39.

Ochi, K., J.C. Kandala & E. Freese, (1981) Initiation of Bacillus subtilis sporulation by the stringent response to partial amino acid deprivation. *J Biol Chem* **256**: 6866-6875.

Paintdakhi, A., B. Parry, M. Campos, I. Irnov, J. Elf, I. Surovtsev & C. Jacobs-Wagner, (2016) Oufti: an integrated software package for high-accuracy, high-throughput quantitative microscopy analysis. *Mol Microbiol* **99**: 767-777.

Picossi, S., B.R. Belitsky & A.L. Sonenshein, (2007) Molecular mechanism of the regulation of Bacillus subtilis gltAB expression by GltC. *J Mol Biol* **365**: 1298-1313.

Radeck, J., K. Kraft, J. Bartels, T. Cikovic, F. Durr, J. Emenegger, S. Kelterborn, C. Sauer, G. Fritz, S. Gebhard & T. Mascher, (2013) The Bacillus BioBrick Box: generation and evaluation of essential genetic building blocks for standardized work with Bacillus subtilis. *J Biol Eng* **7**: 29.

Rosner, A. & H. Paulus, (1971) Regulation of aspartokinase in Bacillus subtilis. The separation and properties of two isofunctional enzymes. *J Biol Chem* **246**: 2965-2971.

Ruane, K.M., A.J. Lloyd, V. Fulop, C.G. Dowson, H. Barreteau, A. Boniface, S. Dementin, D. Blanot, D. Mengin-Lecreulx, S. Gobec, A. Dessen & D.I. Roper, (2013) Specificity determinants for lysine incorporation in Staphylococcus aureus peptidoglycan as revealed by the structure of a MurE enzyme ternary complex. *J Biol Chem* **288**: 33439-33448.

Sezonov, G., D. Joseleau-Petit & R. D'Ari, (2007) Escherichia coli physiology in Luria-Bertani broth. *J Bacteriol* **189**: 8746-8749.

Shan, Y., A. Brown Gandt, S.E. Rowe, J.P. Deisinger, B.P. Conlon & K. Lewis, (2017) ATP-Dependent Persister Formation in Escherichia coli. *MBio* **8**.

Sonenshein, A.L., (2007) Control of key metabolic intersections in Bacillus subtilis. *Nat Rev Microbiol* **5**: 917-927.

Steinchen, W. & G. Bange, (2016) The magic dance of the alarmones (p)ppGpp. *Mol Microbiol* **101**: 531-544.

Strominger, J.L., E. Ito & R.H. Threnn, (1960) Competitive inhibition of enzymatic reactions by oxamycin. *Journal of the American Chemical Society* **82**: 998-999.

Sun, D.X. & P. Setlow, (1991) Cloning, nucleotide sequence, and expression of the Bacillus subtilis ans operon, which codes for L-asparaginase and L-aspartase. *J Bacteriol* **173**: 3831-3845.

Tolner, B., T. Ubbink-Kok, B. Poolman & W.N. Konings, (1995) Characterization of the proton/glutamate symport protein of Bacillus subtilis and its functional expression in Escherichia coli. *J Bacteriol* **177**: 2863-2869.

Tuomanen, E., R. Cozens, W. Tosch, O. Zak & A. Tomasz, (1986) The rate of killing of Escherichia coli by beta-lactam antibiotics is strictly proportional to the rate of bacterial growth. *J Gen Microbiol* **132**: 1297-1304.

Yang, J.H., S.C. Bening & J.J. Collins, (2017) Antibiotic efficacy-context matters. *Curr Opin Microbiol* **39**: 73-80.

Yeats, C., N.D. Rawlings & A. Bateman, (2004) The PepSY domain: a regulator of peptidase activity in the microbial environment? *Trends Biochem Sci* **29**: 169-172.

Zaprasis, A., M. Bleisteiner, A. Kerres, T. Hoffmann & E. Bremer, (2015) Uptake of amino acids and their metabolic conversion into the compatible solute proline confers osmoprotection to Bacillus subtilis. *Appl Environ Microbiol* **81**: 250-259.

Zhang, J.J., F.M. Hu, N.Y. Chen & H. Paulus, (1990) Comparison of the three aspartokinase isozymes in Bacillus subtilis Marburg and 168. *J Bacteriol* **172**: 701-708.

Zhao, H., V. Patel, J.D. Helmann & T. Dorr, (2017) Don't let sleeping dogmas lie: new views of peptidoglycan synthesis and its regulation. *Mol Microbiol* **106**: 847-860.

Zhao, H., Y. Sun, J.M. Peters, C.A. Gross, E.C. Garner & J.D. Helmann, (2016) Depletion of Undecaprenyl Pyrophosphate Phosphatases Disrupts Cell Envelope Biogenesis in Bacillus subtilis. *J Bacteriol* **198**: 2925-2935.

3.7 Supplemental Material

3.7.1 Supplemental Figures

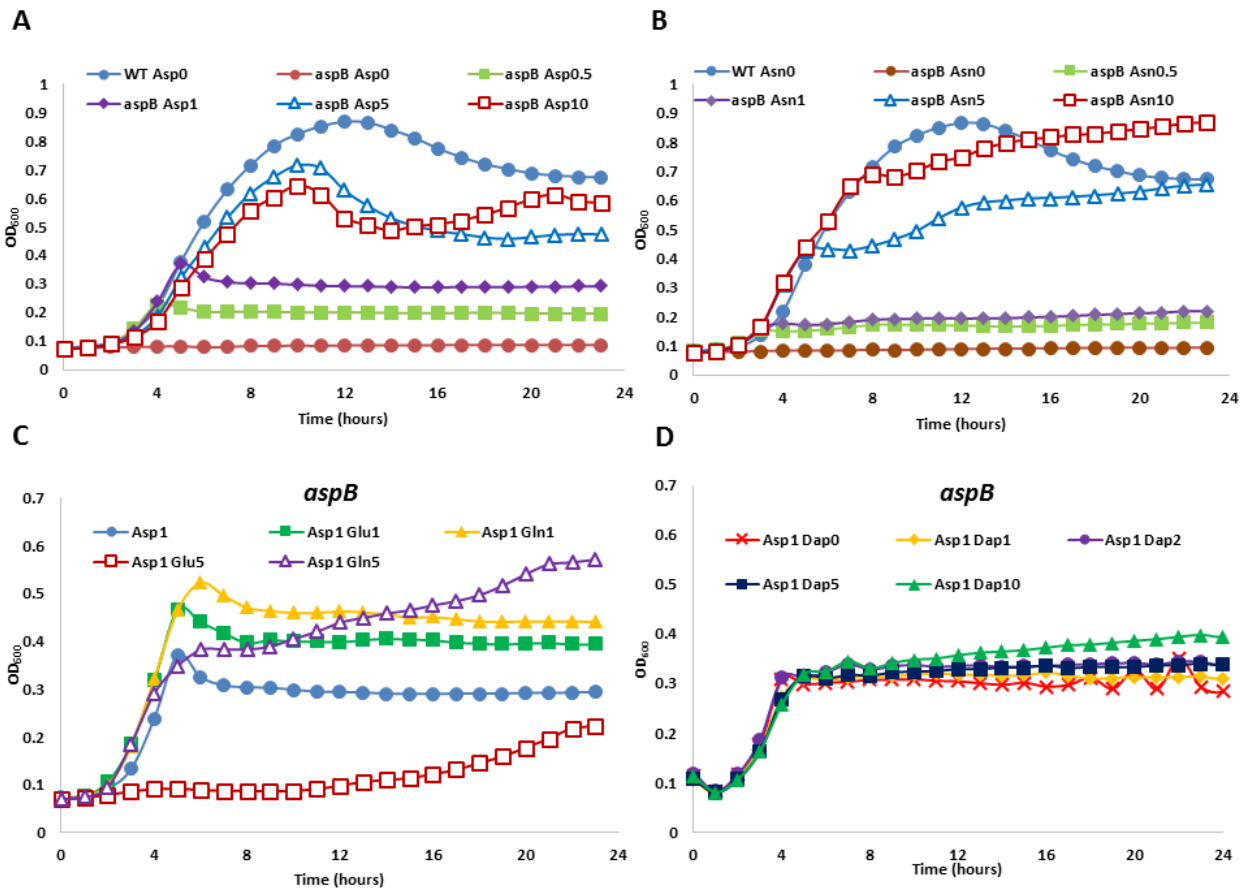

Figure S3.1. Growth curves of wild type and the *aspB* mutant in minimal medium.

A. Growth curves of WT and the *aspB* mutant in MM with or without supplementation with Asp (mM). **B**. Growth curves of WT and the *aspB* mutant in MM with or without supplementation with Asn (mM). **C**. Growth curves of the *aspB* mutant in MM supplemented with 1 mM Asp and different amount of Glu. **D.** Growth curves of the *aspB* mutant in minimal medium supplemented with 1 mM Asp and different amount of DAP, unit for concentration is mM. All growth curves were measured at least 3 times and a representative measurement is shown.

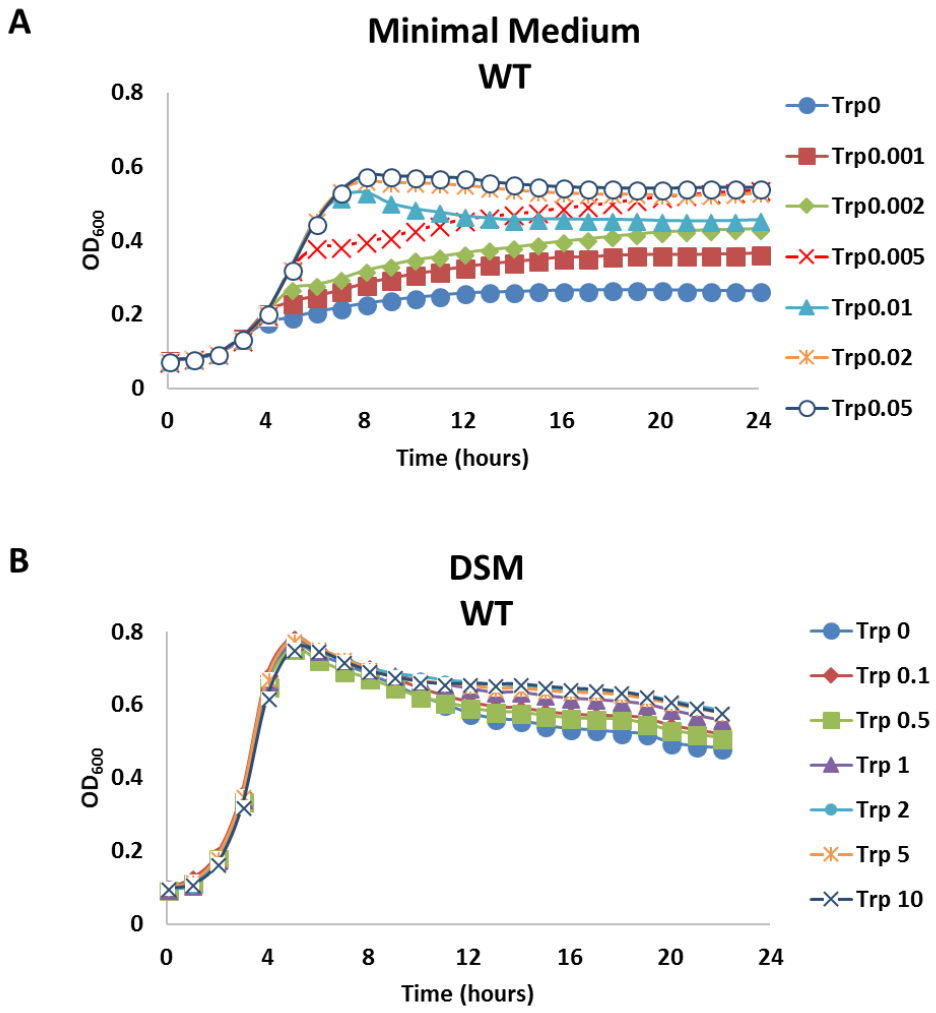

Figure S3.2. Tryptophan is not limited for growth in DSM.

A. Growth curves of WT strain 168 in minimal medium supplemented with different amount of tryptophan. Unit for Trp concentration is mM. WT reaches maximum OD_{600} when 0.005 mM or higher concentration of Trp is provided.
B. Growth curves of the WT in DSM supplemented with different amount of Trp (unit for Trp concentration is mM). Maximum OD_{600} does not increase as up to 10 mM is supplemented. All growth curves were measured at least 3 times and a representative measurement is shown.

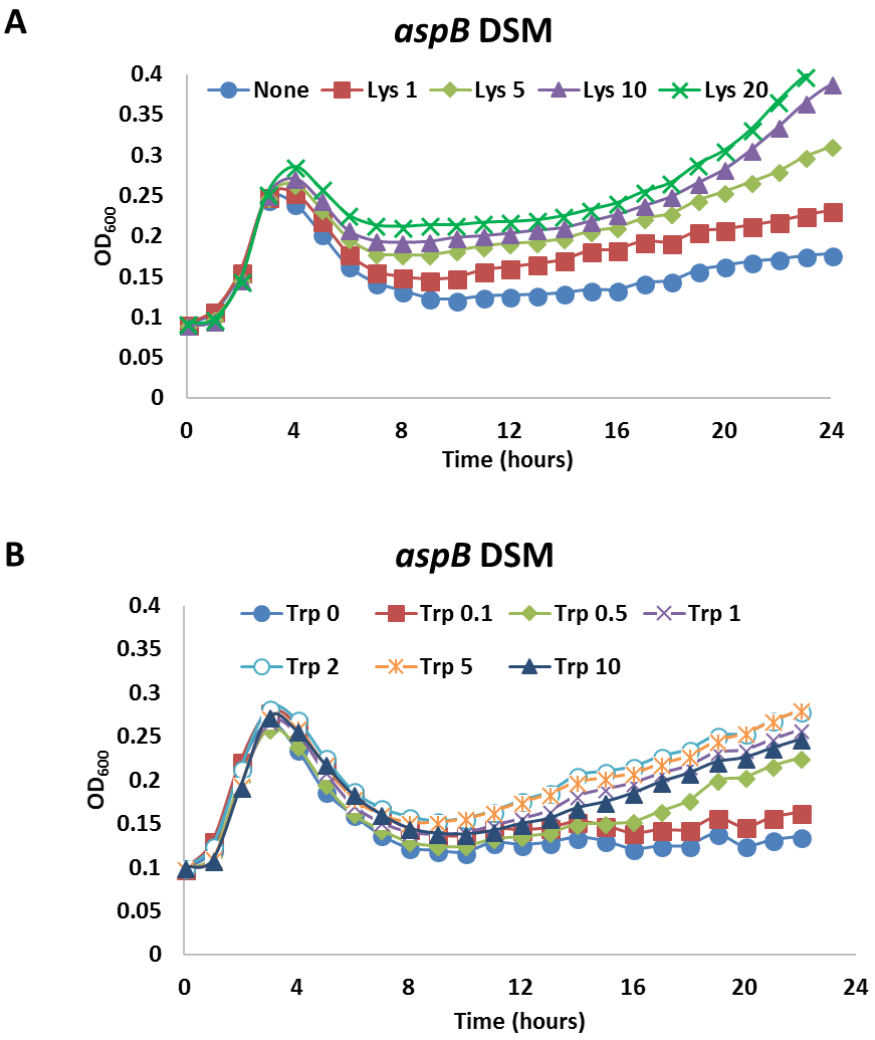

Figure S3.3. Effect of Lys and Trp on the recovery of the aspB mutant after lysis. Unit for Lys and Trp concentration is mM.

A. Growth curves of the *aspB* mutant in DSM supplemented with different amount of Lys.

B. Growth curves of the *aspB* mutant in DSM supplemented with different amount of Trp. All growth curves were measured at least 3 times and a representative measurement is shown.

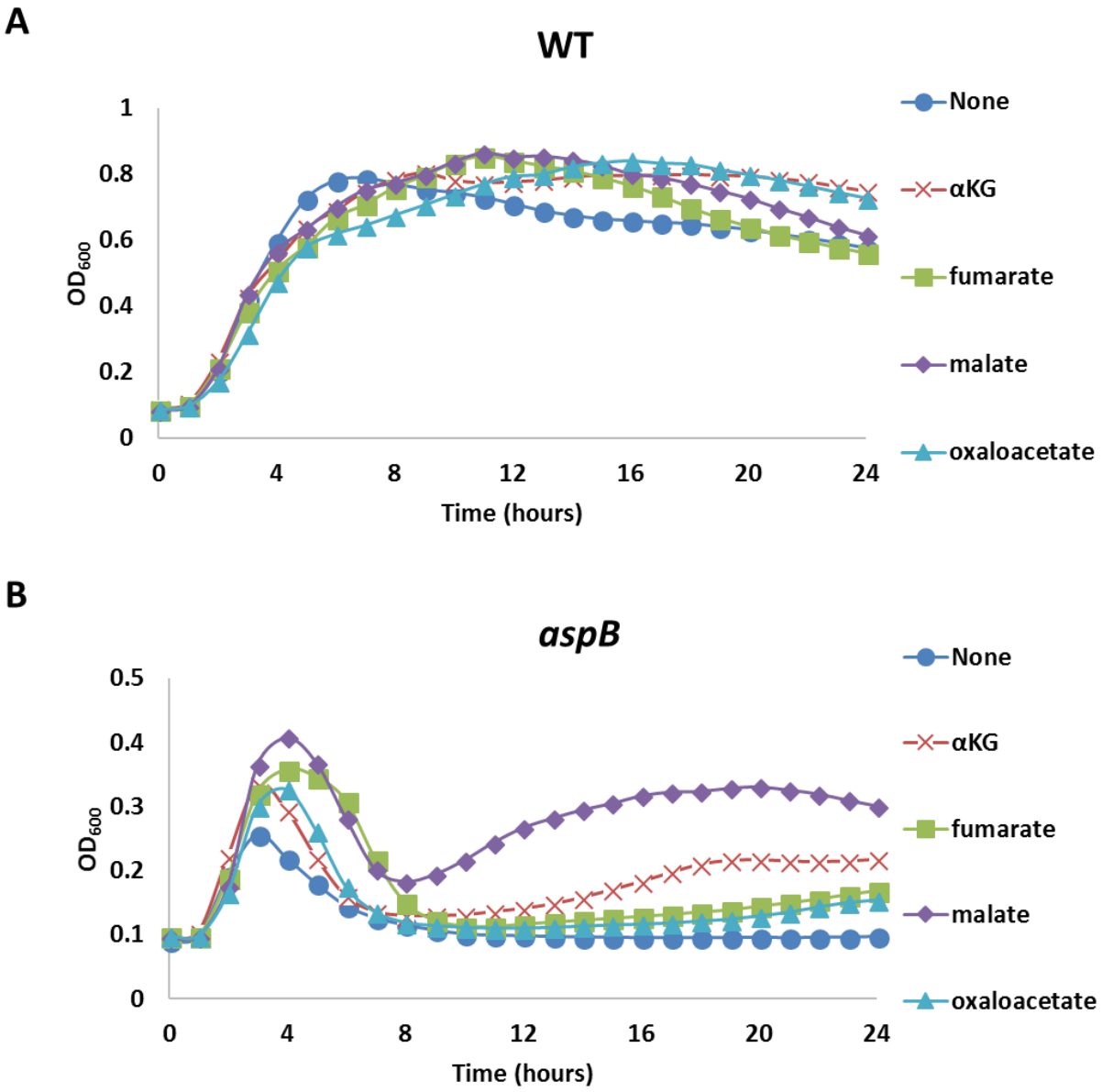

Figure S3.4. Effect of TCA cycle intermediates on the recovery of the aspB mutant after lysis in DSM. All supplements are supplemented to a final concentration of 10 mM.

A. Growth curves of the WT and B. the *aspB* mutant in DSM supplemented with different amount of TCA cycle intermediates. All growth curves were measured at least 3 times and a representative measurement is shown.

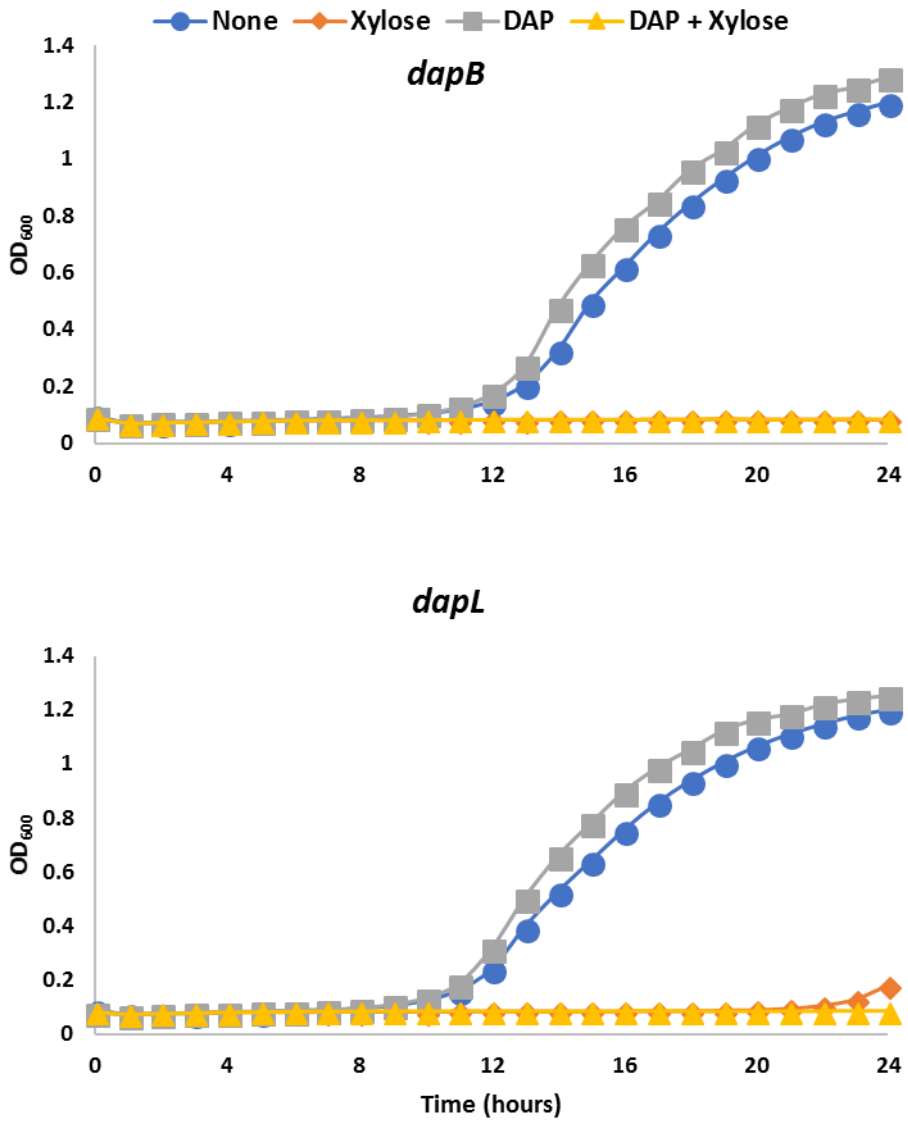

Figure S3.5 Supplement of DAP cannot rescue growth when transcription of essential genes upstream of DAP in the mDAP synthesis pathway are blocked by dCas9. Growth curves of *dapB* and *dapL* CRISPRi strains were preformed in minimal medium supplemented with 3.4 mM of lysine (final concentration). The medium is either additionally supplemented with a final concentration of 2% xylose (to induce dCas9), 10 mM DAP, or 2%xylose + 10 mM DAP.

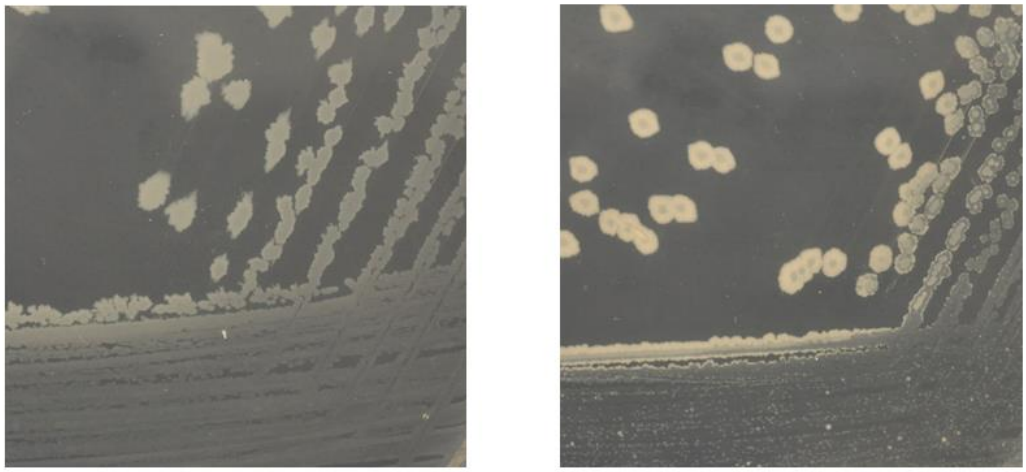

Figure S3.6. Colony morphology of the *aspB* mutant growing on LB (left) and MH (right) after incubation at 37 ˚C for 24 hours.

3.7.2 Supplemental Tables

Table S3.1. Primers used in this study

Primer Number	Primer Name	Sequence
6225	aspB up F	TGCAAAATGTGAGCTTGCCC
6226	aspB up R kan	CCTATCACCTCAAATGGTTCGCTGTGCCAGTGTGGTTGATGGTG
6227	aspB down F kan	CGAGCGCCTACGAGGAATTTGTATCGAGCCATTGAAAGAATCAAGCGT
6228	aspB down R	ATTCTTGGGAACGGGGCTTT
6243	aspB F	GATCCCCGGGAGACGAATTAGGGGGAGTTCAA
6244	aspB R	GATCTCTAGACCCGCTCTTAACTAACCGGG
6326	BKE MLS check R	TTTTCTCGTTCATAGTAGTTCCTCC
6327	BKE MLS check F	CCTTAAAACATGCAGGAATTGACG
6554	BKE-Scar-F	GCAGGCGAGAAAGGAGAGA
6555	BKE-Scar-R	CGAGGCTCCTGTCACTGCT
6808	P_{sigM}-F-EcoRI	AGCTGAATTCGCCGTTTGCATGTAATGTG
6809	P_{sigM}-R-PstI	AGCTCTGCAGCAGTAAGTCTTCAGCAAGATGC
7182	gltA-check-F	CTGCTGATTGCTGATTGGGC
7183	gltA-check-R	AACGGTGTACCGCAATCCAT
8152	gltP-check-F	GGGGACTTTTTCGCCAACAT
8153	gltP-check-R	GTAAACGCAAGACTGGCAGC
8154	yveA-check-F	TTTGTTGGCGACGGGAAAAC
8155	yveA-check-R	GTGCCGGCCTTTTTGACAAT
8156	gltT-check-F	AGGTTAGGTCAAAGCTCACCTG
8157	gltT-check-R	GGGCGGAACTGATCAAAAGC
8183	tcyA-F	AACGATTTATTGCGCGGCTC
8184	tcyA-R	CCCCTGAAAGTATCGGCCAG
8185	tcyC-F	ATGTCATCGAACGGCGTCTT
8186	tcyC-R	GCCAAGGCGGCTTTGTTTTA
8187	tcyJ-F	GGGGAATATCAGACTGGCGG
8188	tcyJ-R	GTTCCAGTTCCGACCGTGAT
8189	tcyN-F	CCAGAGATTACAGGGACGGC

8190	tcyN-R	ATGGCGCACCCCATATTTCA
8191	tcyP-F	AATTCGCACTTGACCCATCG
8192	tcyP-R	TAGGCAAACTGAGACAGCCG
8237	hom-check-F	TCAAAACAGGAGCGGGCTTA
8238	hom-check-R	TGTAAAGTTAGCGCCGGTGT
8240	ypmB-HindIII-F	ATCGAAGCTTAGGAGGTGAGAAGATGAGAAAAAAAGCA
8241	ypmB-XbaI-R	ATCGTCTAGACTAATTCGTCTTAAGGCGTGATATTT
8258	asd-XmaI-F	ATCGCCCGGGAAGCTGATTGGCGGAAGGAG
8259	asd-XbaI-R	ATCGTCTAGACAGGCTGATAGCGCCTTACT
8262	dapA-XmaI-F	ATCGCCCGGGACGCTTTGCATGAAGTGTTTGA
8263	dapA-XbaI-R	ATCGTCTAGATGACCGCGTTTGTTTCACTG

Chapter 4. Dysregulation of a cell envelope stress response sigma factor causes lethal membrane secretion stress

4.1 Abstract

The Gram-positive model organism *Bacillus subtilis* has 19 known sigma factors. Replacement of the primary sigma factor (SigA) with alternative sigma factors allows modification of transcriptional specificity of RNA polymerase (RNAP) and cell differentiation. Sigma M is an extracytoplasmic function (ECF) sigma factor, and responds to cell wall stress by upregulating key genes and alternative pathways in cell wall synthesis. Two membrane bound anti-SigM factors, YhdL and YhdK, sequester and inactivate SigM in the absence of cell wall stress. Null mutations in *yhdK* cause high level SigM activity, slow growth and abnormal cell morphology, while the absence of *yhdL* causes cell death. This stress can be alleviated at either the transcriptional level by reducing SigM activity, or by mutation in the membrane insertase YidC. This work suggests a scenario in which bacterial cells experience a primary stress (cell wall stress) and upregulate an alternative sigma (SigM) in response, thereby potentially imposing on themselves a secondary stress.

4.2 Introduction

In order to survive and thrive in different environment niches and under ever changing growth conditions, bacteria have evolved complex mechanisms to regulate their gene expression in response to environmental cues, and an important way of changing gene expression is the use of alternative sigma factors (Feklistov *et al.*, 2014). Unlike the housekeeping sigma factor (designated SigA in many bacteria) which transcribes essential genes for growth (DNA replication, protein synthesis, etc.), alternative sigma factors are used under conditions in which a subset of

genes are required or beneficial for growth. Under these conditions, one or more alternative sigma factors become active, bind to RNA polymerase (RNAP) core and transcribe a subset of genes specific for the alternative sigma factor (Mascher, 2013).

Bacillus subtilis strain 168 contains eighteen known alternative sigma factors, among which are seven extracytoplasmic function (ECF) sigma factors responding to cell envelope stresses (Souza *et al.*, 2014, Mascher, 2013). While each sigma factor has a specific set of genes under its transcriptional control, there is considerable amount of overlap between sigma factors (Mascher *et al.*, 2007). Among the seven ECF sigma factors, SigM, SigV, SigW and SigX are best studied, and respond to stresses caused by agents inhibiting peptidoglycan (PG) synthesis, lysozyme, detergents and membrane-disrupting agents, and cationic antimicrobials, respectively (Helmann, 2016, Wiegert *et al.*, 2001). The overlap in the SigMWX regulon is highlighted by biochemistry and genetic studies showing that deletion of one sigma factor can only achieve partial loss of resistance against some antibiotics (Huang *et al.*, 1998) (Mascher *et al.*, 2007). Interestingly, a mutant missing all seven ECF sigma factors is more sensitive to many cell envelope targeting compounds, but is overall similar in phenotype to a mutant missing only SigMWX (Asai *et al.*, 2008, Luo *et al.*, 2010). SigV is induced by lysozyme and confers lysozyme resistance by O-acetylation of the PG and D-alanylation of teichoic acids (Ho *et al.*, 2011, Guariglia-Oropeza & Helmann, 2011). The function of the other three ECF sigma factors, SigY, SigZ and YlaC is not clear.

SigM is one of the most well studied ECF sigma factors in *B. subtilis*. SigM transcribes a set of ~60 genes in response to stresses in peptidoglycan (PG) synthesis, with many of them being central to PG synthesis (Eiamphungporn & Helmann, 2008, Jervis *et al.*, 2007). Upon PG synthesis stresses, it can upregulate transcription of key enzymes (PonA, a class A PBP, for example)

(Eiamphungporn & Helmann, 2008), or turn on alternative pathways (such as Amj, alternative to the lipid II flippase MurJ) (Meeske *et al.*, 2015) (reviewed in (Helmann, 2016)). A *sigM* mutant has growth defects in the presence of high salt or 5% ethanol, and is highly sensitive to cell wall targeting antibiotics including β-lactams, bacitracin and moenomycin (Luo & Helmann, 2012, Thackray & Moir, 2003).

Sigma M is co-transcribed in an operon with its two anti-sigma factors, YhdL and YhdK. The operon is transcribed from two promoters, a constitutive SigA-controlled promoter P_A and an autoregulatory SigM-controlled promoter P_M (Figure 4.1A) (Thackray & Moir, 2003). In the absence of cell envelope stresses, the *sigM* operon is mostly transcribed from P_A (Horsburgh & Moir, 1999). Upon co-translation with its two anti-sigma factors, SigM is sequestered on the membrane by YhdL and YhdK, with direct interaction between YhdL and SigM (Yoshimura *et al.*, 2004, Asai, 2018). In response to cell envelope stresses, SigM is released from YhdL and YhdK through an unknown mechanism, binds to RNA polymerase (RNAP) in the cytoplasm and activates transcription of the genes in its regulon (Mascher, 2013). The autoregulatory P_M allows SigM to transcribe its own *sigMyhdLyhdK* operon and form a positive feedback loop as newly synthesized SigM is not bound to its anti-sigma factors in presence of cell wall stress (Thackray & Moir, 2003). It is yet to be understood how the cytoplasmic SigM is inactivated after the stress condition is resolved.

Among the two anti-sigma factors, YhdL is reported to be essential due to high SigM activity in its absence (Thackray & Moir, 2003, Kobayashi *et al.*, 2003). The function of the other anti-sigma factor YhdK is not clear. In this work we show that absence of either anti-sigma factor drastically increases SigM activity and leads to a cell growth defect (Δ*yhdK*) or cell death (Δ*yhdL*). High SigM activity leads to membrane secretion stress, likely caused by overproduction of SigM

transcribed membrane proteins. This stress can be alleviated at either the transcriptional level by reducing SigM activity, or by mutation in the membrane insertase YidC. This work suggests a scenario in which bacterial cells experience a primary stress (cell wall stress) and upregulate an alternative sigma (SigM) in response, thereby potentially imposing on themselves a secondary stress.

4.3 Results

4.3.1 Excess SigM activity is toxic in the absence of anti-sigma factors

Because SigM controls its own transcription from the autoregulatory P_M promoter, we use the activity of this promoter as a proxy for SigM activity and constructed a P_M-lux luciferase reporter to monitor SigM activity during growth (measurement of luminescence every 12 minutes). We found that in a wild type 168 (WT168) strain, SigM is transiently induced by about 10-fold in mid-exponential growth phase and quickly returns to background level when grown in LB medium (Figure 4.1B), similar to a previous report (Horsburgh & Moir, 1999). The transient induction is likely caused by rapid cell growth and the need to upregulate wall synthesis in the exponential growth phase. A *sigM* null mutant does not exhibit this transient induction, suggesting the induction is specific to SigM activity (Figure 4.1B). A *yhdK* null mutant shows much higher SigM activity than WT throughout the growth, with an ~100-fold increase compared to WT at their respective peaks (Figure 4.1C). The *yhdK* mutant also exhibits other growth defects, including long filamentous cell morphology (Figure 4.1D), slow growth in liquid culture (Figure 4.1E), and small colony size (Figure 4.1F).

YhdL is reported to be an essential gene (Kobayashi *et al.*, 2003), and indeed we could not obtain a *yhdL* null mutant in the *B. subtilis* 168 strain background. Transformation of a *yhdL::kan* allele into a strain with P_M-lacZ generates tiny blue colonies and big white colonies that contain

mutations in the *sigM* gene (Figure 4.6C and Sanger sequencing results, data not shown), and the tiny blue colonies do not grow after re-streaking on fresh medium (data not shown). The growth defect of *yhdK/L* mutants is due to high SigM activity, as a strain missing the whole *sigMyhdLyhdK* operon has normal cell morphology and a growth rate similar to WT (Figure 4.1D, E). Overall these results confirm that high SigM activity is toxic to cells, consistent with previous reports.

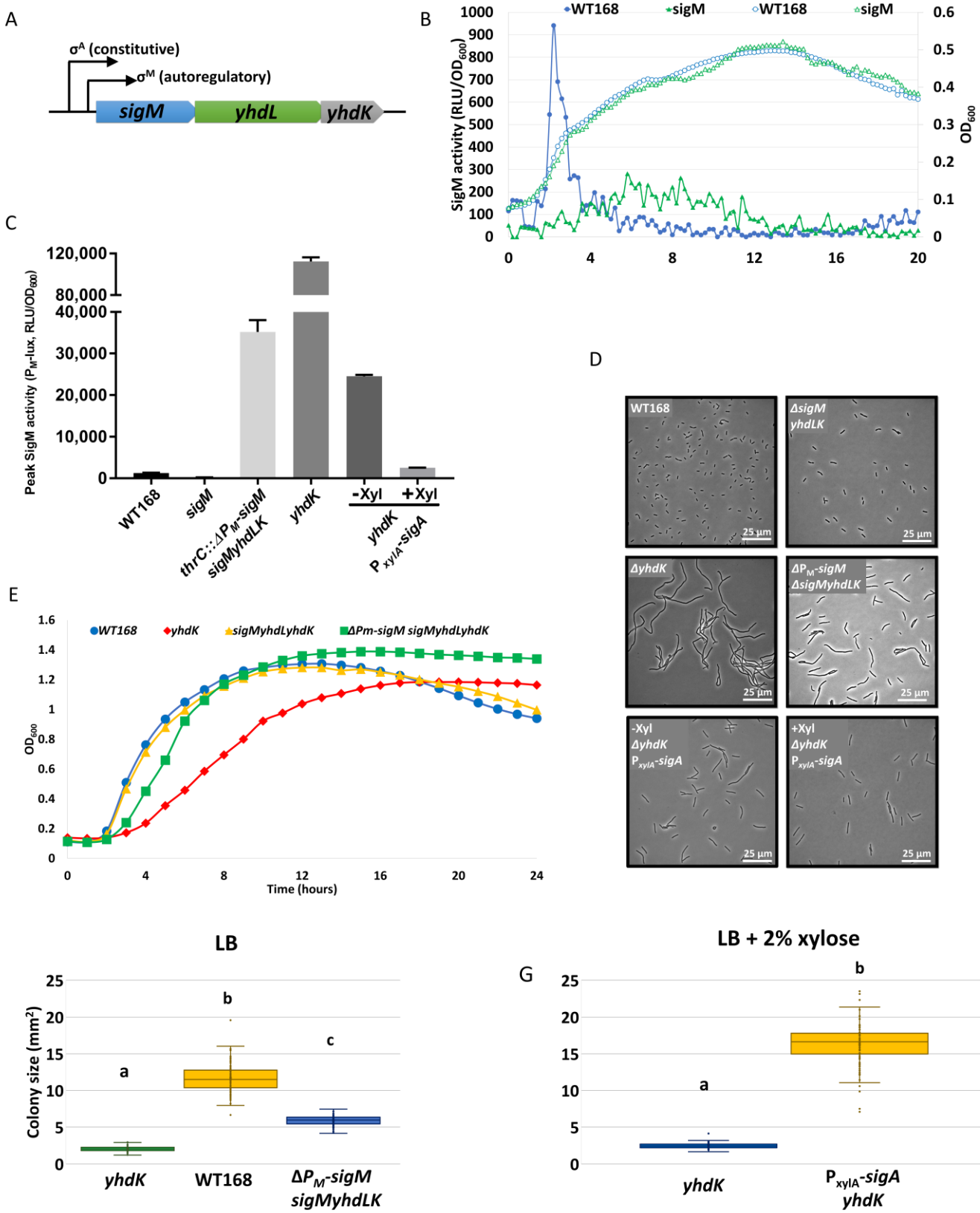
A
σA (constitutive)
σM (autoregulatory)
sigM
yhdL
yhdK
B
WT168
sigM
WT168
sigM
SigM activity (RLU/OD600)
OD600
C
Peak SigM activity (PM-lux, RLU/OD600)
WT168
sigM
thrC::ΔPM-sigM sigMyhdLK
yhdK
-Xyl
+Xyl
yhdK PxylA-sigA
D
WT168
ΔsigM yhdLK
ΔyhdK
ΔPM-sigM ΔsigMyhdLK
-Xyl ΔyhdK PxylA-sigA
+Xyl ΔyhdK PxylA-sigA
25 µm
E
WT168
yhdK
sigMyhdLyhdK
ΔPm-sigM sigMyhdLyhdK
OD600
Time (hours)
F
LB
Colony size (mm2)
a
b
c
yhdK
WT168
ΔPM-sigM sigMyhdLK
G
LB + 2% xylose
a
b
yhdK
PxylA-sigA yhdK

Figure 4.1. Excess SigM activity is toxic in the absence of anti-sigma factors.

(A). Operon structure of *sigMyhdLK*. **(B).** SigM activity monitored using a P_M-lux reporter during growth of WT168 and *sigM* mutant**. (C).** Peak SigM activity in different strain backgrounds. **(D).** Cell morphology of different strains under phase contrast microscope**. (E).** Growth curve of different strains. The OD_{600} was measured using Bioscreen every 15 minutes, and every fourth number is plotted. **(F)**. Colony size of different strains on LB plate after 24 hours of incubation at 37°C. **(G).** Colony size of different strains on LB plate supplemented with 2% xylose (final concentration) after 24 hours of incubation at 37°C.

4.3.2 Alleviation of SigM toxicity by overexpressing SigA or removing the positive feedback of SigM.

We next sought to address the reason for the toxicity from high SigM activity. Because of the limited number of RNAP core enzyme in the cell, different sigma factors need to compete for the core enzyme to transcribe their regulons (Park *et al.*, 2018, Ganguly & Chatterji, 2012, Grigorova *et al.*, 2006). It is possible that high SigM over compete SigA for the latter's essential functions. Alternatively, high SigM activity can cause overexpression of its regulon, of which one or more genes may become toxic when overexpressed. To test if one or both hypotheses are correct, we constructed a P_{xylA}-*sigA* strain in which SigA can be overexpressed from a xylose inducible promoter. Overexpression of SigA can outcompete SigM and reduce SigM toxicity in both the *yhdK* and *yhdL* backgrounds. When SigA is overexpressed, the colony size of the *yhdK* mutant is greatly increased (Figure 4.1G), and a *yhdL* mutant is now viable and the viability is xylose-dependent (data not shown). Using a P_M-lux luciferase reporter, we found that overexpression of *sigA* significantly reduces SigM activity in both *yhdK* and *yhdL* mutant (data not shown).

The high SigM activity is mostly from P_M and the positive feedback loop. In a strain with an ectopic *sigM* only under its P_A but not P_M promoter, the native *sigMyhdLK* operon can be deleted. The mutant has a P_A-*sigM* in the cell without any anti-sigma M factor, and shows an intermediate increase in SigM activity (Figure 4.1C), slightly longer cell morphology (Figure 4. 1E), some retardation in grow rate (Figure 4.1E), and a colony size smaller than WT but bigger than the *yhdK* null mutant (Figure 4.1F). Overexpression of SigA may reduce SigM activity partly by compromising the positive feedback loop, as lowered SigM activity caused by overexpression of SigA will reduce the amount of *sigM* autoregulation. Overall, our results suggest that excess SigM activity is toxic for cells in absence of its anti-sigma factors, mainly from the positive

feedback of the autoregulatory P_M promoter of the *sigMyhdLyhdK* operon, and overexpression of SigA can suppress the toxicity resulting from high SigM.

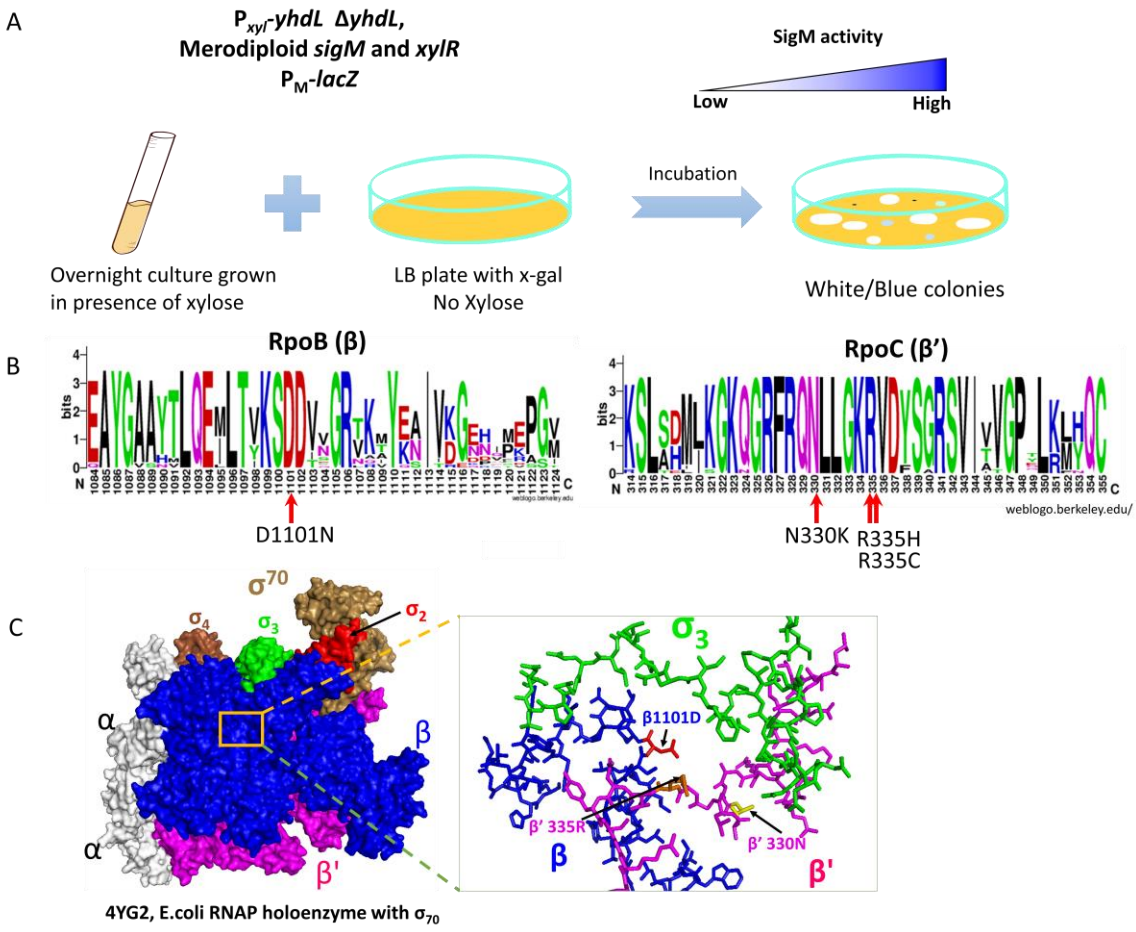

Figure 4.2. Suppressor mutations in core RNA polymerase rescues lethality of *yhdL* null mutation.

(A). Experiment scheme for isolation of suppressors in *yhdL* null mutant background. **(B).** WebLogo of amino acid substitutions in RpoB (β subunit) and RpoC (β' subunit). **(C).** Localization of substitutions in RpoB and RpoC to E. coli RNA polymerase holoenzyme with σ^{70}.

4.3.3 Single amino acid substitutions in RNA polymerase suppress SigM toxicity

Even though overexpression of SigA or breaking the positive feedback loop can rescue cells from lethality of high SigM activity, this observation does not distinguish which hypothesis above (competition with SigA vs. overexpression of toxic protein(s)) is correct, as both genetic modifications would result in less overexpression of potentially toxic protein(s). To identify the potential toxic protein(s), we turned to forward genetics to look for suppressors that can survive high SigM activity, hoping to find suppressors with mutations affecting the expression or activity of potentially toxic proteins. To this end, we constructed a *yhdL* depletion strain with an ectopic xylose-inducible *yhdL* and a deletion of the native *yhdL*. We also introduced a second copy of *sigM* and *xylR* to reduce the chance of getting trivial suppressors that have mutations in *sigM* or *xylR*. A P_M-lacZ reporter was used to visualize high SigM activity with blue color on plates containing X-Gal (5-bromo-4-chloro-3-indolyl β-D-galactopyranoside) (Figure 4.2A). The depletion strain was grown in the presence of xylose to high density, washed twice to remove xylose, and then plated without xylose to select suppressors that can grow in the absence of YhdL (Figure 4.2A). This selection yielded some big white colonies that have mutations in both copies of *sigM* (Sanger sequencing results, data not shown), tiny blue colonies that readily generate white suppressors when re-streaked onto fresh plates, and medium sized light blue colonies that have elevated SigM activity in the absence of YhdL yet are still relatively healthy and do not generate white suppressors when re-streaked (data not shown). Several suppressors of this type were analyzed by whole genome re-sequencing, and four independent suppressor mutations were identified with each containing a single point mutation. These four mutations affect subunits of core RNA polymerase (RNAP), with one mutation affecting RpoB (β) (D1101N), and the other three affecting RpoC (β'): N330K, R335H, and R335C (Figure 4. 2B). These four mutations are

in three conserved amino acids among RpoB/C proteins, suggesting these amino acid residues are important for the conserved structure and function of RNAP (Figure 4.2B).

Because there is no structure available for *B. subtilis* RNAP bound to an ECF sigma factor, we mapped all four mutations to *E. coli* RNAP bound to σ^{70} for insights of how these mutations may affect RNAP-sigma factor interaction. All three affected amino acids ($RpoB^{D1101}$, $RpoC^{N330}$ and $RpoC^{R335}$) map close to the region 3 of *E. coli* σ^{70}, suggesting these amino acids may be important for RNAP-sigma factor interaction. While ECF sigma factors such as SigM do not have a region 3 between region 2 and 4, there is a linker region between region 2 and 4, which may be close to RNAP and important for RNAP-sigma factor interaction. We thus speculate that these mutations in RNAP may affect RNAP-sigma factor interaction, lead to reduced SigM activity, and thus alleviate the toxicity of SigM in the absence of anti-sigma factor YhdL.

To test if these mutations reduce SigM activity, we attempted to reconstruct these mutations at the native locus using CRISPR. We were able to construct $RpoB^{D1101N}$ and $RpoC^{R335H}$ at their native loci, and both the $RpoB^{D1101N}$ and $RpoC^{R335H}$ mutants show slightly slower growth than WT in LB medium (Figure 4.3A). The $RpoC^{R335H}$ mutant exhibits mildly filamentous cell morphology (Figure 4.3B). Attempts to combine both $RpoB^{D1101N}$ and $RpoC^{R335H}$ mutations in one strain were not successful. Using the same P_M-lux reporter described above, we found that the *yhdK* null mutants with $RpoB^{D1101N}$ or $RpoC^{R335H}$ show 1,000-fold or 200-fold reduction of peak SigM activity, respectively, compared to the *yhdK* null mutant with WT RNAP (Figure 4.3C). The filamentous cell morphology of the *yhdK* null is also greatly suppressed by mutations in RNAP (Figure 4.3D), consistent with the idea that the morphology defect of the *yhdK* mutant is from high SigM activity. In addition, *yhdL* can be deleted in the $RpoB^{D1101N}$ and $RpoC^{R335H}$ mutant strains. With the RpoB/C mutations, the *yhdL* null mutants exhibit higher SigM activity than their *yhdK*

null counterparts (Figure 4.3C) and show more severe cell morphology defect (Figure 4.3D). However, even in the absence of *yhdL*, the SigM activity is still 5- to 8-fold lower in these RpoB/C mutants than the *yhdK* null mutant with WT RNAP. Overall these data show that single amino acid substitutions in RpoB or RpoC can suppress the lethality of a *yhdL* deletion, and the growth defect of both *yhdL* and *yhdK* mutations. The SigM activity is reduced with the RpoB/C mutations, possibly due to reduced interaction between the mutant RNAP and Sigma M.

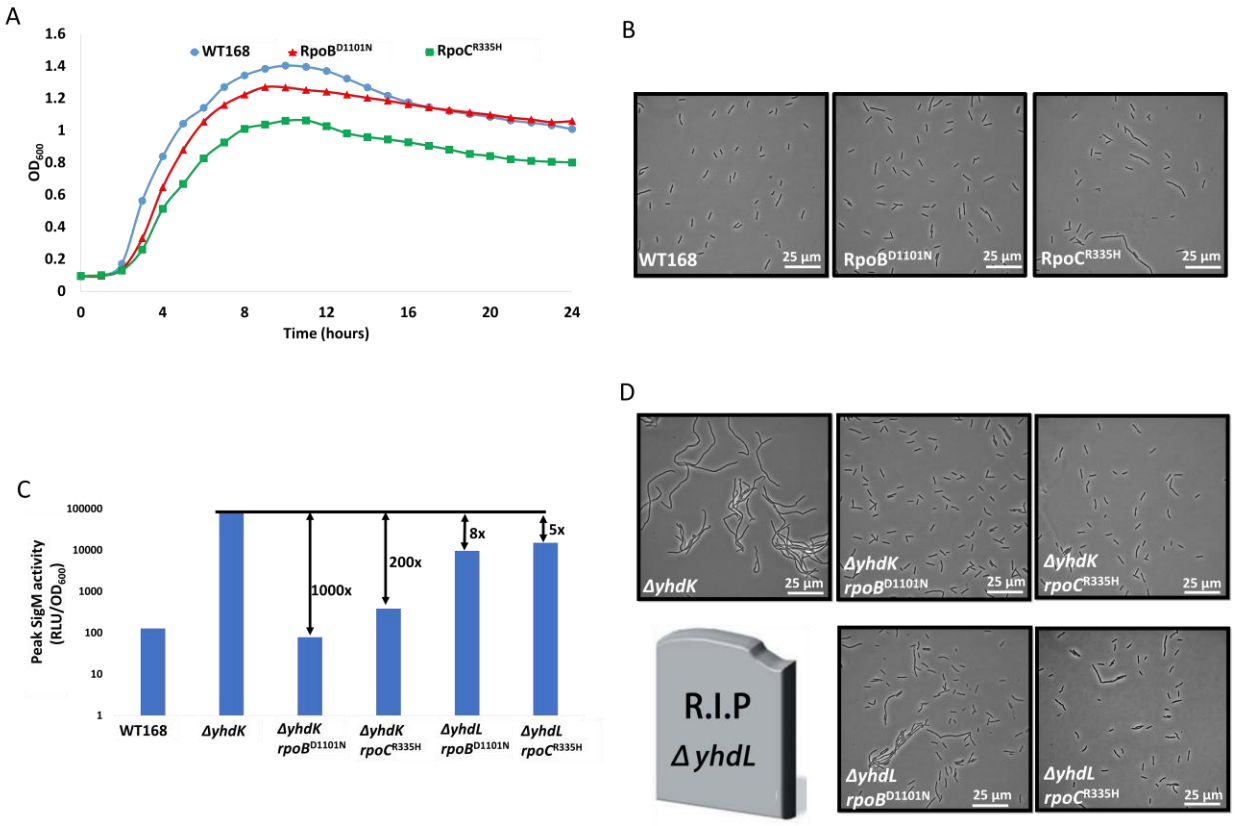

Figure 4.3. Single amino acid substitutions in RNA polymerase suppress SigM toxicity.

(A). Growth curve of WT and *rpoB*/C mutants. **(B).** Cell morphology using phase contrast microscopy of WT and *rpoB*/C mutants. **(C)**. Peak SigM activity of different strains. Fold change between different strains are indicated with arrows and numbers. **(D)**. Cell morphology using phase contrast microscopy of different strains. A *yhdL* null mutant with WT RNA polymerase is lethal, and shown as a tombstone.

4.3.4 Pleiotropic effect of the RpoB^{D1101N} and RpoC^{R335H} substitution on alternative sigma factors

Because mutations in core RNAP may affect its interaction with many sigma factors and thereby alter the transcription efficiency of many genes, we next used sporulation as a representative assay to assess the activity of other sigma factors. Sporulation is a complex developmental process in *B. subtilis* and requires the sequential activation of multiple sigma factors (Piggot & Hilbert, 2004, Stragier & Losick, 1996). To test whether RpoB^{D1101N} and RpoC^{R335H} mutations affect interactions between RNAP and sporulation sigma factors, we measured sporulation efficiency of these mutants after 48 hours of growth in Difco Sporulation Medium (DSM). We found that the RpoB^{D1101N} strain was impaired in the formation of heat resistant spores (0.6% in RpoB^{D1101N} comparing to 66.8% in WT), whereas the RpoC^{R335H} strain had a milder sporulation defect (13.6% in RpoC^{R335H}) (Figure 4.4A). This result suggests that the RpoB^{D1101N} mutant may have sporulation blocked in a certain stage. To find out at which stage sporulation is blocked, we used dual labelling of cells with membrane dyes FM 4-64 and mitotracker green. FM 4-64 can label both the mother cell and forespore membranes before the forespore is engulfed, but cannot penetrate the membrane to label the forespore membrane after the engulfment is complete and two membranes are separated by the cytoplasm of the mother cell. In comparison, mitotracker green can label both membranes before and after the engulfment step (Figure 4.4B). Using these two dyes, we scored cells of WT and RNAP mutants after 4, 7, 14 and 28 hours (over 300 cells per strain per time point) after inoculation in DSM, and found that both RpoB^{D1101N} and RpoC^{R335H} mutants showed reduced rate of asymmetric division, an early morphological landmark of sporulation. More importantly, the RpoB^{D1101N} strain is defective in finishing the engulfment step. In comparison, the RpoC^{R335H} strain can go through the engulfment

step, albeit with a smaller portion of cells than WT at the end of the observed 28 hours. To identify which sporulation factor failed to be activated, we constructed $P_{spoVG42}$-lux, P_{spoIIM}-lux and P_{spoVFA}-lux to directly measure activity of SigH, SigE and SigK, respectively. Our results show that compared to WT cells, SigH activity is increased in the $RpoC^{R335H}$ mutant and decreased in the $RpoB^{D1101N}$ mutant (Figure 4.4C). The construct measuring SigE and SigK activity, however, yielded no signal even in WT background (data not shown). This is likely because of an intrinsic limitation of luciferase reporters, as the generation of signal luminescence uses a lot of ATP, which may be insufficient in sporulating cells. Overall these results suggest that $RpoB^{D1101N}$ and $RpoC^{R335H}$ strains have pleotropic and sometimes different effects in phenotypes that rely on alternative sigma factors, possibly due to altered interaction of mutant RNAP with one or more sigma factors.

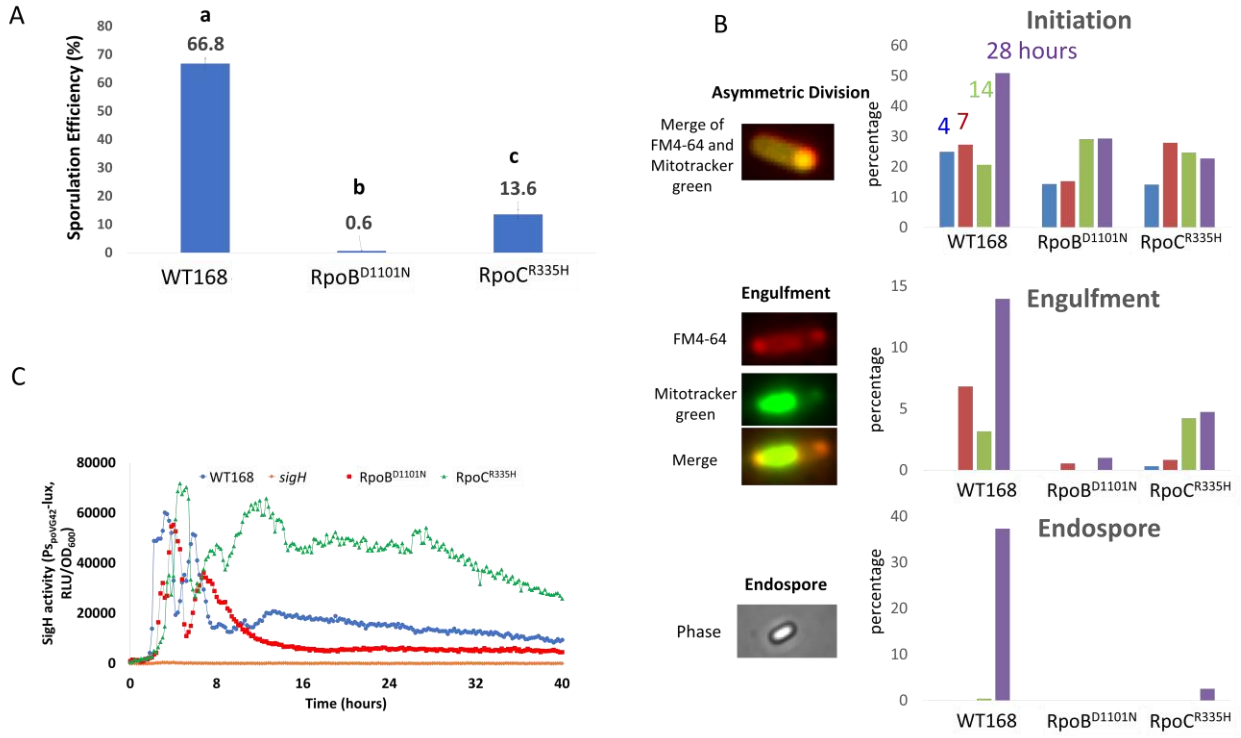

Figure 4.4. Pleiotropic effect of the RpoB^{D1101N} and RpoC^{R335H} substitution on alternative sigma factors.

(A). Efficiency of generating heat resistant endospores of different strains after 48 hours of inoculation in Difco Sporulation Medium (DSM) at 37°C. **(B).** Quantification of different strains going through stages in sporulation after different amount of time after inoculation in DSM at 37°C. Representative images of cells in different sporulation stages are shown on the left. **(C).** SigH activity measured using a Pspo$_{VG42}$-lux reporter in different strain backgrounds.

4.3.5 RpoC^{R335H} substitution causes increased SigW activity

We next tested sensitivity of RpoB^{D1101N} and RpoC^{R335H} mutant strains against several compounds targeting the cell envelope, and found these two mutants are similar to or slightly more sensitive than WT to lysozyme, vancomycin, ampicillin and EDTA (Figure 4.5A). The RpoB^{D1101N} mutant strain is also more sensitive to fosfomycin than WT cells (Figure 4.5B). Surprisingly, we found the RpoC^{R335H} strain is much more resistant to fosfomycin than WT (Figure 4.5B). Fosfomycin resistance is provided by *fosB*, a SigW-dependent gene that encodes a bacillithiol-S-transferase that inactivates fosfomycin (Cao *et al.*, 2001, Lamers *et al.*, 2012, Roberts *et al.*, 2013). To test if the fosfomycin resistance of RpoC^{R335H} mutant is SigW-dependent, we deleted *sigW* gene in RpoC^{R335H} mutant, and found the *rpoC^{R335H} sigW* double mutant is as sensitive to fosfomycin as a *sigW* single mutant with WT RNAP, suggesting the resistance is SigW-dependent, and RpoC^{R335H} mutant likely has increased SigW activity. We next constructed a P_{fosB}-lux reporter strain to directly measure SigW activity in WT and RpoC^{R335H} mutant. We found that even when growing in LB medium without fosfomycin, SigW activity is about 10-fold higher in the RpoC^{R335H} mutant than WT (Figure 4.5C). Overall, our results suggest that the RpoC$_{R335H}$ mutant has increased SigW activity. This increased activity could be due to increased affinity between the mutant RNAP and SigW, although this has not been measured directly.

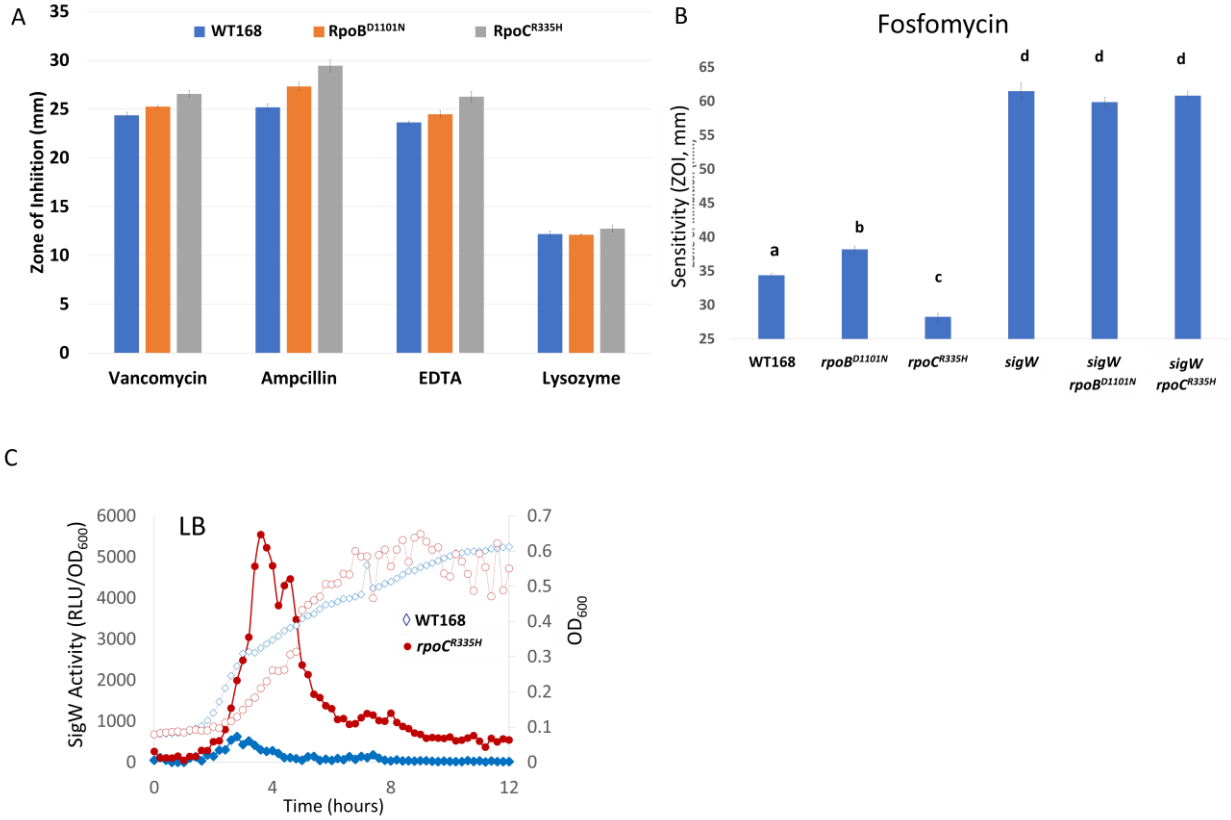

Figure 4.5. RpoC^{R335H} substitution causes increased SigW activity.

(A). Sensitivity of WT and *rpoB*/C mutants to vancomycin, ampicillin, EDTA and lysozyme, measured using zone of inhibition assay. **(B).** Zone of inhibition assay showing sensitivity of different strains to fosfomycin. **(C).** SigW activity measured using a P_{fosB}-lux reporter of WT and RpoC^{R335H} strain.

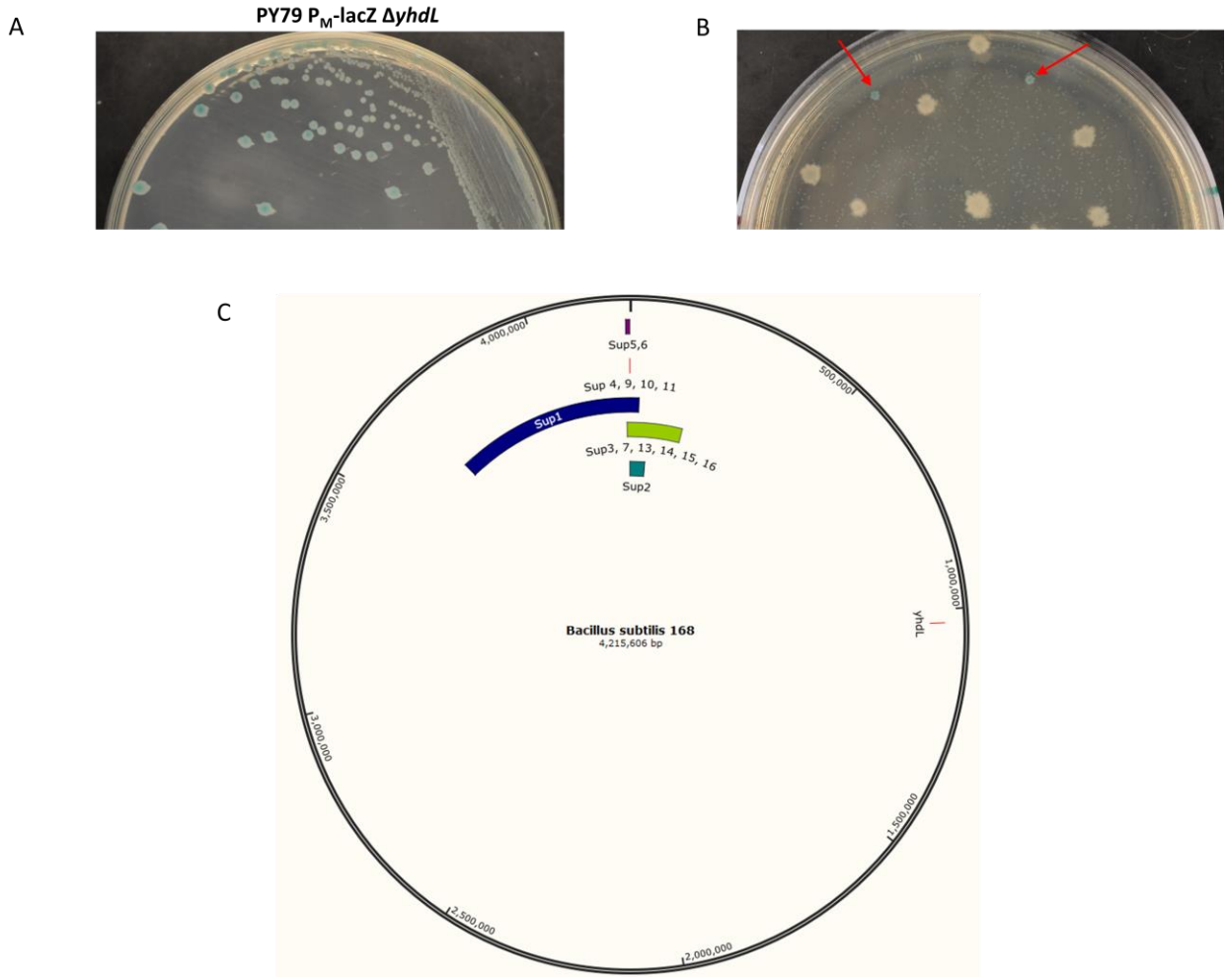

Figure 4.6. SpoIIIJ^{Q140K} substitution is necessary and sufficient for tolerance of high SigM activity.

(A). *yhdL* is not essential in *Bacillus subtilis* strain PY79 background. **(B).** Transformation plate using chromosomal DNA of the viable PY79 *yhdL*::kan to transform 168 strain with a P_M-lacZ reporter. The arrows show intermediate sized blue colonies, suggesting relatively healthy cells with high SigM activity. **(C).** Mapping of co-transformed DNA fragments from 16 transformants onto chromosome of strain 168. Gene *yhdL* and co-transformed DNA are labelled.

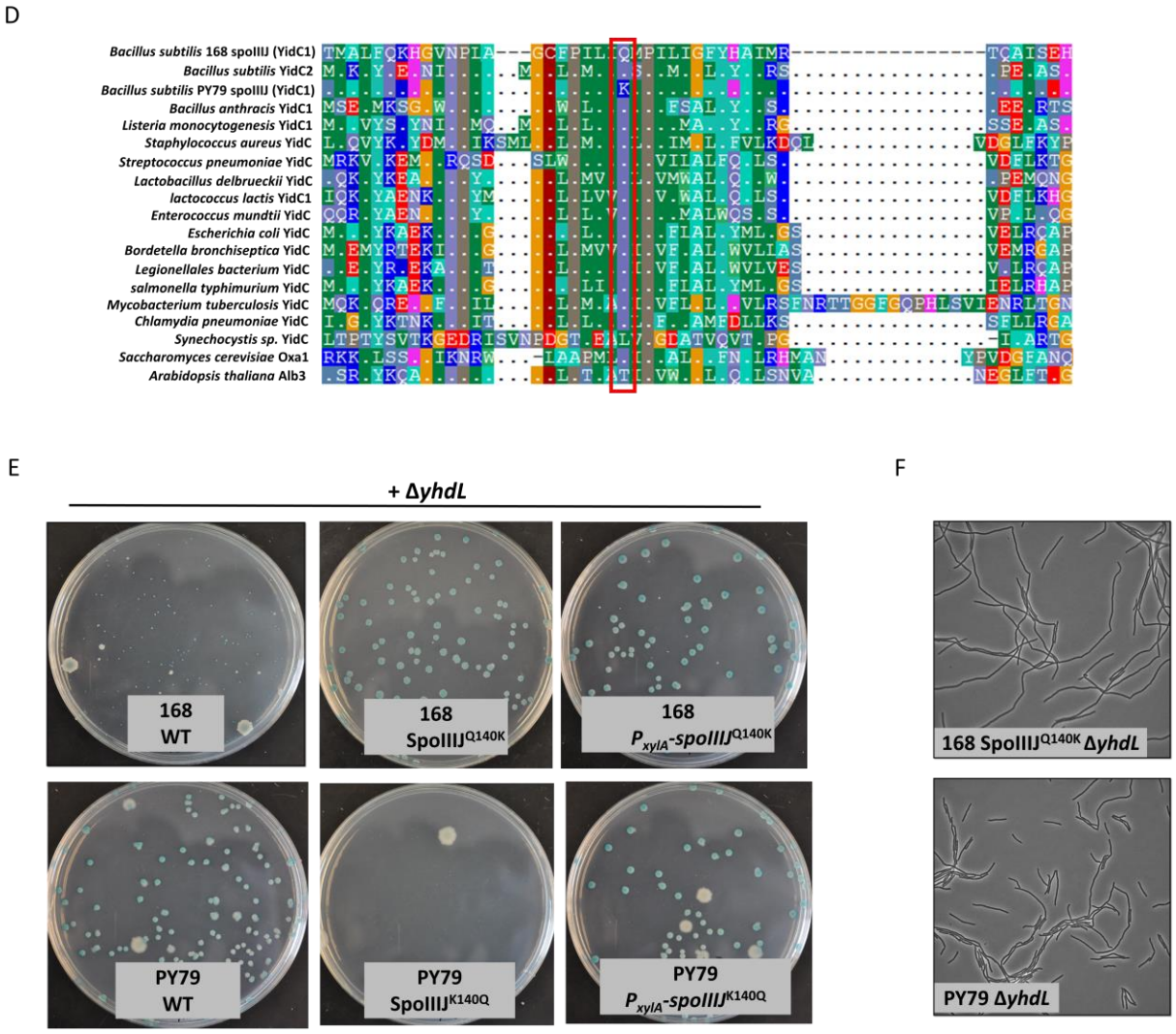

Figure 4.6. SpoIIIJ^{Q140K} substitution is necessary and sufficient for tolerance of high SigM activity (continued).

(D). Alignment of YidC homologs from different firmicute strains and *E. coli.* The red box shows the highly conserved Q140 of SpoIIIJ in *B. subtilis* strain 168. **(E).** Transformation plates of *yhdL* deletion from strains with different *spoIIIJ* alleles. All strains have P_M-lacZ reporter to show blue color on plates containing X-Gal if SigM activity is high. **(F)** Cell morphology of *yhdL* mutants under phase contrast microscope.

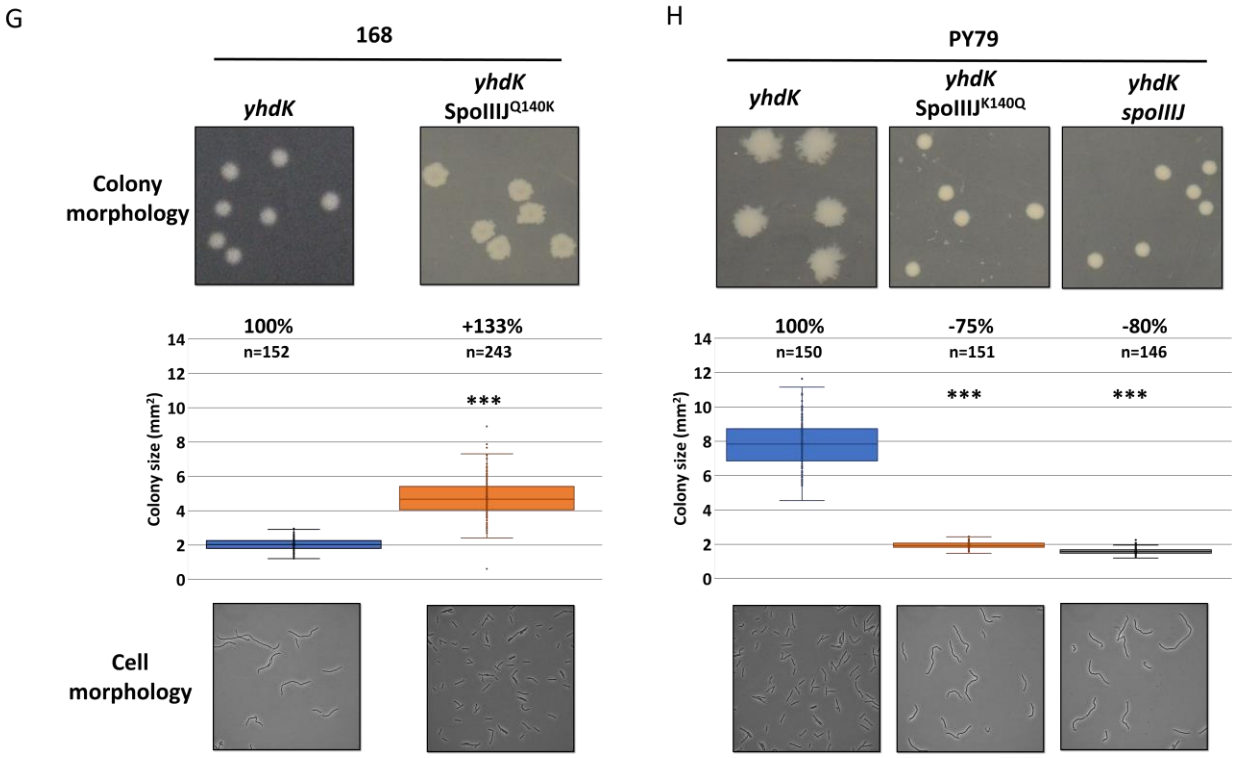

Figure 4.6. SpoIIIJ^{Q140K} substitution is necessary and sufficient for tolerance of high SigM activity (continued).

(G). Colony morphology, size and cell morphology of *yhdK* mutants in strain 168 background with different *spoIIIJ* alleles. **(H).** Colony morphology, size and cell morphology of *yhdK* mutants in strain PY79 background with different *spoIIIJ* alleles.

4.3.6 The gene *yhdL* is not essential in *B. subtilis* strain PY79

Our work above shows that high SigM activity can be alleviated by changes in the transcription level, either by overexpression of SigA, breaking the positive feedback loop, or mutations in RNAP that differentially affect the activity of sigma factors, and likely have reduced affinity for SigM. However, because all these manipulations also reduce the amount of expressed SigM proteins, we cannot draw a conclusion of whether the toxicity of excess SigM is due to its competition against SigA, or a downstream consequence caused by overproduction of certain protein(s). Fortunately, during the pursuit of another project we found that *yhdL* is not essential in PY79, another commonly used laboratory strain of *Bacillus subtilis* (Youngman *et al.*, 1984). In a PY79 background strain containing a P_M-lacZ reporter, deletion of *yhdL* generate transformants with reduced colony size than WT and exhibits high SigM activity as indicated by the blue color on LB plate containing X-Gal (Figure 4.6A, C). This mutant is relatively stable, with occasional appearance of suppressors that have a large white colony morphology (likely containing mutations in *sigM*). To identify the genetic differences that confer tolerance to high SigM in PY79, we compared the genome between *B. subtilis* strain 168 and PY79. There are over a hundred single nucleotide polymorphisms (SNPs) between 168 and PY79, as well as four large deletion from the genome of PY79 (including the SPβ prophage), causing a reduction of 180 kb from the PY79 genome comparing to 168 (Zeigler *et al.*, 2008, Schroeder & Simmons, 2013).

To look for differences that may account for the different tolerance of high SigM, we first compared all the genes in the SigM regulon and the Spx regulon (Spx is a transcription regulator that belongs to the SigM regulon) and found no difference between the coding sequence of these genes. Since we know from the study above that mutations that alter *sigM* transcription can affect SigM activity, we next compared the sequence of *sigA*, *rpoB*/*C* and the surrounding sequence of

sigM, and only identified one region downstream of *sigA* that is different between the two strains. In 168, three transcriptional upshifts are labelled in the region of difference, producing a putative antisense RNA reverse complement to the mRNA of *sigA* (Nicolas et al., 2012). In PY79, 12 bp are missing and this leads to one less predicted promoter for the antisense RNA, potentially causing higher SigA level in PY79 than 168. To test if this difference accounts for the non-essentiality of *yhdL* in PY79, we mutated 168 to delete the promoter that is absent in PY79 using CRISPR. However, *yhdL* is still essential in the 168 antisigA* strain, suggesting that this difference does not play a major, if any, role in the essentiality of *yhdL*.

4.3.7 A single point mutation in SpoIIIJ is necessary and sufficient for tolerance of high SigM activity

We then tried a nonbiased forward genetics-based selection to identify the difference between PY79 and 168 that enables PY79 to tolerate high SigM. Because each competent cell of *B. subtilis* contains about 50 binding sites for DNA uptake, a competent cell can take multiple pieces of DNA during a transformation experiment, a phenomenon known as congression (Dubnau & Cirigliano, 1972). We transformed a 168 strain containing P_M-lacZ with a high concentration of chromosomal DNA from the viable PY79 *yhdL*::kan strain, and selected for kanamycin resistant transformants on a LB plate supplemented with X-Gal. The majority of transformants were tiny blue colonies that cannot be re-streaked onto fresh plates (consistent with the essentiality of the YhdL antisigma factor in the 168 background), with a few big white colonies (likely *sigM* mutants) and intermediate sized blue colonies (Figure 4.6B). The intermediate blue colonies grew to a similar size as a *yhdL* null mutant in PY79, and have a low frequency of generating big white suppressors after re-streaking to a fresh plate, suggesting that in these suppressors the difference

between 168 and PY79 was co-transformed into 168 besides the *yhdL*::kan allele. Whole genome sequencing was performed on these transformants and the reads were mapped to the reference genome of 168 to identify loss or mutation of genes in strain 168. Unmapped reads were *de novo* assembled and BLAST against PY79 reference genome to identify transfer of gene(s) that are unique to PY79. By mapping the transfer of SNPs unique to PY79 into the 168 chromosome we were able to define segments of the genome that had co-transformed with, but were unlinked to, the *yhdL::kan* mutation (Figure 4.6C). Out of 16 sequenced transformants, 14 of them contain a single SNP encoding a missense mutation in the *spoIIIJ* gene ($SpoIIIJ^{Q140K}$).

SpoIIIJ belongs to the YidC membrane insertase family and is responsible for inserting membrane proteins into the lipid membrane, independently or in association with the Sec secretion system (Kumazaki *et al.*, 2014, Tsirigotaki *et al.*, 2017, Hennon *et al.*, 2015). *E. coli* encodes one homolog of YidC, while some bacteria such as *B. subtilis* encodes two homologs, YidC1 (SpoIIIJ) and YidC2 (Hennon *et al.*, 2015, Saller *et al.*, 2009).YidC1 was originally named SpoIIIJ because of its essential role in sporulation (Saller *et al.*, 2009, Errington *et al.*, 1992), although it is also expressed in vegetative cells. The expression of the other YidC homolog YidC2 is regulated by an upstream gene MifM, which monitors the total membrane insertase activity and only allow expression of YidC2 when there is insufficient amount of SpoIIIJ (Chiba & Ito, 2015). Both SpoIIIJ and YidC2 can fulfill the essential function of YidC insertase individually, with SpoIIIJ essential for sporulation (Corte *et al.*, 2014) and YidC2 partly play a role in the development of competence (Saller *et al.*, 2011). Interestingly, an alignment of SpoIIIJ homologs revealed that the Gln 140 is highly conserved among bacteria and only *B. subtilis* PY79 contains Lys at this position (Figure 4.6D).

To test if this Gln to Lys (Q140K) substitution is necessary and sufficient for tolerance of high SigM, we next constructed the SpoIIIJ^{Q140K} mutant in strain 168 using CRISPR and found that *yhdL* is no longer essential in presence of the SpoIIIJ^{Q140K} point mutation (Figure 4.6E). Conversely, changing the Lys 140 into Gln in PY79 abolished the ability of PY79 to tolerate loss of *yhdL* (Figure 4. 6E), suggesting that the SpoIIIJ^{Q140K} point mutation is necessary and sufficient for tolerance of the *yhdL* deletion mutation. The PY79 SpoIIIJ^{K140} is dominant over the 168 SpoIIIJ^{Q140} in the ability to tolerate the *yhdL* deletion, since merodiploid strains (expression of the PY79 SpoIIIJ^{K140} from a xylose-inducible promoter in the presence of 168 SpoIIIJ^{Q140}, or expression of SpoIIIJ^{Q140} in the presence of PY79's native SpoIIIJ^{K140}) expressing both alleles of SpoIIIJ still tolerate loss of *yhdL* (Figure 4.6E). This suggests that SpoIIIJ^{Q140K} results from a gain of function mutation. Phase contrast microscopy reveals that a 168 SpoIIIJ^{Q140K} *yhdL* mutant has a similar but slightly more elongated cell morphology comparing a PY79 *yhdL* mutant (Figure 4.6F), confirming the significant role of SpoIIIJ^{Q140K} in tolerating the *yhdL* null mutation and also suggesting the presence of other minor factor(s). Similarly, the small colony size, as well as the filamentous cell morphology of the 168 *yhdK* mutant can be largely rescued by SpoIIIJ^{Q140K} substitution (Figure 4.6G). A SpoIIIJ^{K140Q} mutation in PY79 converts the edged round big colony morphology of PY79 *yhdK* mutant into the small round morphology of 168 *yhdK*, and cells exhibit increased filamentation (Figure 4.6H). Deletion of *spoIIIJ* in a PY79 *yhdK* mutant mimics a SpoIIIJ^{K140Q} mutation, likely because the cells now rely on the other YidC homolog YidC2, which contains a Q140 in the equivalent position (Saller *et al.*, 2009). Overall, our results show that SpoIIIJ^{Q140K} mutation is necessary and sufficient for *B. subtilis* to tolerate high SigM activity caused by deletion of the anti-sigma factor *yhdL* or *yhdK*.

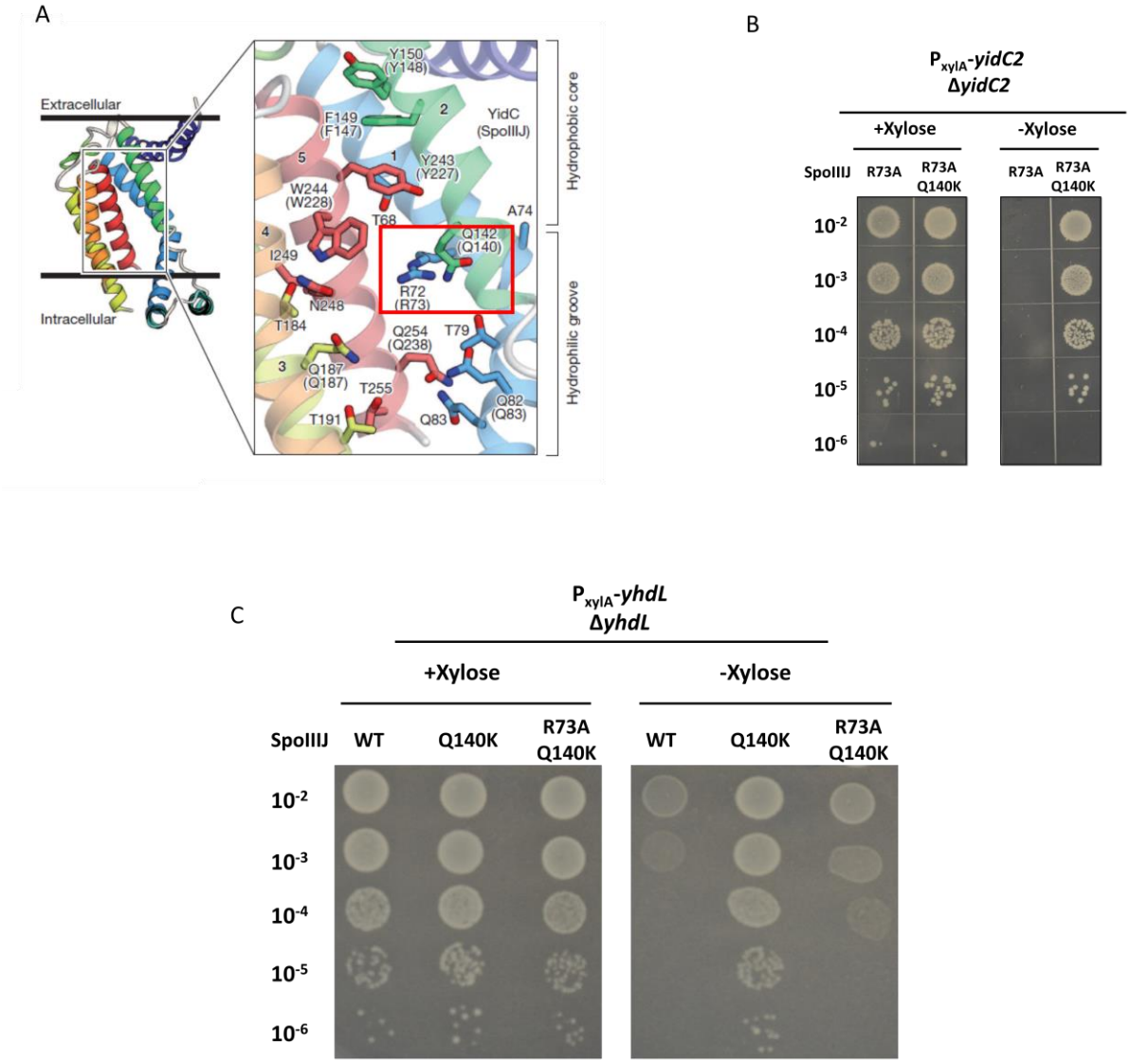

Figure 4.7. SpoIIIJ^{Q140K} has increased positive charge in the substrate binding groove.

(A). Crystal structure of SpoIIIJ from *B. halodurans* (3WO6). **(B).** Spot dilution assay of *yidC2* depletion strains with SpoIIIJ^{R73A} or SpoIIIJ^{R73AQ140K}. **(C)**. Spot dilution assay of *yhdL* depletion strains with WT SpoIIIJ (Q140), SpoIIIJ^{Q140K} or SpoIIIJ^{R73AQ140K}.

4.3.8 SpoIIIJ^{Q140K} mutation causes increased positive charge inside the substrate binding groove

We then try to understand why the SpoIIIJ^{Q140K} substitution can help cells tolerate high SigM activity. The structure of SpoIIIJ from *Bacillus halodurans* reveals a positively charged hydrophilic groove formed by five transmembrane segments (Kumazaki *et al.*, 2014). The positive charge provided by R72 (R73 in *Bacillus subtilis*) is essential for the function of SpoIIIJ and is thought to be important for binding of protein substrates for the membrane insertion step, since an R73A substitution in *B. subtilis* SpoIIIJ completely abolished the essential function of SpoIIIJ *in vivo*, while an R73K substitution retained the function (Kumazaki *et al.*, 2014). Because Q140 is in close spatial proximity to R73 (Figure 4.7A), we hypothesized that the SpoIIIJ^{Q140K} mutation may cause a double positive charge inside the hydrophilic groove. If this hypothesis is correct, we speculated that the essential R73 should no longer be essential in the presence of the Q140K mutation. To test this hypothesis, we constructed a depletion strain of the other YidC homologue YidC2, and mutated the essential R73 into an alanine in the presence of the inducer for YidC2. In the presence of xylose inducer for YidC2, both strains containing SpoIIIJ^{R73A} and SpoIIIJ^{R73AQ140K} mutant are viable (Figure 4.7B). In the absence of the inducer, the mutant expressing only SpoIIIJ^{R73A} failed to grow (Figure 4.7B), consistent with the reported essential function of the positive charge from R73 (Kumazaki *et al.*, 2014). However, the SpoIIIJ^{R73AQ140K} double substitution strain is viable with a similar colony morphology comparing to the strain growing in presence of the inducer (Figure 4.7B), demonstrating that the positive charge resulting from the Q140K substitution is sufficient to replace the essential positive charge from R73. Moreover, *yhdL* is still essential in a strain containing the SpoIIIJ^{R73AQ140K} double mutation (Figure 4.7C), suggesting it is the double positive charge, rather than the Q140K substitution *per se*, that rescues

cells from high SigM toxicity. Overall these results support the idea that the SpoIIIJ^{Q140K} substitution increases the positive charge inside the hydrophilic groove and rescues cells from high SigM toxicity. We hypothesize that the increased positive charge may affect the initial binding of protein substrate into the hydrophilic groove and thus affect the insertase activity of SpoIIIJ.

4.3.9 High SigM activity causes membrane secretion stress

Because the SpoIIIJ^{Q140K} substitution acts downstream of SigM regulon expression and suppresses the lethality of *yhdL* mutant, this suggests that toxicity of high SigM is not only from competition with SigA, but also likely results from overexpression of membrane proteins. SpoIIIJ is involved in insertion of membrane proteins into the membrane, and it is possible that the SpoIIIJ^{Q140K} mutation affects its activity and alleviates the membrane secretion stress. In *B. subtilis*, membrane secretion stress is sensed by the CssRS (control of secretion stress regulator/sensor) two component system. In presence of membrane secretion stress, caused either by overproduction of secreted proteins or high temperature, CssR upregulates expression of membrane proteases HtrA (high temperature requirement) and HtrB to facilitate the re-folding or degradation of misfolded proteins. To test whether high SigM activity causes secretion stress, we constructed a P_{htrA}-lux reporter to monitor the CssR-dependent induction of *htrA*. We found that deletion of *yhdK*, which causes high SigM activity, increases P_{htrA} activity by over four-fold (Figure 4.8A), and this increase can be reduced by the SpoIIIJ^{Q140K} mutation by about 50% (Figure 4.8B). Overall these results support the idea that high SigM causes membrane secretion stress which can be partially alleviated by a mutation in membrane insertase SpoIIIJ.

A

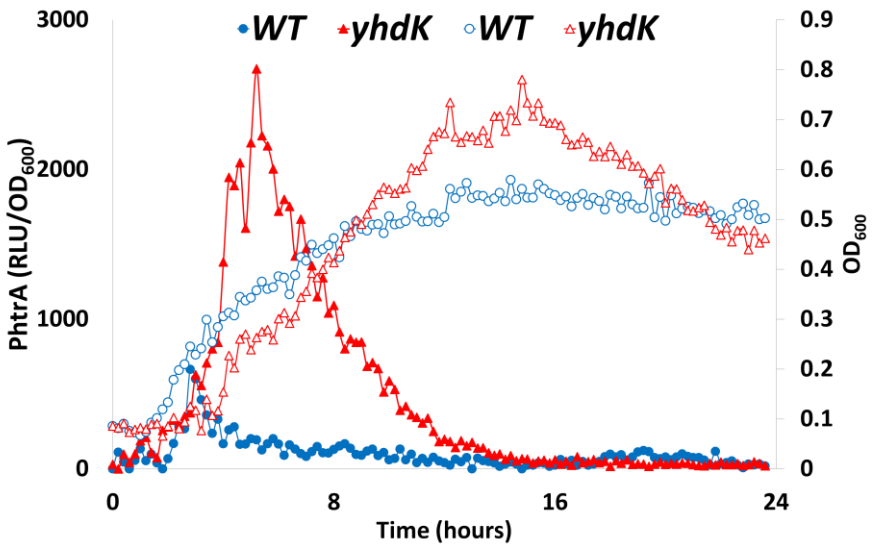

B

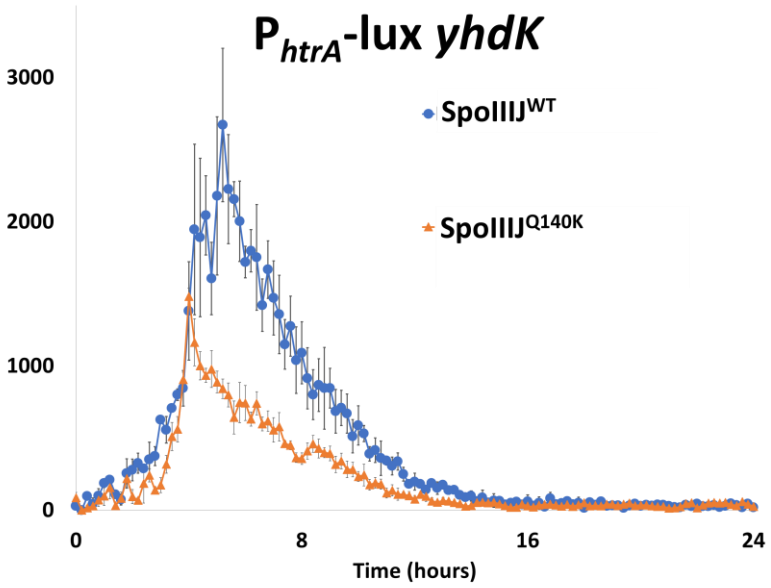

Figure 4.8. SpoIIIJ^{Q140K} substitution relieves secretion stresses caused by high SigM activity.

(A). Quantification of secretion stress measured using a HtrA promoter-luciferase reporter in WT and the *yhdK* mutant. **(B).** P_{htrA}-lux activity in *yhdK* mutants with different *spoIIIJ* alleles.

4.4 Discussion

The use of sigma/anti-sigma factor pairs is common in bacteria to regulate gene expression under different growth conditions, and absence of the anti-sigma factor usually leads to constitutive activity (and often expression) of the corresponding sigma factor (Asai, 2018). In this work, we first found that among the two anti-sigma factors for SigM, the loss of YhdK causes growth defect due to toxicity from high level of SigM, while loss of YhdL is lethal, consistent with previous report (Horsburgh & Moir, 1999). We then moved on to show that reduction of SigM activity at transcriptional level, by overexpression of SigA, abolishing the positive feedback loop for SigM expression, or mutations in RNAP can alleviate SigM toxicity and rescue cell growth in absence of *yhdL* or *yhdK*. During the course of characterizing the mutations in RNAP, we found that the RpoC^{R335H} mutant has greatly increased activity of SigW and mildly increased activity of SigH. This is, to the best of our knowledge, the first work describing an RNAP mutant that exhibits decreased activity to some, but increased activity to multiple other sigma factors.

The serendipitous discovery that *yhdL* is not essential in PY79 led to the identification of SpoIIIJ^{Q140K} allele, which is a unique point mutation among closely related SpoIIIJ/YidC membrane protein insertases and is dominant over the SpoIIIJ^{Q140} allele in rescuing cells from high SigM toxicity. Based on available structural information of SpoIIIJ from *B. halodurans*, we propose that this substitution increases the positive charge inside the substrate binding groove. Indeed, in a SpoIIIJ^{R73AQ140K} double mutant which still contains the Q140K mutation but not the increased positive charge, cells are vulnerable to high SigM activity and *yhdL* remains essential.

How does the increased positive charge rescue cells from high SigM activity? Because the *sigM* regulon includes many membrane proteins, high SigM activity leads to overexpression of these proteins and causes membrane secretion stress. Since many essential membrane proteins

need to be correctly inserted into the membrane by YidC and/or the Sec machinery for their function, overexpression of membrane/secreted proteins may lead to abnormal/insufficient insertion of some essential membrane proteins. Indeed, using a P_{htrA}-lux reporter, we found that cells undergo strong secretion stress in absence of *yhdK*, and this stress can be significantly relieved by the SpoIIIJ^{Q140K} allele (Figure 4.8). Because the positive charge in the substrate binding groove was previously shown to be essential for the essential function of SpoIIIJ, we speculate that the change in this charge may lead to changes in substrate binding and/or the membrane insertion step. The identification of the affected membrane proteins will be the subject of future investigation.

While a changed substrate specificity of SpoIIIJ^{Q140K} is one plausible explanation for the cells' tolerance of high SigM, another possibility relies on the fact that SpoIIIJ/YidC interacts with Sec machinery for membrane protein folding after secretion (Beck *et al.*, 2001), as well as membrane proteases if the protein cannot be folded correctly (van Bloois *et al.*, 2008). It is thus possible that the SpoIIIJ^{Q140K} mutant protein may have altered interaction with one or more membrane proteases. Preliminary data suggest that increased production of membrane protease HtrB is detrimental for the fitness of the *yhdK* mutant. How does SpoIIIJ^{Q140K} allele affect HtrB activity and whether there are other proteases involved will be the focus of future work.

One important finding of this work is that it reveals a connection between high SigM activity and membrane secretion stress. Because cells use a positive feedback loop to turn on SigM to a very high level when they face cell wall stresses, it is very likely that by overexpressing proteins important to fight cell wall stress, bacteria impose themselves to a secondary secretion stress. Indeed, preliminary data suggest that many cell wall targeting antibiotics also induce the CssRS two-component system for secretion stress. More work is needed in this aspect to

potentially guide the use of multiple antibiotics to fight infectious diseases, with one traditional antibiotic targeting an essential bacterial pathway and the other one targeting the new Achilles' heel that bacteria imposed upon themselves when dealing with the first antibiotic.

4.5 Material and Methods

4.5.1 Strains, plasmids and growth condition

Bacteria were grown in liquid lysogeny broth (LB) medium with shaking, or on LB plates (1.5% agar; Difco) at 37 ˚C unless otherwise stated. Plasmids were constructed using standard methods (Luo *et al.*, 2010), and amplified in *E. coli* DH5α before transforming into *B. subtilis*. For selection of transformants, 100 μg/ml ampicillin was used for *E. coli*. Antibiotics used for selection of *B. subtilis* transformants include: kanamycin 15 μg/ml, spectinomycin 100 μg/ml, macrolide-lincosamide-streptogramin B (MLS, contains 1 μg/ml erythromycin and 25 μg/ml lincomycin), neomycin 10 μg/ml, chloramphenicol 10 μg/ml.

4.5.2 Genetic techniques

Chromosomal and plasmid DNA transformation was performed as previously stated (Luo & Helmann, 2012). Markerless in-frame deletion mutants were constructed from BKE strains as described (Meeske *et al.*, 2015). Briefly, BKE strains were acquired from the Bacillus Genetics Stock Center, chromosomal DNA was extracted, and the mutation containing an *erm* cassette was transformed into our WT 168 or PY79 strain. The *erm* cassette was subsequently removed by introduction of plasmid pDR244, which was later cured by growing at the non-permissive temperature of 42 ˚C. Gene deletions were confirmed by PCR screening using flanking primers. Transduction was performed to move SPβ derivatives into the 168 strain as previously described

(Harwood & Cutting, 1990). Unless otherwise described, all PCR products were generated using *B. subtilis* 168 strain chromosomal DNA as template. DNA fragments used for gene over-expression were sequence verified. Null mutant construction was PCR screen verified to have the right size band.

4.5.3 Whole genome sequencing and sequence analysis

Chromosomal DNA of suppressor strains was extracted using Qiagen DNeasy Blood & Tissue Kit. DNA was then sent for sequencing using Illumina HiSeq2500 High Output Mode with Single-end 100 bp reads. Sequencing results were analyzed using CLC workbench version 8.5.1. Single nucleotide variants (SNVs) were detected using default settings.

4.5.4 Disk diffusion assays

Disk diffusion assays were performed as previously described (Kingston *et al.*, 2014). Overnight cultures of test strains were re-inoculated into fresh LB liquid medium and grown to early log phase (OD_{600} ~0.4), and a 100 µl aliquot of the culture was mixed briefly with 4 ml LB soft agar (containing 0.75% agar, kept at 50 ˚C) before being poured onto LB plates (containing 15 ml LB with 1.5% agar). Plates were then cooled and dried in a laminar airflow hood for 5 minutes. Filter paper disks were placed on the surface of the plate, and chemicals were added to the paper disks. Plates were then incubated at 37˚C for 16 h before the diameter of the zone of inhibition was measured. Numbers reported are diameter minus the 6.5 mm diameter of the filter paper disk. The chemicals added to the disks include: ampicillin 1 mg, vancomycin 100 µg, fosfomycin 1 mg, lysozyme 100 µg, EDTA 10 µl of 0.5 M (pH 8.0) solution.

4.5.5 WebLogo for conserved region of RpoB and RpoC

Conserved region near the suppressor mutations of RpoB and RpoC were generated using WebLogo (Crooks *et al.*, 2004). The list of bacterial species of RpoB includes *Bacillus subtilis, Escherichia coli, Thermus aquaticus, Mycobacterium tuberculosis, Staphylococcus aureus, Streptococcus pneumoniae, Salmonella typhimurium, Legionella pneumophila, Chlamydia trachomatis, Lactobacillus delbrueckii, Enterococcus faecium, Pseudomonas aeruginosa, Vibrio cholerae, Cronobacter sakazakii, Paenibacillus polymyxa* and *Acetobacter malorum.* The list of bacterial species of RpoC includes *Bacillus subtilis, Escherichia coli, Thermus aquaticus, Salmonella typhimurium, Photobacterium profundum, Rhodobacter sphaeroides, Legionella pneumophila, Shigella flexneri, Chlamydia muridarum, Lactococcus lactis, Listeria innocua serovar, Mycobacterium tuberculosis, Acinetobacter baylyi, Clostridium tetani, Staphylococcus aureus, Enterococcus faecium,* and *Streptococcus pneumoniae.*

4.5.6 Colony size measurement

Colony size was measured using Fiji Image J (Schindelin *et al.*, 2012). Briefly, bacterial cells were grown to mid-exponential phase (OD_{600}~0.3-0.4), then serial diluted to desired concentrations. Diluted cells were plated onto fresh LB plates (15 ml medium per plate, diameter of the plate is 9 cm), and multiple dilution rates were used. Plates were incubated at 37 °C for 24 hours. Plates containing 10-50 separate single colonies were used for size measurement, because this number of colonies per plate ensures sufficient sample size and does not cause reduced colony size due to crowdedness and nutrient limitation. Pictures of plates were taken with a ruler as a length reference, and colony size was measured using Fiji Image J per software's instruction. For each strain, at least 100 colonies were measured, and box and whisker plots were used.

4.6 References

Asai, K., (2018) Anti-sigma factor-mediated cell surface stress responses in Bacillus subtilis. *Genes Genet Syst* **92**: 223-234.

Asai, K., K. Ishiwata, K. Matsuzaki & Y. Sadaie, (2008) A viable Bacillus subtilis strain without functional extracytoplasmic function sigma genes. *J Bacteriol* **190**: 2633-2636.

Beck, K., G. Eisner, D. Trescher, R.E. Dalbey, J. Brunner & M. Muller, (2001) YidC, an assembly site for polytopic Escherichia coli membrane proteins located in immediate proximity to the SecYE translocon and lipids. *EMBO Rep* **2**: 709-714.

Cao, M., B.A. Bernat, Z. Wang, R.N. Armstrong & J.D. Helmann, (2001) FosB, a cysteine-dependent fosfomycin resistance protein under the control of sigma(W), an extracytoplasmic-function sigma factor in Bacillus subtilis. *J Bacteriol* **183**: 2380-2383.

Crooks, G.E., G. Hon, J.M. Chandonia & S.E. Brenner, (2004) WebLogo: a sequence logo generator. *Genome Res* **14**: 1188-1190.

Dubnau, D. & C. Cirigliano, (1972) Fate of transforming DNA following uptake by competent Bacillus subtilis. Formation and properties of products isolated from transformed cells which are derived entirely from donor DNA. *J Mol Biol* **64**: 9-29.

Eiamphungporn, W. & J.D. Helmann, (2008) The Bacillus subtilis sigma(M) regulon and its contribution to cell envelope stress responses. *Mol Microbiol* **67**: 830-848.

Feklistov, A., B.D. Sharon, S.A. Darst & C.A. Gross, (2014) Bacterial sigma factors: a historical, structural, and genomic perspective. *Annu Rev Microbiol* **68**: 357-376.

Ganguly, A. & D. Chatterji, (2012) A comparative kinetic and thermodynamic perspective of the sigma-competition model in Escherichia coli. *Biophys J* **103**: 1325-1333.

Grigorova, I.L., N.J. Phleger, V.K. Mutalik & C.A. Gross, (2006) Insights into transcriptional regulation and sigma competition from an equilibrium model of RNA polymerase binding to DNA. *Proc Natl Acad Sci U S A* **103**: 5332-5337.

Helmann, J.D., (2016) Bacillus subtilis extracytoplasmic function (ECF) sigma factors and defense of the cell envelope. *Curr Opin Microbiol* **30**: 122-132.

Horsburgh, M.J. & A. Moir, (1999) Sigma M, an ECF RNA polymerase sigma factor of Bacillus subtilis 168, is essential for growth and survival in high concentrations of salt. *Mol Microbiol* **32**: 41-50.

Jervis, A.J., P.D. Thackray, C.W. Houston, M.J. Horsburgh & A. Moir, (2007) SigM-responsive genes of Bacillus subtilis and their promoters. *J Bacteriol* **189**: 4534-4538.

Kobayashi, K., S.D. Ehrlich, A. Albertini, G. Amati, K.K. Andersen, M. Arnaud, K. Asai, S. Ashikaga, S. Aymerich, P. Bessieres, F. Boland, S.C. Brignell, S. Bron, K. Bunai, J. Chapuis, L.C. Christiansen, A. Danchin, M. Debarbouille, E. Dervyn, E. Deuerling, K. Devine, S.K. Devine, O. Dreesen, J. Errington, S. Fillinger, S.J. Foster, Y. Fujita, A. Galizzi, R. Gardan, C. Eschevins, T. Fukushima, K. Haga, C.R. Harwood, M. Hecker, D. Hosoya, M.F. Hullo, H. Kakeshita, D. Karamata, Y. Kasahara, F. Kawamura, K. Koga, P. Koski, R. Kuwana, D. Imamura, M. Ishimaru, S. Ishikawa, I. Ishio, D. Le Coq, A. Masson, C. Mauel, R. Meima, R.P. Mellado, A. Moir, S. Moriya, E. Nagakawa, H. Nanamiya, S. Nakai, P. Nygaard, M. Ogura, T. Ohanan, M. O'Reilly, M. O'Rourke, Z. Pragai, H.M. Pooley, G. Rapoport, J.P. Rawlins, L.A. Rivas, C. Rivolta, A. Sadaie, Y. Sadaie, M. Sarvas, T. Sato, H.H. Saxild, E. Scanlan, W. Schumann, J.F. Seegers, J. Sekiguchi, A. Sekowska, S.J. Seror, M. Simon, P. Stragier, R. Studer, H. Takamatsu, T. Tanaka, M. Takeuchi, H.B. Thomaides, V. Vagner, J.M. van Dijl, K. Watabe, A. Wipat, H. Yamamoto, M. Yamamoto,

Y. Yamamoto, K. Yamane, K. Yata, K. Yoshida, H. Yoshikawa, U. Zuber & N. Ogasawara, (2003) Essential Bacillus subtilis genes. *Proc Natl Acad Sci U S A* **100**: 4678-4683.

Kumazaki, K., S. Chiba, M. Takemoto, A. Furukawa, K. Nishiyama, Y. Sugano, T. Mori, N. Dohmae, K. Hirata, Y. Nakada-Nakura, A.D. Maturana, Y. Tanaka, H. Mori, Y. Sugita, F. Arisaka, K. Ito, R. Ishitani, T. Tsukazaki & O. Nureki, (2014) Structural basis of Sec-independent membrane protein insertion by YidC. *Nature* **509**: 516-520.

Luo, Y., K. Asai, Y. Sadaie & J.D. Helmann, (2010) Transcriptomic and phenotypic characterization of a Bacillus subtilis strain without extracytoplasmic function sigma factors. *J Bacteriol* **192**: 5736-5745.

Luo, Y. & J.D. Helmann, (2012) Analysis of the role of Bacillus subtilis sigma(M) in beta-lactam resistance reveals an essential role for c-di-AMP in peptidoglycan homeostasis. *Mol Microbiol* **83**: 623-639.

Mascher, T., (2013) Signaling diversity and evolution of extracytoplasmic function (ECF) sigma factors. *Curr Opin Microbiol* **16**: 148-155.

Mascher, T., A.B. Hachmann & J.D. Helmann, (2007) Regulatory overlap and functional redundancy among Bacillus subtilis extracytoplasmic function sigma factors. *J Bacteriol* **189**: 6919-6927.

Meeske, A.J., L.T. Sham, H. Kimsey, B.M. Koo, C.A. Gross, T.G. Bernhardt & D.Z. Rudner, (2015) MurJ and a novel lipid II flippase are required for cell wall biogenesis in Bacillus subtilis. *Proc Natl Acad Sci U S A* **112**: 6437-6442.

Mendez, R., A. Gutierrez, J. Reyes & L. Marquez-Magana, (2012) The extracytoplasmic function sigma factor SigY is important for efficient maintenance of the Spbeta prophage that encodes sublancin in Bacillus subtilis. *DNA Cell Biol* **31**: 946-955.

Nicolas, P., U. Mader, E. Dervyn, T. Rochat, A. Leduc, N. Pigeonneau, E. Bidnenko, E. Marchadier, M. Hoebeke, S. Aymerich, D. Becher, P. Bisicchia, E. Botella, O. Delumeau, G. Doherty, E.L. Denham, M.J. Fogg, V. Fromion, A. Goelzer, A. Hansen, E. Hartig, C.R. Harwood, G. Homuth, H. Jarmer, M. Jules, E. Klipp, L. Le Chat, F. Lecointe, P. Lewis, W. Liebermeister, A. March, R.A. Mars, P. Nannapaneni, D. Noone, S. Pohl, B. Rinn, F. Rugheimer, P.K. Sappa, F. Samson, M. Schaffer, B. Schwikowski, L. Steil, J. Stulke, T. Wiegert, K.M. Devine, A.J. Wilkinson, J.M. van Dijl, M. Hecker, U. Volker, P. Bessieres & P. Noirot, (2012) Condition-dependent transcriptome reveals high-level regulatory architecture in Bacillus subtilis. *Science* **335**: 1103-1106.

Park, J., M. Dies, Y. Lin, S. Hormoz, S.E. Smith-Unna, S. Quinodoz, M.J. Hernandez-Jimenez, J. Garcia-Ojalvo, J.C.W. Locke & M.B. Elowitz, (2018) Molecular Time Sharing through Dynamic Pulsing in Single Cells. *Cell Syst* **6**: 216-229 e215.

Saller, M.J., F. Fusetti & A.J. Driessen, (2009) Bacillus subtilis SpoIIIJ and YqjG function in membrane protein biogenesis. *J Bacteriol* **191**: 6749-6757.

Schindelin, J., I. Arganda-Carreras, E. Frise, V. Kaynig, M. Longair, T. Pietzsch, S. Preibisch, C. Rueden, S. Saalfeld, B. Schmid, J.Y. Tinevez, D.J. White, V. Hartenstein, K. Eliceiri, P. Tomancak & A. Cardona, (2012) Fiji: an open-source platform for biological-image analysis. *Nat Methods* **9**: 676-682.

Souza, B.M., T.L. Castro, R.D. Carvalho, N. Seyffert, A. Silva, A. Miyoshi & V. Azevedo, (2014) sigma(ECF) factors of gram-positive bacteria: a focus on Bacillus subtilis and the CMNR group. *Virulence* **5**: 587-600.

Thackray, P.D. & A. Moir, (2003) SigM, an extracytoplasmic function sigma factor of Bacillus subtilis, is activated in response to cell wall antibiotics, ethanol, heat, acid, and superoxide stress. *J Bacteriol* **185**: 3491-3498.

Tsirigotaki, A., J. De Geyter, N. Sostaric, A. Economou & S. Karamanou, (2017) Protein export through the bacterial Sec pathway. *Nat Rev Microbiol* **15**: 21-36.

van Bloois, E., H.L. Dekker, L. Froderberg, E.N. Houben, M.L. Urbanus, C.G. de Koster, J.W. de Gier & J. Luirink, (2008) Detection of cross-links between FtsH, YidC, HflK/C suggests a linked role for these proteins in quality control upon insertion of bacterial inner membrane proteins. *FEBS Lett* **582**: 1419-1424.

Wiegert, T., G. Homuth, S. Versteeg & W. Schumann, (2001) Alkaline shock induces the Bacillus subtilis sigma(W) regulon. *Mol Microbiol* **41**: 59-71.

Yoshimura, M., K. Asai, Y. Sadaie & H. Yoshikawa, (2004) Interaction of Bacillus subtilis extracytoplasmic function (ECF) sigma factors with the N-terminal regions of their potential anti-sigma factors. *Microbiology* **150**: 591-599.

Zeigler, D.R., Z. Pragai, S. Rodriguez, B. Chevreux, A. Muffler, T. Albert, R. Bai, M. Wyss & J.B. Perkins, (2008) The origins of 168, W23, and other Bacillus subtilis legacy strains. *J Bacteriol* **190**: 6983-6995.

4.7 Supplemental Tables

Table S4.1. Strains used in this study

Strain Number	Genotype
HB17474	*sigM* null markerless
HB17494	*sigM* null markerless P_M-*luxABCDE*
HB20830	*yhdK*::*erm*
HB20833	*yhdK*::*erm*, P_M-*luxABCDE*
HB20928	*rpoB* "3301G to A" CRISPR
HB20930	*rpoC* "1004 C to A" CRISPR
HB20934	HB20928 with *yhdL*::*kan*
HB20937	HB20930 with *yhdL*::*kan*
HB20940	PY79 BAM1077 ΔP_M-*rodA yhdL*::*kan*
HB21075	HB20928 with P_M-*lacZ*
HB21077	HB20930 with P_M-*lacZ*
HB21079	HB20928 with P_M-*lux*
HB21081	HB20930 with P_M-*lux*
HB21083	HB20928 with P_M-*lacZ yhdL*::*kan*
HB21086	HB20930 with P_M-*lacZ yhdL*::*kan*
HB21089	HB20928 with P_M-*lux yhdL*::*kan*
HB21092	HB20930 with P_M-*lux yhdL*::*kan*
HB21105	*ganA*::P_{xyl}-*sigA*
HB21107	*ganA*::P_{xyl}-*yhdL*-cat
HB21108	P_{xyl}-*yhdL*-cat *yhdLK*::*kan*
HB21166	HB20928 with P_M-*lux yhdK*::*erm*
HB21168	HB20930 with P_M-*lux yhdK*::*erm*
HB21174	PY79 P_M-*lux*
HB21175	PY79 P_M-*lacZ*
HB21228	168 P_M-*lacZ* AntiSigA*
HB21248	PY79 P_M-*lacZ yhdL*::*kan*
HB21281	HB20930 with *sigW*::*erm*
HB21285	HB20928 with *sigW*::*erm*
HB22578	P_{fosB}-*lux*
HB22580	HB20928 with P_{fosB}-*lux*
HB22582	HB20930 with P_{fosB}-*lux*
HB22745	P_M-*lux sigMyhdLyhdK*::*tet*
HB22775	*ganA*::P_{xyl}-*sigA* P_M-*lacZ*
HB22781	168 P_M-*lacZ* *spoIIIJ*$_{PY79}$
HB22787	P_{xyl}-*sigA yhdL*::*kan*
HB22789	168 P_M-*lacZ* *spoIIIJ*$_{PY79}$ *yhdL*::*kan*
HB22799	*sigE* null markerless
HB22800	*sigH* null markerless
HB22801	*spoIIIC* null markerless

HB22802	*spoIVCB* null markerless
HB22803	*oxaAB* (*yidC2*) null markerless
HB22807	P_{spoIIM}-*lux*
HB22808	$P_{spoVG42}$-*lux*
HB22809	P_{spoVFA}-*lux*
HB22825	HB20928 with P_{spoIIM}-*lux*
HB22827	HB20930 with P_{spoIIM}-*lux*
HB22829	*sigE* null markerless P_{spoIIM}-*lux*
HB22830	HB20928 with $P_{spoVG42}$-*lux*
HB22832	HB20930 with $P_{spoVG42}$-*lux*
HB22834	*sigH* null markerless $P_{spoVG42}$-*lux*
HB22835	HB20928 with P_{spoVFA}-*lux*
HB22837	HB20930 with P_{spoVFA}-*lux*
HB22839	*spoIIC* null markerless P_{spoVFA}-*lux*
HB22840	*spoIVCB* null markerless P_{spoVFA}-*lux*
HB22925	PY79 P_M-*lacZ* $spoIIIJ_{PY79}$
HB22926	PY79 P_M-*lacZ spoIIIJ* null markerless
HB22965	168 P_M-*lux* $spoIIIJ_{PY79}$
HB22966	168 $spoIIIJ_{PY79}$
HB22974	*ganA*::P_{xyl}-$SpoIIIJ_{168}$
HB22975	*ganA*::P_{xyl}-$SpoIIIJ_{PY79}$
HB22983	P_M-*lacZ ganA*::P_{xyl}-$SpoIIIJ_{168}$
HB22984	P_M-*lacZ ganA*::P_{xyl}-$SpoIIIJ_{PY79}$
HB22986	PY79 P_M-*lacZ ganA*::P_{xyl}-$SpoIIIJ_{168}$
HB22987	PY79 P_M-*lacZ ganA*::P_{xyl}-$SpoIIIJ_{PY79}$
HB23524	168 *spoIIIJ* R73A
HB23526	PY79 *spoIIIJ* R73A
HB23530	*yidC2* null markerless pAX01-*yidC2*
HB23532	168 *spoIIIJ* R73A pAX01-*yidC2*
HB23533	PY79 *spoIIIJ* R73A pAX01-*yidC2*
HB23610	168 *spoIIIJ* R73A pAX01-*yidC2 yidC2*::kan
HB23611	PY79 *spoIIIJ* R73A pAX01-*yidC2 yidC2*::kan
HB23619	P_{xyl}-*sigA* P_M-*lux*
HB23650	P_{htrA}-*lux*
HB23659	P_{htrA}-*lux* $spoIIIJ_{PY79}$
HB23692	168 spoIIIJR73A Q140K
HB23693	168 spoIIIJR73A Q140K P_{xyl}-*yidC2 yidC2* null markerless
HB23696	168 spoIIIJR73A Q140K P_{xyl}-*yhdL-xylR*-cat
HB23697	168 spoIIIJR73A Q140K P_M-*lacZ*
HB23698	168 spoIIIJR73A Q140K P_{xyl}-*yhdL-xylR*-cat *yhdL*::*kan*
HB23719	168 spoIIIJQ140K P_{xyl}-*yhdL*-cat *yhdL*::*kan*
HB23720	PY79 P_M-*spoVG-lacZ* P_{xyl}-*yhdL*-cat *yhdL*::*kan*

Table S4.2. Primers used in this study

Primer Number	Name	Sequence
6582	yhdL-cln-up-F	GCCGTTTTCGTTGCGAGAAT
6583	yhdL-cln-up-R	CGCCGACATTCGCTGATTTTTCCTGGTCGCTCATTTCCC
6584	yhdL-cln-mid-F	GGGAAATGAGCGACCAGGAAAAATCAGCGAATGTCGGCG
6585	yhdL-cln-mid-R	CCTATCACCTCAAATGGTTCGCTGTCCGAAAACCGGTATAACGAAA
6586	yhdL-cln-down-F	CGAGCGCCTACGAGGAATTTGTATCGAGATACGAATTTACAGTTTGGCT
6587	yhdL-cln-down-R	ACGAATCGGGCAATCATGTG
6588	chr-sigM-seq-F	CCATTGTGCCACTCCTTCAC
6589	chr-sigM-seq-R	TGCAGTCATTTCCTGGTCGC
6590	pAX01-check-F	GGGGGAAATGACAAATGGTCC
6591	pAX01-check-R	ACGAAAGGGCCTCGTGATAC
6599	Pxyl-yhdL-F-BamHI	ATCGGGATCCTAGAGGGGAGAAAAGGCAATGATGAATGAAGAATTTAAAAAGC
6600	Pxyl-yhdL-R-SacII	ATCGCCGCGGTCCAGCCGAATACATTGTG
6693	pAX01-erm-cm-up-F	GCCGCACTCTTCCTTTTTCAA
6694	pAX01-erm-cm-up-R	CTTGATAATAAGGGTAACTATTGCCTTTGGTTGAGTACTTTTTCACTCG
6695	pAX01-erm-cm-down-F	GGGTAACTAGCCTCGCCGGTCCACGCTGGGGGAGGAAATAATTCTATGAGTCGC
6696	pAX01-erm-cm-down-R	TCGGCATTTTTGCATGGAGC
6759	yhdL-check-F	ACGCTGGGAAGCTACCTCTA
6760	yhdL-check-R	TCTGCTTTTGCGGTCGTTTG
6808	PsigM-F-EcoRI	AGCTGAATTCGCCGTTTGCATGTAATGTG
6809	PsigM-R-PstI	AGCTCTGCAGCAGTAAGTCTTCAGCAAGATGC
6814	pBs1ClacZ(lux)-check-F	AAAGGATTTGAGCGTAGCGA
6815	pBs1ClacZ-check-R	TTGGGTAACGCCAGGGTTTT
6816	pBs3Clux-check-R	GAGAGTCCTCCTGTCGACCT
7249	yhdL-in-check-F	GAAAACACAGCACCGGCAAT
7250	yhdL-in-check-R	AATTCCACCTCGCCGACATT
7324	rpoB-gRNA-F	TACGGACTGTTAAGTCTGATGACG
7325	rpoB-gRNA-R	AAACCGTCATCAGACTTAACAGTC
7326	rpoB-repair-up-F	AAGGCCAACGAGGCCTGCGCTTCGCAATCTTGATG
7327	rpoB-repair-up-R	CTTCGTATGTTTTCACACGTCCAACAACATCATTAGACTTAACAGTCAGAATTTCTTGA
7328	rpoB-repair-down-F	TCAAGAAATTCTGACTGTTAAGTCTAATGATGTTGTTGGACGTGTGAAAACATACGAAG
7329	rpoB-repair-down-R	AAGGCCTTATTGGCCTACGGCGTTGTCCTTGTGAA
7340	rpoC10034-gRNA-F	TACGGGTAAACGTGTCGATTACTC
7341	rpoC10034-gRNA-R	AAACGAGTAATCGACACGTTTACC
7344	rpoC1004-repair-up-R	CAACAACGATTACAGAACGTCCTGAATAGTCCACATGTTTACCAAGAAGGTTTTGACGGA
7345	rpoC1004-repair-down-F	TCCGTCAAAACCTTCTTGGTAAACATGTGGACTATTCAGGACGTTCTGTAATCGTTGTTG
7346	rpoC10034-repair-WT-up-R	CGATTACAGAACGTCCTGAATAGTCCACACGTTTACCAAGAAGGTTTTGACGGAAA
7347	rpoC10034-repair-WT-down-F	TTTCCGTCAAAACCTTCTTGGTAAACGTGTGGACTATTCAGGACGTTCTGTAATCG
7348	pJOE8999-check-F	CCTTTTTGCGTGTGATGCGA
7349	pJOE8999-check-R	GTCAGCTAGGAGGTGACTGA
7405	SigA-R-SacII	ATCGCCGCGGACAAAATTGAATAGAAACATGCCT
7406	SigA-F-SpeI	ATCGACTAGTTTGCGGAGGAGCAAATAGAT

7537	sigA-gRNA-F	TACGCATTATACAATAGAATAAAA
7538	sigA-gRNA-R	AAACTTTTATTCTATTGTATAATG
7539	sigA-repiar-up-F	AAGGCCAACGAGGCCTTCCTTCCCCGTTAATTTGT
7540	sigA-repiar-up-R	CCATATTTTCTATTGTAAGCGTGAGATTTAGGCATGTTTCTATTCA
7541	sigA-repiar-down-F	TGAATAGAAACATGCCTAAATCTCACGCTTACAATAGAAAATATGG
7542	sigA-repiar-down-R	AAGGCCTTATTGGCCTCGGGTTAACCTTCTTTCTG
7543	sigA-seq-F	CCTTTTTGATCCTTCCCCCT
7544	sigA-seq-R	AGGTCGGCAAAGTATTTGGA
7656	PfosB-XbaI-F	CTAGACTGTATGAAACTTTCTTATGAAAAAAGTCGTATATGTGGATGATCAGCTTCTGCA
7657	PfosB-PstI-R	GAAGCTGATCATCCACATATACGACTTTTTTCATAAGAAAGTTTCATACAGT
7815	spoIIIJ-seq-F	ACGGGAGATAACTACGGGCT
7816	spoIIIJ-seq-R	GCTTCATCGACATTTCGCCC
7827	sigM-int-F	CCGCTGTCTGGCACGAAATA
7828	sigM-int-R	TTTTCAAGTGGCGCGAAACG
7866	spoIIIJ-gRNA-F	TACGATCCAATTAAAATCGGCATC
7867	spoIIIJ-gRNA-R	AAACGATGCCGATTTTAATTGGAT
7868	spoIIIJ-up-F	AAGGCCAACGAGGCCTATTGCCAGAAAACCGGCGA
7869	spoIIIJ-up-R	TCGCATGATAGAATCCAATTAAGATAGGCATCTTGATCAAAATCGGGAAACATCCC
7870	spoIIIJ-down-F	GGGATGTTTCCCGATTTTGATCAAGATGCCTATCTTAATTGGATTCTATCATGCGA
7871	spoIIIJ-down-R	AAGGCCTTATTGGCCATCAGACTTCCCGGCAATGG
8110	PspoIIM-XbaI-F	ATCGTCTAGACATACAGCAGTTGATGATAAGG
8111	PspoIIM-PstI-R	ATCGCTGCAGCGCTCTAGTGATTTGATTTAATA
8112	PspoVFA-XbaI-F	ATCGTCTAGAGCGGGCTCTAAAGAAAACAT
8113	PspoVFA-PstI-R	ATCGCTGCAGCTGGATCTCTAGTTGTTAAGC
8114	sigH-check-F	ATTTTCGGACAGGGGGCATT
8115	sigH-check-R	GGTTTCCGCATGTCTTGCAT
8116	sigE-check-F	CAGGGGAGTTGGTCAGCAAA
8117	sigE-check-R	ACCCCGCAGATTTCGACTTT
8118	spoIIIC-check-F	TGCCTGCAACTTGGACTGAT
8119	spoIIIC-check-R	AGCTTTTAGAACGTCCGGCT
8120	yidC2-check-F	TCCTGCTCTAACGGCAATCG
8121	yidC2-check-R	CTTTTTGCACGGGGTTGCTT
8122	spoIVCB-check-F	ACAGGCCTGCCATCCATTTT
8123	spoIVCB-check-R	GGCCGCAAGCGTCTTTTAAC
8132	PspoVG42-up-F	ATCGTCTAGAATAAGAAAAGTGATTCTGGGAGA
8133	PspoVG42-up-R	TCCTGCTCGTTTTTAAAATATTTTTTaAAAAAATAGGATATAGTTACACAATTAGGT
8134	PspoVG42-down-F	ACTATATCCTATTTTTTtAAAAAATATTTTAAAAACGAGCAGGA
8135	PspoVG42-down-R	ATCGCTGCAGTCCCTATATAAAAGCATTAGTGTATCA
8246	spoIIIJ-PY79-to-168-down-F	CATTGGCGGGATGTTTCCCGATCTTGATCCAGATGCCGATTTTAATTGGA
8247	spoIIIJ-PY79-to-168-up-R	AAAATCGGCATCTGGATCAAGATCGGGAAACATCCCGCCAATG
8248	spoIIIJ-PY79-to-168-gRNA-F	TACGATCGGCATCTTGATCAAAAT
8249	spoIIIJ-PY79-to-168-gRNA-R	AAACATTTTGATCAAGATGCCGAT
8278	spoIIIJ-R73A-gRNA-F	TACGAATTAATAAACGAATTAAAA
8279	spoIIIJ-R73A-gRNA-R	AAACTTTTAATTCGTTTATTAATT
8280	SpoIIIJ-R73A-repair-up-R	GCTGCTTAATCATCAGCGGTAAAATTAATAATGCAATTAAAATGGTAACTAGAATAATTGAAAGC

8281	SpoIIIJ-R73A-repair-down-F	GCTTTCAATTATTCTAGTTACCATTTTAATTGCATTATTAATTTTACCGCTGATGATTAAGCAGC
8282	spoIIIJ-SpeI-F	ATCGACTAGTAGATTAATTATAGGAGGAAATGTTGT
8283	spoIIIJ-BamHI-R	ATCGGGATCCAGCAGTCACATTCCTCACTTTT
8347	spoIIIJ-XmaI-F	ATCGCCCGGGAGATTAATTATAGGAGGAAATGTTGT
8348	SpoIIIJ-XbaI-R	ATCGTCTAGAAGCAGTCACATTCCTCACTTTT